

Westinghouse Non-Proprietary Class 3

WCAP-15834
Revision 1

July 2002

WCOBRA/TRAC AP1000
ADS-4/IRWST PHASE MODELING



WCAP-15834

**WCOBRA/TRAC AP1000
ADS-4/IRWST Phase Modeling**

W. L. Brown
Systems Analysis Engineering

R. M. Kemper
Systems Analysis Engineering

R. F. Wright
Passive Plant Engineering

Revision 0 – May 2002

Revision 1 – July 2002

Westinghouse Electric Company LLC
P.O. Box 355
Pittsburgh, PA 15230-0355

© 2002 Westinghouse Electric Company LLC
All Rights Reserved

TABLE OF CONTENTS

LIST OF TABLES.....v

LIST OF FIGURES..... vii

LIST OF ACRONYMS AND ABBREVIATIONSxi

EQUATION NOMENCLATURE xii

SUMMARY xiii

1 INTRODUCTION..... 1-1

2 WCOBRA/TRAC APPLICATION TO THE ADS-4 IRWST INITIATION PHASE 2-1

2.1 INTRODUCTION..... 2-1

2.2 FLOW MODELS AND VALIDATION 2-1

2.2.1 Models and Correlations 2-2

2.2.2 Separate Effects Test Validation 2-16

2.2.3 References 2-21

2.3 OSU APEX FACILITY VALIDATION OF WCOBRA/TRAC-AP 2-46

2.3.1 WCOBRA/TRAC OSU Test Facility Model 2-47

2.3.2 Assessment of WCOBRA/TRAC-AP Predictions 2-51

2.3.3 References 2-52

3 AP1000 PLANT SIMULATIONS 3-1

3.1 PLANT MODELING..... 3-1

3.1.1 Vessel Component..... 3-1

3.1.2 Primary Loop 3-2

3.1.3 Pressurizer 3-2

3.1.4 Steam Generators 3-2

3.1.5 Reactor Coolant Pumps..... 3-2

3.1.6 Loop Lines 3-2

3.1.7 Accumulators 3-2

3.1.8 Core Makeup Tanks 3-3

3.1.9 Passive Residual Heat Removal Heat Exchanger/In-Containment
Refueling Water Storage Tank..... 3-3

3.1.10 In-Containment Refueling Water Storage Tank (IRWST)..... 3-3

3.1.11 Automatic Depressurization System Stage 1 to 3 Valves..... 3-3

3.1.12 Automatic Depressurization System Stage 4 Valves..... 3-3

3.1.13 Safety Injection During the ADS-4 IRWST Initiation Phase 3-3

3.1.14 Break Component..... 3-4

3.1.15 Initial and Boundary Conditions 3-4

3.2 LIMITING CASE RESULTS 3-4

3.2.1 Double-Ended DVI Line Break..... 3-4

3.2.2 Inadvertent ADS Actuation Scenario 3-5

3.3 REFERENCES..... 3-6

TABLE OF CONTENTS (cont.)

4 CONCLUSIONS..... 4-1

APPENDIX A ASSESSMENT OF THE EFFECTS OF ENTRAINMENT IN AP1000 SBLOCA ANALYSIS

A.1 INTRODUCTION.....A.1-1

A.2 SCALING ASSESSMENT OF ENTRAINMENTA.2-1

A.3 EFFECT OF ENTRAINMENT IN THE AP1000 UPPER PLENUM FOLLOWING LOCA EVENTSA.3-1

A.4 ENTRAINMENT SENSITIVITY STUDIES WITH WCOBRA/TRAC.....A.4-1

A.5 CONCLUSIONS.....A.5-1

LIST OF TABLES

Table 2-1 Test Matrix Parameters..... 2-24

LIST OF FIGURES

Figure 1-1 AP1000 Passive Safety Injection Flow Schematic 1-7

Figure 2-1 Generalized Flow Regime Map for Horizontal Two-Phase Flow..... 2-27

Figure 2-2 Equilibrium Liquid Level vs. Martinelli Parameter, X 2-28

Figure 2-3 Basic Mesh Cell 2-29

Figure 2-4 WCOBRA/TRAC-AP Representation of Interfacial Heat Transfer 2-30

Figure 2-5 Schematic Diagram of the Experimental System (Lim, et al., 1981) 2-31

Figure 2-6 WCOBRA/TRAC Noding 2-32

Figure 2-7 Measured Water Thickness Versus Axial Position for Various Liquid (WI) Flowrates and Inlet Water Layer Thickness of 1.583 cm..... 2-33

Figure 2-8 Measured Water Thickness at 0.157 m From the Channel Inlet Versus Liquid and Steam Flowrates 2-34

Figure 2-9 Calculated Liquid Level (Run 275) 2-35

Figure 2-10 Calculated and Measured Liquid Levels Versus Axial Position (Run 275) 2-36

Figure 2-11 Calculated Steam Pressure (Run 275)..... 2-37

Figure 2-12 Calculated and Measured Steam Pressure Versus Axial Position (Run 275)..... 2-38

Figure 2-13 Calculated Steam Flowrate (Run 275) 2-39

Figure 2-14 Calculated and Measured Steam Flowrate Versus Axial Position (Run 275) 2-40

Figure 2-15 Comparison of Condensation Heat Transfer Correlations 2-41

Figure 2-16 Predicted Versus Measured Liquid Level at Various Axial Locations 2-42

Figure 2-17 Predicted Versus Measured Steam Flowrate at Various Axial Locations..... 2-43

Figure 2-18 Predicted Versus Measured Liquid Temperature at the Channel Exit..... 2-44

Figure 2-19 Predicted Versus Measured Steam Pressure Drop at Various Axial Locations 2-45

Figure 2-20 OSU WCOBRA/TRAC Schematic Diagram..... 2-53

Figure 2-21 OSU WCOBRA/TRAC Vessel Model (Front View) 2-54

LIST OF FIGURES (cont.)

Figure 2-22 OSU Vessel Model – Section 1 2-55

Figure 2-23 OSU Vessel Model – Section 2 2-56

Figure 2-24 OSU Vessel Model – Section 3 2-57

Figure 2-25 OSU Vessel Model – Section 4 2-58

Figure 2-26 OSU Vessel Model – Section 5 2-59

Figure 2-27 OSU Vessel Model – Section 6 2-60

Figure 2-28 OSU Vessel Model – Section 7 2-61

Figure 2-29 WCOBRA/TRAC Prediction vs. Test SB18 Data: Pressurizer Collapsed
Liquid Level..... 2-62

Figure 2-30 WCOBRA/TRAC Prediction vs. Test SB18 Data: Total ADS-4 Integrated
Liquid Flow Rate 2-63

Figure 2-31 WCOBRA/TRAC Prediction of Test SB18 Downcomer Collapsed Liquid Level.... 2-64

Figure 2-32 WCOBRA/TRAC Prediction of Test SB18 Core Collapsed Liquid Level..... 2-65

Figure 2-33 WCOBRA/TRAC Prediction of Test SB18 Core/Upper Plenum Collapsed
Liquid Level..... 2-66

Figure 2-34 WCOBRA/TRAC Prediction vs. Test SB18 Data: Downcomer Pressure 2-67

Figure 3-1 AP1000 WCOBRA/TRAC Vessel Model (Front View)..... 3-7

Figure 3-2 AP1000 Vessel Model – Section 1 3-8

Figure 3-3 AP1000 Vessel Model – Section 2 3-9

Figure 3-4 AP1000 Vessel Model – Section 3 3-10

Figure 3-5 AP1000 Vessel Model – Section 4 3-11

Figure 3-6 AP1000 Vessel Model – Section 5 3-12

Figure 3-7 AP1000 Vessel Model – Section 6 3-13

Figure 3-8 AP1000 WCOBRA/TRAC Schematic Diagram..... 3-14

Figure 3-9 AP1000 DEDVI Break Downcomer Pressure 3-15

LIST OF FIGURES (cont.)

| | | |
|-------------|---|------|
| Figure 3-10 | AP1000 DEDVI Break IRWST Flow Rate..... | 3-16 |
| Figure 3-11 | AP1000 DEDVI Break CMT and Accumulator Flow Rate | 3-17 |
| Figure 3-12 | AP1000 DEDVI Break Intact Loop ADS-4 – Integrated Liquid Flow | 3-18 |
| Figure 3-13 | AP1000 DEDVI Break Intact Loop ADS-4 – Integrated Vapor Flow | 3-19 |
| Figure 3-14 | AP1000 DEDVI Break Single Failure Loop ADS-4 – Integrated Liquid Flow..... | 3-20 |
| Figure 3-15 | AP1000 DEDVI Break Single Failure Loop ADS-4 – Integrated Vapor Flow..... | 3-21 |
| Figure 3-16 | AP1000 DEDVI Break Vessel Mass Inventory | 3-22 |
| Figure 3-17 | AP1000 DEDVI Break Integrated Core Inlet Flow | 3-23 |
| Figure 3-18 | AP1000 Inadvertent ADS Actuation Scenario – Downcomer Pressure..... | 3-24 |
| Figure 3-19 | AP1000 Inadvertent ADS Actuation Scenario – Total IRWST Injection Flow Rate..... | 3-25 |
| Figure 3-20 | AP1000 Inadvertent ADS Actuation Scenario – Total CMT Injection Flow Rate..... | 3-26 |
| Figure 3-21 | AP1000 Inadvertent ADS Actuation Scenario Intact Loop ADS-4 – Integrated Liquid Flow | 3-27 |
| Figure 3-22 | AP1000 Inadvertent ADS Actuation Scenario Intact Loop ADS-4 – Integrated Vapor Flow | 3-28 |
| Figure 3-23 | AP1000 Inadvertent ADS Actuation Scenario Single Failure Loop ADS-4 – Integrated Liquid Flow | 3-29 |
| Figure 3-24 | AP1000 Inadvertent ADS Actuation Scenario Single Failure Loop ADS-4 – Integrated Vapor Flow | 3-30 |
| Figure 3-25 | AP1000 Inadvertent ADS Actuation Scenario Break Vessel Mass Inventory..... | 3-31 |
| Figure 3-26 | AP1000 Inadvertent ADS Actuation Scenario Break Integrated Core Inlet Flow | 3-32 |

LIST OF ACRONYMS AND ABBREVIATIONS

| | |
|--------|---|
| ACC | accumulators |
| ADS | automatic depressurization system |
| CCFL | counter current flow limitation |
| CMT | core makeup tank |
| CVS | chemical and volume control system |
| DCD | design control document |
| DVI | direct vessel injection |
| ECCS | emergency core cooling system |
| H2TS | hierarchical, two-tiered scaling |
| HX | heat exchanger |
| IRWST | in-containment refueling water storage tank |
| KI | Kataoka-Ishii |
| LOCA | loss-of-coolant accident |
| LTC | long-term cooling |
| NRC | Nuclear Regulatory Commission |
| OSU | Oregon State University |
| PCS | passive containment cooling system |
| PIRT | phenomena identification and ranking tables |
| PRHR | passive residual heat removal |
| PWR | pressurized water reactor |
| PXS | passive core cooling system |
| RCP | reactor coolant pump |
| RCS | reactor coolant system |
| RNS | normal residual heat removal system |
| SAR | Safety Analysis Report |
| SBLOCA | small-break loss-of-coolant accident |
| SG | steam generator |
| SIMARC | simulator advanced real-time code |

EQUATION NOMENCLATURE

| | | | |
|----------|--|---------------------|--|
| A | Area | Z | Transverse direction, Subchannel Coordinates |
| C_o | Distribution parameter | | |
| d | Offtake diameter | | |
| D | Pipe diameter | <u>Greek</u> | |
| D_H | Hydraulic diameter | ρ | Density |
| E_{fg} | Entrainment ratio | δ | Angle |
| F_r | Froude Number | ν | Kinematic viscosity |
| g | Gravitational acceleration | α | Void fraction |
| G | Mass flux | σ | Surface tension |
| h | Enthalpy, or height | μ | Viscosity |
| h_L | Mixture level | τ | Interfacial shear stress |
| H | Heat Transfer coefficient | Δ | Delta, or difference |
| i | Interfacial | ϕ | Phase |
| j | Superficial velocity | Φ | 2-phase multiplier |
| k | Thermal conductivity, or unit vector indicating flow direction | <u>Subscripts</u> | |
| K | Interfacial friction factor | b | Bubble |
| N_{it} | Viscosity number | g | Saturated vapor |
| P | Pressure | l | Liquid field, or subcooled liquid |
| P_f | Friction perimeter | v | Vapor field |
| P_H | Heated perimeter | f | Saturated liquid |
| P_r | Prandtl number | fo | Liquid only |
| q'' | Heat flux | m | Mixture |
| R | Resistance, hydraulic | sat | Saturated |
| R_e | Reynolds number | sub | Subcooled |
| T | Temperature | w | Wall |
| V_s | Settling velocity | <u>Superscripts</u> | |
| x | Vertical direction, Cartesian coordinates, or flow quality | e | Entrained field |
| X | Phasic pressure drop ratio in two-phase flow | k | Continuous phase |
| U | Vertical velocity component, Subchannel coordinates | x | Vertical direction, Cartesian Coordinate |
| V_{gj} | Drift velocity | S | Superficial |
| z | Transverse direction, Cartesian coordinates, or elevation | * | Indicates dimensionless quantity |
| | | - | Indicates average quantity |
| | | ^ | Indicates vector quantity |

SUMMARY

In NUREG-1512, "Final Safety Evaluation Report Related to the Certification of the AP600 Standard Design," dated September 1998, the NRC approved the use of the Westinghouse NOTRUMP safety analysis code for the purpose of performing small break loss of coolant accidents (SBLOCA) for the AP600, in accordance with Appendix K of 10 CFR Part 50. In this evaluation, the staff identified that the NOTRUMP code did not include an explicit modeling of some phenomena that may affect the performance of the passive safety systems during the SBLOCA events. To compensate for the lack of an explicit momentum flux model in NOTRUMP, Westinghouse imposed penalties to the NOTRUMP code calculations to effectively inhibit the depressurization capability of the automatic depressurization system, and thus reduce the predicted safety injection flow, for the purpose of conservatively bounding the effect of momentum flux on the NOTRUMP predictions. This conservative approach was found to be acceptable for the AP600, due to several factors, including the following:

- Validation of the NOTRUMP code against AP600 separate effects and integral systems test programs.
- Large conservatisms inherent in the approved methodology (including Appendix K decay heat of 120 percent of nominal).
- Large safety margins of the passive safety systems, demonstrated in the confirmatory tests that were conducted by the NRC at the APEX test facility, at Oregon State University, and the ROSA-AP600 test facility, at the Japan Atomic Energy Research Institute.
- Large safety margins of the AP600 SBLOCA analysis results, which show that SBLOCA is a non-limiting LOCA event with no core uncover for break sizes up to, and including the double-ended rupture of a direct vessel injection line break (DEDVI), which disables 50 percent of the installed safety injection flow paths.

In the AP1000 Pre-Certification review, Westinghouse demonstrated, through the evaluation of important phenomena and through scaling of the AP600 tests, that the AP600 test program used to support Design Certification was applicable to the AP1000. This leads to the conclusion that the safety analysis codes that were validated and approved for the AP600 are then appropriate for use in performing AP1000 safety analysis in support of AP1000 Design Certification. In the AP1000 Design Control Document, submitted as part of the Westinghouse Application for Design Certification, it can be seen that the AP1000 plant behavior is similar to the AP600, and the performance of the AP1000 safety systems demonstrate margin to the regulatory limits.

One of the considerations in the approval of the NOTRUMP code for AP1000 was the Westinghouse commitment to perform a supplemental analysis of the AP1000 SBLOCA event, for the period of time in the transient when phenomena, such as momentum flux and hot leg / upper plenum entrainment, could affect the predicted analytical results from the NOTRUMP code. This supplemental analysis is performed with a version of the WCOBRA-TRAC computer code. Models and correlations to predict important phenomena during the ADS-4 IRWST initiation Phase of an AP1000 SBLOCA are included. The reason for using the WCOBRA-TRAC code is that this code is a modern, state-of-the-art analysis code that models the phenomena that were not explicitly modeled in NOTRUMP. The purpose of this supplemental

analysis is to demonstrate that NOTRUMP provides a conservative simulation of ADS-4 venting and the onset of IRWST injection for AP1000.

This report provides a description of the supplemental analysis model, and includes validation of this model against suitable test data. It is shown that this model performs a reasonable simulation of a suitable test performed at the APEX test facility. This model is then used to perform plant calculations. The results of these plant calculations are then compared to the NOTRUMP calculations presented in Chapter 15 of the AP1000 Design Control Document. Based on a comparison of these calculations to the DCD analyses, it is demonstrated that the NOTRUMP DCD analyses provide a conservative prediction of the ECCS performance of the AP1000. It is concluded that the NOTRUMP DCD calculational approach compensates for the lack of explicit phenomenological modeling in NOTRUMP (such as momentum flux and upper plenum / hot leg entrainment) that could affect the predictions of the SBLOCA accident. Large margin to regulatory limits are demonstrated in the analytical results of the SBLOCA events for AP1000.

Westinghouse and the NRC performed a pre-certification review of the AP1000 to determine whether the testing performed in support of AP600 Design Certification are applicable to the AP1000 Design Certification. In addition, the analysis codes that were validated against the AP600 passive safety system tests were reviewed for their applicability to AP1000. The results of this review were documented in NRC letter "Applicability of AP600 Standard Plant Design Analysis Codes, Test Program and Exemptions to the AP1000 Standard Plant Design," dated March 25, 2002. In this letter, the NRC staff concludes that the tests and analysis codes used to support AP600 Design Certification can be used to support AP1000. In this letter, the staff also identified exceptions to this conclusion that need to be resolved during Design Certification. The most notable of these exceptions is that Westinghouse had not demonstrated that the existing AP600 tests provide data over the range of conditions necessary to validate entrainment models in the NOTRUMP and WCOBRA/TRAC codes that are used for small-break LOCA analyses. This issue is addressed in Appendix A of this report.

Appendix A provides the results of assessments to determine the importance of the phenomena of upper plenum and hot leg entrainment on the performance of the passive safety systems, following a small-break LOCA. In this appendix, it is concluded that the passive safety system performance following a small-break LOCA is not significantly affected by these phenomena, and the predictions of the consequences of a small-break LOCA performed for the AP1000 conservatively bound the consequences of these design basis accidents. The large margin to regulatory limits demonstrated in the analytical results of the SBLOCA events for AP1000 are maintained, even when unrealistic uncertainties of upper plenum and hot leg entrainment are considered. Therefore, it is concluded that these phenomena are not important with respect to overall passive safety system performance, and that additional AP1000 testing and code validation is not needed for AP1000 Design Certification.

1 INTRODUCTION

Westinghouse Electric Company has designed an advanced 600 MWe nuclear power plant called the AP600. The AP600 uses passive safety systems to enhance plant safety and to satisfy U.S. licensing requirements. The use of passive safety systems provides significant and measurable improvements in plant simplification, safety, reliability, investment protection, and plant costs. These systems use only natural forces such as gravity, natural circulation, and compressed gas to provide the driving forces for the systems to adequately cool the reactor core following an accident. The AP600 received Design Certification by the Nuclear Regulatory Commission (NRC) in December 1999.

To further improve AP600 economics, Westinghouse initiated development of the AP1000 standard nuclear reactor design, with an output of approximately 1100 MWe, based upon the AP600 design. The design features of the plant, including the passive safety systems, have been selected to preserve key features and performance characteristics embodied in the AP600. By preserving the design basis of the AP600 in the AP1000, Westinghouse seeks to preserve the licensing basis of the plant as well. The AP1000 passive safety injection systems are shown in Figure 1-1.

The AP1000 is a Westinghouse advanced reactor designed to enhance plant safety with accident mitigation features that, once actuated, depend only on natural forces, such as gravity and natural circulation, to perform all required safety functions.

The AP1000 primary system is a two-loop design. Each loop contains one hot leg, two cold legs, and one steam generator (SG) with two canned motor reactor coolant pumps (RCPs) attached directly to the SG outlet channel head. The passive safety systems comprise the following:

- Two full-pressure core makeup tanks (CMTs) that provide borated makeup water to the primary system at full system pressure.
- Two accumulators (ACCs) that provide borated water to the reactor vessel if the primary pressure ≤ 700 psia.
- A passive residual heat removal (PRHR) heat exchanger (HX), comprised of a C-shaped tube bundle submerged in the in-containment refueling water storage tank (IRWST), that can remove heat from the primary system at full system pressure.
- The automatic depressurization system (ADS), which is comprised of a set of valves connected to the reactor coolant system (RCS) at the pressurizer steam space and the two hot legs. The valves connected to the pressurizer vent to the IRWST through a sparger. The valves connected to the hot leg vent to the containment. These valves are opened sequentially to provide controlled depressurization of the primary system.
- An IRWST that provides a large source of core cooling water, which drains by gravity after the ADS has actuated.
- A passive containment cooling system (PCS) that utilizes the AP1000 steel containment shell to transfer heat to the environment (ultimate heat sink).

Westinghouse submitted the "AP1000 PIRT and Scaling Assessment" (Reference 2) report to the NRC. The report provides Phenomena Identification and Ranking Tables (PIRT) for the AP1000 and demonstrates through scaling that the AP600 test program is applicable to the AP1000 and sufficiently covers the range of conditions expected for the AP1000. The report concludes that the AP600 test program provides a test database sufficient for code validation for AP1000 in accordance with 10CFR Part 52. The Reference 2 PIRT increases the importance of some post-ADS phenomena.

This report documents the approach to supplement the NOTRUMP code approved for AP600 in its application to AP1000 Design Certification by using WCOBRA/TRAC to predict the ADS-4 IRWST initiation phase.

Section 2 provides the validation of the WCOBRA/TRAC code for predicting phenomena during ADS-4 operation and addresses the acceptability of the WCOBRA/TRAC code for the analysis of AP1000 loss-of-coolant accident (LOCA) events during this phase. Section 3 provides an analysis of AP1000 during this phase. Section 4 provides conclusions regarding the capability of NOTRUMP to conservatively predict AP1000 small break LOCA transients.

Westinghouse and the NRC performed a pre-certification review of the AP1000 to determine whether the testing performed in support of AP600 Design Certification is applicable to the AP1000 Design Certification. In addition, the analysis codes that were validated against the AP600 passive safety system tests were reviewed for their applicability to AP1000. The results of this review were documented in NRC letter "Applicability of AP600 Standard Plant Design Analysis Codes, Test Program and Exemptions to the AP1000 Standard Plant Design," dated March 25, 2002. In this letter, the NRC staff concludes that the tests and analysis codes used to support AP600 Design Certification can be used to support AP1000. In this letter, the staff also identified exceptions to this conclusion that need to be resolved during Design Certification. The most notable of these exceptions is that Westinghouse had not demonstrated that the existing AP600 tests provide data over the range of conditions necessary to validate entrainment models in the NOTRUMP and WCOBRA/TRAC codes that are used for small-break LOCA analyses. This issue is addressed in Appendix A of this report.

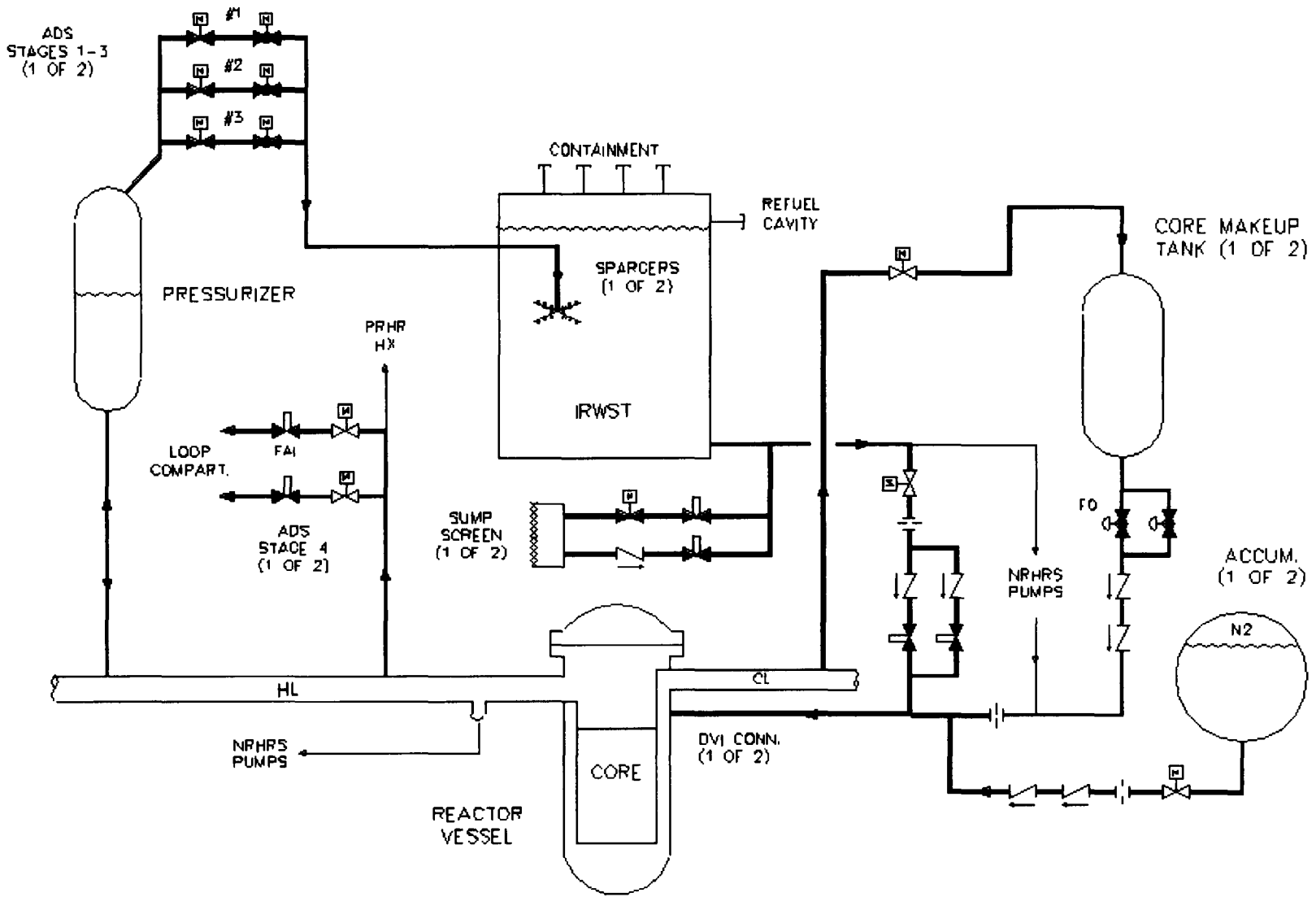


Figure 1-1 AP1000 Passive Safety Injection Flow Schematic

2 WCOBRA/TRAC APPLICATION TO THE ADS-4 IRWST INITIATION PHASE

2.1 INTRODUCTION

The Automatic Depressurization System (ADS) Stage 4 in-containment refueling water storage tank (IRWST) initiation phase of the small break LOCA event for AP1000 is characterized by the following phenomena: significant momentum flux pressure drop in the ADS-4 flowpaths, entrainment in the reactor vessel and hot legs, and draining of the pressurizer and surge line mass. To account for these phenomena, a modified version of WCOBRA/TRAC-MOD7A designated as “WCOBRA/TRAC-AP” is used to supplement NOTRUMP. In comparison to the NOTRUMP code, WCOBRA/TRAC provides a more detailed model of the physical processes encountered during these conditions as follows:

The momentum equation as solved in the TRAC components used for ADS Stage 4 (ADS-4) piping contains all significant terms, including the momentum flux terms, as discussed in Section 2-5 of WCAP-12945-P-A (Reference 3).

COBRA channels are used to model the hot legs in the AP1000 supplemental calculation. Within the hot legs, horizontal flow regimes are identified using the Taitel-Dukler flow map (Reference 1). The Ishii-Grolmes (Reference 2) criteria are used to predict the onset of entrainment off the horizontal surface. Entrainment into the ADS Stage 4 offtake piping atop the hot legs is determined using a Froude-number relationship. In the event that entrainment is predicted to occur, the quality in the ADS-4 pipe is calculated using a correlation for a vertical upward branch connection.

Prediction of the mixture swell in a WCOBRA/TRAC channel depends on interfacial drag between the vapor and liquid phases. Models and correlations are available that calculate interfacial shear in both vertical and horizontal flows. Models for flow regime transition and bubble rise in the code allow for phase separation and entrainment.

Subsection 2.2 is intended to describe the models and correlations that have been included in the WCOBRA/TRAC-AP code to enable it to compute the important phenomena during the ADS-4 IRWST initiation phase of a small break LOCA in AP1000. The subsection presents the code features for modeling horizontal flow behaviors and for calculating the entrainment into the branch line at a “TEE” vertical connection, such as the ADS-4 offtake piping atop the hot legs in the AP1000 design. The performance of the code in predicting the horizontal flow behaviors observed in a separate effect test conducted at atmospheric pressure is also presented. Subsection 2.3 presents the OSU APEX facility integral systems validation using Test SB18.

2.2 FLOW MODELS AND VALIDATION

Horizontal stratification, counter-current flow and counter-current flow limitations (CCFL), and transition between flow regimes in WCOBRA/TRAC depend on interfacial drag between phases in lateral flow. WCOBRA/TRAC-AP allows for horizontal flow regime modeling using correlations for drag to allow stratification. Section 15 of Volume 3 of WCAP-12945-P-A (Reference 3) reported an assessment and calculations of flow in horizontal pipes represented by COBRA channels. The evaluation showed that

WCOBRA/TRAC has the capability to predict counterflow and CCFL at horizontal locations within the reactor coolant system. A further assessment of WCOBRA/TRAC-AP presented in subsection 2.2.2 shows it capable of predicting horizontal stratified flow behaviors with the accuracy necessary for the ADS-4 IRWST initiation phase of small break LOCA analyses for AP1000.

Horizontal flow regimes and the transition criteria from one regime to another have been the subjects of several studies. The most notable result is the Taitel-Dukler flow regime map for horizontal flows (Reference 1), which takes into account both pipe diameters and fluid properties on each of the flow pattern transitions. The Taitel-Dukler flow regime map and transition criteria include a dependence on pipe diameter. This provides a means of examining the scale diameter dependence of the WCOBRA/TRAC models for horizontal flow.

Subsection 2.2.2 presents the results of WCOBRA/TRAC simulations of tests reported in Lim (Reference 4) investigating the horizontal two-phase flow in a channel. The wavy or stratified flow regime condensation and pressure drop data were obtained, together with steam flowrate and water layer thickness data at various locations in a four-foot long experimental channel.

The carry over of droplets from the upper plenum into the hot legs by the flow of steam above the mixture level is assigned a medium (M) ranking for the ADS-4 operation time period in the AP1000 small break LOCA PIRT in WCAP-15613 (Reference 5). Entrainment in the flow from the hot legs into the ADS-4 piping is assigned a high (H) ranking for AP1000, increased from the medium (M) ranking of AP600. This carryover by drops entrained in the steam is modeled in detail in WCOBRA/TRAC-AP.

2.2.1 Models and Correlations

2.2.1.1 Liquid Entrainment Onset Correlations

General Form of Entrainment Onset Correlations into Branch Pipes

The general form of most entrainment onset correlations for offtake pipes found in the literature is as follows:

$$Fr_g \left(\frac{\rho_g}{\rho_l - \rho_g} \right)^{0.5} = C_1 \left[\frac{z_b}{d} \right]^{C_2} \quad (2-1)$$

The key elements of this correlation form consist of the Froude number (Fr), density ratio ($\rho/\Delta\rho$), and a geometric ratio (z/d) of entrainment onset height (z) to offtake diameter (d). The coefficient C_1 and exponent C_2 are functions of the orientation and geometry of the offtake.

Side Offtake Orientation

Craya (Reference 6) developed a theoretical onset of liquid entrainment for discharge from a side offtake neglecting viscosity and surface tension effects. Craya's theoretical result was obtained by treating the offtake as a potential flow point sink. From this he arrived at onset correlations for orifice-type offtakes and slot-type offtakes as follows:

$$Fr_g \left(\frac{\rho_g}{\rho_l - \rho_g} \right)^{0.5} = C_1 \left[\frac{z_b}{d} \right]^{2.5} \quad \text{for orifice} \quad (2-2)$$

$$Fr_g \left(\frac{\rho_g}{\rho_l - \rho_g} \right)^{0.5} = C_1 \left[\frac{z_b}{d} \right]^{1.5} \quad \text{for slot} \quad (2-3)$$

Note that the form is similar for orifice and slot, however, the exponents for the geometric ratio (z/d) are 2.5 and 1.5, respectively.

Top Offtake Orientation

Rouse (Reference 7) developed a correlation for onset of liquid entrainment for top offtake configurations as follows:

$$Fr_g \left(\frac{\rho_g}{\rho_l - \rho_g} \right)^{0.5} = C_1 \left[\frac{z_b}{d} \right]^2 \quad (2-4)$$

It is important to note here that the exponent for the geometric ratio is 2.0, which is different from those obtained by Craya for side offtake orientations. Ardon and Bryce (Reference 8) provide a summary of exponents and coefficients recommended for use in Froude number type correlations in the open literature. For the top offtake orientation, Ardon and Bryce propose the vertical upward branch correlation of Schrock et al. (Reference 9) to compute the discharge flow quality in the offtake branch when entrainment occurs as presented in subsection 2.2.1.5.

Issues with General Correlation Form for Entrainment

While it appears from several data sets that the general correlation form for entrainment onset provides reasonable agreement or representation, there is room for improvement in several areas:

1. Viscous effects are neglected. Interfacial shear stress between the gas and liquid phases would be expected to play some role in liquid entrainment such as found in the work of Ishii and Grolmes (Reference 2). However, there is no viscosity term or viscosity-related non-dimensional parameter in the general correlation.
2. Liquid surface tension and intermolecular force effects are neglected. It is expected that surface tension is important in resisting the onset of entrainment. Intermolecular liquid forces are

probably involved in a liquid siphoning-type effect that is seen in experiments once entrainment onset is reached.

3. The offtake branch, orifice, or slot is treated in most cases (with the exception of the work by Soliman and Sims [Reference 10]) as a point sink. This treatment may be appropriate for very large tanks or reservoirs with relatively small diameter offtakes, but may not be so good for reactor coolant piping connected to a branch pipe.
4. The potential flow solution treatment such as that of Craya and others neglects liquid velocity in liquid phase streamlines and even neglects the very presence of the liquid phase itself in obtaining a potential flow solution for the flowing gas field. Again, neglecting liquid velocity in large reservoirs or tanks may be reasonable, but it would be a more difficult case to make for reactor coolant piping connected to a breakflow path.

A liquid entrainment correlation for flow into branch pipes using a more realistic potential flow, Bernoulli type solution which addresses the concerns outlined earlier (i.e., viscosity, surface tension, etc.) has not been developed and correlated against data sets. Therefore, [

] ^{a,c}

2.2.1.2 Horizontal Flow Regime Map

Model Basis

Predicting the flow regime for two-phase flow in horizontal pipes is important in representing the ADS-4 IRWST initiation phase of a small break LOCA transient for AP1000; the realistic, mechanistic model of Taitel and Dukler (Reference 1) for predicting flow regime transitions provides this capability in WCOBRA/TRAC-AP. This physically based, semi-theoretical model provides an unambiguous analytical prediction of the transition between horizontal flow regimes. It is a preferred approach because it takes into account the different influences of pipe diameter and fluid properties on each flow pattern transition.

Five flow regimes (Reference 1) are considered in this model: intermittent (slug and plug), stratified smooth, stratified wavy, dispersed bubble, and annular/annular dispersed liquid flow. Transitions between horizontal pipe flow regimes are determined using the following dimensionless groups:

$$X = \left[\frac{(dP/dx)_l^S}{(dP/dx)_v^S} \right]^{1/2} \quad (2-5)$$

$$T = \left[\frac{|(dP/dx)_l^S|}{(\rho_l - \rho_v)g \cos \delta} \right]^{1/2} \quad (2-6)$$

$$F = \frac{\rho_v}{(\rho_l - \rho_v)} \frac{U_v^S}{\sqrt{Dg \cos \delta}} \quad (2-7)$$

$$K = \left[\frac{\rho_v U_v^{S^2} U_l^S}{(\rho_l - \rho_v) g_l v_l \cos \delta} \right]^{1/2} \quad (2-8)$$

Each quantity in the above groups is available from the prevailing flow conditions.

The horizontal tube flow regime flow transition boundaries are shown in Figure 2-1. Specific transitions are controlled by the dimensionless groups as follows:

| | |
|--|------|
| Stratified to annular | X, F |
| Stratified to intermittent | X, F |
| Intermittent to dispersed bubble | X, T |
| Stratified smooth to stratified wavy | X, K |
| Annular dispersed liquid to intermittent and to dispersed bubble | X |

where:

- X is the phasic pressure drop ratio (Lockhart and Martinelli, 1949) where $|dP/dx|^S$ designates the pressure drop of one phase flowing alone
- T considers the ratio of turbulent to gravity forces acting on the gas
- F is the Froude number times the square root of the density ratio
- K is the product of F and the square root of the superficial Reynolds number of the liquid
- δ is the angle at which the pipe is inclined to the horizontal

In Reference 1, Taitel-Dukler show that predictions from this model agree very well with data for cocurrent flow through pipes.

Model as Coded

Flowrates, fluid conditions and properties, pressures, and diameter are available from WCOBRA/TRAC input and output for a given timestep. The VESSEL channel formulation calculates the flow between two cells for three separate fields: continuous liquid, continuous vapor, and entrained liquid droplets.

The fluid properties [

] ^{a,c}

[

] ^{a,c}

Next, the equilibrium liquid level $\left(\frac{h_L}{D}\right)$ is calculated for the $\delta = 0$ case from the Taitel-Dukler function that is graphically represented in Figure 2-2.

Referring to Figure 2-1, $X = 1.6$ is the limit line B.

For Curve A, Froude number (F) is calculated [

] ^{a,c}

[

]^{a,c}

Lastly, curve D is defined.

On curve D, parameter T, which is the ratio of turbulent force to the gravity force acting on gas, is calculated from:

$$T = \left[\frac{8\tilde{A}_G}{\tilde{S}_1 \tilde{U}_L^2 (\tilde{U}_L \tilde{D}_L)^{-0.2}} \right]^{1/2} \quad (2-12)$$

[

]^{a,c}

By equating

$$T = \left[\frac{4 C_{FF} (Re_f^{-0.2}) (\rho_l U_L^S)^2}{D \cdot 2 \rho_l} \right]^{1/2} \frac{1}{(\rho_l - \rho_v) g} \quad (2-13)$$

and solving for, U_L^S as,

$$U_L^S = \frac{1}{\rho_l} \left[\frac{T^2 \cdot (\rho_l - \rho_v) g}{\frac{2 C_{FF}}{D \rho_l} Re_f^{-0.2}} \right]^{1/2} \quad (2-14)$$

The gap superficial velocities are compared against $X = 1.6$, Equations 2-13 and 2-14, to determine the flow regime. Currently, four flow regimes, namely, stratified, annular dispersed liquid, dispersed bubble, and intermittent are recognized.

Scaling Considerations

Pipe diameter is one of the parameters that affects the flow regime transitions in the Taitel-Dukler horizontal flow regime map, through its presence in the "F" term. Therefore, the method is general, and may be used with confidence to predict flow regimes at various scales of operation; at larger diameters the regime boundaries are displaced relative to their location with a small pipe diameter.

Likewise, the use of prevailing fluid properties in this model considers variations in pressure, temperature, and quality such as those that occur during the ADS-4 IRWST initiation phase of a small break LOCA transient.

Conclusions

The Taitel-Dukler method for determining flow regime transitions in horizontal two-phase flow has been incorporated into WCOBRA/TRAC-AP. This method provides a mechanistic prediction of flow regime based on realistic theoretical considerations. The agreement with concurrent flow data is judged to be very good in Reference 1.

2.2.1.3 Horizontal Stratified Interfacial Drag

Model Basis

This model is based on stratified flow steam-water data in a rectangular channel (Jensen, Reference 11). The model is mechanistically based on the turbulent motion of the liquid near the interface. In addition, the interfacial shear and interfacial heat transfer are consistent with each other.

The interfacial friction factor K is computed according to Equations 5.5 and 5.6 of Jensen (Reference 11):

$$K_{ix,vl,HS} = 0.5 \cdot f_i \cdot |W_{vl}| \cdot A_{HS} / \Delta Z \quad (2-15)$$

where:

A_{HS} is the vapor/liquid stratified interface area

$$f_i = 0.01 \quad \text{if } U' < 17.6 \quad (2-16)$$

$$= 14.6 \times 10^{-6} (U')^{1.8} \quad \text{if } U' \geq 17.6 \quad (2-17)$$

where:

$$U' = \frac{U_v - U_l}{1.414 \left(\frac{\sigma(\rho_l - \rho_v)g}{\rho_l^2} \right)^{1/4}} \quad (2-18)$$

U_v and U_l are the vapor and liquid velocities, respectively.

Model as Coded

Note that the friction factors are discontinuous at $U' = 17.6$ and also between developed and undeveloped flows.

The horizontal stratification is checked [

]^{a,c} to identify the flow regime according to the Taitel-Dukler (Reference 1) flow regime map. The parameters used in the determination of the horizontal flow regime are the total liquid superficial velocity, total vapor superficial velocity, gap average vapor density, gap average liquid density, the vapor viscosity, liquid viscosity, total gap void fraction, hydraulic diameter of flow channel, and mixture level.

The drag term for the horizontally stratified flow is modified in [

]^{a,c}

Conclusions

The ability to identify horizontal stratified flow regimes has been implemented in WCOBRA/TRAC-AP, together with a method for calculating the interfacial drag for two-phase flow in these regimes.

2.2.1.4 Entrainment in Horizontal Stratified Flow

Model Basis

When horizontal stratification is identified, the Ishii-Grolmes (Reference 2) criteria are checked; if the criteria are satisfied, the calculation of entrainment off of the horizontal surface is enabled.

Ishii and Grolmes describe entrainment in horizontal cocurrent flow as the stripping of drops from the top of waves. They describe four mechanisms, but the shearing off of the top of roll waves by turbulent gas flow is expected to be significant for the ADS-4 IRWST initiation. Ishii and Grolmes state that this mechanism is valid for liquid $Re > 160$ in horizontal concurrent flow. For roll wave entrainment, Ishii and Grolmes provide two correlations based upon Re :

For $Re > 1635$:

$$\frac{\mu_l U_g}{\sigma} \sqrt{\frac{\rho_g}{\rho_l}} \geq N_\mu^{0.8} \text{ for } N_\mu < \frac{1}{15}$$

$$\frac{\mu_l U_g}{\sigma} \sqrt{\frac{\rho_g}{\rho_l}} \geq 0.1146 \text{ for } N_\mu < \frac{1}{15}$$

For $Re < 1635$:

$$\frac{\mu_l U_g}{\sigma} \sqrt{\frac{\rho_g}{\rho_l}} \geq 11.78 N_\mu^{0.8} Re_l^{-1/3} \text{ for } N_\mu < \frac{1}{15}$$

$$\frac{\mu_l U_g}{\sigma} \sqrt{\frac{\rho_g}{\rho_l}} \geq 1.35 Re_l^{-1/3} \text{ for } N_\mu < \frac{1}{15}$$

Re is based upon liquid film thickness, U_g is the minimum gas velocity for entrainment to occur, and N_μ represents viscosity number.

The entrainment source term in the continuity cell is evaluated when the Ishii-Grolmes criteria are satisfied for gap flow connections according to the model used by Hanratty (Reference 12):

$$Re = K_a U_v \sqrt{\rho_v \rho_l} \text{ (lb/s - ft}^2\text{)} \quad (2-19)$$

where:

$K_a = 0.2$ is currently used.

The size of the entrained droplets is determined by Tatterson's (Reference 13) model:

$$D_e = 0.0112 \left(\frac{D_g \sigma}{0.5 f_i \rho_v U_v^2} \right)^{1/2} \quad (2-20)$$

This correlation is for vertical annular flow, and the characteristic length is the pipe diameter. It will be implemented here by assuming that the characteristic length is the hydraulic diameter (D_g) of the gap above the mixture elevation.

De-entrainment onto the interface is assumed to be dominated by the terminal velocity of the droplets. The settling velocity (V_s) is the minimum of the Stokes flow solution Equation 9.13 (Wallis, Reference 14):

$$V_{s,1} = \frac{1}{18} \frac{D_e^2 g (\rho_l - \rho_v)}{\mu_l} \quad (2-21)$$

and the turbulent flow solution Equation 12.29 (Wallis):

$$V_{s,2} = \sqrt{\frac{D_e (\rho_l - \rho_v) g}{\rho_v}} \quad (2-22)$$

where:

D_e is the average diameter of the entrained drops in the vapor above the mixture. The net flux of droplets into the mixture is:

$$R_{de} = \rho_l \alpha_e (V_s - U_{v,ver}) \quad (2-23)$$

where:

$U_{v,ver}$ is the average vertical vapor velocity above the mixture and $V_s = \min(V_{s,1}, V_{s,2})$.

Model as Coded

As previously described, the horizontal stratified flow model is activated []^{a,c} to identify the flow regime according to the Taitel-Dukler flow regime map. The parameters used in the determination of the horizontal flow regime are the total liquid superficial velocity, total vapor superficial velocity, gap average vapor density, gap average liquid density, the vapor viscosity, liquid viscosity, total gap void fraction, hydraulic diameter of flow channel, and mixture level.

Within the structure of WCOBRA/TRAC, entrainment must be treated []^{a,c} The

entrainment and de-entrainment source calculations are then performed using the techniques described earlier in this section.

Scaling Considerations

In WCOBRA/TRAC-AP, entrainment is modeled [

] ^{a,c}

Conclusions

The ability to identify horizontal stratified flow regimes has been implemented in WCOBRA/TRAC-AP, together with the calculation of entrainment at the vapor-liquid stratified interface for two-phase flow in these regimes.

2.2.1.5 Flow Regime Conditions Upstream of the ADS-4 Delivery Piping (Entrainment/Vapor Pull-through Model)

Model Basis

During the ADS-4 IRWST initiation phase of a small break LOCA event, flow in the hot leg pipes will eventually become two-phase and stratify. A stratified flow regime near or upstream of the ADS-4 valves may lead to liquid entrainment in the hot legs and in the ADS-4 delivery piping depending upon local characteristics such as the velocity of the gas phase and the height of liquid in the pipe relative to the ADS-4 branch elevation.

Nearly all entrainment onset correlations found in the literature were developed from stratified, potential flow, Bernoulli-type solutions. In these correlations, the Froude number (ratio of inertia to gravity forces) is usually a predominant term.

The general form of most entrainment onset correlations found in the literature is as follows:

$$Fr_k = \frac{U_k}{\sqrt{d \cdot g \frac{\Delta\rho}{\rho_k}}} = C_1 \left[\frac{Z_b}{d} \right]^{C_2} \quad (2-24)$$

where:

k indicates the continuous phase.

The key elements of this correlation form consist of the Froude number (Fr), density ratio $\Delta\rho/\rho_k$, and a geometric ratio (Z_b/d) of entrainment onset height (Z_b) to offtake diameter (d). The coefficient C_1 and exponent C_2 are functions of the orientation and geometry of the offtake.

Different offtake orientations lead to different values of C_1 and C_2 in the equation 2-24 for the flow.

The following exponent and multiplier values in the correlation form for entrainment are provided by Anderson (Reference 15):

$$C_1 = 0.35, C_2 = 2.50 \text{ for liquid entrainment into a top branch} \quad (2-25)$$

The above values are used in WCOBRA/TRAC-AP to predict the AP600 integral effects tests during the ADS-4 IRWST initiation phase.

When entrainment is predicted to occur, the quality in the offtake will differ from that in the donor cell. In WCOBRA/TRAC-AP, the discharge flow quality in the offtake branch is calculated by the following correlation as proposed by Ardron and Bryce (Reference 8):

Vertical upward branch, from Schrock et al., (Reference 9):

$$x = R^{3.25(1-R)^2} \quad (2-26)$$

where:

$$R = lh / Z_b$$

and h is the distance between the branch pipe and the liquid surface,

Z_b is the critical distance at which the entrainment begins.

Model as Coded

The model as coded proceeds through a sequence of calculational steps to determine the entrainment from a channel in the hot leg pipes. [

] ^{a,c}

[

] ^{a,c}

Scaling Considerations

Ardron and Bryce (Reference 8) based their selections of correlations from a review of several series of tests carried out to study two-phase flow in offtake branches at top, bottom and central position connections to a larger diameter horizontal pipe containing stratified flow. In these experiments, pressures ranged from 0.2-6.2MPa. Ardron and Bryce concluded that this data base was adequate to assess the modeling of horizontal stratification entrainment to a PWR RCS loop pipe break.

Conclusions

Appropriate correlations are included in WCOBRA/TRAC-AP to provide the capability to calculate: (1) the onset of entrainment from the hot legs into the ADS-4 pipes and (2) the flow quality in the ADS-4 pipes during the ADS-4 IRWST initiation phase for a postulated AP1000 small break LOCA event.

2.2.1.6 Interfacial Heat Transfer in the Horizontal Stratified Regime

The horizontal stratified heat transfer model is utilized in a continuity cell where the horizontal stratified flow is identified in the connecting gap according to the Taitel-Dukler (Reference 1) flow regime map.

If the flow regime is determined to be annular-dispersed or dispersed bubble according to the Taitel-Dukler flow regime map, the appropriate interfacial heat/mass transfer is used.

Model Basis

The interfacial heat transfer model developed by Jensen (Reference 11) is mechanistically based on the turbulent motion of the liquid near the interface, and is consistent with the interfacial drag model. Equation 5.11 (Jensen) states:

$$\frac{Nu_x}{Pr_l^{0.5}} = 0.0405 \cdot \left(\frac{u^* \cdot x}{\nu} \right)^{1.1} \quad (2-27)$$

where:

$$Nu_x = \frac{h_i \cdot x}{k_l}$$

$$u^* = \sqrt{\frac{\tau}{\rho_1}} = \sqrt{\frac{f_i \cdot \rho_v \cdot U_r^2}{2 \cdot \rho_1}} \quad (2-28)$$

where x is the lateral distance, τ is the interfacial shear stress, U_r is the relative velocity, and ν is the kinematic viscosity. Note that while this is not the final recommended correlation, it is not very different from the final version (Figure 5.24 of Jensen). The interfacial friction is obtained from the value without condensation (subsection 2.2.1.3), but needs to be adjusted to account for condensation. This is done by applying Equation 2.31 (Jensen, Reference 11) as follows:

$$\tau_c = \tau + \frac{\Gamma_c \cdot U_v}{144 \cdot g_c} \quad (2-29)$$

where the τ is in psia and the condensation rate (Γ_c) is in lb/ft²/s.

Rearranging Equation 2-27 yields,

$$h_{il} = 0.0405 \cdot k_l \cdot Pr_l^{0.5} \cdot \left(\frac{u^*}{\nu} \right)^{1.1} \cdot x^{0.1} \quad (2-30)$$

Model as Coded

Since h_{il} is a very weak function of the lateral distance x , the [

$$]^{a,c} \quad (2-31)$$

The heat transfer coefficient h_{il} is then multiplied by the appropriate interfacial area to yield the condensation heat transfer coefficient (HASCL) as:

$$HASCL = h_{il} \cdot Area$$

where Area = continuity cell area as seen in Figure 2-3.

Conclusions

The ability to identify horizontal stratified flow regimes has been implemented in WCOBRA/TRAC-AP, together with a method for calculating the interfacial heat transfer for two-phase flow in these regimes. The capability of WCOBRA/TRAC-AP to predict the thermal conditions in the stratified horizontal two-phase flow regime is demonstrated by the test simulations shown in the following subsection.

2.2.2 Separate Effects Test Validation

The predicted performance of AP1000 during the ADS-4 IRWST initiation phase of a small break LOCA transient is influenced by the two-phase flow regime present in the horizontal hot leg pipes. In the WCOBRA/TRAC-AP computer code, the Taitel and Dukler flow regime map (Reference 1) is used to define the horizontal pipe flow regime. At the relatively low flowrates associated with ADS-4 operation during a small break LOCA, the horizontal two-phase flow is often in the stratified wavy and/or stratified smooth flow regimes.

Within WCOBRA/TRAC-AP logic, the horizontal flow regime is []^{a,c} the Taitel and Dukler regime map. If the path is determined to be stratified, the Jensen and Yuen model (Reference 11) is applied to calculate the interfacial drag and condensation that occurs; entrainment at the interface between gas and liquid is calculated when the Ishii-Grolmes criteria are satisfied (Reference 2). Because the interfacial drag and entrainment modeling for horizontal stratified flow are basic processes that are directly related to high-ranked items in the AP1000 small break LOCA PIRT given in WCAP-15613 (Reference 5), individual validation of each of these models is needed to confirm their accuracy. This is accomplished using the experimental WCOBRA/TRAC-AP simulations presented in the following sections.

Physical Processes

In the condition of a smooth, equilibrium-stratified flow, the wall resistance of the liquid is similar to that for open-channel flow and that of the gas is similar to closed-duct flow. Because the gas phase velocity is much larger than the velocity at the gas-liquid interface, the gas side interfacial shear stress is evaluated using the equation for gas wall shear. The interfacial drag is thus easily defined theoretically.

Entrainment from the liquid film at the stratified flow two-phase interface is accounted for in determining the mass inventory of the RCS during the ADS-4 IRWST initiation phase of a small break LOCA in AP1000.

WCOBRA/TRAC-AP Models

Phenomena associated with the ADS-4 IRWST initiation phase of a small break LOCA—the interfacial drag, entrainment, and condensation—are discussed in this section.

Interfacial Drag

The models and correlations used to calculate interfacial drag in horizontal stratified flow are described in subsection 2.2.1.3. In particular, the work reported by Jensen and Yuen (Reference 11) is used.

Entrainment

Subsection 2.2.1.4 describes the models and correlations in WCOBRA/TRAC-AP that are used to calculate the horizontal flow processes.

In general, entrainment is the result of interfacial shear between vapor and a liquid film. In WCOBRA/TRAC-AP, liquid is moved from the continuous liquid field to the entrained field when the interfacial shear forces acting on the liquid are sufficient. In de-entrainment, liquid is moved from the entrained field to the continuous liquid field. A summary of the applicable models in WCOBRA/TRAC-AP is as follows:

- Entrainment in Film Flow

WCOBRA/TRAC determines film entrainment rates by comparing the entrainment rate based on a stable film flow to an empirical entrainment rate based on the work of Walley (Reference 17). Refer to subsection 4-6-2 of Reference 3 for details.

- Entrainment in Bottom Reflood

The model for entrainment in the core near the quench front is based on a model by Kataoka and Ishii (Reference 16) assuming vapor bubbling through a liquid pool.

- Entrainment at a Horizontally Stratified Surface

In the ADS-4 IRWST initiation phase of small break LOCA events, if the vapor velocity is sufficient, entrainment can occur from a horizontal interface of vapor and liquid. Refer to subsection 2.2.1.4.

- De-entrainment in Film Flow and Crossflow De-entrainment

The model to estimate the de-entrainment of entrained drops into the continuous liquid field uses an empirical model by Cousins (Reference 18). Entrained liquid in the upper plenum can de-entrain on structures there as the two-phase mixture flows from the vessel into the hot legs. WCOBRA/TRAC uses a model based on experiments by Dallman and Kirchner (Reference 19) to determine the amount of de-entrainment in the upper plenum and other regions of the reactor vessel. These models, which are used in large break LOCA analyses, are not applied in the WCOBRA/TRAC analyses presented in this report.

- De-entrainment at Area Changes

De-entrainment occurs as a two-phase mixture encounters a flow restriction such as a tie plate. WCOBRA/TRAC uses a simple area ratio to de-entrain a fraction of the droplet field where an area reduction occurs in the reactor vessel.

- De-entrainment at Solid Surfaces and Liquid Pools

Drops are assumed to de-entrain when the drops flow into a cell with a solid surface at the opposite face or when the drops flow into a cell which is in a bubbly flow regime.

Condensation

WCOBRA/TRAC-AP uses a model for interfacial heat and mass transfer similar to other best estimate codes. As described in Section 5 of WCAP-12945 (Reference 3), four components are evaluated to calculate interfacial heat and mass transfer; they may be described as:

$$\begin{aligned}
 \Gamma_{SCL} &= \frac{HA_{SCL}(T_l - T_i)}{H_v - H_f} \\
 \Gamma_{SHL} &= \frac{HA_{SHL}(T_l - T_i)}{H_g - H_l} \\
 \Gamma_{SCV} &= \frac{HA_{SCV}(T_v - T_i)}{H_v - H_f} \\
 \Gamma_{SHV} &= \frac{HA_{SHV}(T_v - T_i)}{H_g - H_l}
 \end{aligned}
 \tag{2-32}$$

where:

Γ_{SCL} = condensation to subcooled liquid

Γ_{SHL} = evaporation from superheated liquid

Γ_{SCV} = condensation from subcooled vapor

Γ_{SHV} = evaporation to superheated vapor

Figure 2-4 provides a pictorial representation of the WCOBRA/TRAC-AP approach. []^{a,c}

Assessment of WCOBRA/TRAC-AP Horizontal Stratified Flow Models

The performance of the horizontal stratified flow models in WCOBRA/TRAC-AP are established in predicting a pertinent separate effect test to demonstrate that the models are adequate for the ADS-4 IRWST initiation phase of AP1000 small break LOCA applications. The interfacial drag predictive capability is validated against relevant experimental data (Reference 4); these data are also used to validate the interfacial condensation heat transfer.

Test Facility Description and Modeling

The test facility of Lim (Reference 4) used a rectangular channel to measure condensation of steam in cocurrent, horizontal flow. The channel was constructed of stainless steel with Pyrex glass windows; its dimensions were 160.1 cm long, 6.35 cm high, and 30.48 cm wide. Data were taken in the course of 35 runs. Controlled parameters in the experiments included water and steam inlet temperatures, mass flowrates, and water layer thickness at the inlet. The range of steam (maximum velocity 18 m/s) and water (maximum velocity 41 cm/s) flowrates were restricted by either the initiation of bridging

phenomena or the occurrence of a hydraulic jump. Inlet steam pressure was approximately 1 atmosphere. Steam velocity, static pressure (for some experiments), and water layer thicknesses were measured at five locations along the channel. The water inlet temperature was also measured. Figure 2-5 is a schematic diagram of the experimental system.

Figure 2-6 presents the WCOBRA/TRAC noding of the test facility. [

] ^{a,c}

As shown in Figure 2-6, the experimental channel is modeled axially [

] ^{a,c} This was considered sufficient to provide enough resolution to compare with experimental measurements, which are available at only five axial locations.

The experimental channel is divided [

] ^{a,c}

The experimental report (Lim, et al., 1981) offers no data on liquid level in the discharge tank during the experiments and on the tank dimensions. Because it is impractical to simulate a constant liquid level in the tank due to condensation in the channel, the liquid level in the tank was allowed to rise during the simulation, but it was always kept below the liquid level in the channel. Condensation was turned off in

[

] ^{a,c}

[

] ^{a,c}

The liquid level at the channel inlet [

] ^{a,c} As shown in

Figures 2-7 and 2-8, the liquid profile away from the channel inlet is determined only by the steam and water flowrates. The "line" in Figure 2-8 is a linear correlation plane oriented in parallel to the reader's line of sight. Because essentially all of the variation in the liquid water thickness in the experimental channel can be attributed to the variations in steam and water flowrates, the effect of the initial water layer thickness on the flow pattern away from the inlet can be ignored.

The experimental results used in this analysis are reported to be at steady-state. That is, the water level, pressure, temperature, and steam flow in the channel were stable and not varying significantly.

The WCOBRA/TRAC simulations were run [

] ^{a,c}

Calculational Results

A total of 35 tests are reported in Lim (Reference 4) as shown in Table 2-1. Those tests in which the horizontal two-phase flow is fully within the wavy or stratified flow regimes (32 in number) were simulated. The experimental results and test conditions for the tests simulated with WCOBRA/TRAC-AP are shown in Table 2-1. Steam density and steam and water velocities were input as boundary conditions in the model's steam and liquid fill components, respectively.

In Table 2-1, steam flowrate and water layer thickness data at locations 1, 2, 3, 4, and 5 correspond to 6.18, 12.05, 23.08, 34.18, and 48.14 inches from the experimental channel inlet. Static pressure difference measurements at 4.88, 10.75, 21.77, 32.87, and 47.24 inches are listed as being at locations 1 through 5. Nomenclature is provided on the table.

Steam density input is calculated using NIST/ASME steam properties for given values of the steam inlet temperature and constant pressure of 16 psi. Due to small variations in the liquid temperature and density among the tests and along the experimental channel, a constant liquid density corresponding to the average liquid temperature of 148.6°F is assumed. Steam and water inlet velocities in the model fill components (Figure 2-6) are calculated using a constant flow area of 0.2083 ft².

The WCOBRA/TRAC-AP predictions for a typical case (Run 275) are presented in Figures 2-9, 2-11, and 2-13. Predicted values of liquid level, steam pressure, and steam flowrate are shown for the duration of the test at a number of axial locations. In Figures 2-10, 2-12, and 2-14, the average calculated values of these parameters are compared with the experimental data. There is a reasonably good agreement between the measured and predicted average values of liquid level and pressure drop¹ in the channel as seen in Figures 2-10 and 2-12. While the liquid level at 47.27 inches is significantly underpredicted, the observed trend of the liquid level to recover toward the channel outlet is well reproduced by WCOBRA/TRAC-AP (Figure 2-10). WCOBRA/TRAC-AP overpredicted the steam flowrate axially as seen in Figure 2-14; underpredicting the steam condensation rate is the cause. This matter was investigated further; the condensation heat transfer correlation used in WCOBRA/TRAC-AP (Reference 11), and one derived from the experimental data, were compared to each other for typical flow conditions in the channel. This comparison is presented in Figure 2-15: the solid line is the WCOBRA/TRAC correlation result, and the dashed line(s) the correlation from the experiment.

The alternative correlation for a smooth interface based on this test data (Lim, et al., 1981) is given by:

$$Nu_{x_{As}} := 0.631 \cdot (Re_g)^{0.58} \cdot (Re_l)^{0.09} \cdot (Pr_l)^{0.3} \quad (2-33)$$

where:

$Nu_{x_{As}}$ = is the Nusselt number (Nu)

¹ Note that the pressure actually increases as the steam flow proceeds through the channel.

The principal difference between the correlations is that the Nu value in WCOBRA/TRAC-AP is [

]^{a,c}

The cumulative results of all tests simulated are shown in Figures 2-16 through 2-19, which show scatter plots of predicted versus measured quantities of the liquid level, steam mass flowrate, liquid temperature at the channel exit, and the pressure drop in the channel, respectively. For most of the cases, liquid level predictions are within ± 0.2 inches of the measurements. The steam flowrate is overestimated almost everywhere in the test section, particularly near the channel exit. As a result, the liquid temperature at the channel exit is underpredicted by 20° to 40°F. The large majority (approximately 80 percent) of the pressure drop predictions is within ± 33 percent of the experimental data, as shown in Figure 2-19.

Conclusions

WCOBRA/TRAC-AP predictions of two-phase flow in a horizontal channel were verified against data for a rectangular channel with cocurrent water flow at atmospheric pressure. A model of the experimental channel, consisting of []^{a,c} The pertinent cases among the 35 test cases reported in Lim (Reference 4) were simulated. For most of the cases, liquid level predictions are within ± 0.2 inches of the measurements. Depending on the axial position, steam flowrate can be overestimated by a factor of 2 or more (near the channel exit). As a result, the liquid temperature at the channel exit is underpredicted by 20° to 40°F. To address this, values of the condensation heat transfer coefficient calculated by the code were compared with those given by the correlation used in WCOBRA/TRAC-AP and one derived from the experimental data. The difference in the condensation heat transfer coefficient is determined to be due to the correlation used in the code. Condensation heat transfer in AP1000 hot leg horizontal stratified flow is a minor effect during the ADS-4 IRWST initiation phase as saturated or near-saturated conditions exist during this phase of the transient.

Most of the pressure drop predictions are within ± 33 percent of the experimental data, and the number of points for which the pressure drop is underpredicted is approximately the same as the number for which it is overpredicted. Inasmuch as hot leg steam velocities are low when horizontal stratified flow conditions exist in the AP1000 hot legs during the ADS-4 IRWST initiation phase of a small break LOCA event, the hot leg pressure drop prediction is not of major importance in predicting ADS-4 performance.

2.2.3 References

1. Taitel, Y., and Dukler, A. E., 1976, "A Model for Predicting Flow Regime Transitions in Horizontal and Near Horizontal Gas-Flow," AICHE Journal, Vol. 22, No. 1, pp. 47-55.
2. Ishii, M. and Grolmes, M., 1975, "Inception Criteria for Droplet Entrainment in Two-Phase Concurrent Film Flow," AICHE Journal, Vol. 21, No. 2, pp. 308-318.

3. Bajorek, S. M., et al., 1998, "Code Qualification Document for Best Estimate LOCA Analysis," WCAP-12945-P-A, Volumes 1 and 3.
4. Lim, I. S., et al., 1981, "Cocurrent Steam-water Flow in a Horizontal Channel," NUREG/CR-2289.
5. WCAP-15613, "AP1000 PIRT and Scaling Assessment," Westinghouse Electric Company LLC, February 2001.
6. Craya, A., 1949, "Theoretical Research on the Flow of Non-homogeneous Fluids," La Houille Blanche, pp. 44-55.
7. Rouse, H., 1956, "Seven Exploratory Studies in Hydraulics," Proc. ASCE, Vol. 82.
8. Ardron, K. H., and Bryce, W. M., 1990, "Assessment of Horizontal Stratification Entrainment Model in RELAP5/MOD2 by comparison with Separate Effects Experiments," Nuclear Engineering and Design, Vol. 122, pp. 263-271.
9. Schrock, V. E., et al., "Small Break Critical Discharge – the Roles of Vapor and Liquid Entrainment in a Stratified Two-Phase Region Upstream of the Break," USNRC Report NUREG/CR-4761 (December 1986).
10. Soliman, H. M. and Sims, G. E., 1992, "Theoretical Analysis of the Onset of Liquid Entrainment for Orifices of Finite Diameter," Int. Journal of Multiphase Flow, Vol. 18, pp. 229-235.
11. Jensen, R. J. and Yuen, M. C., 1982, "Interphase Transport in Horizontal Stratified Cocurrent Flow," NUREG/CR-2334.
12. Hanratty, T. J., and Engen, J. M., 1957, "Interaction Between a Turbulent Air Stream and a Moving Water Surface," AIChE Journal, Vol. 3, No. 3, p. 299.
13. Tatterson, D. F., et al., 1977, "Drop Sizes in Annular Gas-Liquid Flows," AIChE Journal, Vol. 23, No. 1, pp. 68-76.
14. Wallis, G. B., 1969, One-Dimensional Two-Phase Flow, McGraw-Hill.
15. Anderson, J. L. and Benedetti, R. L., 1986, "Critical Flow Through Small Pipe Breaks," EPRI/NP-4532.
16. Kataoka, I. and Ishii, M., 1983, "Mechanistic Modeling and Correlations for Pool Entrainment Phenomena," NUREG/CR-3304.
17. Walley, P. B., et al., 1973, "Experimental Wave and Entrainment Measurements in Vertical Annular Two-Phase Flow," AERE-R7521, Atomic Energy Research Establishment, Harwell, England.

18. Cousins, L. B., et al., 1965, "Liquid Mass Transfer in Annular Two-Phase Flow," Paper C4, Symposium on Two-Phase Flow, Vol. 2, Exeter, England.
19. Dallman, J. C. and Kirchner, W. L., 1980, "De-Entrainment Phenomena on Vertical Tubes in Droplet Cross Flow," NUREG/CR-1421.

| Table 2-1 Test Matrix Parameters | | | | | | | | | | | |
|----------------------------------|----------------------|----------|-------|-------|-------|-------|-------|----------------------|--------------------|--------------------|--------------------|
| No. | Units ^(a) | Location | | | | | | W_L^{in} (lb/s) | T_G^{in} (°F) | T_L^{in} (°F) | T_L^{ex} (°F) |
| | | Inlet | 1 | 2 | 3 | 4 | 5 | | | | |
| 211 | W_G (lb/s) | 0.09 | 0.083 | 0.077 | 0.069 | 0.065 | 0.064 | 0.866 | 281 | 76.7 | 160 |
| | δ_L (in) | 0.623 | 0.534 | 0.393 | 0.223 | 0.222 | 0.241 | | | | |
| | ΔP (psi) | 0 | 7E-05 | 1E-04 | 2E-04 | 3E-04 | 3E-04 | | | | |
| 231 | W_G (lb/s) | 0.09 | 0.082 | 0.074 | 0.063 | 0.06 | 0.059 | 0.896 | 271 | 33.8 | 118 |
| | δ_L (in) | 0.623 | 0.626 | 0.487 | 0.317 | 0.293 | 0.317 | | | | |
| | ΔP (psi) | 0 | 1E-04 | 2E-04 | 3E-04 | 4E-04 | 5E-04 | | | | |
| 251 | W_G (lb/s) | 0.09 | 0.077 | 0.072 | 0.06 | 0.055 | 0.054 | 1.17 | 272 | 33.8 | 98.1 |
| | δ_L (in) | 0.623 | 0.624 | 0.55 | 0.349 | 0.403 | 0.436 | | | | |
| | ΔP (psi) | 0 | 3E-04 | 5E-04 | 7E-04 | 7E-04 | 7E-04 | | | | |
| 253 | W_G (lb/s) | 0.143 | 0.129 | 0.12 | 0.086 | 0.063 | 0.039 | 1.447 | 281 | 70.88 | 156 |
| | δ_L (in) | 0.623 | 0.569 | 0.444 | 0.3 | 0.417 | 0.484 | | | | |
| | ΔP (psi) | 0 | 7E-04 | 1E-03 | 0.002 | 0.002 | 0.002 | | | | |
| 255 | W_G (lb/s) | 0.204 | 0.188 | 0.167 | 0.113 | 0.081 | 0.061 | 1.57 | 278 | 72.68 | 175 |
| | δ_L (in) | 0.623 | 0.411 | 0.291 | 0.208 | 0.218 | 0.433 | | | | |
| | ΔP (psi) | 0 | 0.001 | 0.002 | 0.004 | 0.004 | 0.004 | | | | |
| 257 | W_G (lb/s) | 0.275 | 0.248 | 0.222 | 0.163 | 0.128 | 0.101 | 1.573 | 287 | 72.86 | 190 |
| | δ_L (in) | 0.623 | 0.298 | 0.208 | 0.173 | 0.178 | 0.23 | | | | |
| | ΔP (psi) | 0 | 0.002 | 0.004 | 0.006 | 0.007 | 0.007 | | | | |
| 273 | W_G (lb/s) | 0.144 | 0.119 | 0.096 | 0.061 | 0.042 | 0.025 | 2.253 | 280 | 77.54 | 144 |
| | δ_L (in) | 0.623 | 0.783 | 0.643 | 0.525 | 0.591 | 0.642 | | | | |
| | ΔP (psi) | 0 | 7E-04 | 0.001 | 0.002 | 0.002 | 0.002 | | | | |
| 275 | W_G (lb/s) | 0.202 | 0.169 | 0.14 | 0.097 | 0.069 | 0.047 | 2.244 | 285 | 79.7 | 163 |
| | δ_L (in) | 0.623 | 0.623 | 0.51 | 0.403 | 0.352 | 0.622 | | | | |
| | ΔP (psi) | 0 | 0.001 | 0.002 | 0.004 | 0.004 | 0.005 | | | | |

a. Definitions for all units are listed at the end of this table.

| No. | Units | Location | | | | | | W_L^{in} (lb/s) | T_G^{in} (°F) | T_L^{in} (°F) | T_L^{ex} (°F) |
|-----|------------------|----------|-------|-------|-------|-------|-------|----------------------|--------------------|--------------------|--------------------|
| | | Inlet | 1 | 2 | 3 | 4 | 5 | | | | |
| 277 | W_G (lb/s) | 0.277 | 0.24 | 0.212 | 0.156 | 0.117 | 0.08 | 2.289 | 287 | 76.1 | 175 |
| | δ_L (in) | 0.623 | 0.427 | 0.334 | 0.307 | 0.283 | 0.314 | | | | |
| | ΔP (psi) | 0 | 0.002 | 0.004 | 0.006 | 0.007 | 0.008 | | | | |
| 293 | W_G (lb/s) | 0.144 | 0.106 | 0.084 | 0.05 | 0.033 | 0.019 | 3.17 | 279 | 76.82 | 126 |
| | δ_L (in) | 0.623 | 0.956 | 0.819 | 0.658 | 0.702 | 0.754 | | | | |
| | ΔP (psi) | 0 | 7E-04 | 0.002 | 0.002 | 0.002 | 0.003 | | | | |
| 295 | W_G (lb/s) | 0.199 | 0.155 | 0.127 | 0.08 | 0.055 | 0.034 | 3.148 | 284 | 78.44 | 144 |
| | δ_L (in) | 0.623 | 0.869 | 0.693 | 0.551 | 0.652 | 0.726 | | | | |
| | ΔP (psi) | 0 | 5E-04 | 0.002 | 0.004 | 0.004 | 0.005 | | | | |
| 297 | W_G (lb/s) | 0.276 | 0.224 | 0.193 | 0.141 | 0.101 | 0.064 | 3.165 | 287 | 79.34 | 161 |
| | δ_L (in) | 0.623 | 0.605 | 0.444 | 0.446 | 0.389 | 0.419 | | | | |
| | ΔP (psi) | 0 | 0.001 | 0.004 | 0.006 | 0.007 | 0.008 | | | | |
| 353 | W_G (lb/s) | 0.144 | 0.132 | 0.127 | 0.09 | 0.067 | 0.043 | 1.5 | 281 | 76.73 | 160 |
| | δ_L (in) | 0.873 | 0.653 | 0.528 | 0.309 | 0.242 | 0.451 | | | | |
| 357 | W_G (lb/s) | 0.274 | 0.255 | 0.231 | 0.173 | 0.138 | 0.109 | 1.489 | 288 | 77 | 192 |
| | δ_L (in) | 0.873 | 0.493 | 0.303 | 0.203 | 0.173 | 0.213 | | | | |
| 373 | W_G (lb/s) | 0.141 | 0.125 | 0.114 | 0.077 | 0.049 | 0.03 | 2.233 | 281 | 75.92 | 139 |
| | δ_L (in) | 0.873 | 0.828 | 0.665 | 0.453 | 0.363 | 0.585 | | | | |
| 377 | W_G (lb/s) | 0.272 | 0.246 | 0.218 | 0.155 | 0.112 | 0.074 | 2.236 | 288 | 76.1 | 175 |
| | δ_L (in) | 0.873 | 0.653 | 0.456 | 0.316 | 0.282 | 0.302 | | | | |
| 393 | W_G (lb/s) | 0.141 | 0.118 | 0.102 | 0.06 | 0.042 | 0.024 | 3.143 | 280 | 78.62 | 127 |
| | δ_L (in) | 0.873 | 0.931 | 0.776 | 0.562 | 0.606 | 0.711 | | | | |
| 397 | W_G (lb/s) | 0.277 | 0.233 | 0.201 | 0.144 | 0.104 | 0.067 | 3.095 | 288 | 77.36 | 161 |
| | δ_L (in) | 0.873 | 0.688 | 0.638 | 0.441 | 0.367 | 0.393 | | | | |
| 153 | W_G (lb/s) | 0.146 | 0.13 | 0.117 | 0.071 | 0.05 | 0.031 | 1.5 | 221 | 73.04 | 165 |
| | δ_L (in) | 0.375 | 0.568 | 0.524 | 0.414 | 0.541 | 0.573 | | | | |
| 157 | W_G (lb/s) | 0.285 | 0.254 | 0.227 | 0.169 | 0.135 | 0.124 | 1.463 | 241 | 75.74 | 194 |
| | δ_L (in) | 0.375 | 0.306 | 0.279 | 0.196 | 0.241 | 0.484 | | | | |
| 173 | W_G (lb/s) | 0.147 | 0.128 | 0.105 | 0.063 | 0.043 | 0.041 | 2.311 | 220 | 73.4 | 144 |
| | δ_L (in) | 0.375 | 0.779 | 0.71 | 0.546 | 0.663 | 0.681 | | | | |

| No. | Units | Location | | | | | | W_L^{in} (lb/s) | T_G^{in} (°F) | T_L^{in} (°F) | T_L^{ex} (°F) |
|-----|-----------------|----------|-------|-------|-------|-------|-------|----------------------|--------------------|--------------------|--------------------|
| | | Inlet | 1 | 2 | 3 | 4 | 5 | | | | |
| 177 | W_G (lb/s) | 0.285 | 0.262 | 0.217 | 0.159 | 0.115 | 0.086 | 2.315 | 241 | 80.06 | 177 |
| | δ_L (in) | 0.375 | 0.503 | 0.438 | 0.335 | 0.36 | 0.381 | | | | |
| 453 | W_G (lb/s) | 0.142 | 0.131 | 0.123 | 0.099 | 0.08 | 0.063 | 1.504 | 280 | 122.2 | 182 |
| | δ_L (in) | 0.623 | 0.6 | 0.544 | 0.43 | 0.535 | 0.567 | | | | |
| 455 | W_G (lb/s) | 0.207 | 0.193 | 0.176 | 0.138 | 0.119 | 0.108 | 1.5 | 284 | 119.5 | 190 |
| | δ_L (in) | 0.623 | 0.445 | 0.361 | 0.299 | 0.305 | 0.507 | | | | |
| 457 | W_G (lb/s) | 0.282 | 0.261 | 0.238 | 0.199 | 0.179 | 0.165 | 1.496 | 287 | 118.4 | 197 |
| | δ_L (in) | 0.623 | 0.407 | 0.293 | 0.257 | 0.252 | 0.263 | | | | |
| 459 | W_G (lb/s) | 0.344 | 0.315 | 0.294 | 0.254 | 0.236 | 0.223 | 1.562 | 288 | 125.8 | 201 |
| | δ_L (in) | 0.623 | 0.329 | 0.257 | 0.227 | 0.214 | 0.249 | | | | |
| 473 | W_G (lb/s) | 0.141 | 0.125 | 0.112 | 0.084 | 0.064 | 0.045 | 2.344 | 280 | 123.8 | 172 |
| | δ_L (in) | 0.623 | 0.766 | 0.663 | 0.526 | 0.61 | 0.675 | | | | |
| 475 | W_G (lb/s) | 0.199 | 0.176 | 0.156 | 0.119 | 0.094 | 0.079 | 2.286 | 284 | 119.5 | 180 |
| | δ_L (in) | 0.623 | 0.635 | 0.53 | 0.444 | 0.367 | 0.632 | | | | |
| 477 | W_G (lb/s) | 0.285 | 0.256 | 0.233 | 0.187 | 0.158 | 0.132 | 2.337 | 287 | 117.9 | 189 |
| | δ_L (in) | 0.623 | 0.491 | 0.367 | 0.336 | 0.298 | 0.333 | | | | |
| 493 | W_G (lb/s) | 0.143 | 0.118 | 0.102 | 0.072 | 0.056 | 0.037 | 3.002 | 278 | 119.7 | 164 |
| | δ_L (in) | 0.623 | 0.906 | 0.825 | 0.665 | 0.728 | 0.77 | | | | |
| 495 | W_G (lb/s) | 0.2 | 0.17 | 0.149 | 0.109 | 0.083 | 0.064 | 3.007 | 285 | 119.8 | 172 |
| | δ_L (in) | 0.623 | 0.812 | 0.735 | 0.546 | 0.451 | 0.721 | | | | |
| 497 | W_G (lb/s) | 0.282 | 0.252 | 0.225 | 0.178 | 0.142 | 0.11 | 3.156 | 287 | 119.3 | 181 |
| | δ_L (in) | 0.623 | 0.622 | 0.458 | 0.426 | 0.392 | 0.426 | | | | |

W_G = steam mass flowrate
 δ_L = water layer thickness
 ΔP = differential pressure
 W_L^{in} = inlet liquid mass flowrate
 T_G^{in} = inlet vapor temperature
 T_L^{in} = inlet liquid temperature
 T_L^{ex} = outlet liquid temperature

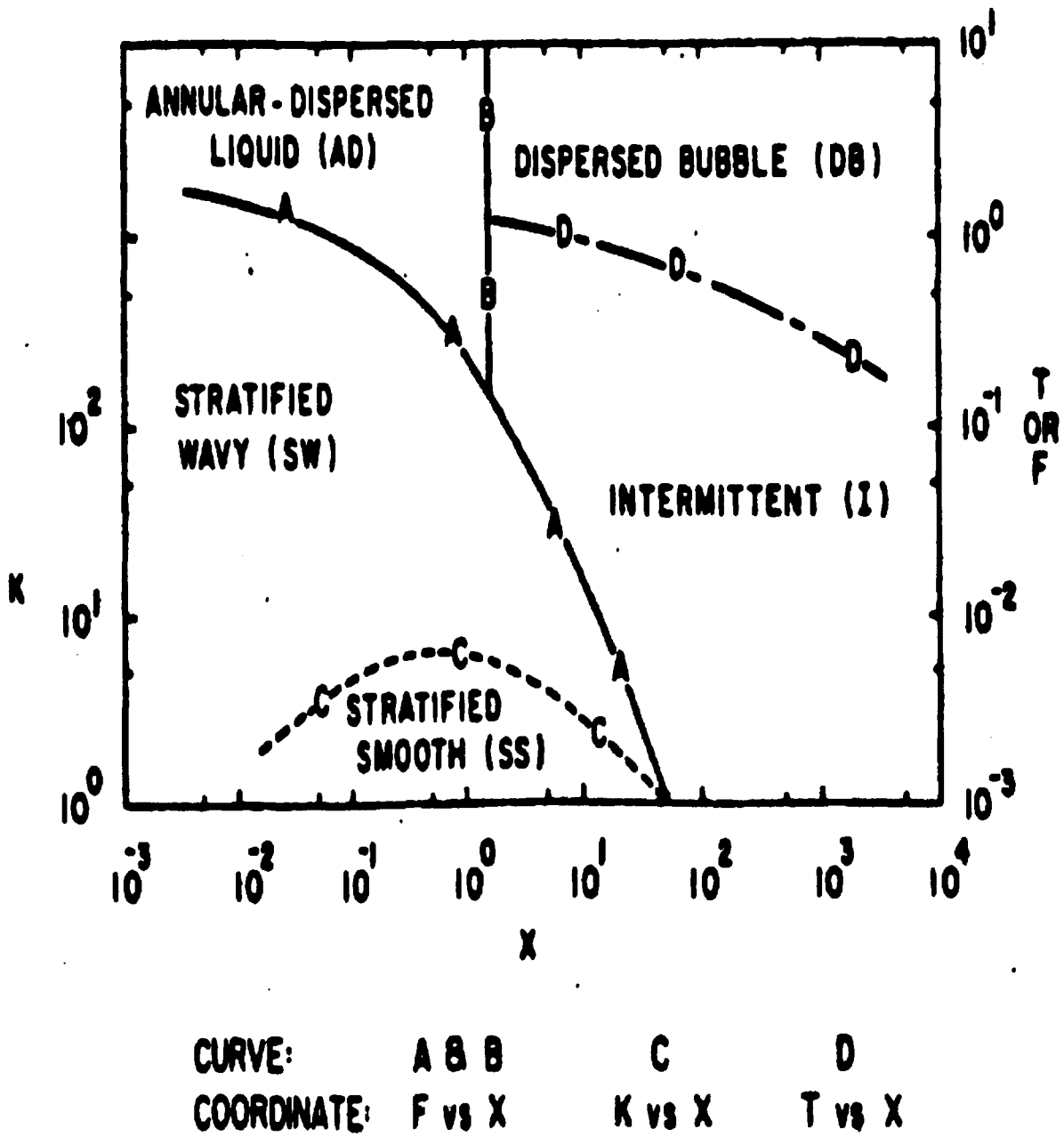


Figure 2-1 Generalized Flow Regime Map for Horizontal Two-Phase Flow

Equilibrium Liquid Level (HL/D)

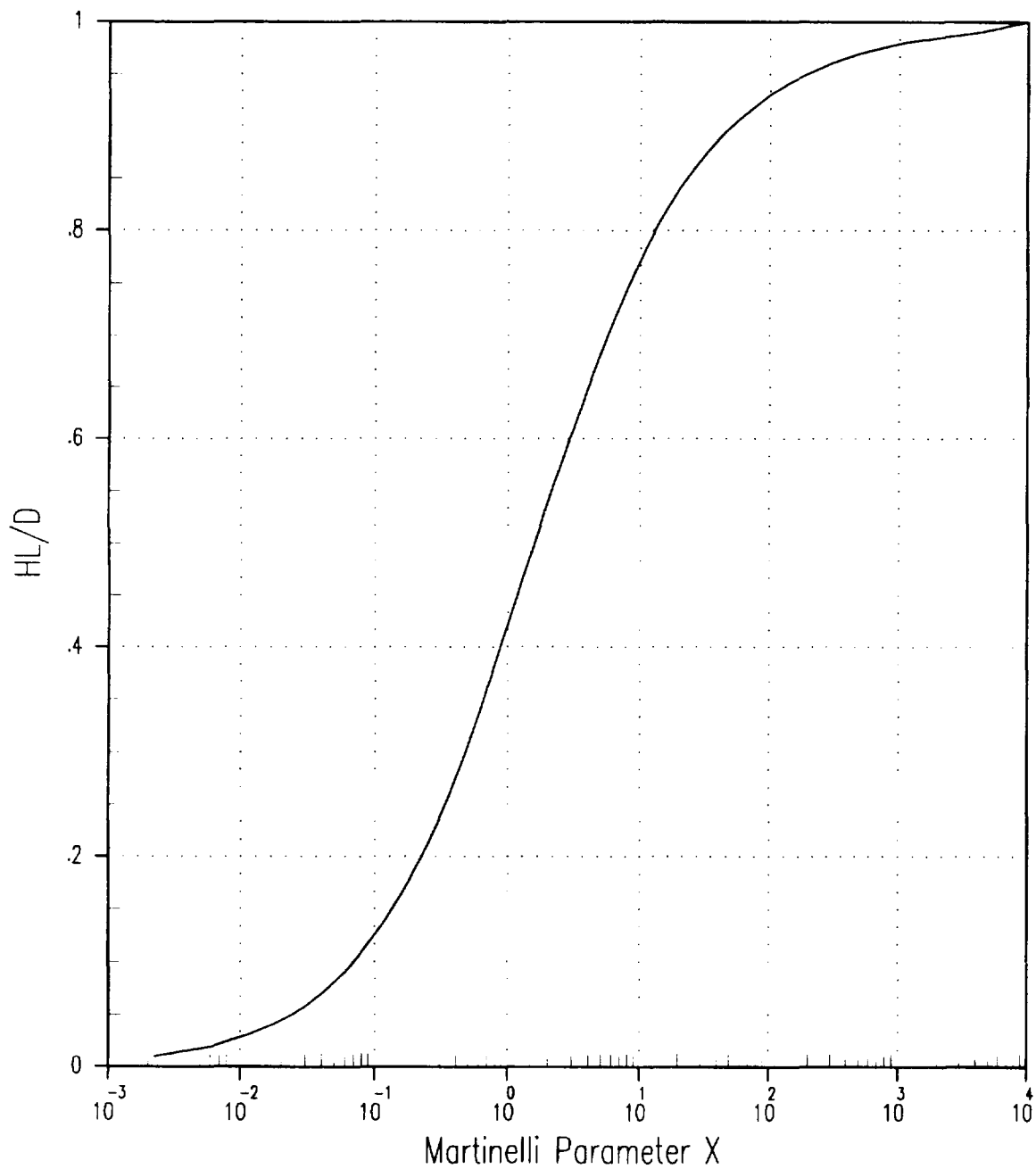


Figure 2-2 Equilibrium Liquid Level vs. Martinelli Parameter, X

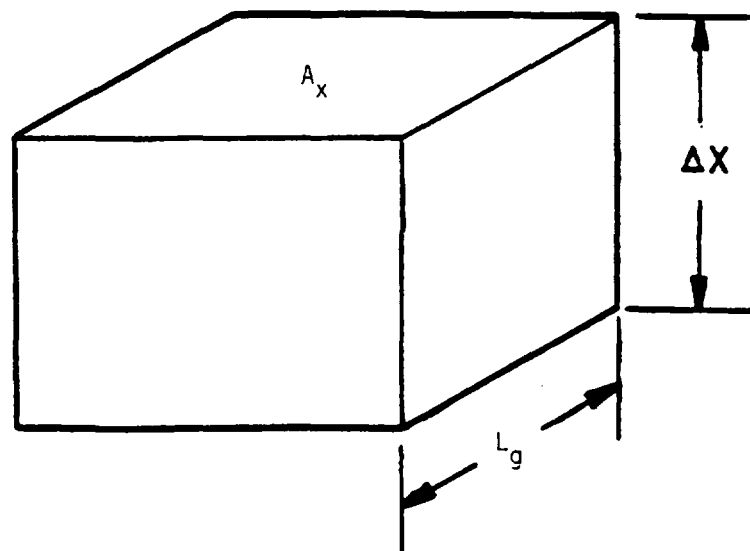


Figure 2-3 Basic Mesh Cell

a,c

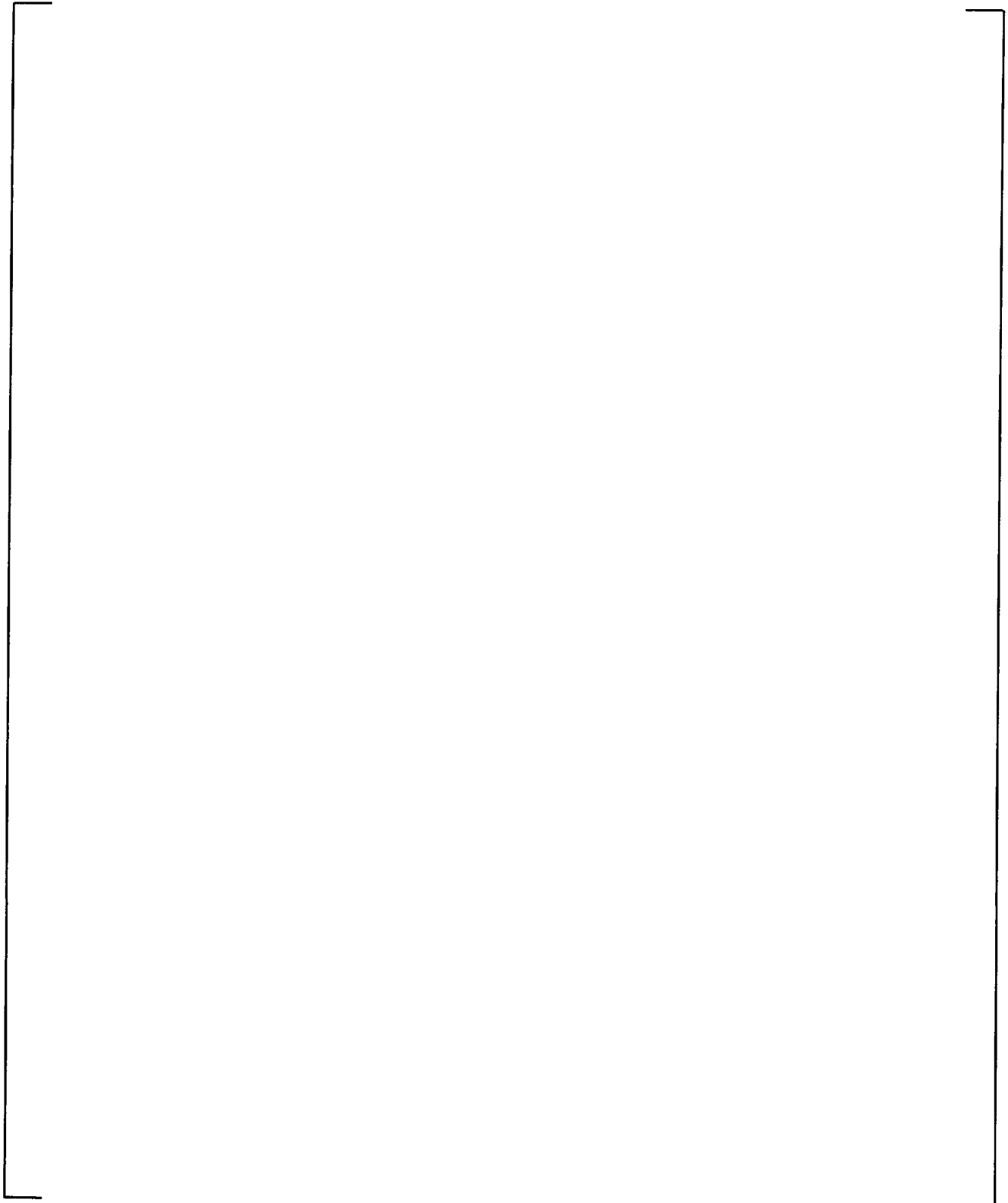


Figure 2-4 WCOBRA/TRAC-AP Representation of Interfacial Heat Transfer

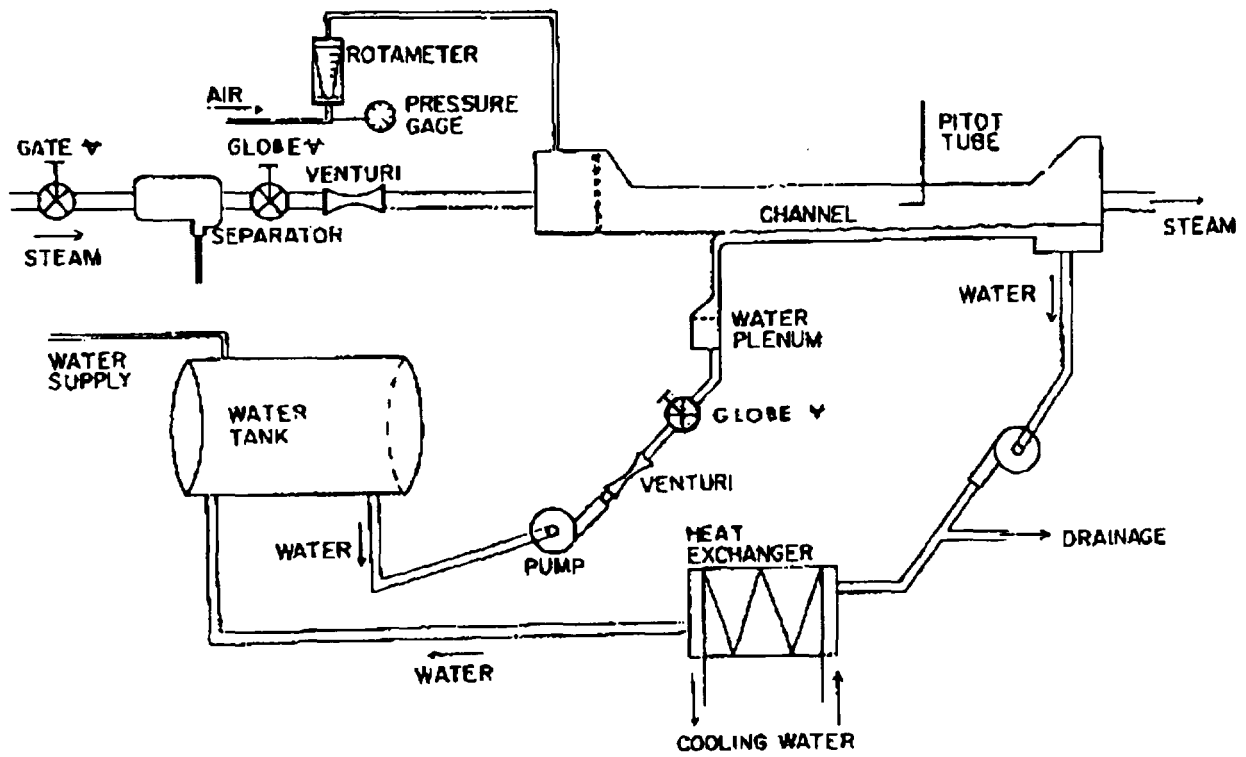


Figure 2-5 Schematic Diagram of the Experimental System (Lim, et al., 1981)

a,c

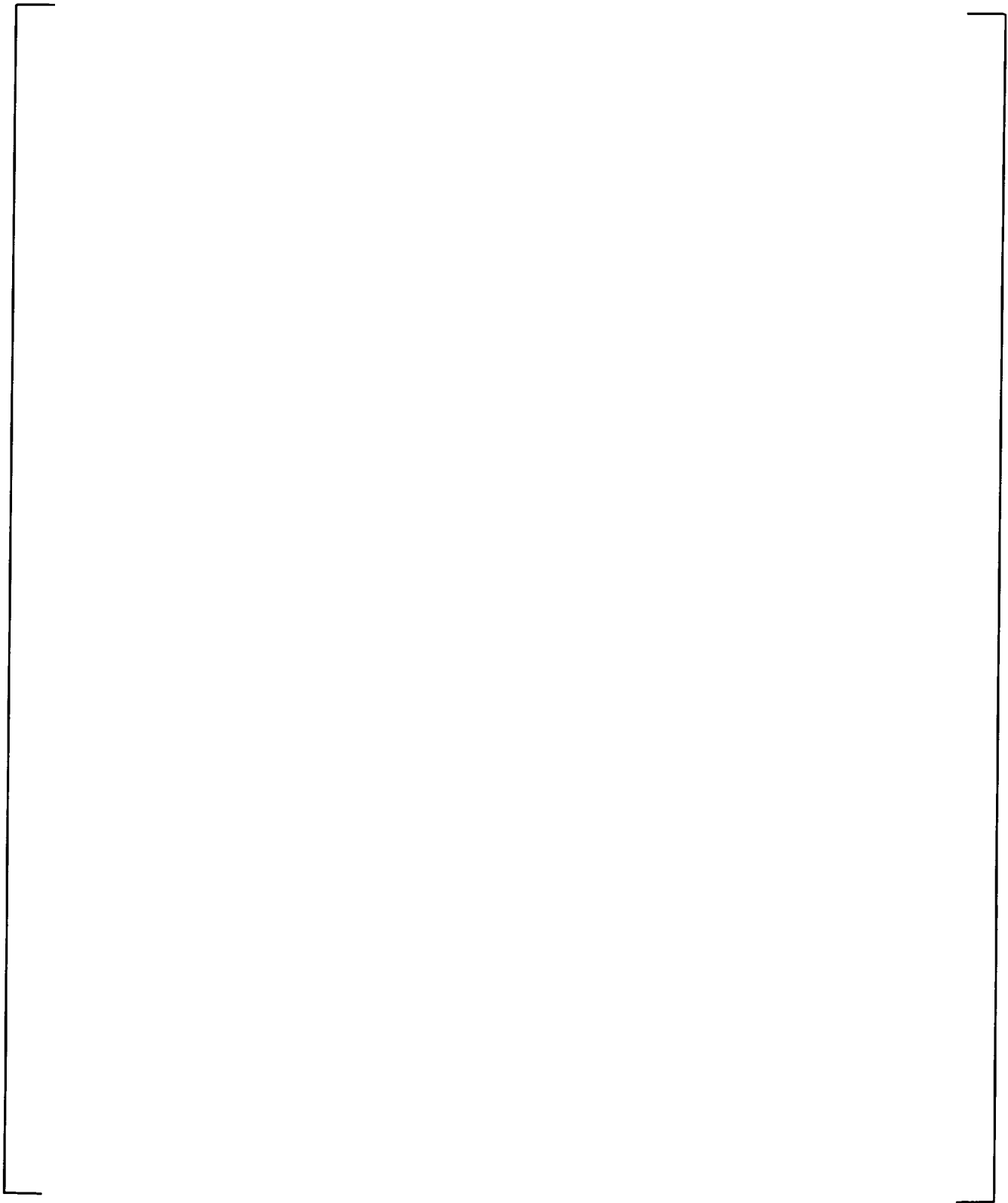


Figure 2-6 WCOBRA/TRAC Noding

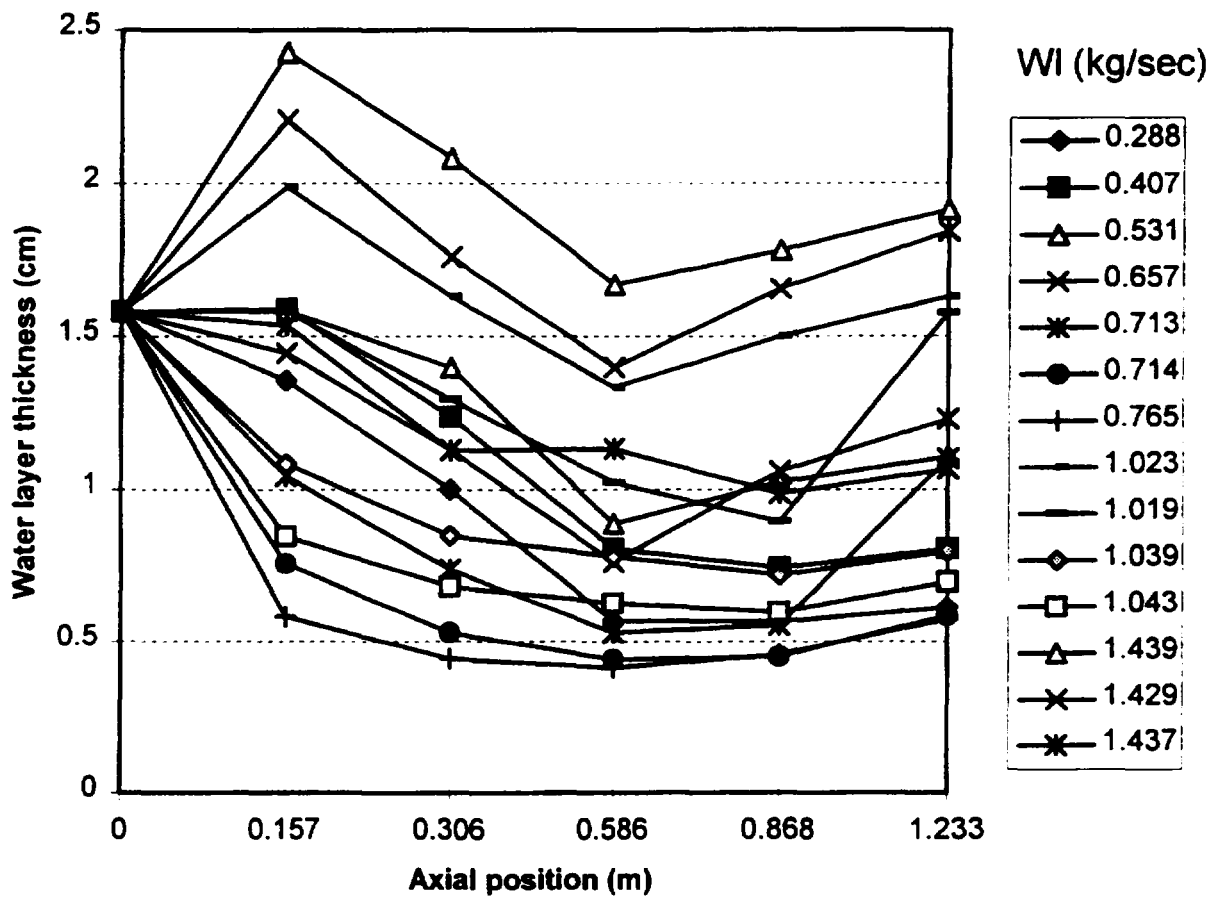


Figure 2-7 Measured Water Thickness Versus Axial Position for Various Liquid (WI) Flowrates and Inlet Water Layer Thickness of 1.583 cm

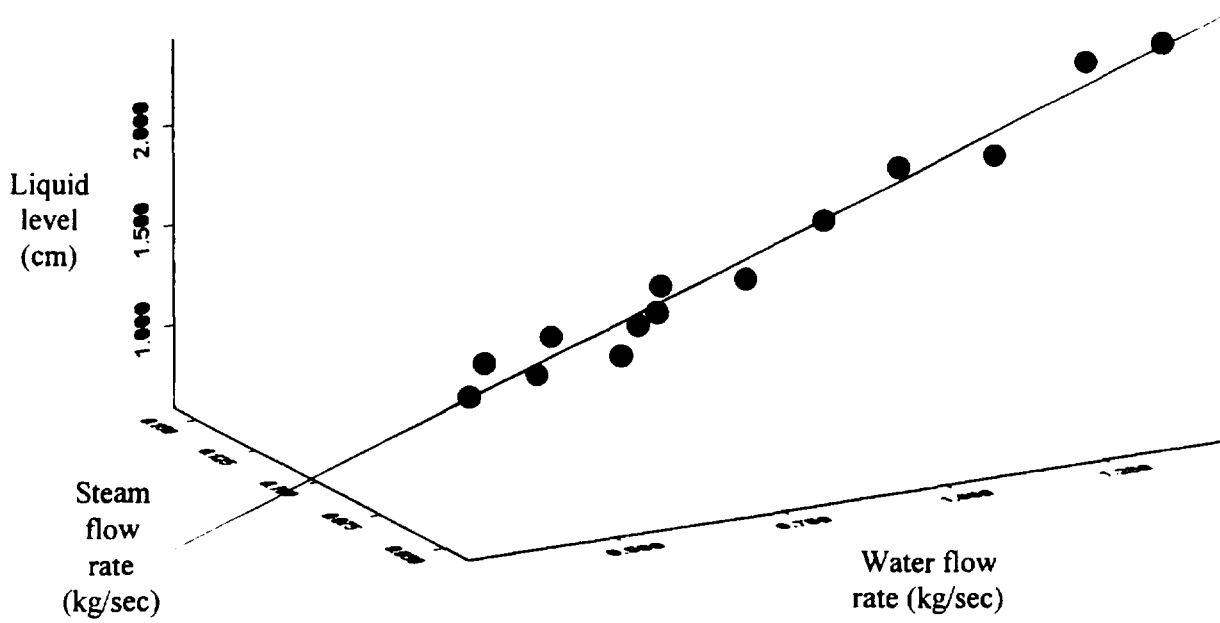


Figure 2-8 Measured Water Thickness at 0.157 m From the Channel Inlet Versus Liquid and Steam Flowrates

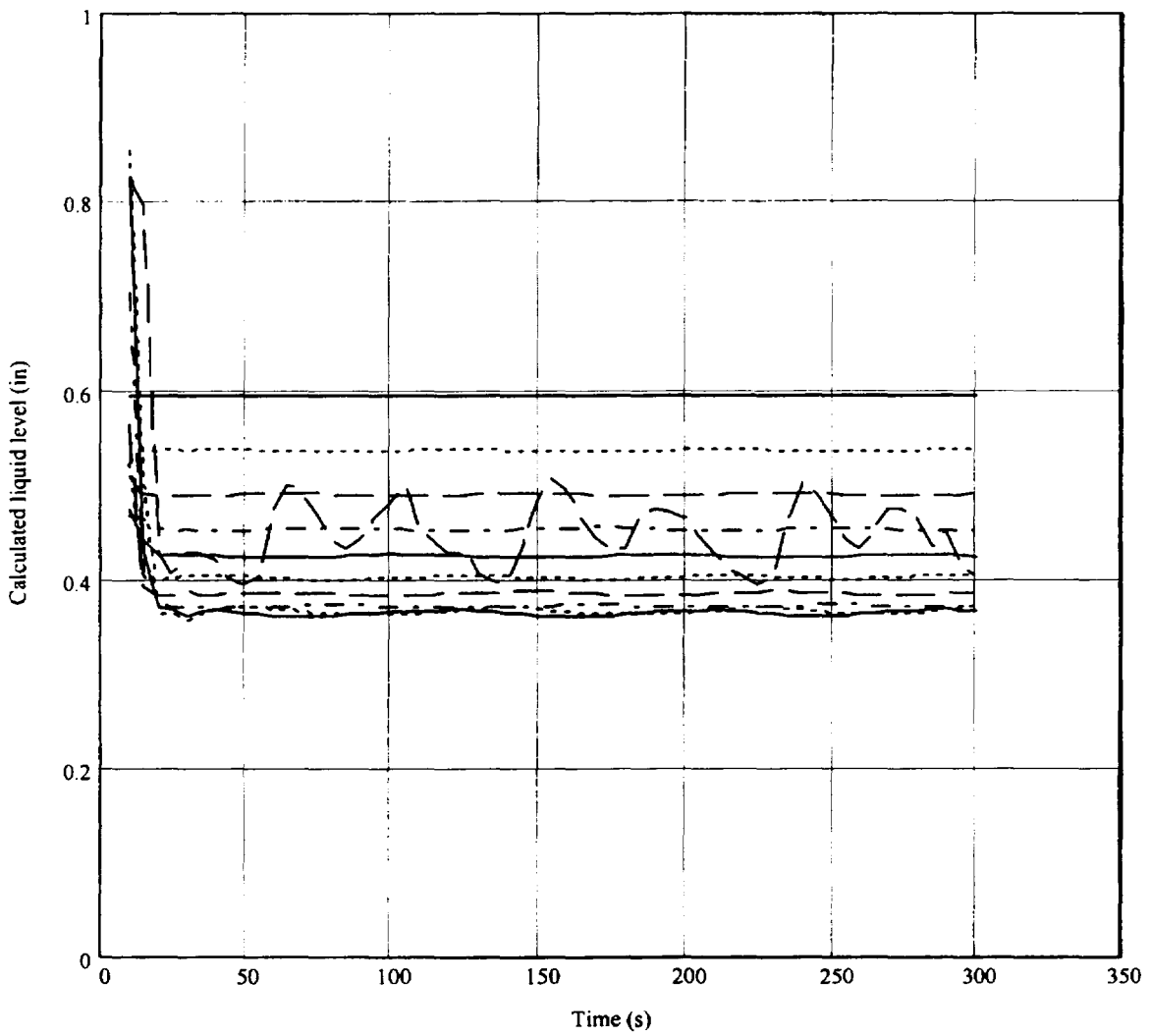


Figure 2-9 Calculated Liquid Level (Run 275)

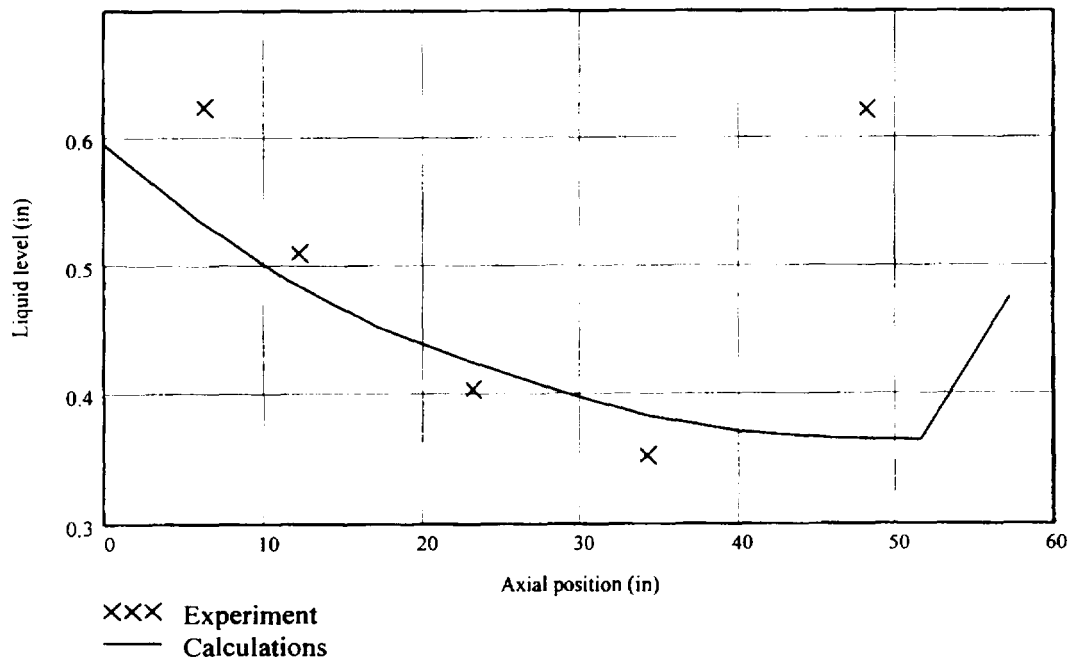


Figure 2-10 Calculated and Measured Liquid Levels Versus Axial Position (Run 275)

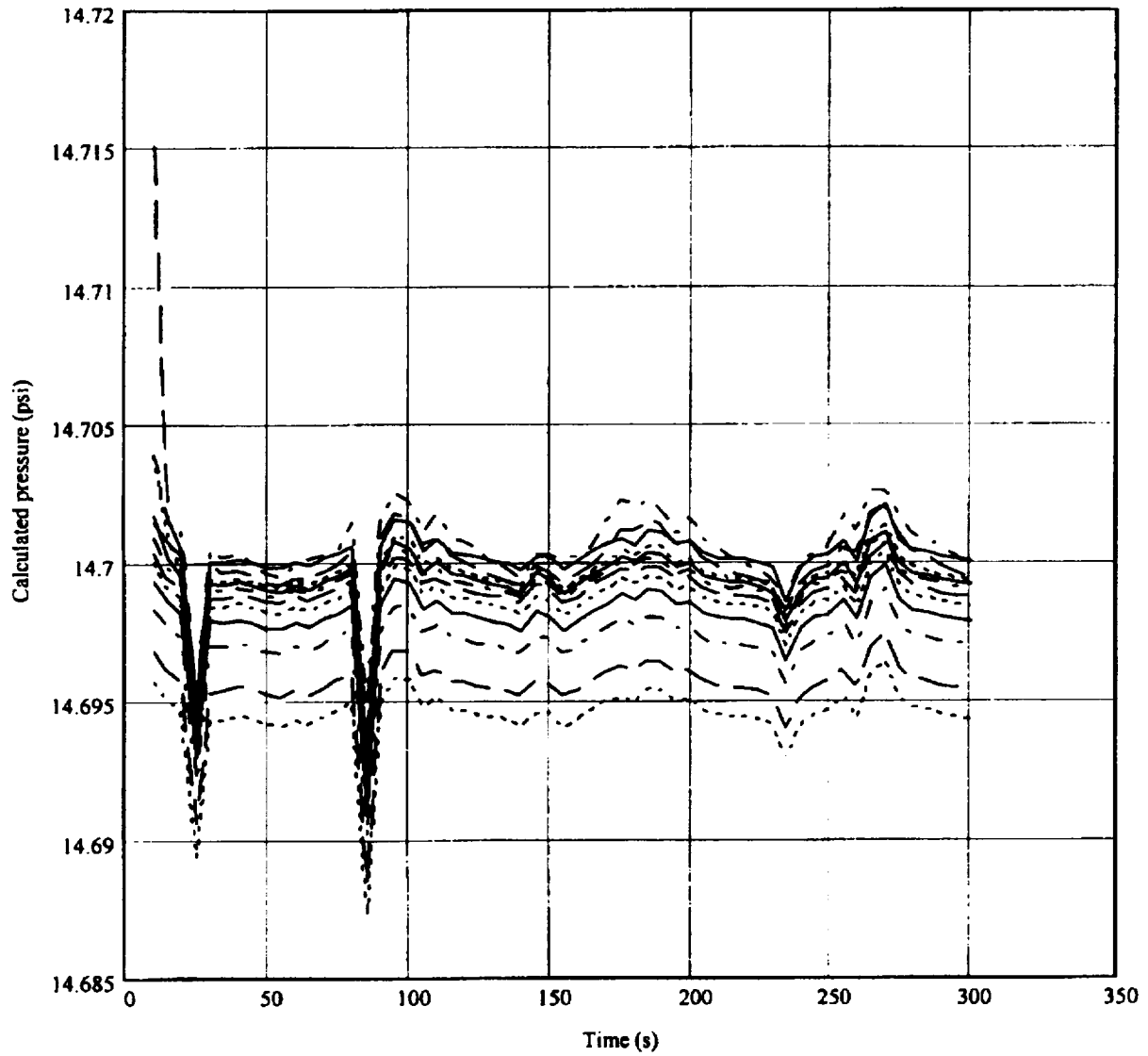


Figure 2-11 Calculated Steam Pressure (Run 275)

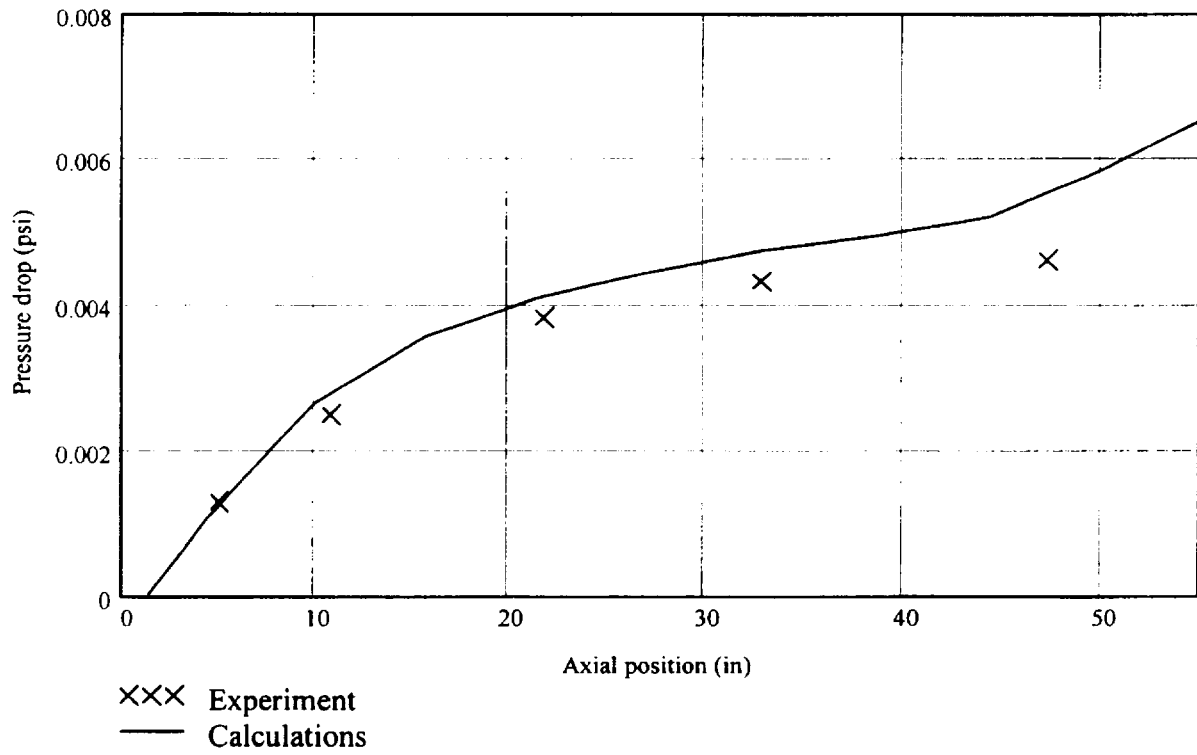


Figure 2-12 Calculated and Measured Steam Pressure Versus Axial Position (Run 275)

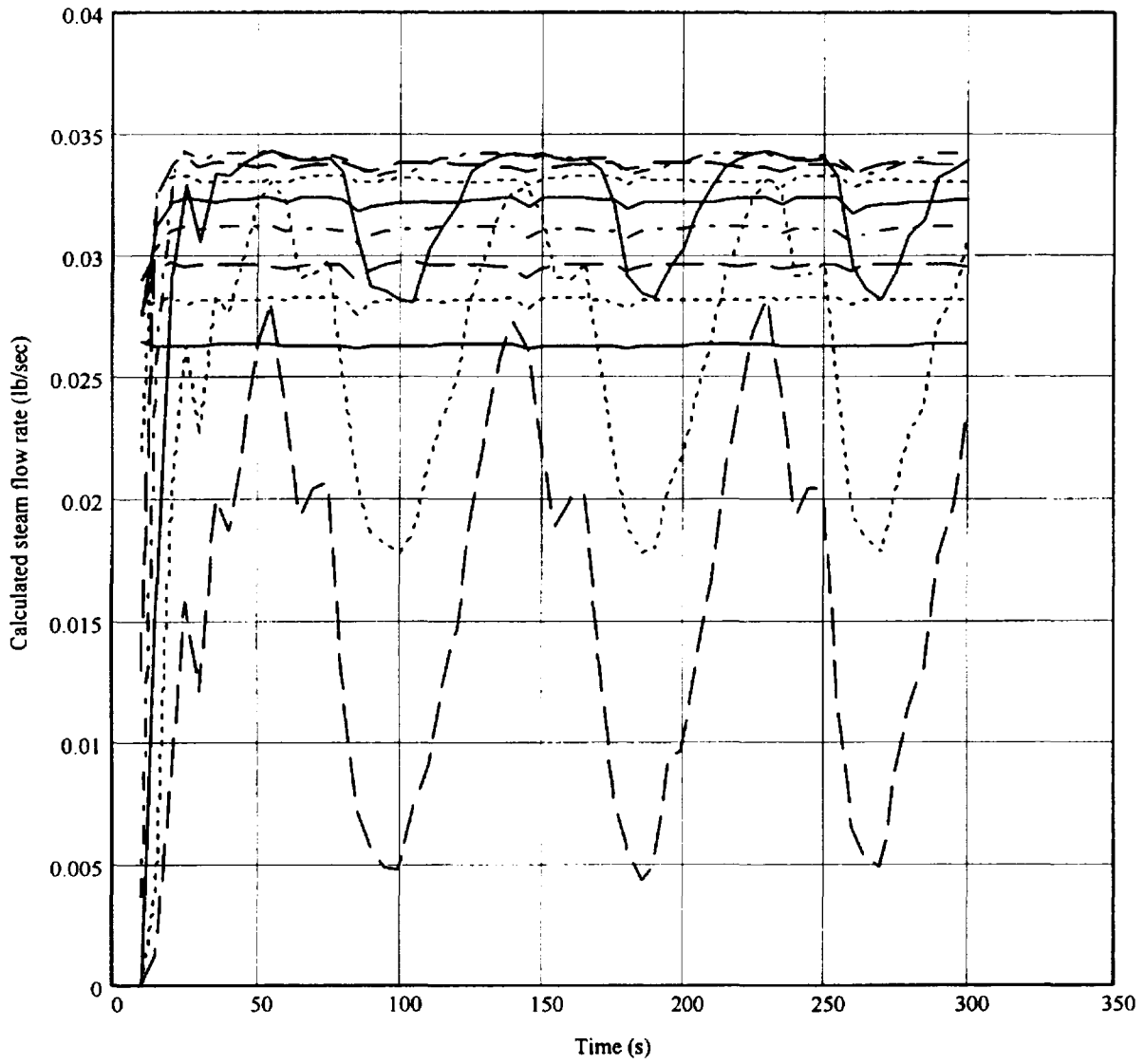


Figure 2-13 Calculated Steam Flowrate (Run 275)

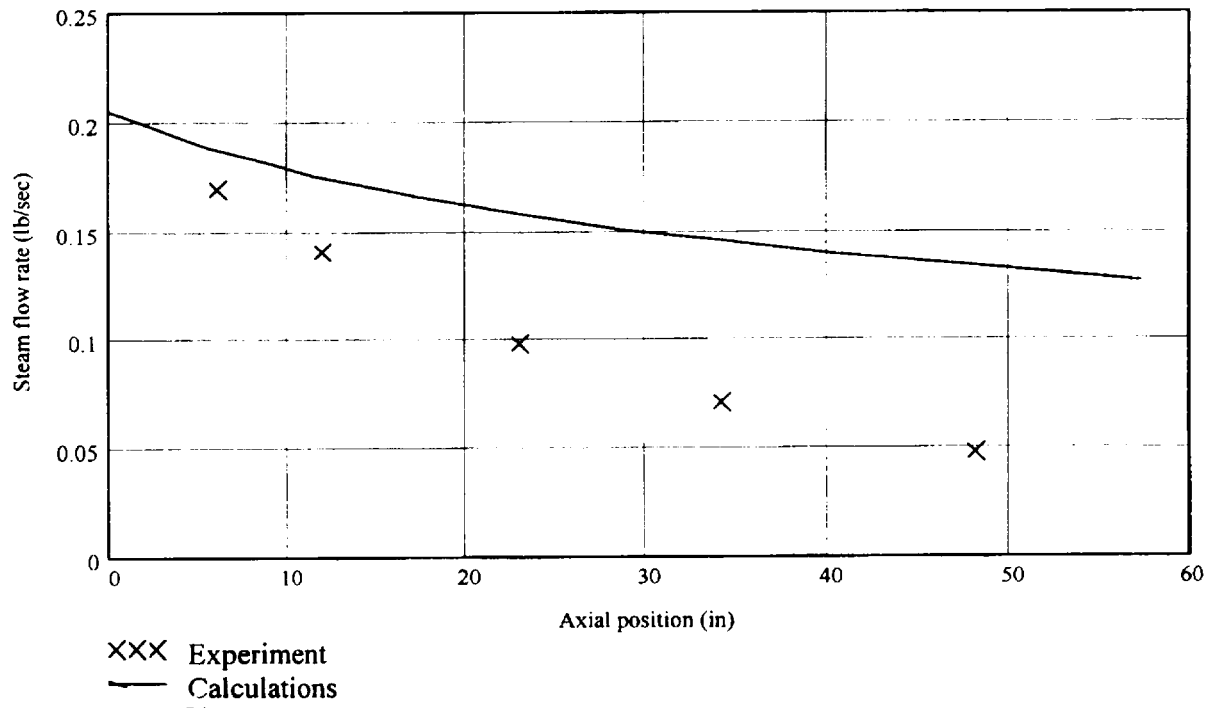


Figure 2-14 Calculated and Measured Steam Flowrate Versus Axial Position (Run 275)

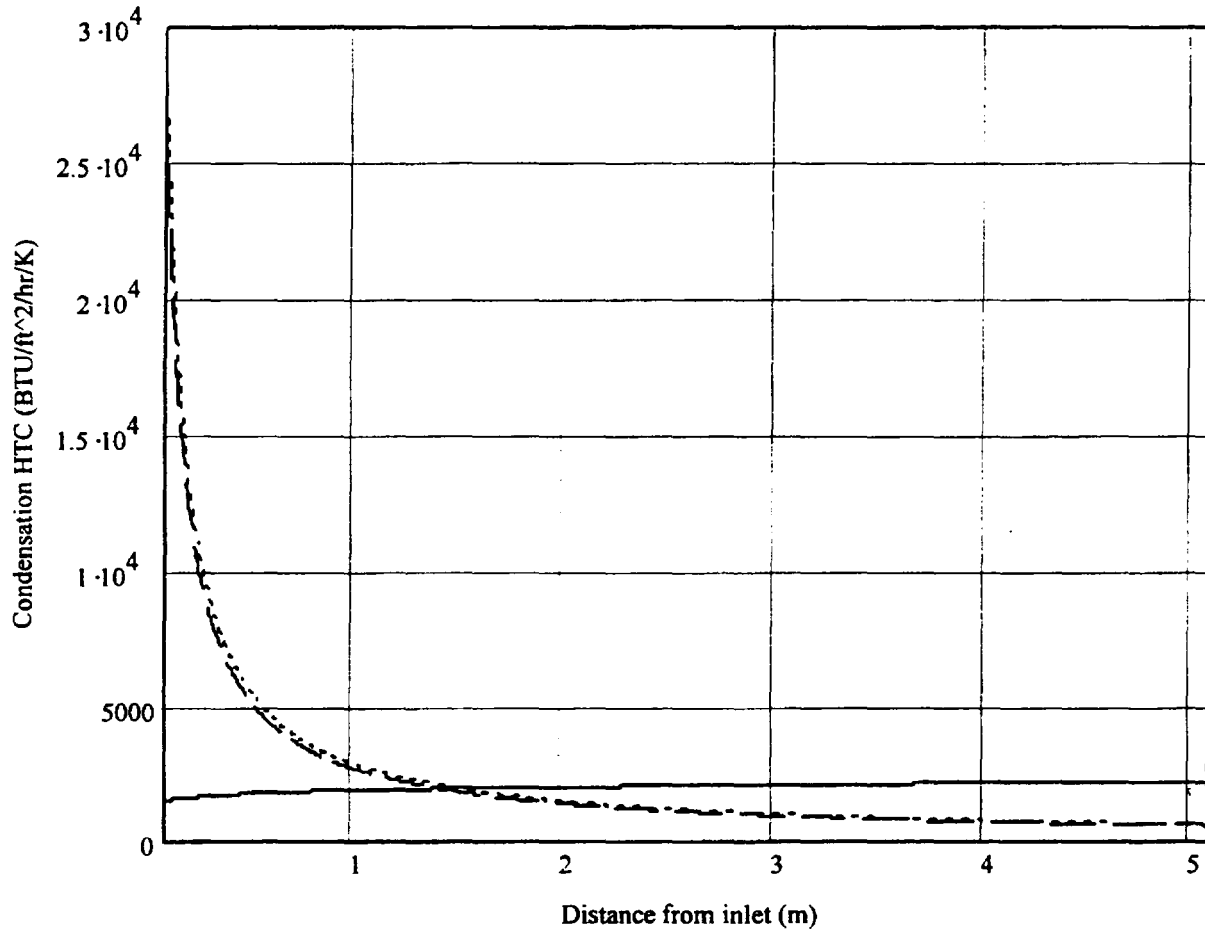


Figure 2-15 Comparison of Condensation Heat Transfer Correlations

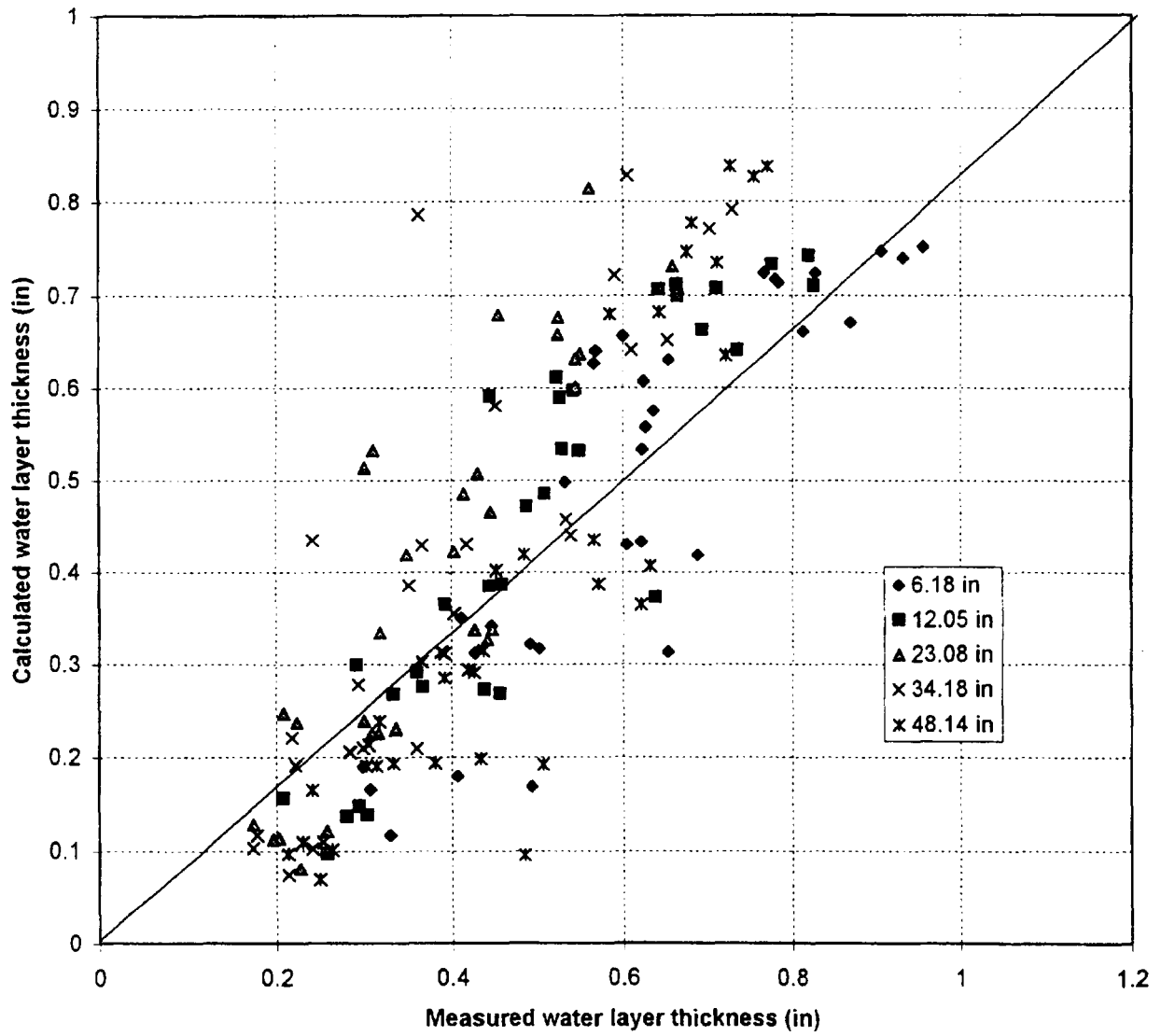


Figure 2-16 Predicted Versus Measured Liquid Level at Various Axial Locations

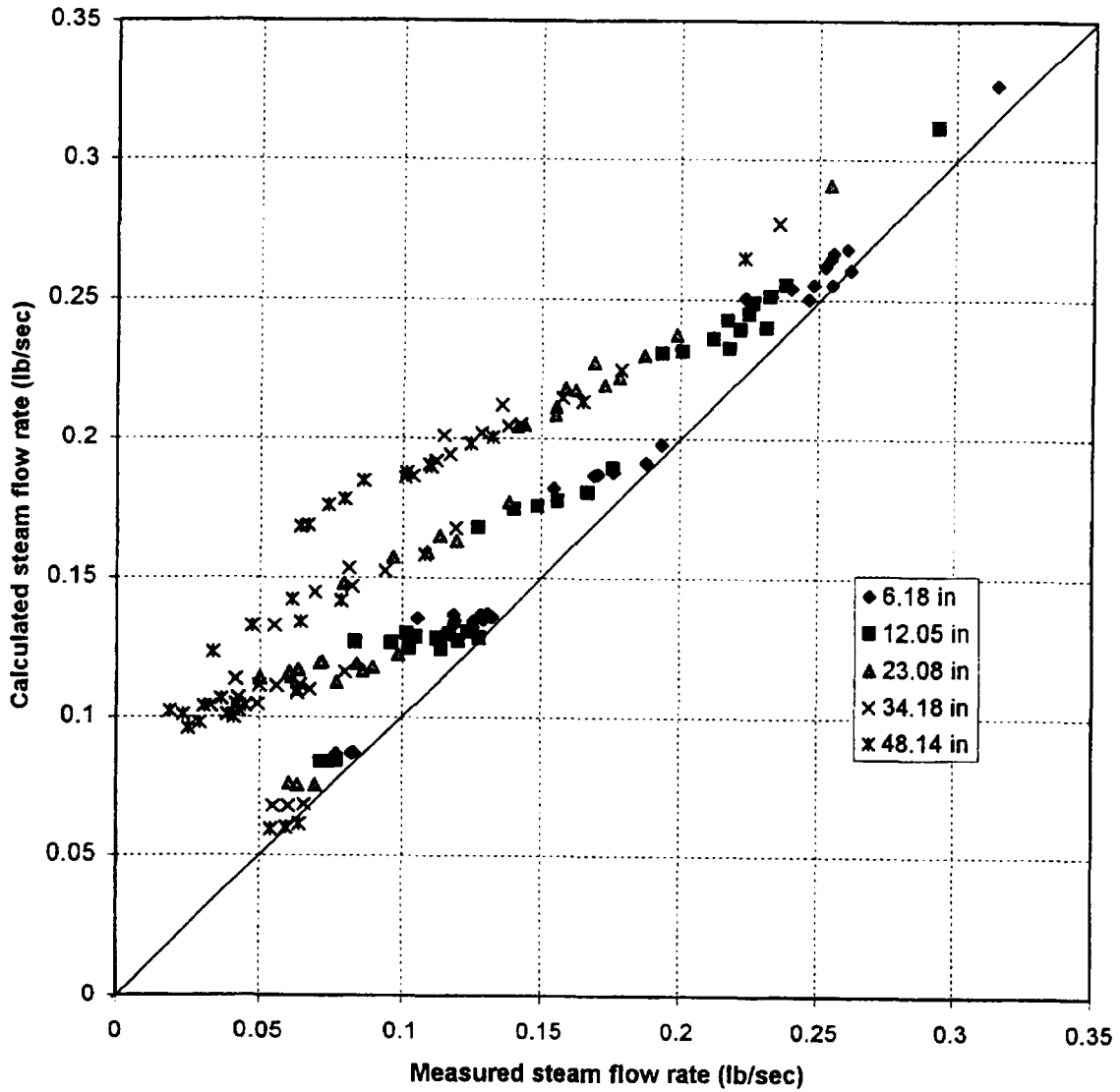


Figure 2-17 Predicted Versus Measured Steam Flowrate at Various Axial Locations

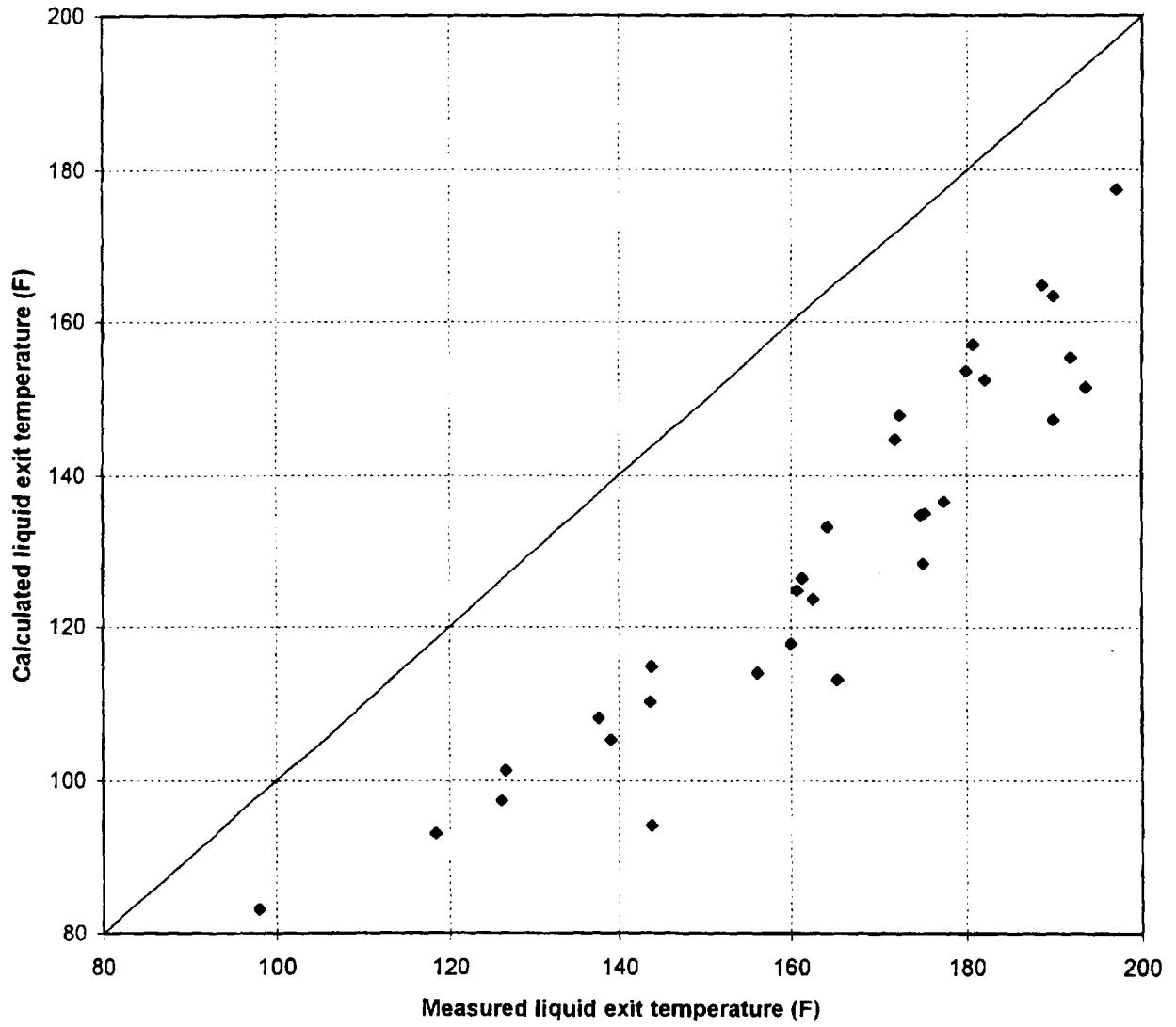
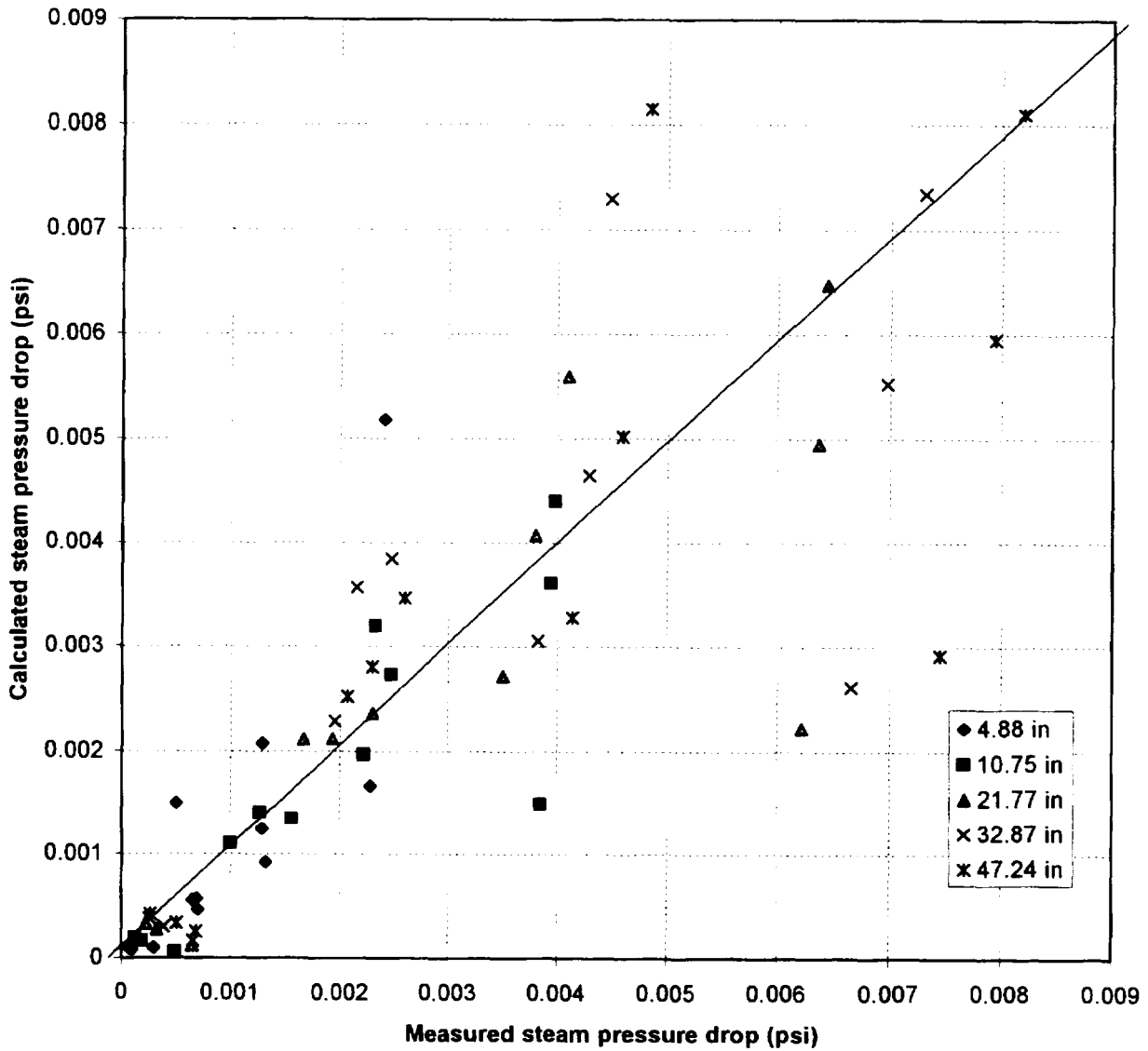


Figure 2-18 Predicted Versus Measured Liquid Temperature at the Channel Exit



(Measurements were taken only during the following runs: 211, 231, 251, 253, 255, 257, 273, 275, 277, 293, 295, and 297)

Figure 2-19 Predicted Versus Measured Steam Pressure Drop at Various Axial Locations

2.3 OSU APEX FACILITY VALIDATION OF WCOBRA/TRAC-AP

In addition to the separate effects test validation reported in the previous section, WCOBRA/TRAC-AP has been validated against Test SB18 of the OSU APEX facility matrix to assess its capability to predict the ADS-4 IRWST initiation phase transient in the upper plenum/hot leg/pressurizer region of interest. The scaling of the OSU APEX facility, which is a 1/4-height, reduced-pressure model of the AP600, has been demonstrated to be adequate for AP1000, such that the data obtained is considered applicable to the larger plant (Reference 1). Test SB18 is simulated [

] ^{a,c}

The WCOBRA/TRAC-AP code version employed in the test SB18 simulation contains the models described in subsection 2.2.1 and the "AP" modeling previously described in Reference 2 superimposed on the Mod 7A Rev. 5 code version, which contains the changes as reported in Reference 3.

The test data report for the OSU tests is given in the OSU Final Data Report (Reference 4), which describes the test facility, the valid instrumentation, and the test facility performance for the different tests. The OSU Test Analysis Report (Reference 5) examines in additional detail the thermal-hydraulic behavior of the test facility and the phenomenon observed in the tests, as identified in the phenomena identification ranking table (PIRT).

The OSU APEX test facility is a 1/4-height, reduced-pressure model of the AP600 and AP1000 and the passive emergency core cooling systems. The test facility located at the Radiation Center at the University in Corvallis, Oregon, includes the RCS, SGs, passive core cooling system (PXS), ADS, and nonsafety-related injection systems, such as the normal residual heat removal system (RNS) and the chemical and volume control system (CVS). The test facility, fabricated from austenitic stainless steel designed for normal operation at 450°F and 400 psig, was scaled using the hierarchical, two-tiered scaling analysis (H2TS) method developed by the U.S. NRC. Simulated piping breaks were tested in the hot leg (HL), cold leg (CL), pressure balance line between the cold leg and the core makeup tank (CMT), and the direct vessel injection (DVI) line. Decay heat that scaled to 3 percent of the full power (about 2 minutes after shutdown) was supplied by electrically heated rods in the reactor vessel. Simulated transients were programmed by the control system to proceed automatically. About 850 data channels were recorded by the data acquisition system (DAS) and downloaded to compact disks for subsequent data reduction and plotting. The OSU test facility was specifically designed to examine the transient (SBLOCA) periods as well as the long-term-cooling (LTC) aspects of the AP600 passive safety systems. The applicability of the OSU APEX facility data to the AP1000 has been demonstrated in Reference 1.

The OSU APEX test facility was constructed specifically to investigate the AP600 passive system characteristics. The facility design models the detail of the AP600 geometry, including the primary system, pipe routings, and layout for the passive safety systems. The primary system consists of one hot leg and two cold legs, with two active pumps and an SG for each of the two loops. There are two CMTs, each connected to a cold leg of one primary loop. The pressurizer is connected to the other primary loop, as in the AP600 plant design. Gas-driven accumulators are connected to the DVI lines. The discharge

lines from a CMT and one of the two IRWST and reactor sump lines are connected to each DVI line. The two independent lines of each stage of ADS 1, 2, and 3 are modeled by one line containing an orifice. Two-phase flow from ADS 1–3 is separated in a swirl-vane separator, and liquid and vapor flows are measured to obtain the total flow rate. The separated flow streams are then recombined and discharged into the IRWST through a sparger. Thus, mass and energy flow from the ADS into the IRWST are preserved. Following actuation, two-phase flow through the ADS-4 flowpaths depressurize the test reactor vessel until IRWST injection is achieved and beyond.

The period for simulation included not only IRWST injection, but also IRWST draining and sump injection to simulate the LTC mode of the AP600. The time scale for the OSU test facility is about one-half; that is, the sequence of events occurred about twice as fast in the test facility as in the AP600. The OSU facility provides data for validating the WCOBRA/TRAC computer code capability to predict the ADS-4 IRWST initiation phase transient.

2.3.1 WCOBRA/TRAC OSU Test Facility Model

The Oregon State University (OSU) test facility is a quarter-scale model of the Westinghouse AP600 and AP1000 systems. It is a low-pressure, integral systems facility designed for test conditions up to 400 psig and 450°F. The facility consists of the following AP600 systems:

- Reactor coolant system (RCS)
- Steam generator (SG) system – primary side
- Passive core cooling system (PXS)
- Partial chemical and volume control system (CVS)
- Partial nonsafety-related normal residual heat removal system (RNS)
- Automatic depressurization system (ADS)

Detailed descriptions of these systems are given in References 4 and 6.

The WCOBRA/TRAC-AP nodalization to analyze the ADS-4 IRWST initiation phase models components of the OSU test facility, as discussed below. Figure 2-20 shows the components simulated in the model. Junctions connecting components are identified with circles. The following subsections describe the main components.

2.3.1.1 Vessel Component

The WCOBRA/TRAC VESSEL component is shown in Figures 2-21 through 2-28. This component simulates the OSU test vessel that contains electrical heater rods as the energy source. As shown,

[] ^{a,c}

Section 1, shown in Figure 2-22, represents the lower plenum; [] ^{a,c}

Section 2, shown in Figure 2-23, represents [] ^{a,c}

[]^{a,c}

Sections 3 through 5, shown in Figures 2-24 to 2-26, represent [

] ^{a,c}

Sections 6 and 7, shown in Figures 2-27 and 2-28, [

] ^{a,c}

2.3.1.2 Primary Loop

The primary loop includes the following major components: [

] ^{a,c}

2.3.1.3 Pressurizer

The pressurizer vent line connects to the ADS Stages 1 to 3 (ADS 1-3) valves. Because [

] ^{a,c}

2.3.1.4 Steam Generators

The code's STGEN component models the SGs [

] ^{a,c}

2.3.1.5 Reactor Coolant Pumps

The RCPs are part of the SG lower plenum. [

] ^{a,c}

2.3.1.6 Loop Lines

The code's PIPE, TEE, and VALVE components [

] ^{a,c}

2.3.1.7 Accumulators

The two accumulators are not modeled because they are empty before the ADS-4 IRWST initiation phase begins.

2.3.1.8 Core Makeup Tanks

The core makeup tanks and the balance lines that connect the top of the CMTs to the cold legs [

] ^{a,c}

2.3.1.9 Passive Residual Heat Removal Heat Exchanger/In-Containment Refueling Water Storage Tank

Test data indicate that the passive residual heat removal heat exchanger (PRHR HX) is [

] ^{a,c}

2.3.1.10 In-Containment Refueling Water Storage Tank (IRWST)

[

] ^{a,c}

2.3.1.11 Automatic Depressurization System Stage 1 to 3 Valves

Component 46 models the ADS 1-3 valves. In the AP600 and AP1000 plants, each set of valves has two flow paths. The OSU test facility [

] ^{a,c}

2.3.1.12 Automatic Depressurization System Stage 4 Valves

Components 64 and 67 represent ADS Stage 4-1 and 4-2 valves, respectively. These valves reduce RCS pressure through HL-1 and HL-2. In the AP600 and AP1000 plants, each fourth stage has two flow paths. In the OSU test facility, [

] ^{a,c}

2.3.1.13 Safety Injection During the ADS-4 IRWST Initiation Phase

As previously noted, [

] ^{a,c}

2.3.1.14 Break Component

The code's BREAK component represents [

] ^{a,c}

2.3.1.15 Boundary Condition Calculations

The phenomena of interest in [

] ^{a,c}

[

] ^{a,c}

2.3.2 Assessment of WCOBRA/TRAC-AP Predictions

The definitions used for quantification are as follows (as excerpted from Section 1.5 of Reference 3):

- **EXCELLENT** – The calculation lies within the data uncertainty band at all times during the transient phase of interest. This is interpreted that the code had no deficiencies that are significant. No action is required for this level of agreement.
- **REASONABLE** – The calculation sometime lies within the data uncertainty bands and shows the same trends as the data. This is interpreted that the code deficiencies are minor. Minor actions and/or discussions are used to explain differences.
- **MINIMAL** – Major data trends and phenomena are not predicted. The code has significant deficiencies, and incorrect conclusions may be drawn based on the calculations without the benefit of data. If the deviation of the code calculations is known, then the minimal agreement may be acceptable for lower-ranked items in the PIRT.
- **INADEQUATE** – Modeling the phenomena is beyond the capability of the code. The question then becomes how important are these phenomena for describing the transient and having confidence in the results and their application to the plant.

This section will focus on the results of the Test SB18 simulation. The time scale of the plots presented is that of the test; the code prediction time values are adjusted so that the ADS-4 actuation time of each is

[] ^{a,c} and in
 Figures 2-29 through 2-34. Figure 2-29 compares the pressurizer level predicted by WCOBRA/TRAC with the Test SB18 data as shown in Figure 5.2.2-35 of Reference 5. The WC/T level agrees extremely well with the data through [] ^{a,c}, at which time it falls below; overall, the agreement is judged as reasonable. The total mass predicted to be released from the ADS-4 flowpaths combined is in reasonable agreement with the data total, as shown in the Figure 2-32 comparison with the test values reported in Reference 5, Figure 5.2.2-62. The code prediction of liquid entrainment through an ADS-4 path is a function of the predicted liquid level in the attached hot leg pipe; subsection 2.2.1 provides discussion of this and other hot leg models developed for this application. The comparison of ADS-4 flow rates is made for only liquid [] ^{a,c}

The WCOBRA/TRAC predicted collapsed liquid levels in the vessel downcomer, core, and upper plenum are shown in Figures 2-31, 2-32, and 2-33, respectively. These figures show that the code [

] ^{a,c} Figure 2-34

compares the code-predicted downcomer pressure with the Test SB18 value. The agreement is judged to be reasonable. Overall, the WCOBRA/TRAC prediction of the ADS-4 IRWST initiation phase is in reasonable agreement with the Test SB18 data, and the code may be used in AP1000 plant calculations of the ADS-4 IRWST initiation phase to supplement NOTRUMP.

2.3.3 References

1. WCAP-15613, "AP1000 PIRT and Scaling Assessment," Westinghouse Electric Company LLC, February 2001.
2. Garner, D. C., et al., "WCOBRA/TRAC OSU Long-Term Cooling Final Validation Report," March 1998.
3. Letter LTR-NRC-01-6 from H. A. Sepp, Westinghouse, to J. S. Wermiel, USNRC, "10CFR50.46 Annual Notification and Reporting for 2000," March 13, 2001.
4. Dumsday, C. L., Carter, M., Copper, M. H., Lau, L. K., Loftus, M. J., Nayyar, V. K., Tupper, R. B., and Willis, J. W., WCAP-14252, Volumes 1-4, "AP600 Low Pressure Integral Systems Test at Oregon State University, Final Data Report," May 1995.
5. WCAP-14292, Revision 1, "AP600 Low-Pressure Integral Systems Test at Oregon State University Test Analysis Report," September 1995.
6. WCAP-14124, Volume I and Volume II, "AP600 Low Pressure Integral Systems Test at Oregon State University, Facility Description Report," July 1994.
7. Takeuchi, Kenji, Young, M. Y., and Gagnon, A. F., "Flooding in the Pressurizer Surge Line of AP600 Plant and Analyses of APEX Data," Nuclear Engineering & Design 192 (1999), pp. 45-58.

a,c

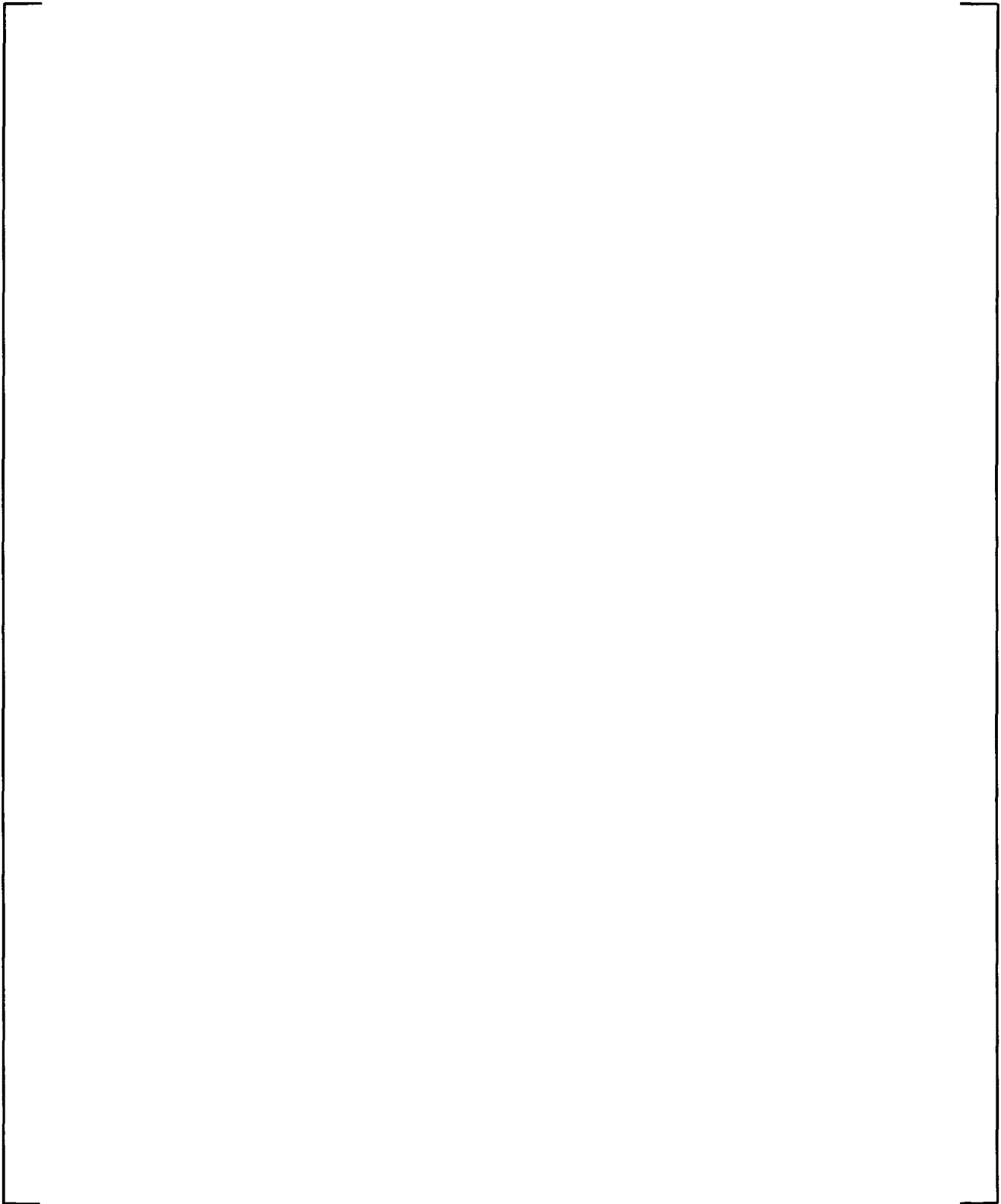


Figure 2-20 OSU WCOBRA/TRAC Schematic Diagram

a,c

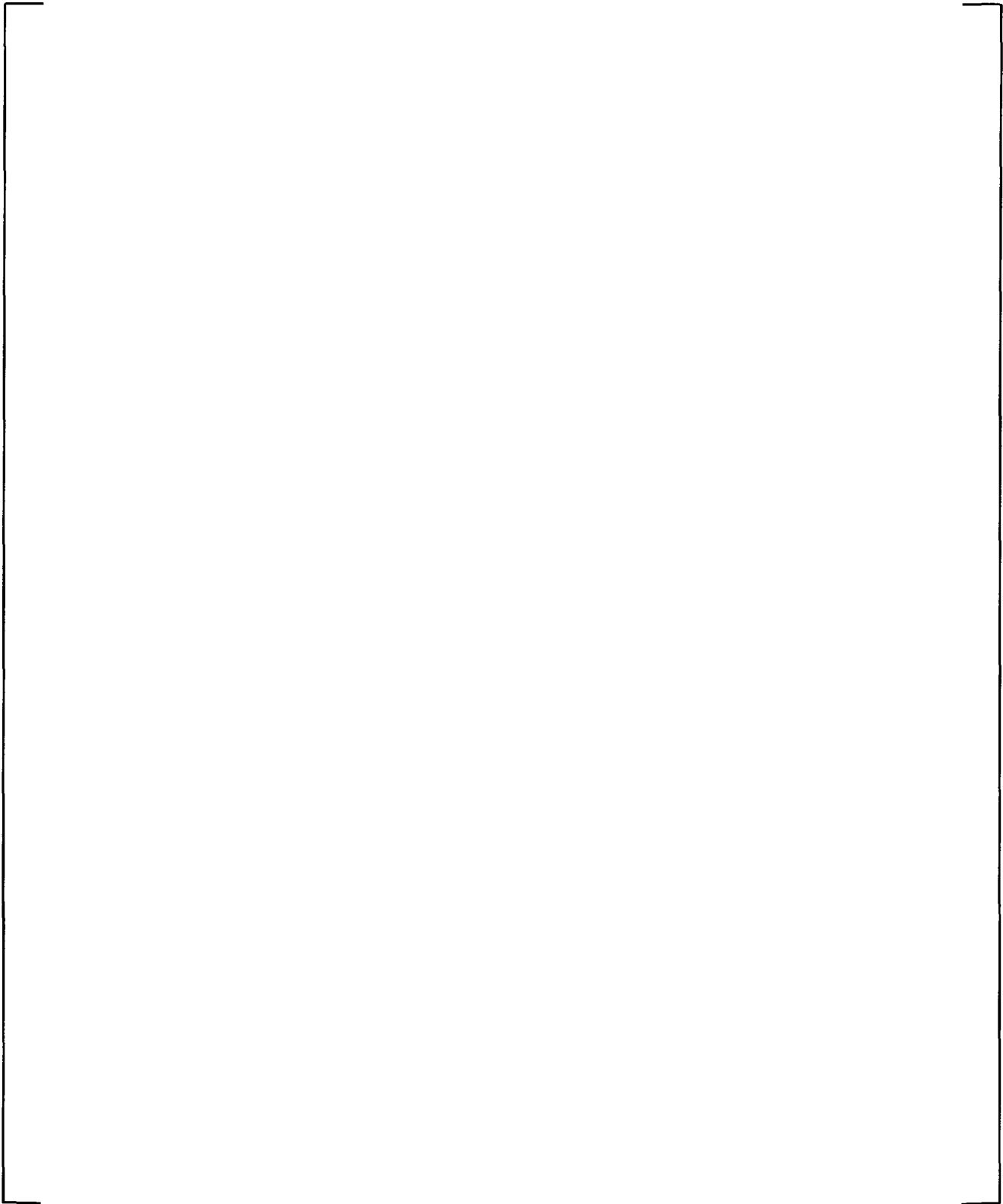


Figure 2-21 OSU WCOBRA/TRAC Vessel Model (Front View)

a,c

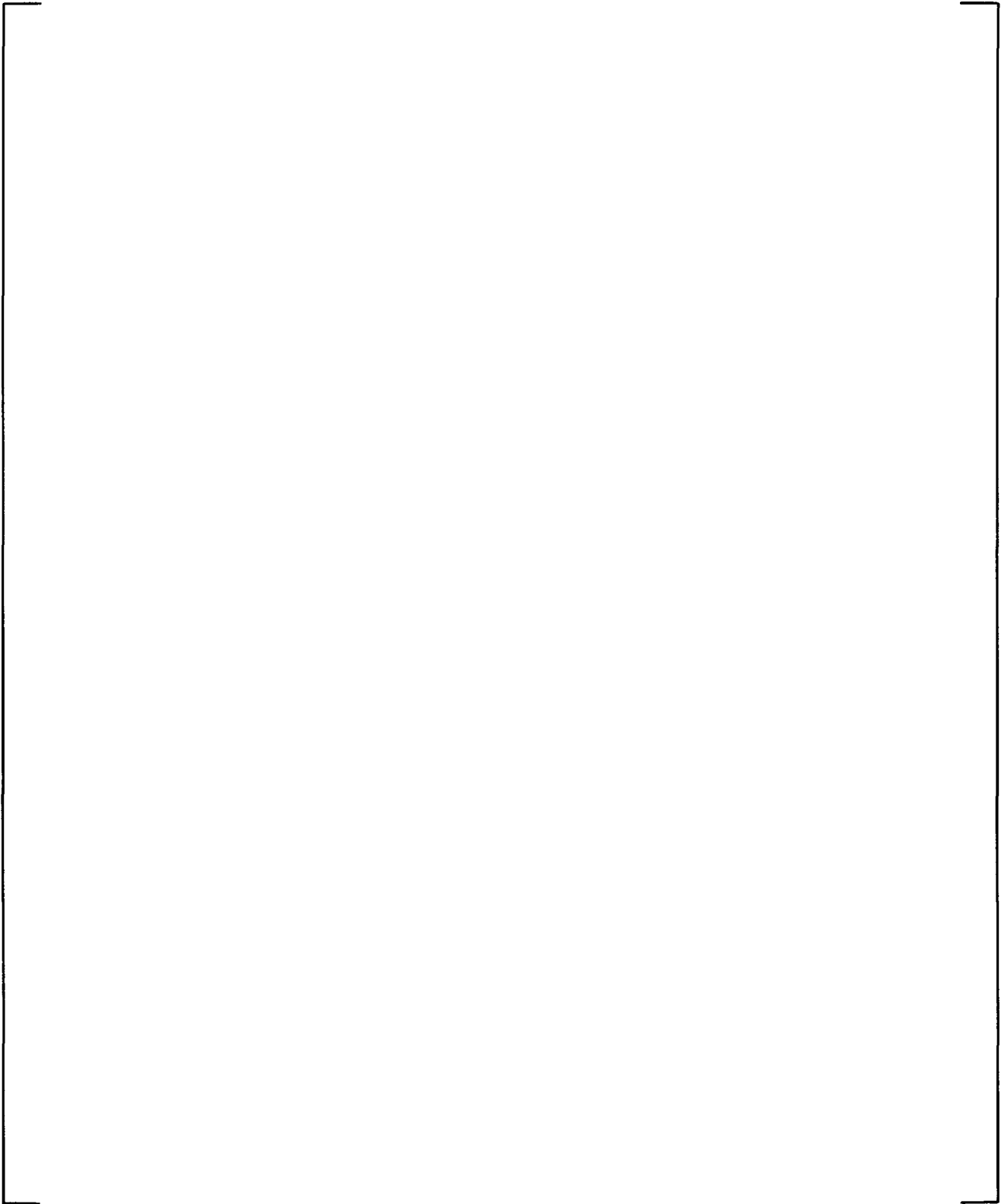


Figure 2-22 OSU Vessel Model – Section 1

a,c

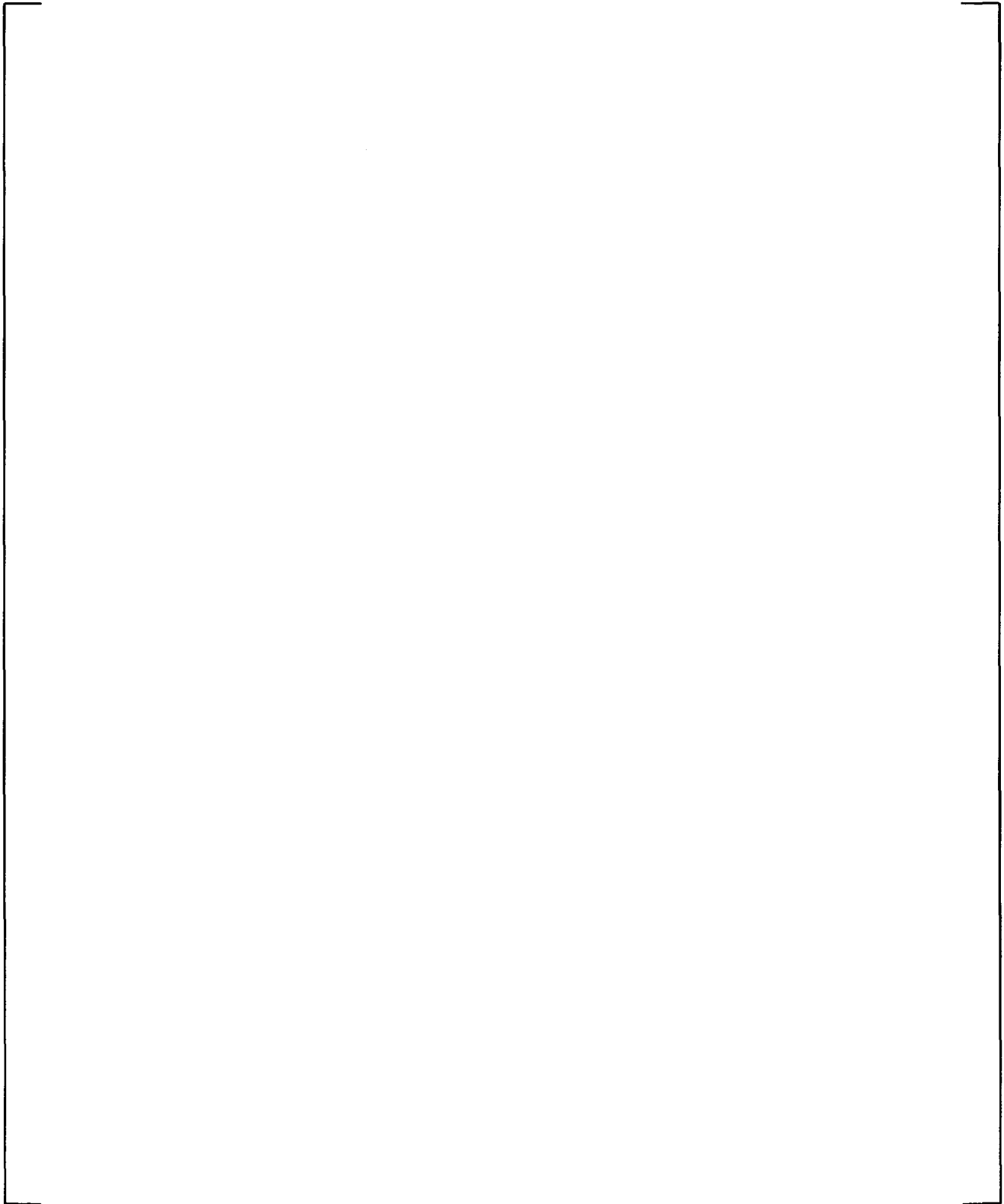


Figure 2-23 OSU Vessel Model – Section 2

a,c

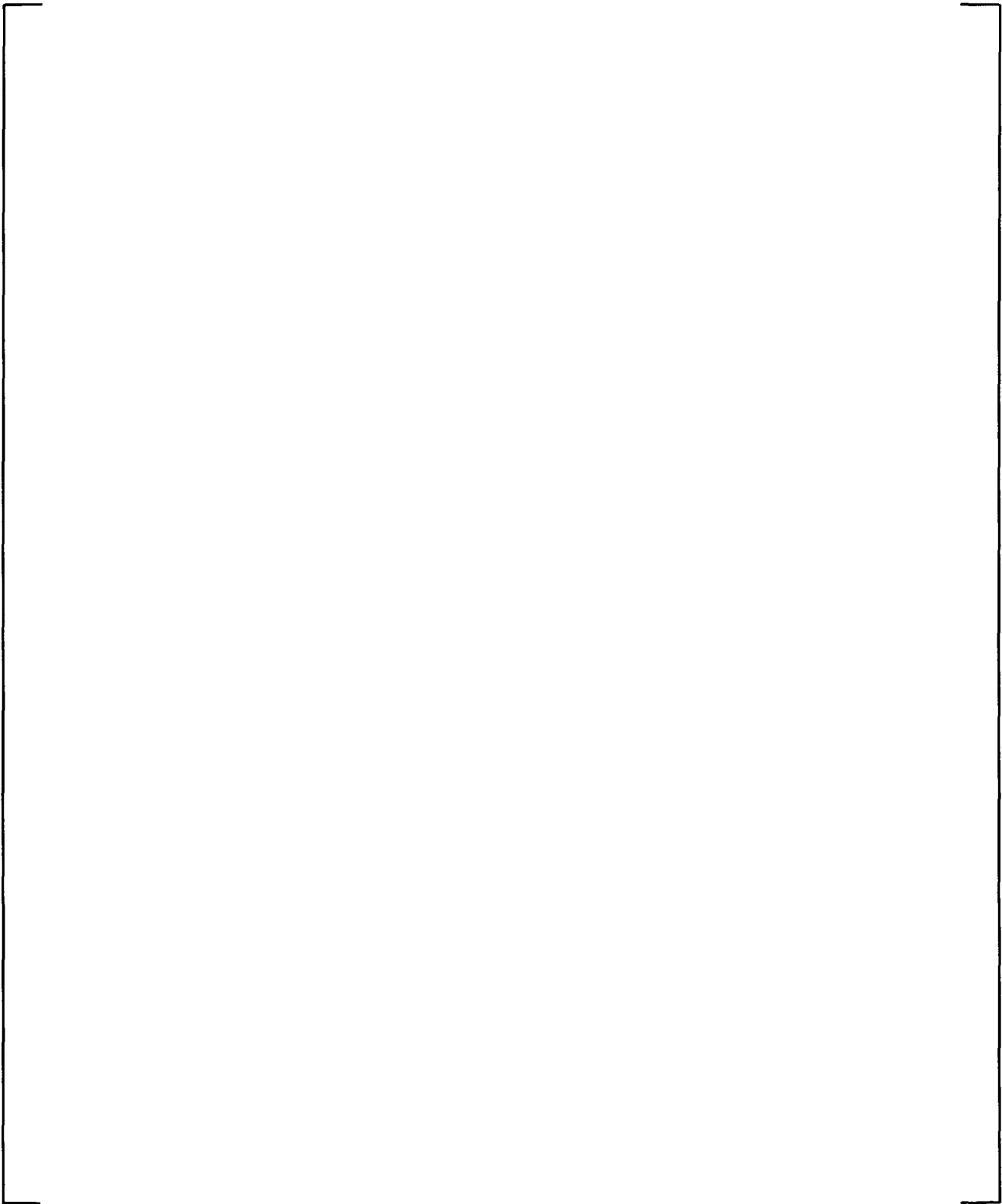


Figure 2-24 OSU Vessel Model – Section 3

a,c

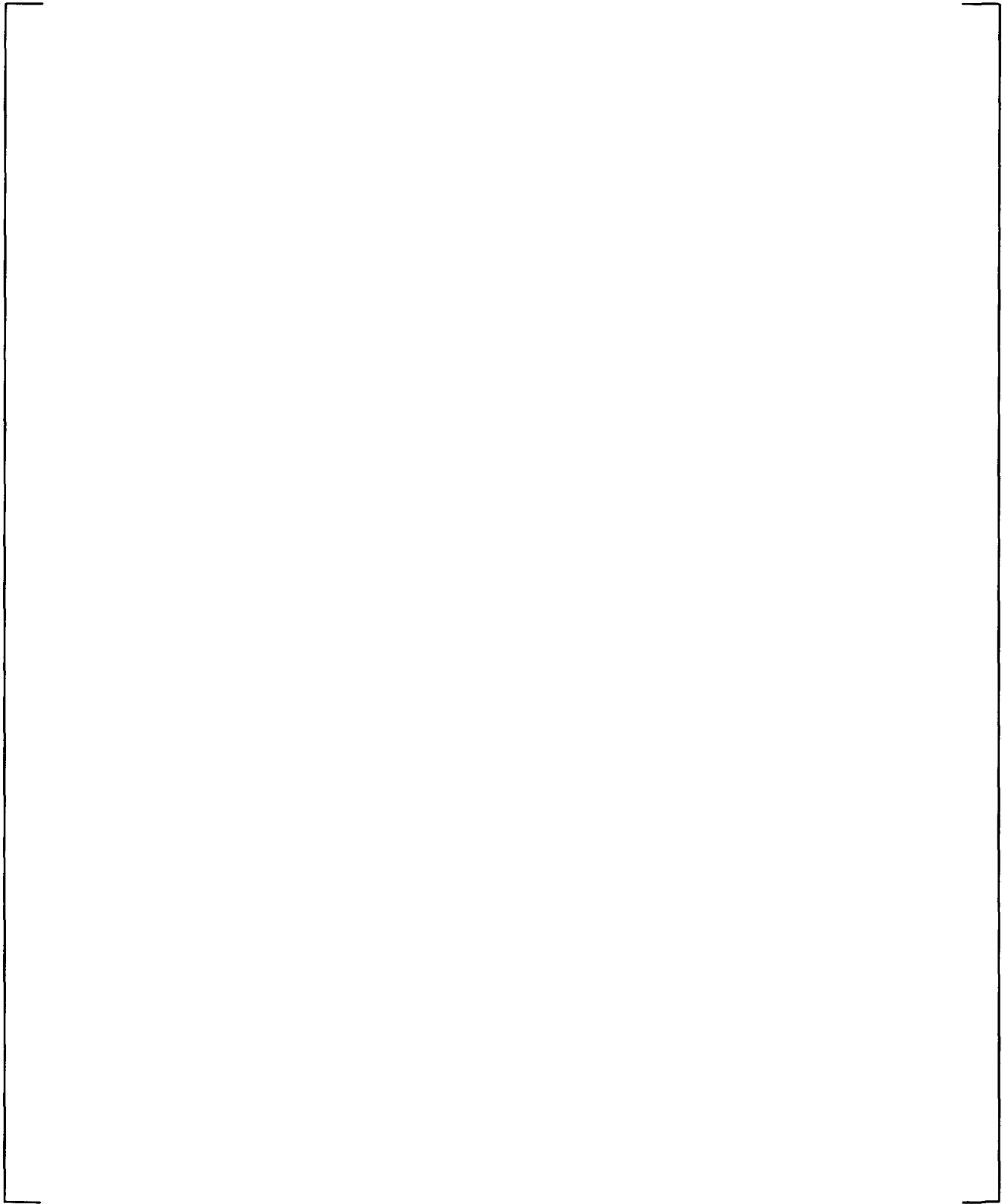


Figure 2-25 OSU Vessel Model – Section 4

a,c

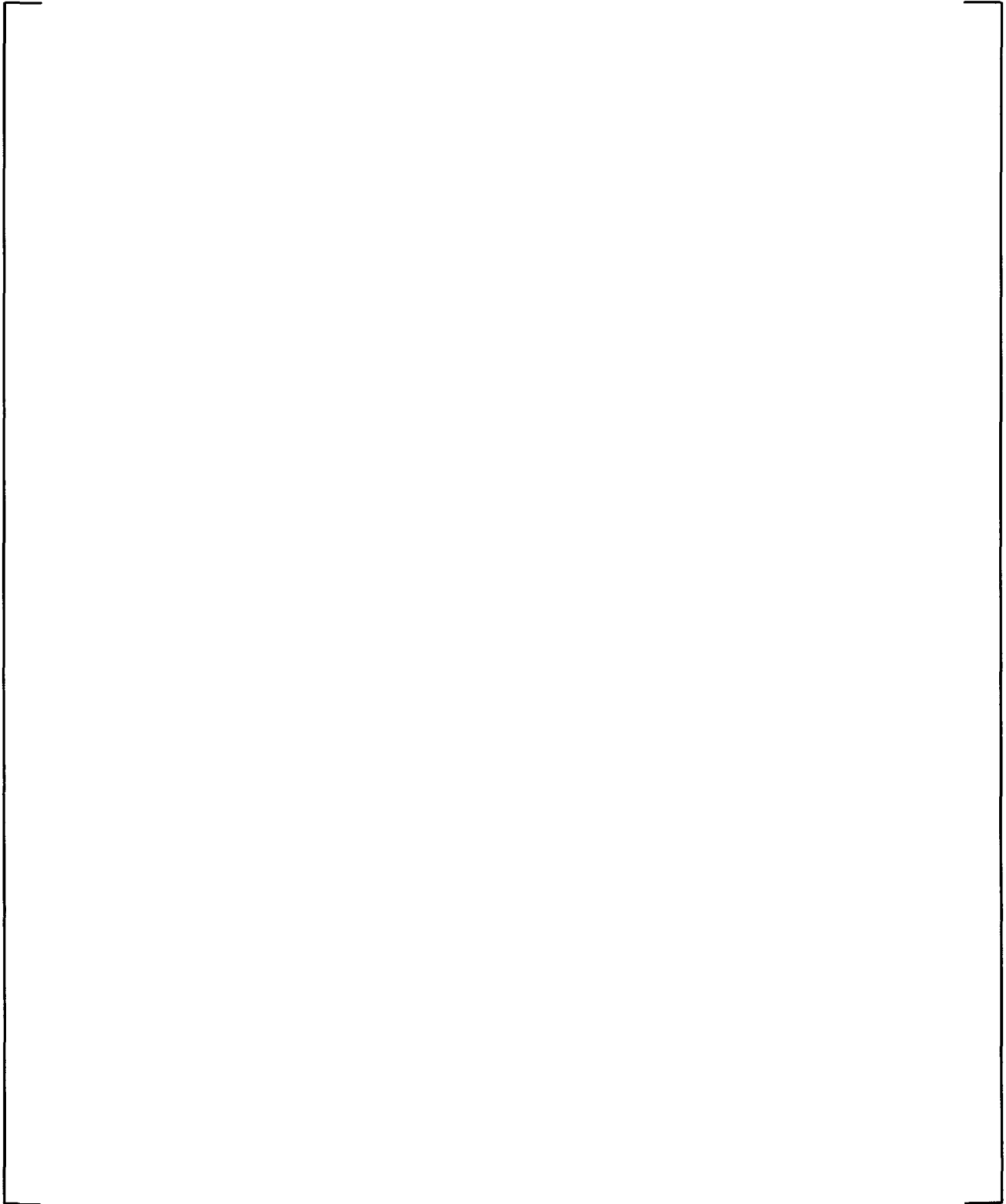


Figure 2-26 OSU Vessel Model – Section 5

a,c

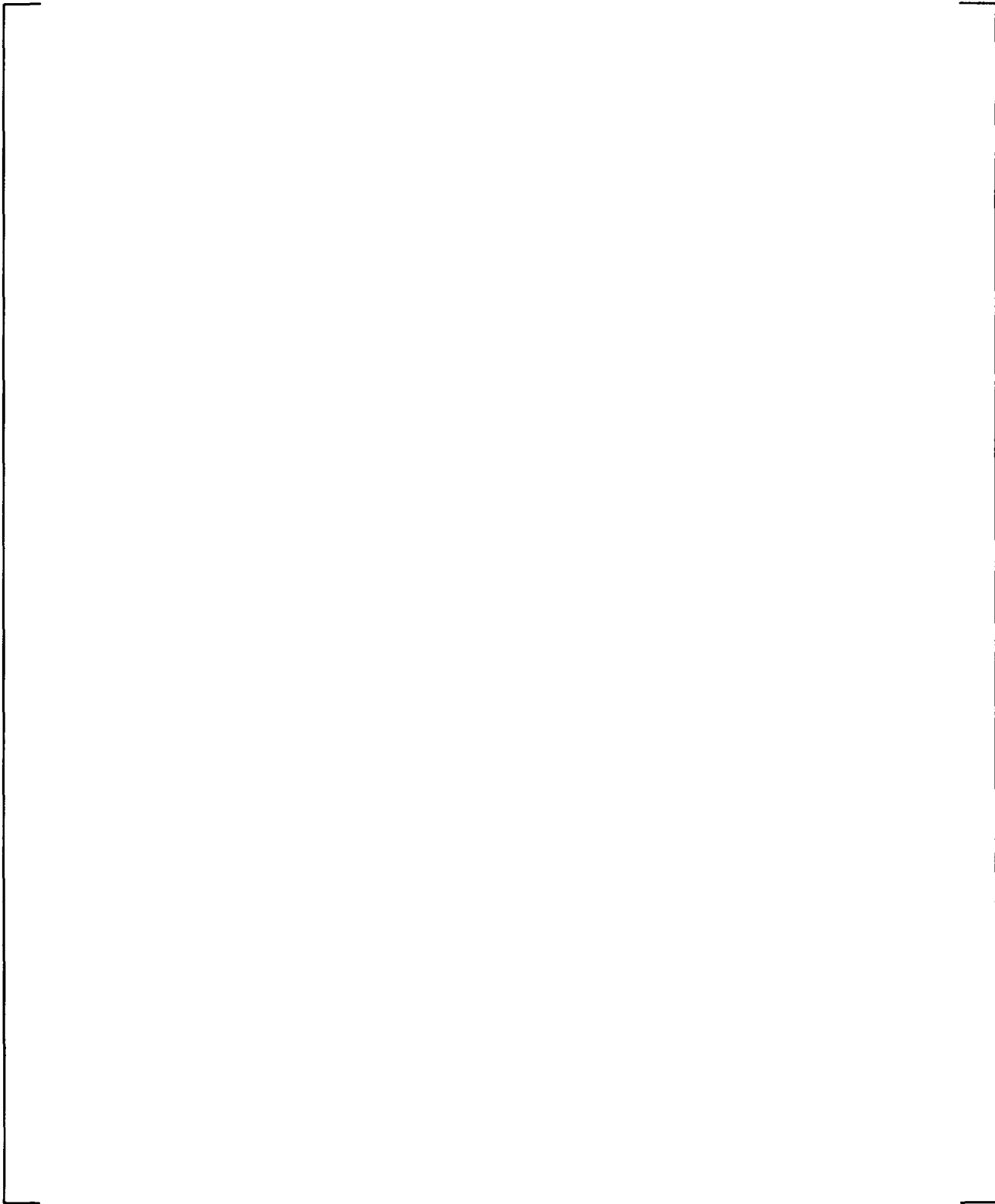


Figure 2-27 OSU Vessel Model – Section 6

a,c

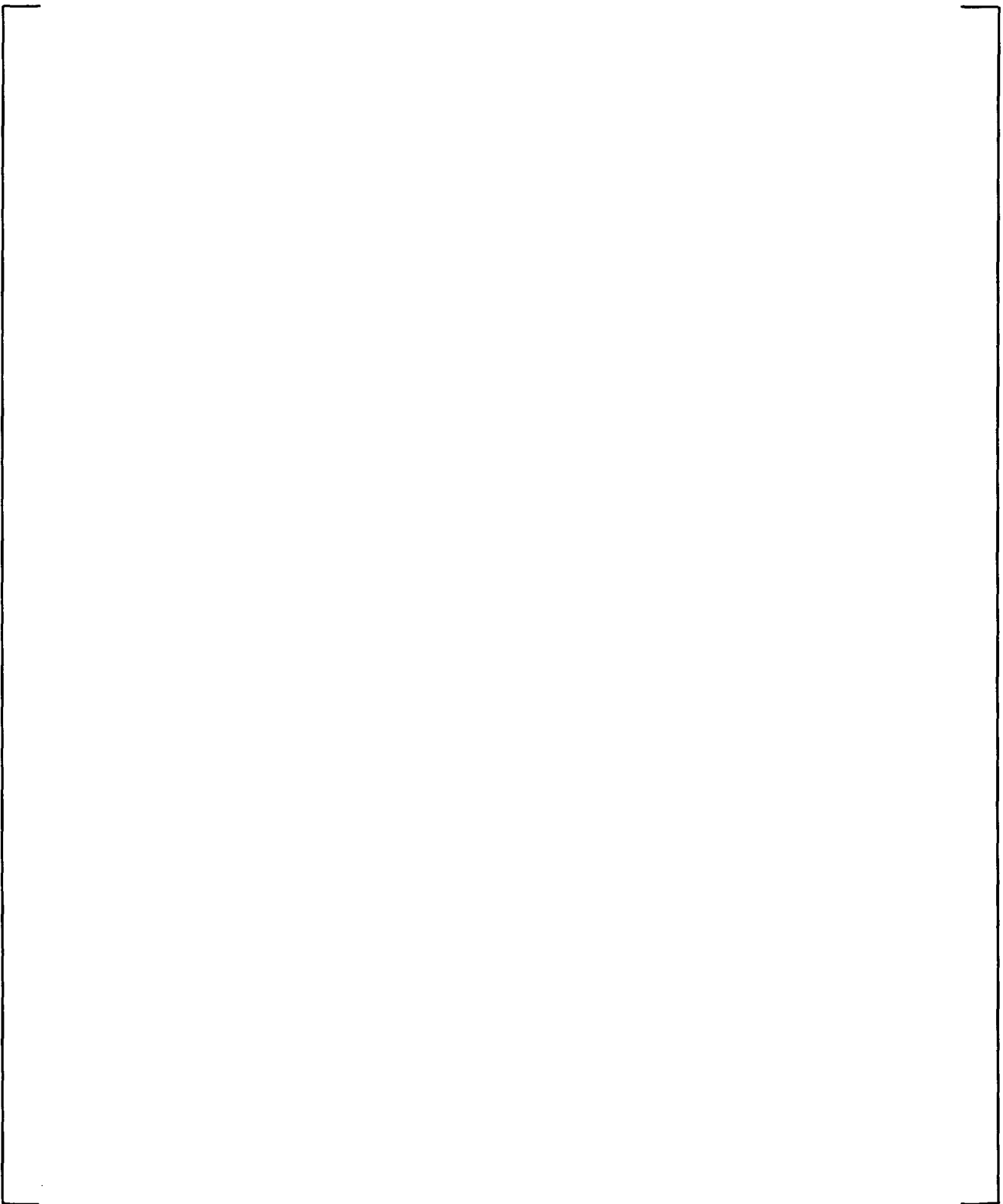


Figure 2-28 OSU Vessel Model – Section 7

(a,b,c)

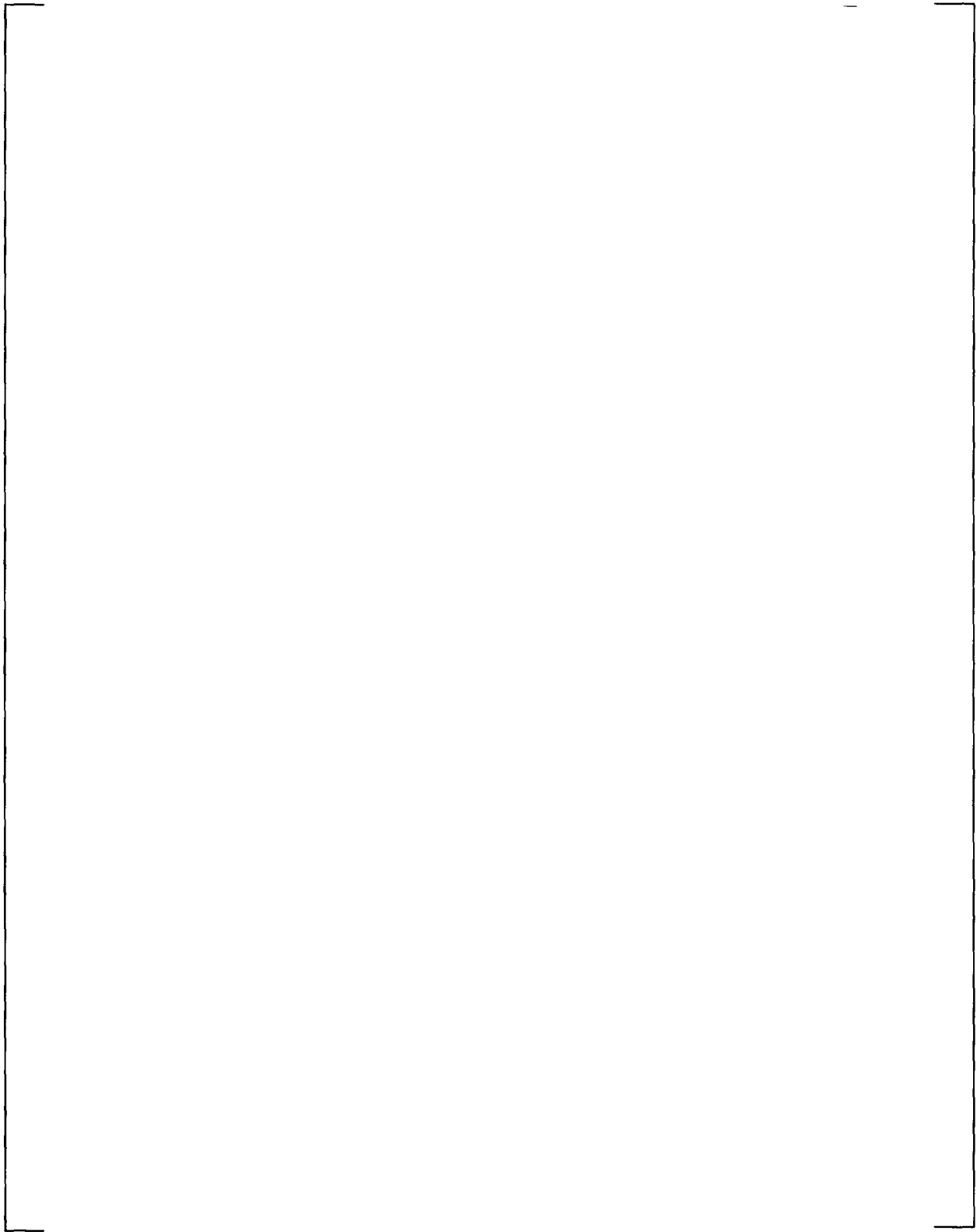


Figure 2-29 WCOBRA/TRAC Prediction vs. Test SB18 Data: Pressurizer Collapsed Liquid Level

(a,b,c)

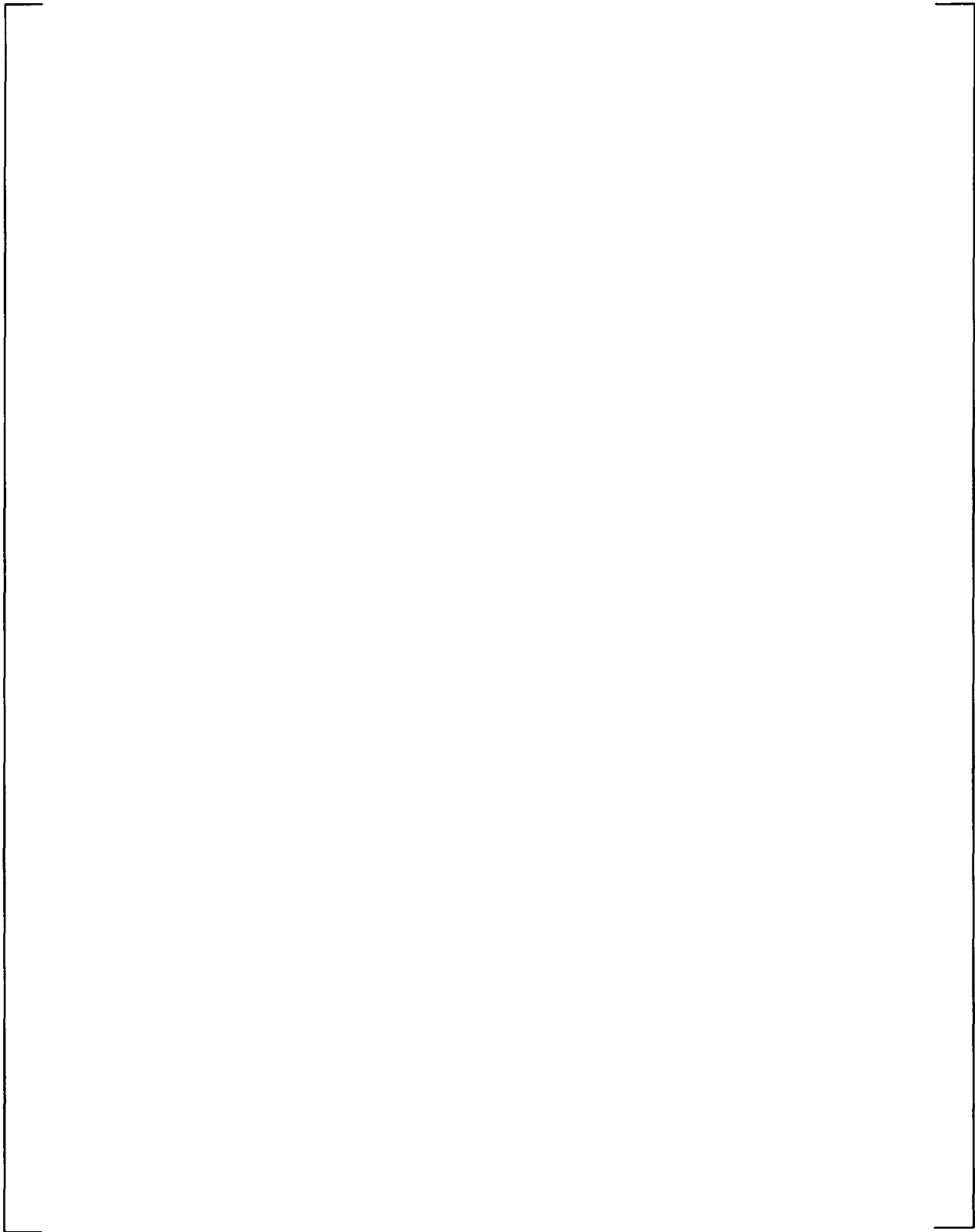


Figure 2-30 WCOBRA/TRAC Prediction vs. Test SB18 Data: Total ADS-4 Integrated Liquid Flow Rate

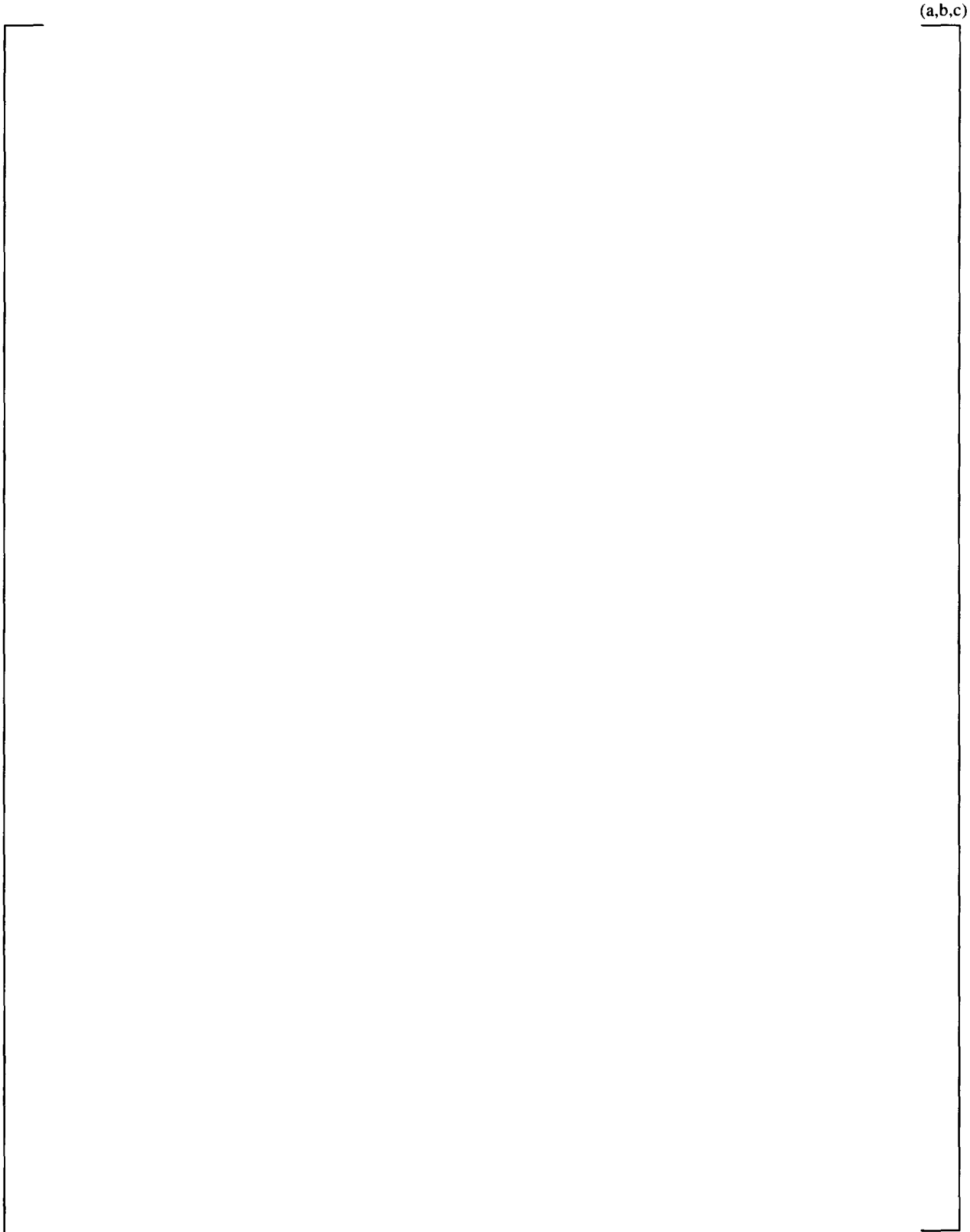


Figure 2-31 WCOBRA/TRAC Prediction of Test SB18 Downcomer Collapsed Liquid Level

(a,b,c)

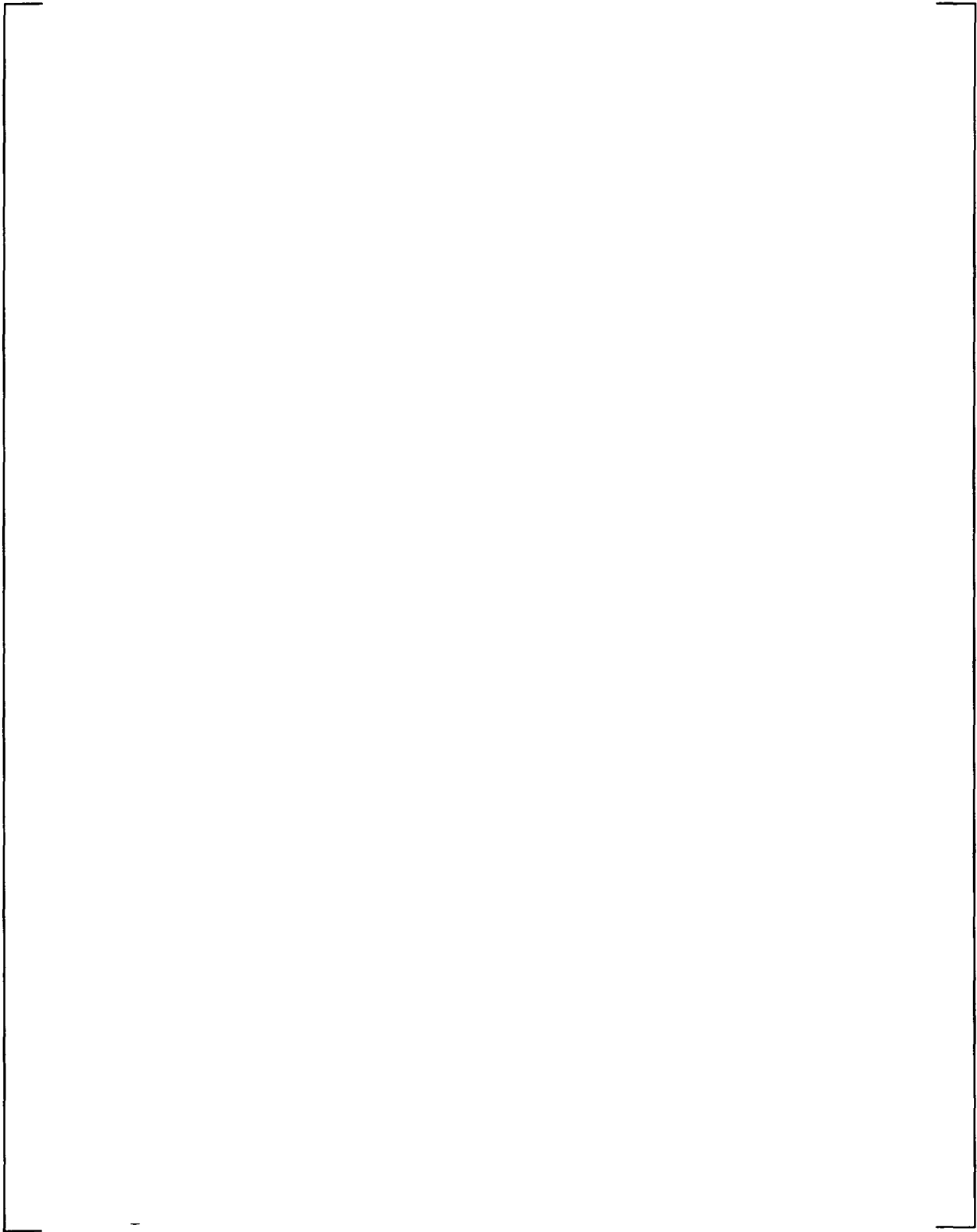


Figure 2-32 WCOBRA/TRAC Prediction of Test SB18 Core Collapsed Liquid Level

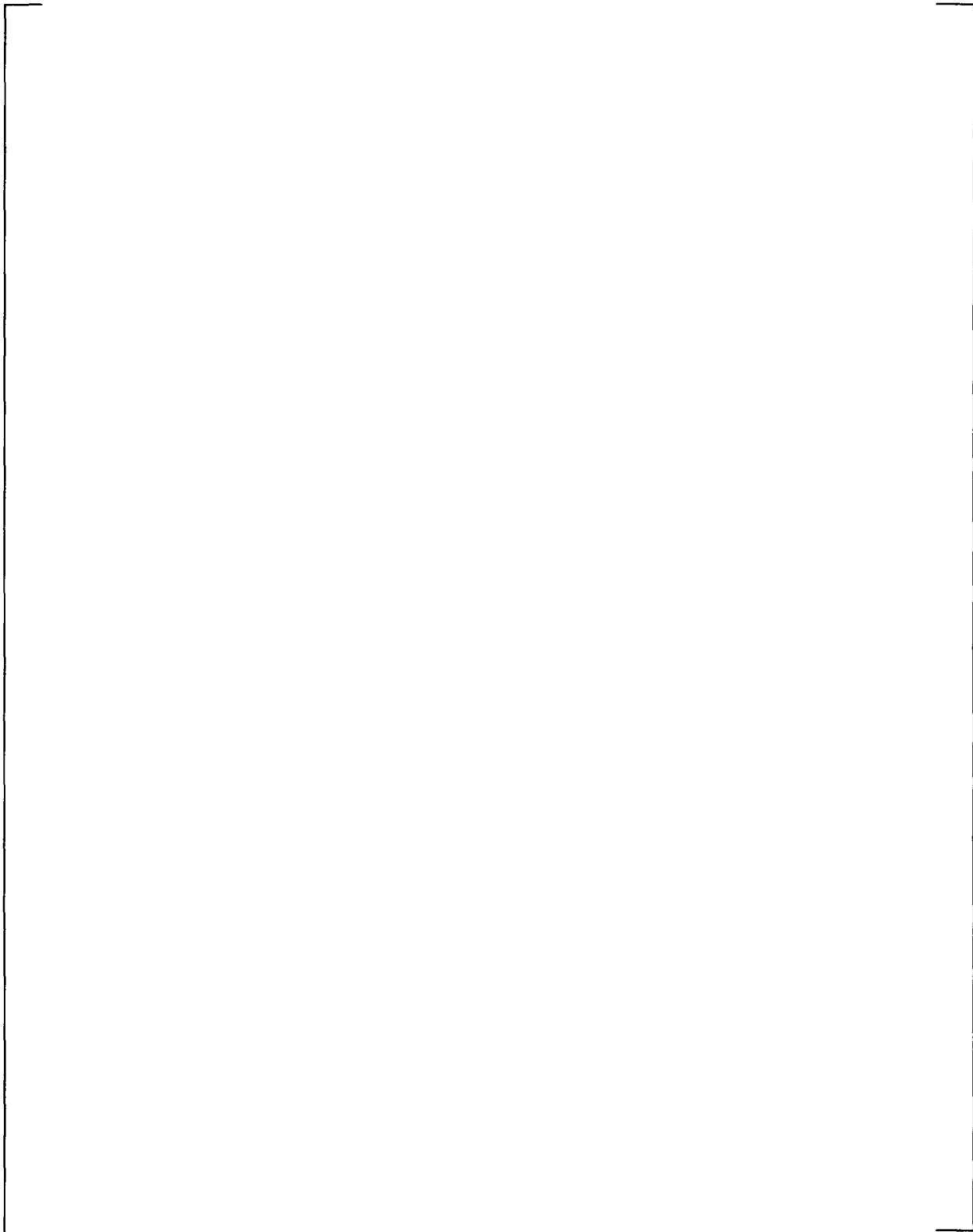


Figure 2-33 WCOBRA/TRAC Prediction of Test SB18 Core/Upper Plenum Collapsed Liquid Level

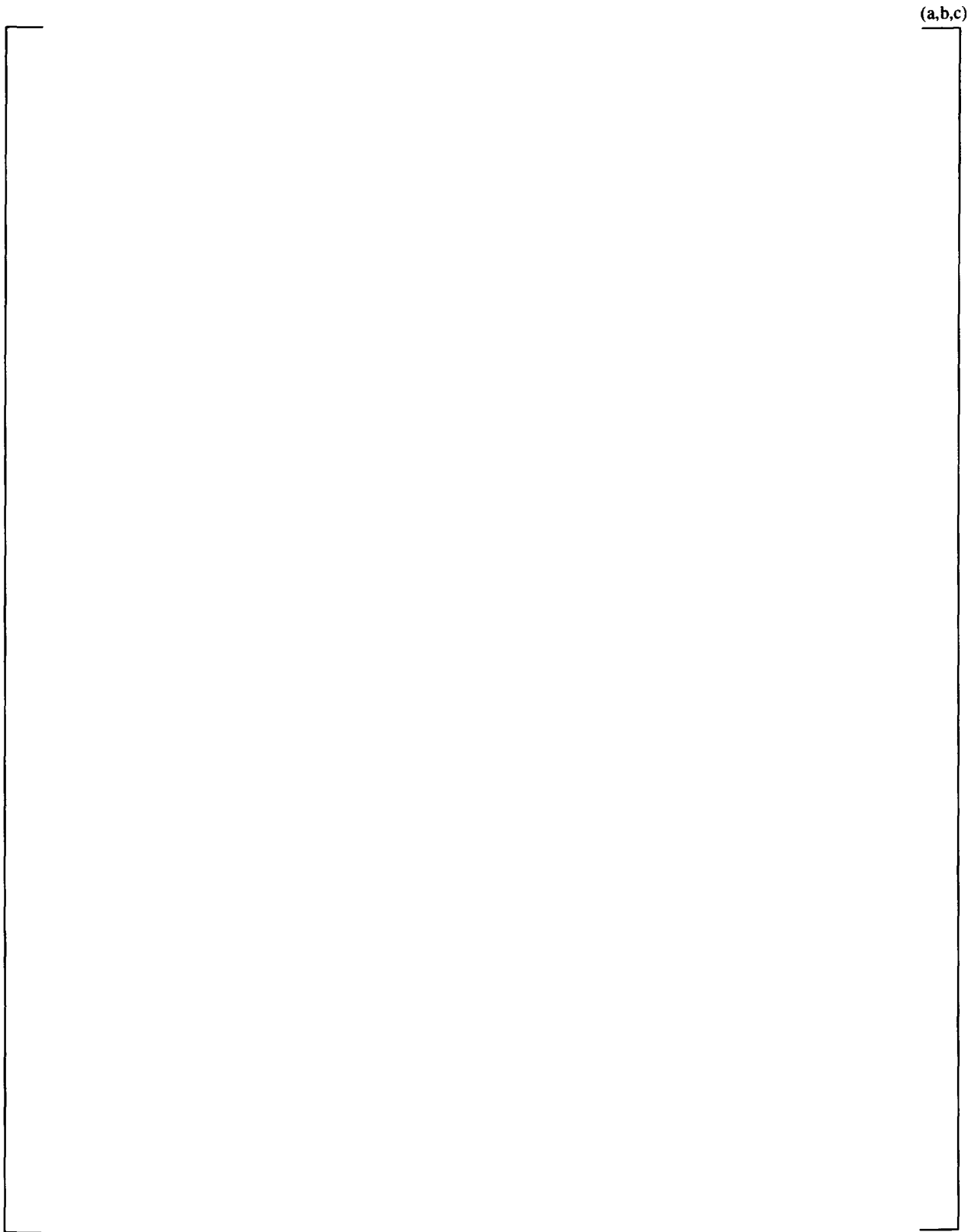


Figure 2-34 WCOBRA/TRAC Prediction vs. Test SB18 Data: Downcomer Pressure

3 AP1000 PLANT SIMULATIONS

The validation presented in Section 2 qualifies WCOBRA/TRAC to predict the ADS-4 IRWST initiation phase behavior of the AP1000. This section presents the AP1000 analyses performed in support of the NOTRUMP small break LOCA analysis in the AP1000 Design Control Document (DCD) (Reference 1).

3.1 PLANT MODELING

The WCOBRA/TRAC-AP nodalization to analyze the ADS-4 IRWST initiation phase transient for AP1000 is consistent with the OSU test facility model discussed in subsection 2.3.1. Figure 3-8 shows the components that are simulated in the AP1000 plant model. Junctions connecting components are identified with circles. The following subsections describe the modeling used to represent the main components.

3.1.1 Vessel Component

The WCOBRA/TRAC VESSEL component is shown in Figure 3-1. As shown, [

] ^{a,c}

Section 1, shown in Figure 3-2, represents the lower plenum; [

] ^{a,c}

Section 2, shown in Figure 3-3, represents [

] ^{a,c}

Sections 3 and 4, shown in Figures 3-4 and 3-5, represent [

] ^{a,c}

Sections 5 and 6, shown in Figures 3-6 and 3-7, both [

] ^{a,c}

Vertical flow channels simulate the axial flow paths, and [

] ^{a,c}

3.1.2 Primary Loop

The primary loop includes the following major components: [

] ^{a,c}

3.1.3 Pressurizer

The pressurizer vent line connects to the ADS Stages 1 to 3 (ADS 1–3) valves. Because [

] ^{a,c}

3.1.4 Steam Generators

The code's STGEN component models the SGs [

] ^{a,c}

3.1.5 Reactor Coolant Pumps

The RCPs are mounted on the SG lower plenums in AP1000. [

] ^{a,c}

3.1.6 Loop Lines

The code's PIPE and TEE components [

] ^{a,c}

3.1.7 Accumulators

The two accumulators are not modeled in the Inadvertent ADS Actuation scenario because they are empty before the ADS-4 IRWST initiation phase begins. For the DEDVI break simulation, [

] ^{a,c}.

3.1.8 Core Makeup Tanks

The core makeup tanks and the balance lines that connect the top of the CMTs to the cold legs [

] ^{a,c}

3.1.9 Passive Residual Heat Removal Heat Exchanger/In-Containment Refueling Water Storage Tank

Test data indicate that the passive residual heat removal heat exchanger (PRHR HX) is [

] ^{a,c}

3.1.10 In-Containment Refueling Water Storage Tank (IRWST)

[

] ^{a,c}

3.1.11 Automatic Depressurization System Stage 1 to 3 Valves

Components 48 and 88 model the ADS 1–3 valves. In the AP1000, each set of valves has two flow paths. These VALVE components are open during the ADS-4 IRWST initiation phase.

[

] ^{a,c}

3.1.12 Automatic Depressurization System Stage 4 Valves

Components 159, 199, 259, and 299 represent ADS Stage 4 valves. Each hot leg has two ADS-4 flow paths. The limiting single failure of an ADS Stage 4 valve to actuate is modeled in WCOBRA/TRAC as the failure of component 159. Component 199 opens when the ADS-4 actuation signal is received, and components 259 and 299 open 60 seconds later.

3.1.13 Safety Injection During the ADS-4 IRWST Initiation Phase

As in the OSU Test SB18 simulation, [

] ^{a,c} Component 777 is the FILL component attached to the second intact DVI line in the Inadvertent ADS scenario.

[

] ^{a,c}

3.1.14 Break Component

The code's BREAK component [

] ^{a,c}

Each open ADS-4 flow path consists of a large diameter pipe leading into a constricted area at the squib valve location. A specific model to simulate this orifice-like break geometry was generated as documented in Reference 3 as the "Small break LOCA break model." This model is applied to calculate the flow rate through the valves at the end of the ADS-4 flow paths. It is also used to model the flow through the venturi of the broken DVI pipe in the DEDVI break simulation.

3.1.15 Initial and Boundary Conditions

The initial conditions used in the AP1000 [

] ^{a,c} 10CFR50 Appendix K core decay heat

is used in the WCOBRA/TRAC simulation.

3.2 LIMITING CASE RESULTS

Two cases from the AP1000 DCD Section 15.6.5.4B small break LOCA analysis are analyzed, the double-ended DVI line break at 25 psia containment pressure and the inadvertent ADS actuation case. These are the minimum passive safety injection flow and the minimum reactor coolant system venting capability cases, respectively, from the AP1000 DCD small break LOCA analyses. In each case, the failure of one ADS-4 valve to open is assumed. For the DEDVI break, Component 778 is the broken DVI pipe instead of an intact injection line. WCOBRA/TRAC simulations of the ADS-4 IRWST initiation phase of these cases are compared with the corresponding NOTRUMP predictions, from Section 15.6.5.4B of the AP1000 DCD, in the following sections.

3.2.1 Double-Ended DVI Line Break

The double-ended DVI line break is the minimum passive safety injection flow capability case from the AP1000 DCD. The failure of one ADS-4 valve to open is assumed in both simulations. The WCOBRA/TRAC simulation of the ADS-4 IRWST initiation phase of the DEDVI line break is compared

with the corresponding NOTRUMP predictions from Section 15.6.5.4B of the AP1000 DCD in this section. The Appendix K-specified ANS 1971 + 20% core decay heat is used in both analyses.

Figure 3-9 presents the WCOBRA/TRAC downcomer pressure prediction of the ADS-4 IRWST initiation phase superimposed on the NOTRUMP result from Section 15.6.5.4B of the AP1000 DCD. The actuation of ADS-4 occurs at 492 seconds. Opening of the ADS-4 flow paths continues the RCS depressurization from approximately 100 psia down to near containment pressure. The RCS pressure tends to stabilize when the energy being discharged from the RCS approaches the energy from the core decay heat and from metal heat. The NOTRUMP prediction levels off in the rate of depressurization at a higher pressure than the WCOBRA/TRAC prediction. This is expected because at a given fluid pressure and quality, the small-break LOCA break flow model in WCOBRA/TRAC delivers more flow through the ADS-4 flow paths than does NOTRUMP using its critical flow model and the ADS-4 flow path resistance increase methodology. Depressurization to the IRWST actuation pressure occurs more rapidly in WCOBRA/TRAC than in NOTRUMP due to the increased rate of energy removal. The IRWST flow rates upon actuation are compared in Figure 3-10. The core makeup tanks still contain a significant amount of water at the time of IRWST injection in the two analyses. The intact CMT and accumulator flow rate is shown in Figure 3-11.

The ADS-4 predicted liquid and vapor flow rates of the two code simulations are compared in Figures 3-12 to 3-15. The more detailed flow regime models and the small-break LOCA break flow model in WCOBRA/TRAC result in higher flow rates through the ADS-4 flow paths.

Comparison of calculated reactor vessel inventory is shown in Figure 3-16. The earlier IRWST injection for the WCOBRA/TRAC case results in the earlier establishment of a stable vessel inventory, which is being replenished by injection from the CMT and IRWST.

The higher WCOBRA/TRAC flow rate through the ADS-4 flow paths also results in a higher mass flow rate through the core than in the NOTRUMP prediction as shown in Figure 3-17. The higher core cooling flow predicted by WCOBRA/TRAC provides a more dynamic heat transfer environment than in NOTRUMP. In both cases, the heat transfer regime on the fuel rods enables the clad temperatures to remain near the coolant saturation temperature.

3.2.2 Inadvertent ADS Actuation Scenario

The Inadvertent ADS scenario is the minimum venting capability case from the AP1000 DCD. The failure of one ADS-4 valve to open is assumed in both simulations. The WCOBRA/TRAC simulation of the ADS-4 IRWST initiation phase of this scenario is compared with the corresponding NOTRUMP predictions from Section 15.6.5.4B of the AP1000 DCD in this section. The Appendix K-specified ANS 1971 + 20% core decay heat is used in both analyses.

Figure 3-18 presents the WCOBRA/TRAC downcomer pressure prediction of the ADS-4 IRWST initiation phase superimposed on the NOTRUMP result from Section 15.6.5.4B of the AP1000 DCD. The actuation of ADS-4 occurs at 1746 seconds. Opening of the ADS-4 flow paths continues the RCS depressurization from approximately 100 psia down to near containment pressure. The RCS pressure tends to stabilize when the energy being discharged from the RCS approaches the energy from the core decay heat and from metal heat. The NOTRUMP prediction levels off in the rate of depressurization at a

higher pressure than the WCOBRA/TRAC prediction. This is expected because at a given fluid condition, the best estimate break flow model in WCOBRA/TRAC delivers more flow through the ADS-4 flow paths than does NOTRUMP using its critical flow model and the ADS-4 flow path resistance increase methodology. Depressurization to the IRWST actuation pressure occurs more rapidly in WCOBRA/TRAC than in NOTRUMP due to the increased rate of energy removal. The IRWST flow rates upon actuation are compared in Figure 3-19. In the WCOBRA/TRAC analysis the IRWST begins to inject before the core makeup tanks have emptied, so there is no gap in safety injection flow. In contrast, NOTRUMP predicts a period almost 10 minutes in length during which no safety injection water is delivered into the reactor vessel. The CMT injection flow rate is shown in Figure 3-20.

The ADS-4 predicted liquid and vapor flow rates of the two code simulations are compared in Figures 3-21 to 3-24. The more detailed flow regime models and the best estimate break flow model in WCOBRA/TRAC result in higher flow rates through the ADS-4 flow paths.

Comparison of calculated reactor vessel inventory is shown in Figure 3-25. The earlier IRWST injection for the WCOBRA/TRAC case results in an earlier recovery of vessel inventory. In both cases the inventory begins to increase once the RCS pressure stabilizes and as decay heat decreases. Inventory is being replenished by injection from the CMT and/or IRWST. The minimum vessel inventory is approximately the same in the WCOBRA/TRAC and NOTRUMP predictions on Figure 3-25. In Figure 3-25 the NOTRUMP plot is adjusted to account for a 3% volume increase introduced according to the Appendix K methodology.

The higher WCOBRA/TRAC flow rate through the ADS-4 flow paths also results in a higher mass flow rate through the core than in the NOTRUMP prediction as shown in Figure 3-26. The higher core cooling flow predicted by WCOBRA/TRAC provides a more dynamic heat transfer environment than in NOTRUMP. In both cases, the heat transfer regime on the fuel rods enables the clad temperatures to remain near the coolant saturation temperature.

3.3 REFERENCES

1. AP1000 Design Control Document, Westinghouse Electric Company LLC, Revision 2, April 2002.
2. Takeuchi, Kenji, Young, M. Y., and Gagnon, A. F., "Flooding in the Pressurizer Surge Line of AP600 Plant and Analyses of APEX Data," Nuclear Engineering & Design 192 (1999), pp. 45-58.
3. WCOBRA/TRAC User's Manual, Revision 9, September 2001, Westinghouse Electric Company, Proprietary.

a,c

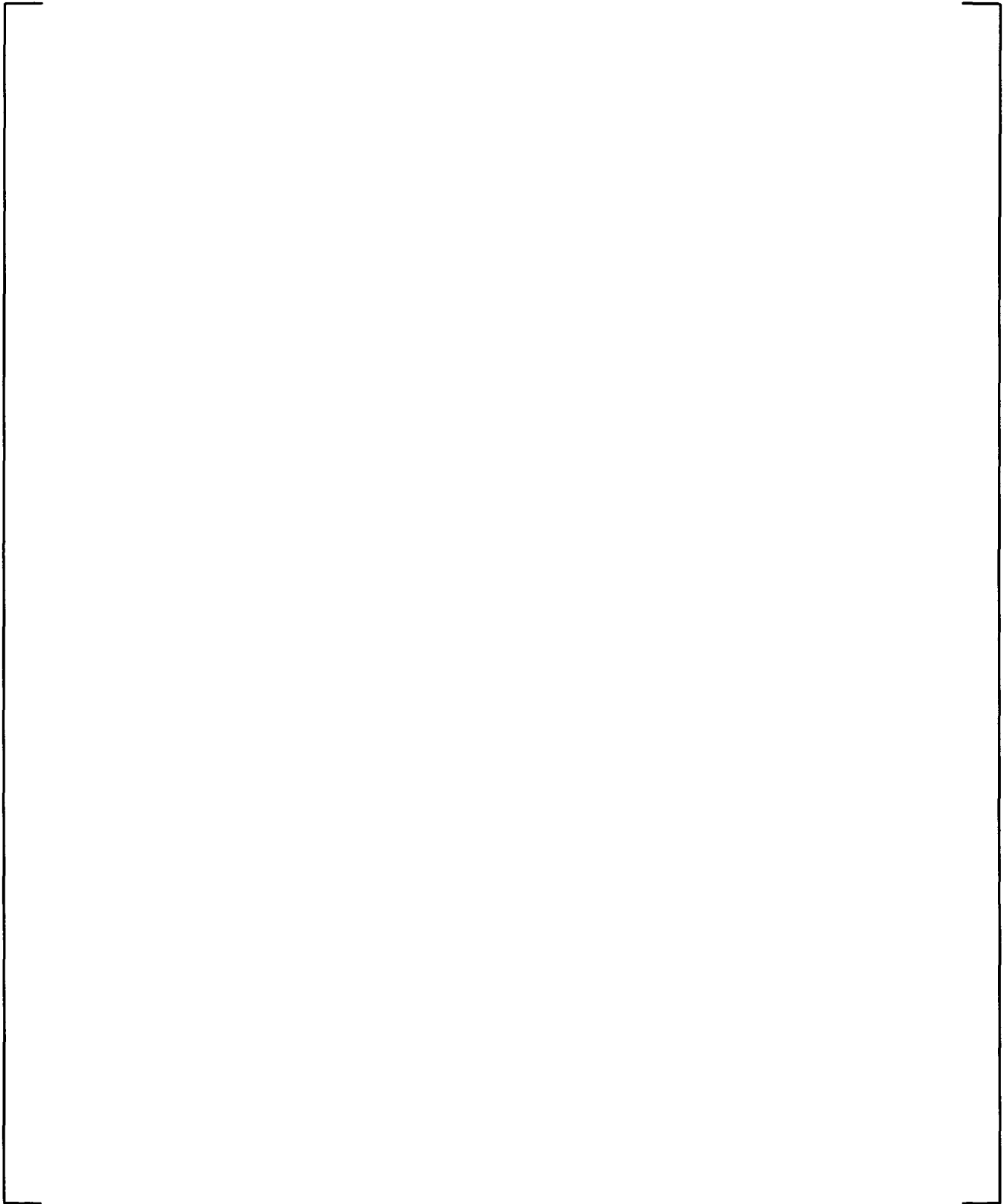


Figure 3-1 AP1000 WCOBRA/TRAC Vessel Model (Front View)

a,c

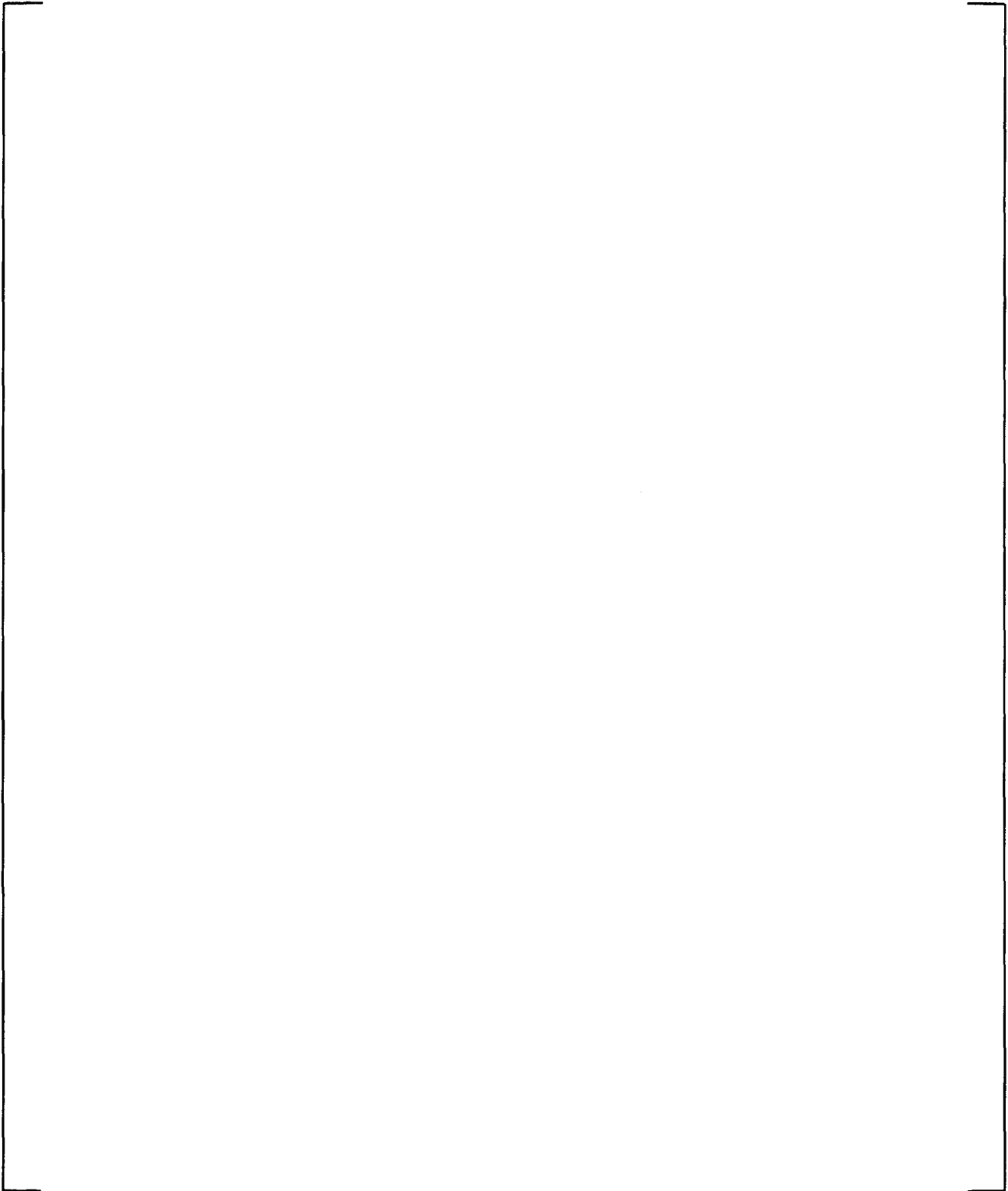


Figure 3-2 AP1000 Vessel Model – Section 1

a,c

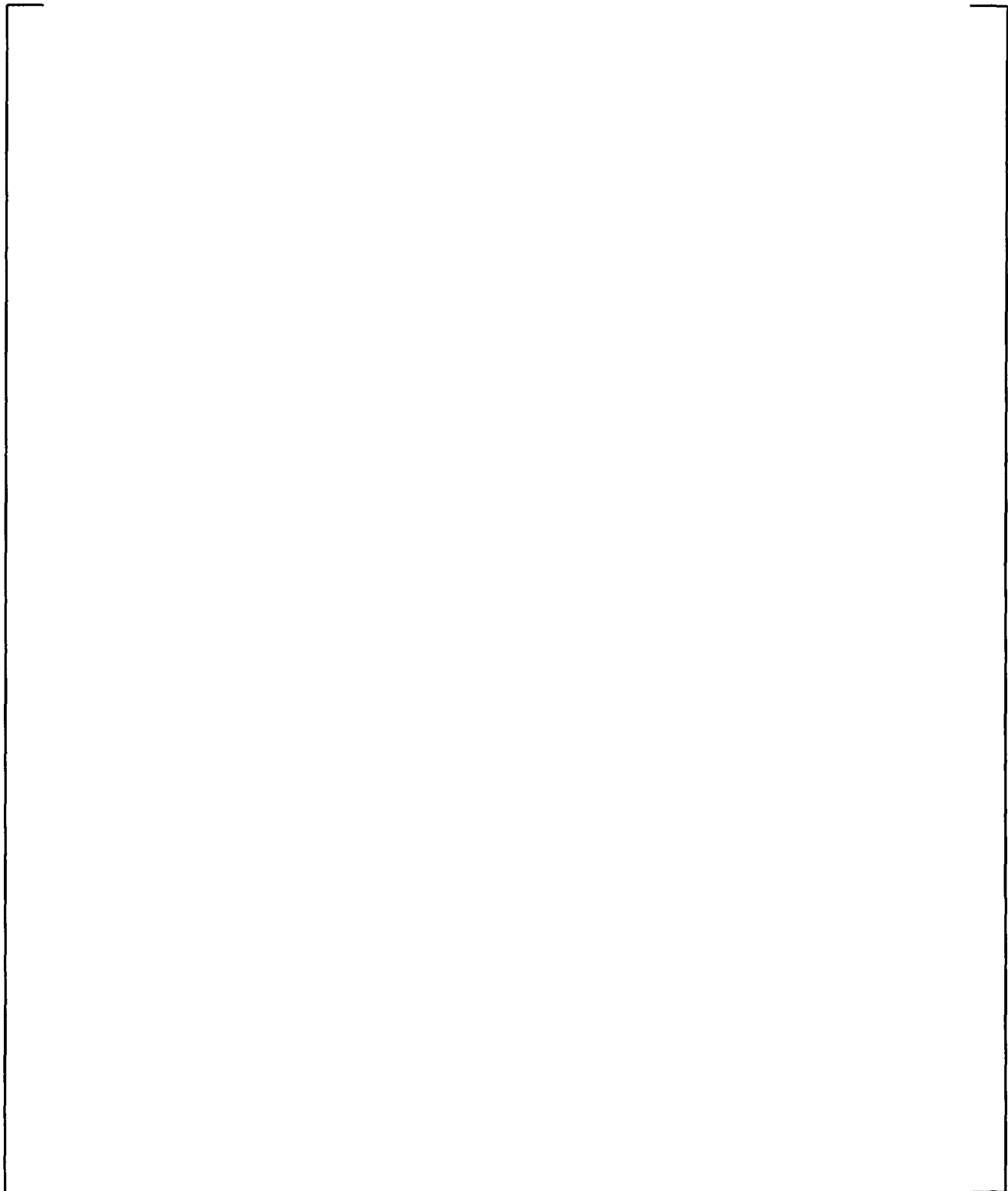


Figure 3-3 AP1000 Vessel Model – Section 2

a.c

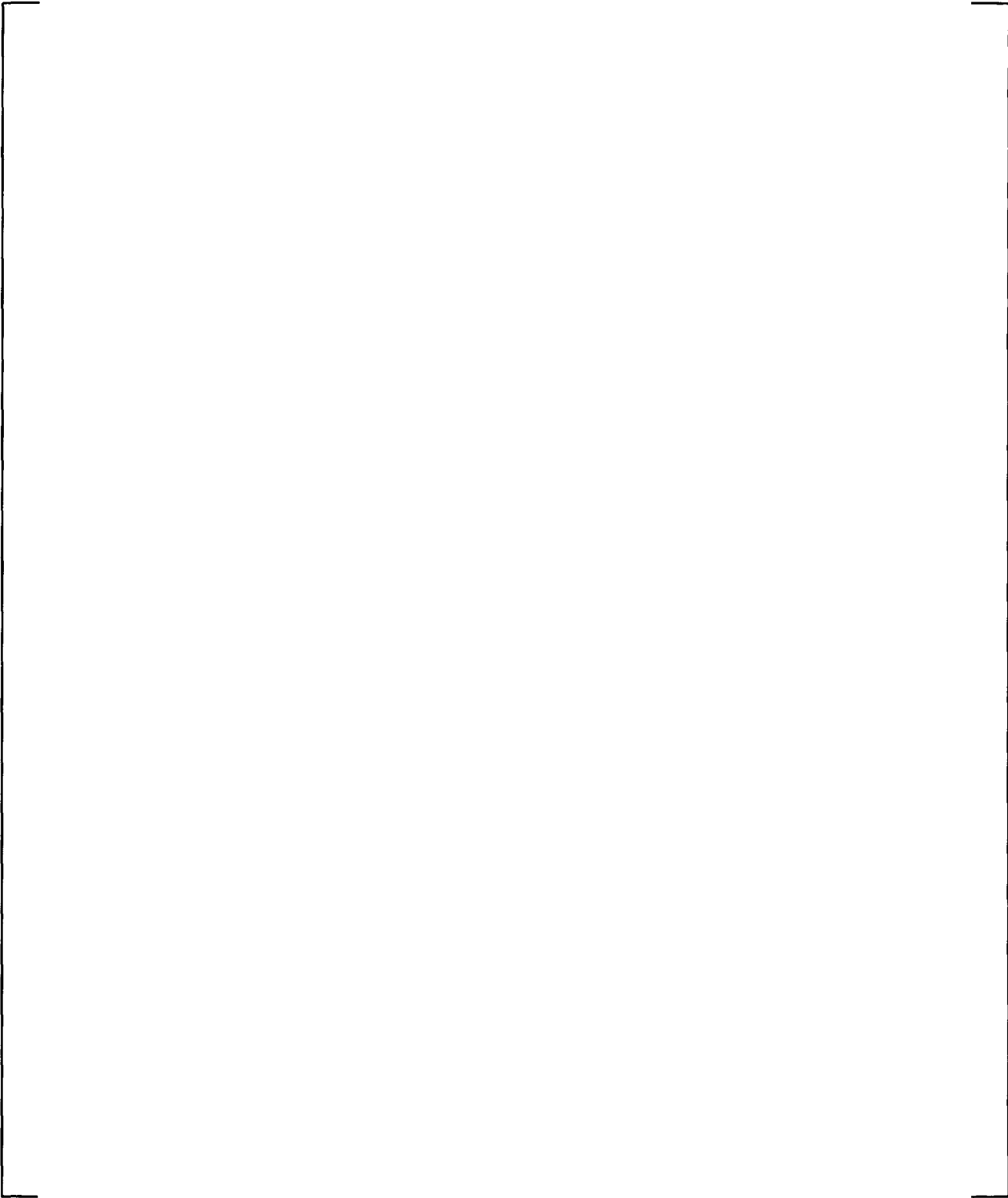


Figure 3-4 AP1000 Vessel Model – Section 3

a,c

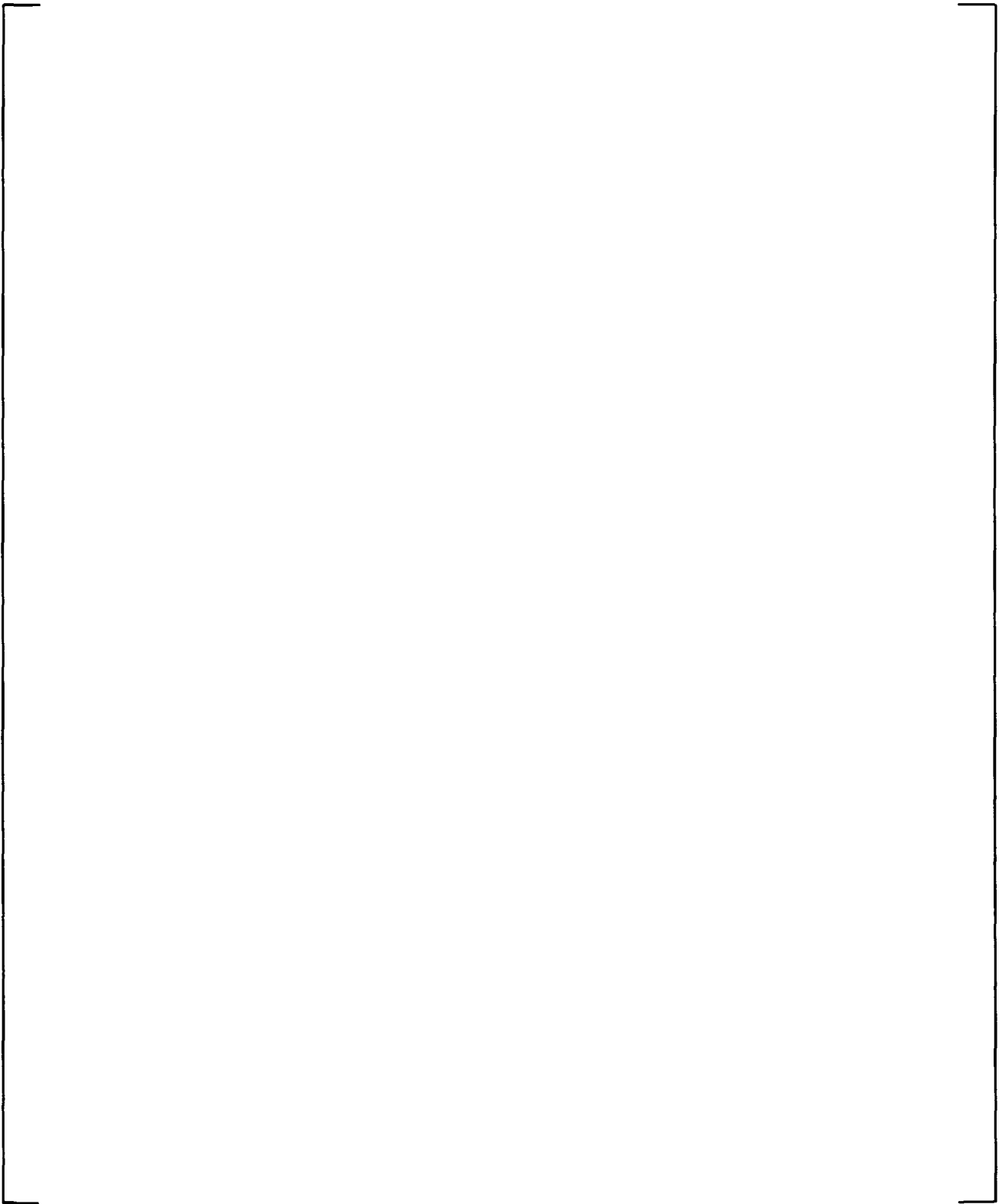


Figure 3-5 AP1000 Vessel Model – Section 4

a,c



Figure 3-6 AP1000 Vessel Model – Section 5

a,c

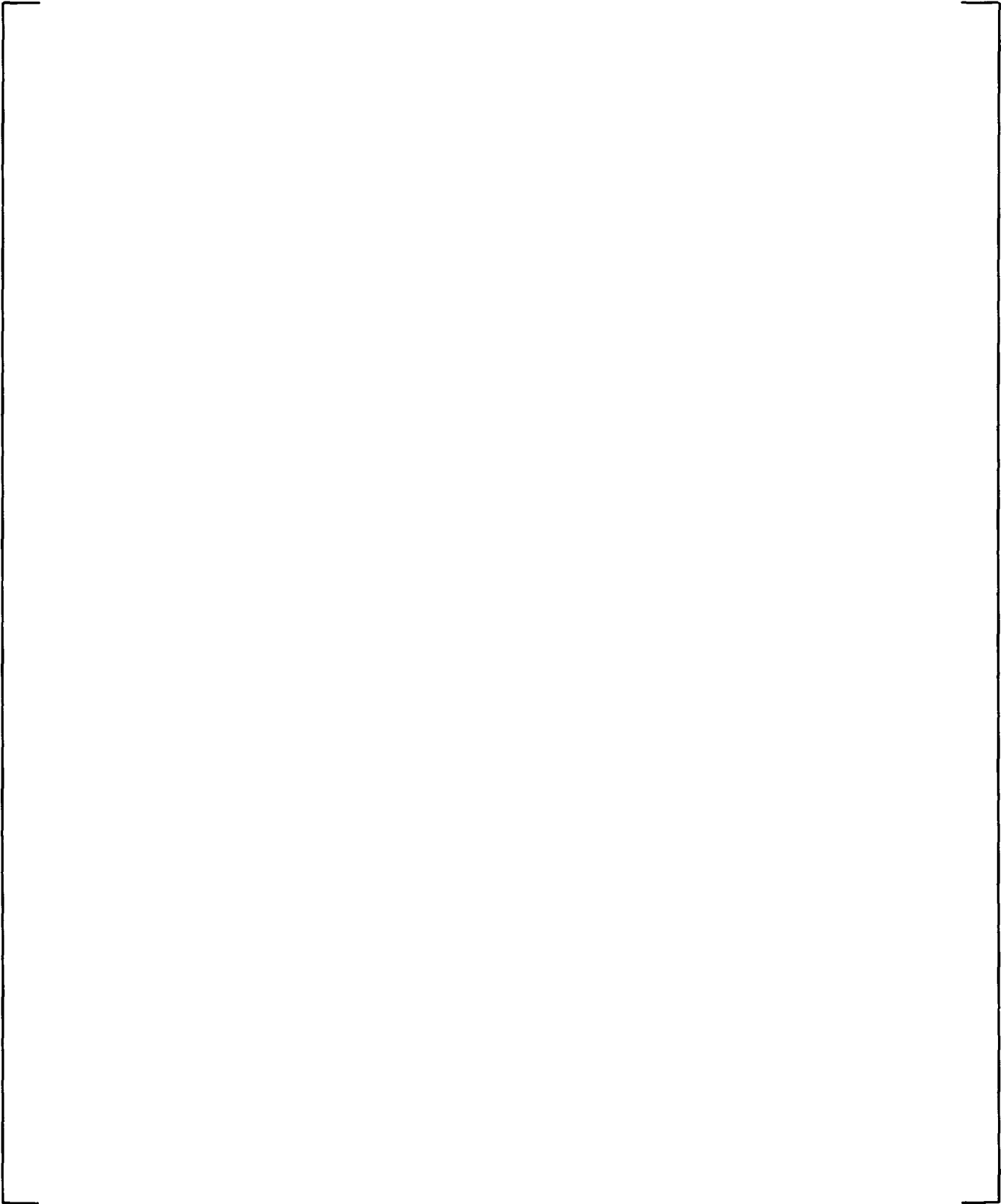


Figure 3-7 AP1000 Vessel Model – Section 6

a,c

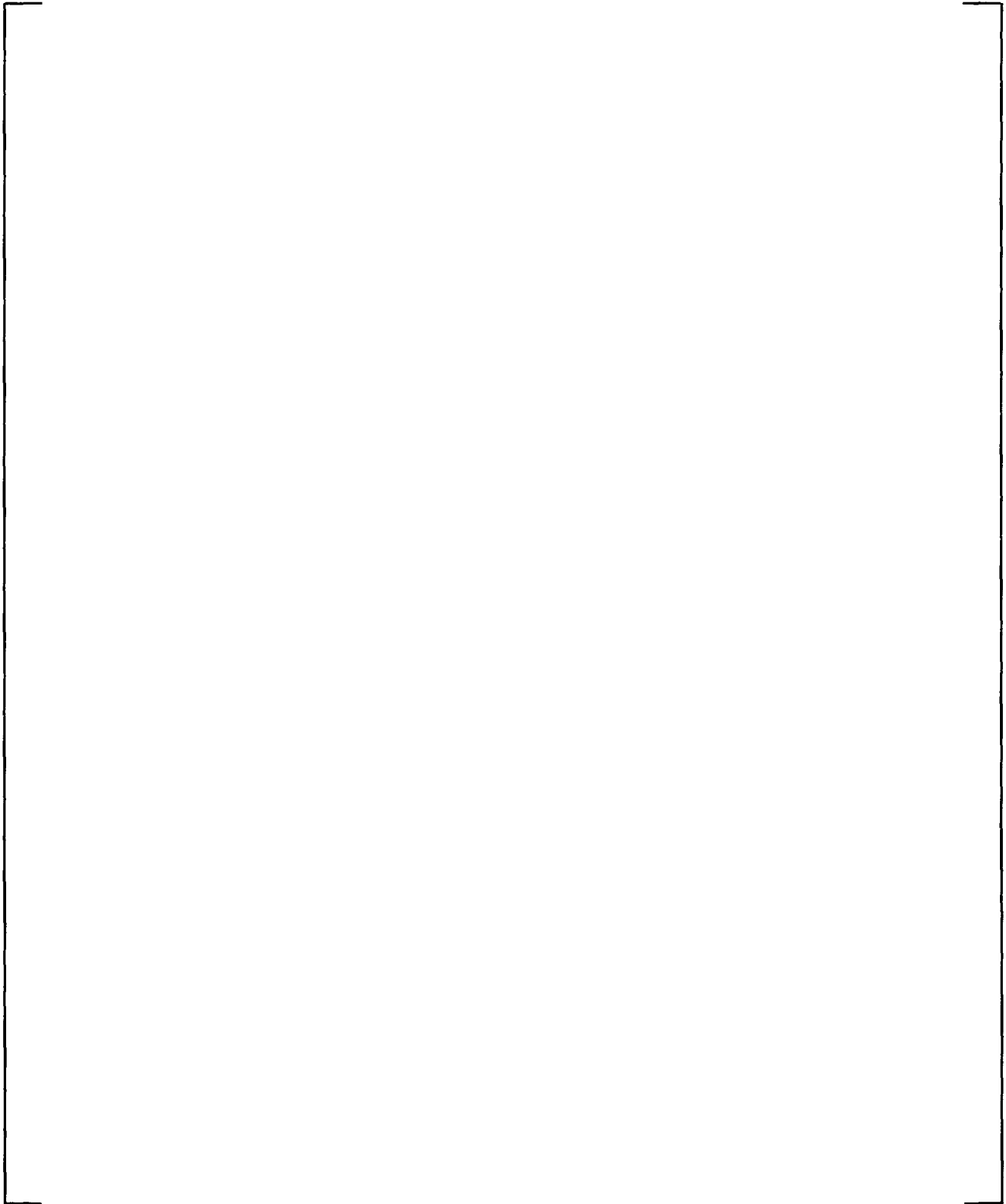


Figure 3-8 AP1000 WCOBRA/TRAC Schematic Diagram

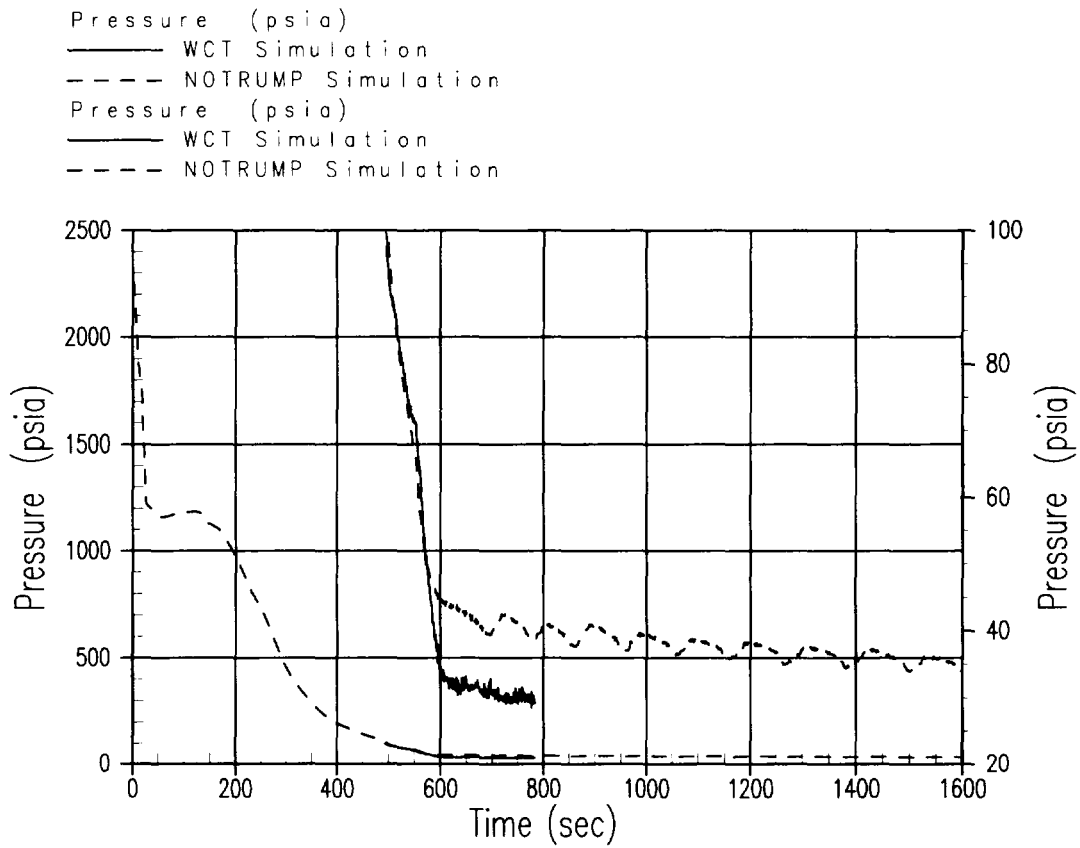


Figure 3-9 AP1000 DEDVI Break Downcomer Pressure

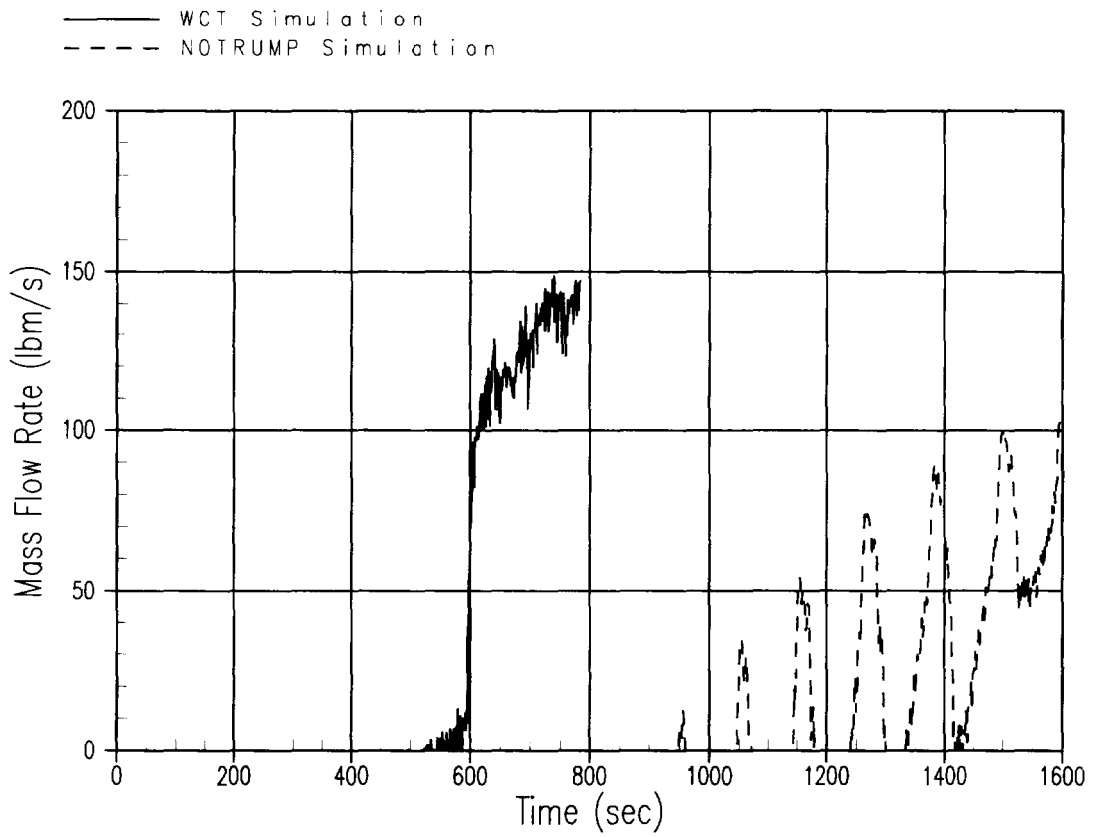


Figure 3-10 AP1000 DEDVI Break IRWST Flow Rate

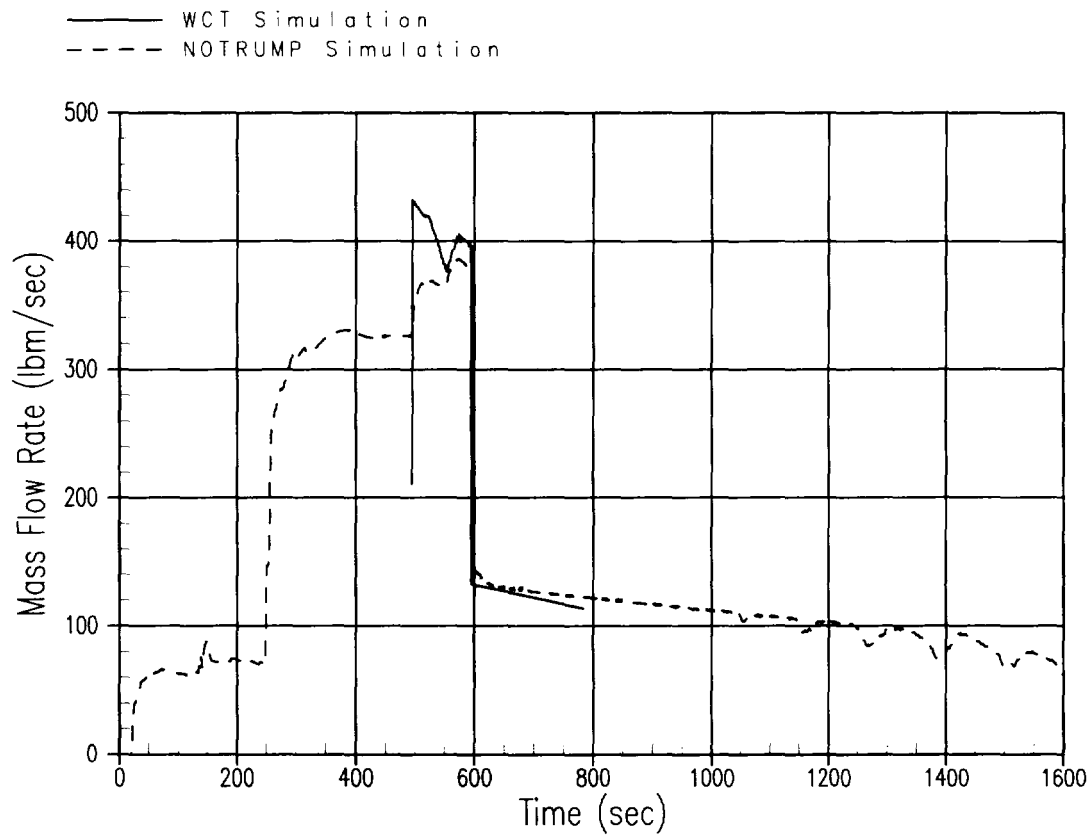


Figure 3-11 AP1000 DEDVI Break CMT and Accumulator Flow Rate

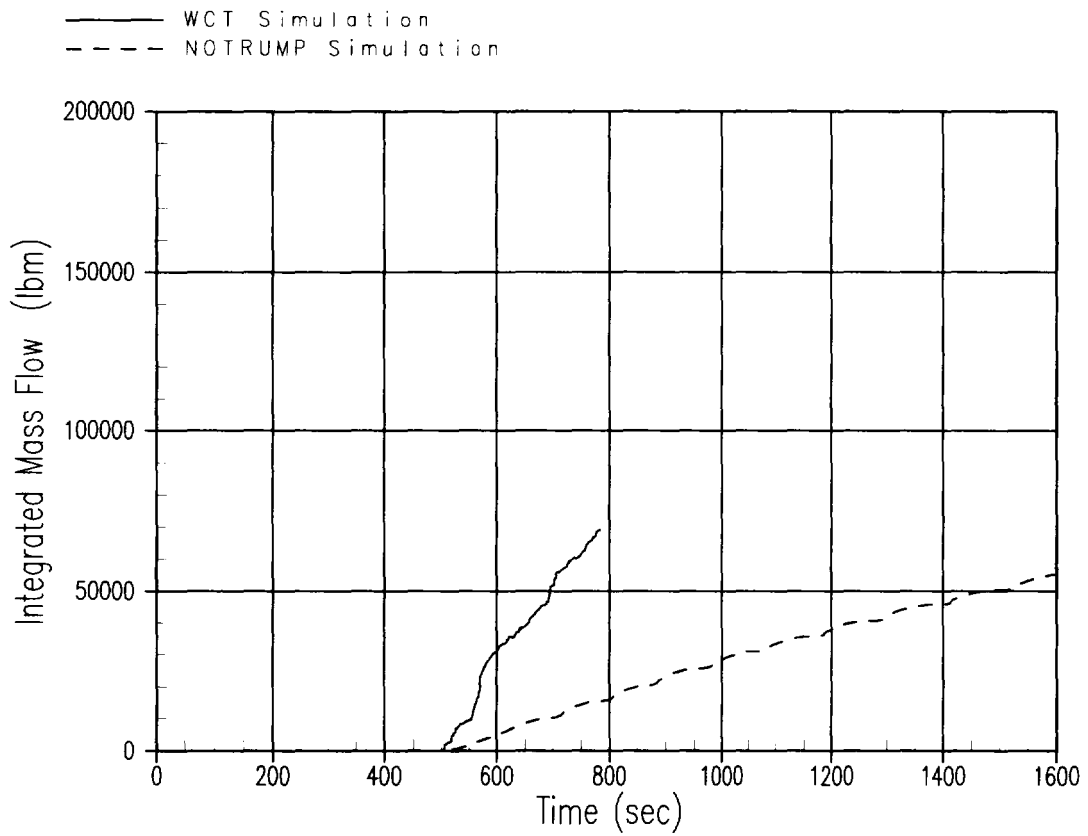


Figure 3-12 AP1000 DEDVI Break Intact Loop ADS-4 - Integrated Liquid Flow

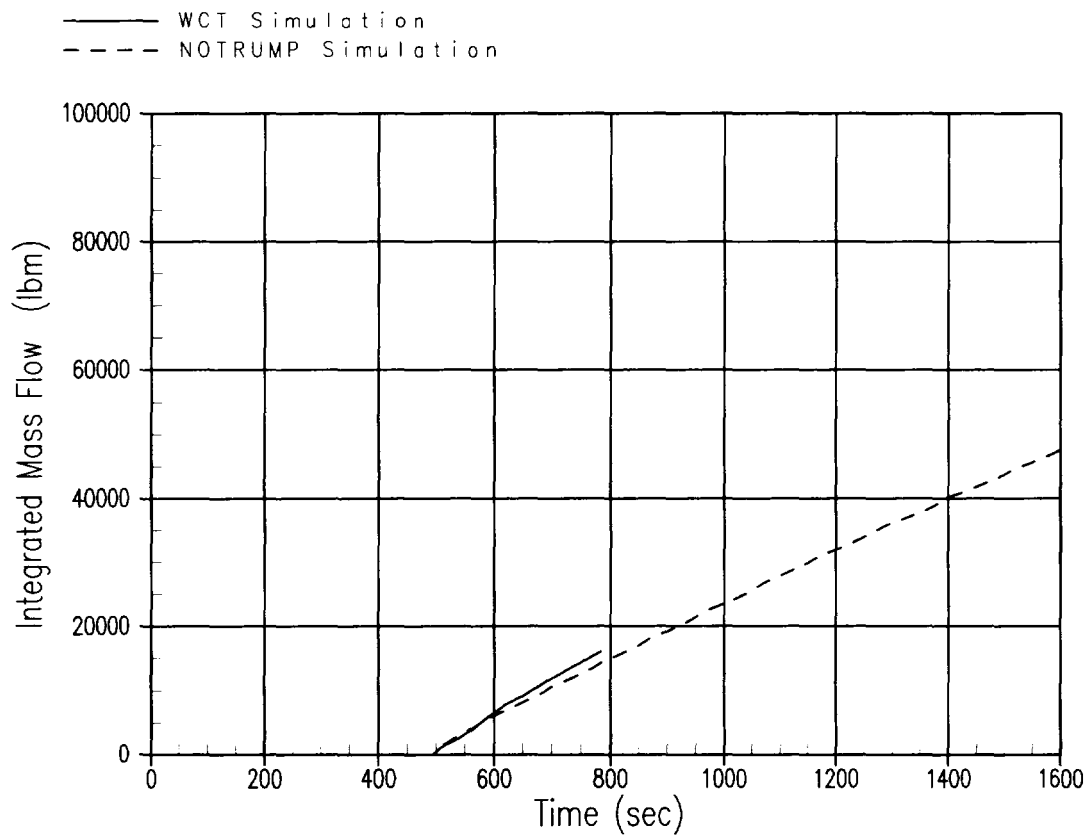


Figure 3-13 AP1000 DEDVI Break Intact Loop ADS-4 – Integrated Vapor Flow

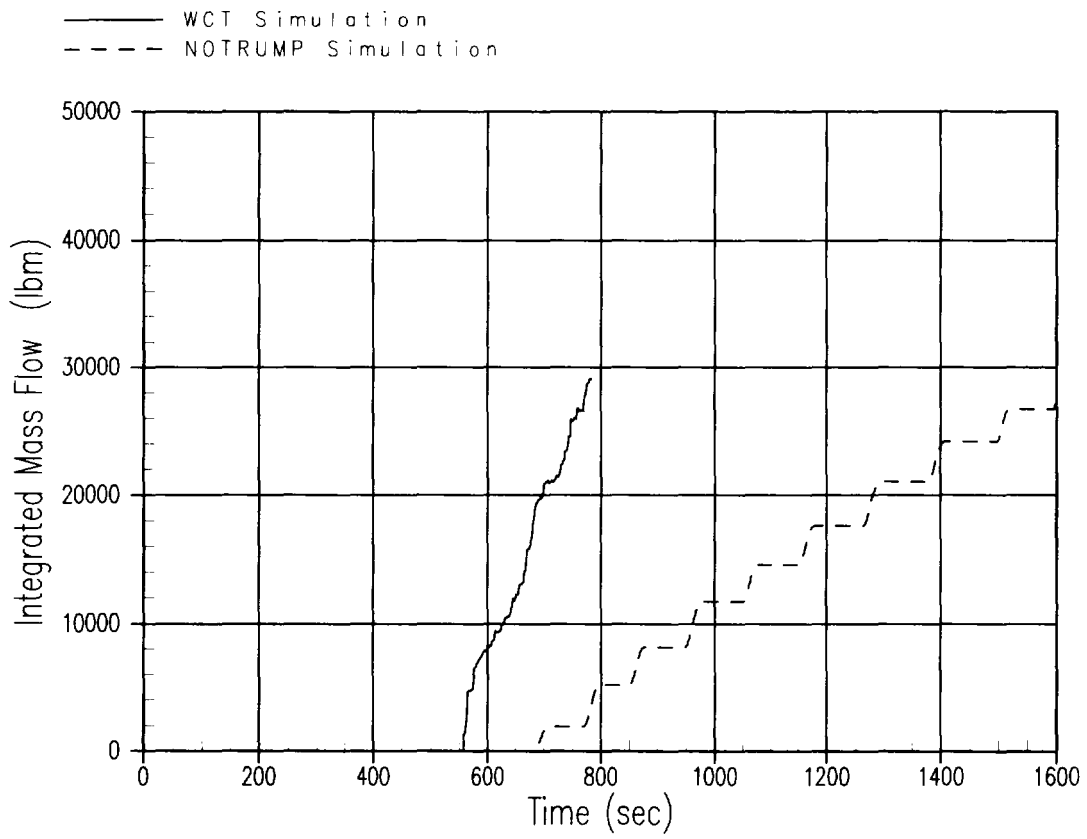


Figure 3-14 AP1000 DEDVI Break Single Failure Loop ADS-4 - Integrated Liquid Flow

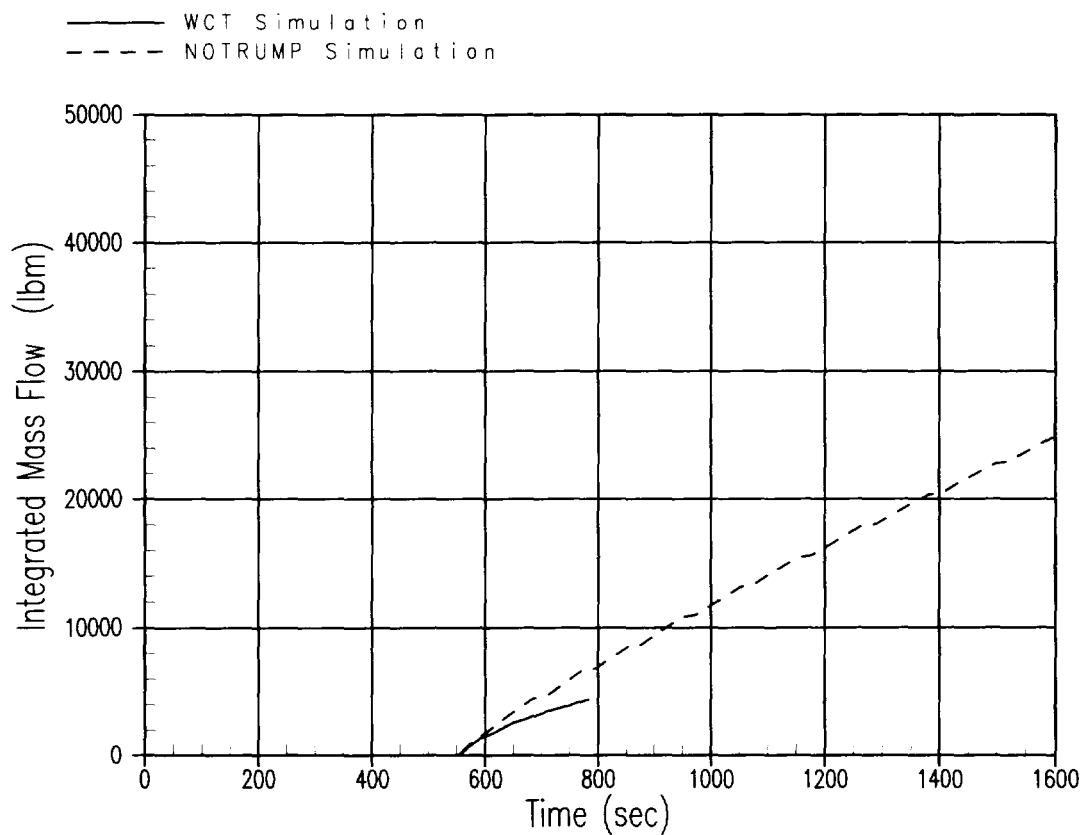


Figure 3-15 AP1000 DEDVI Break Single Failure Loop ADS-4 – Integrated Vapor Flow

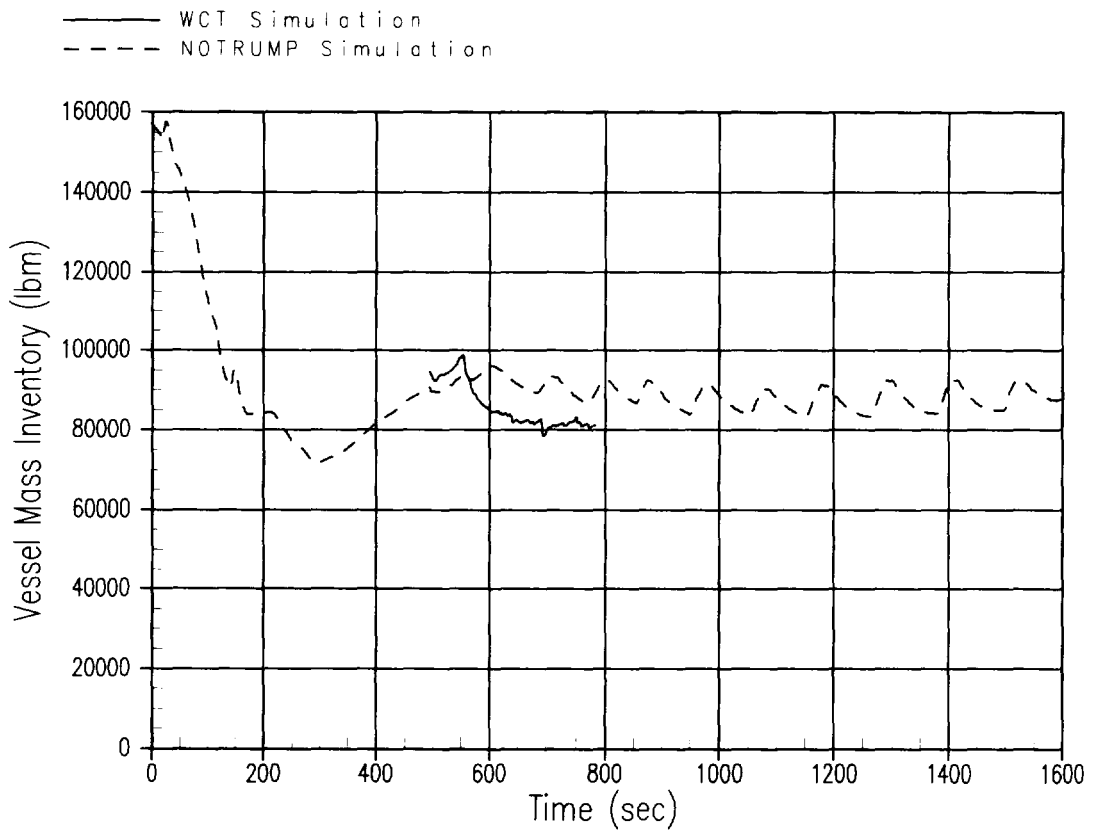


Figure 3-16 AP1000 DEDVI Break Vessel Mass Inventory

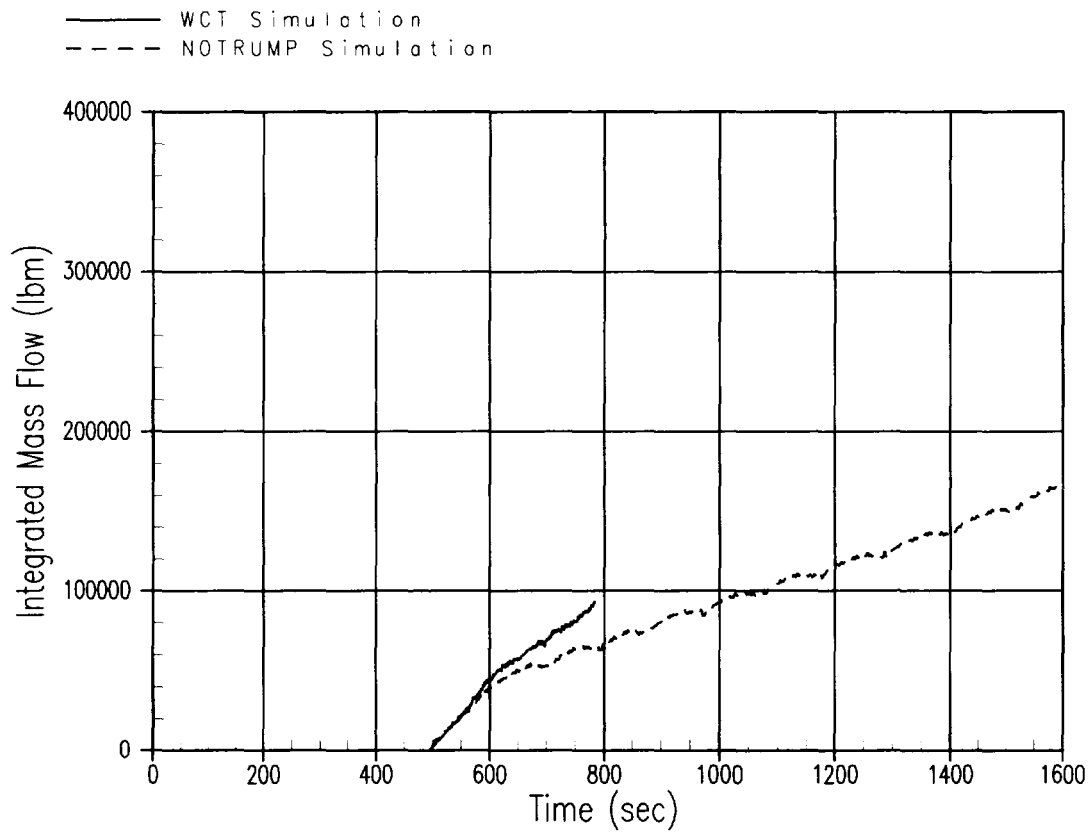


Figure 3-17 AP1000 DEDVI Break Integrated Core Inlet Flow

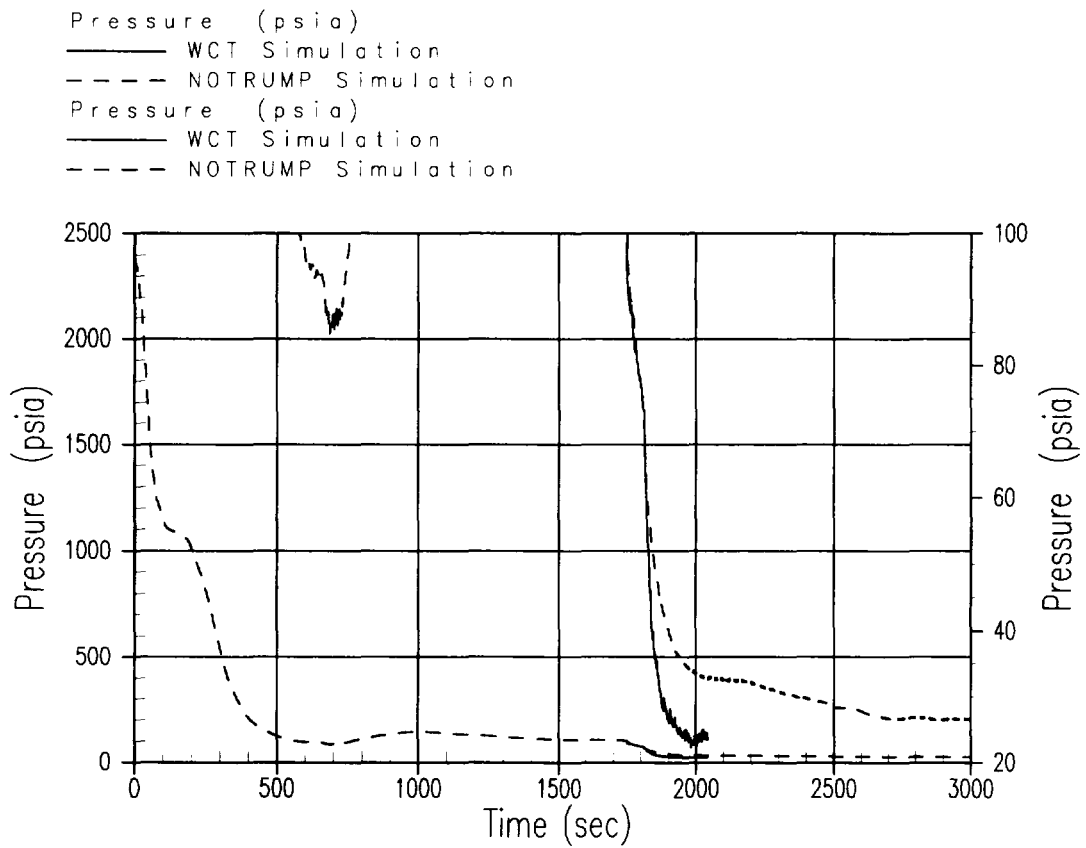


Figure 3-18 AP1000 Inadvertent ADS Actuation Scenario – Downcomer Pressure

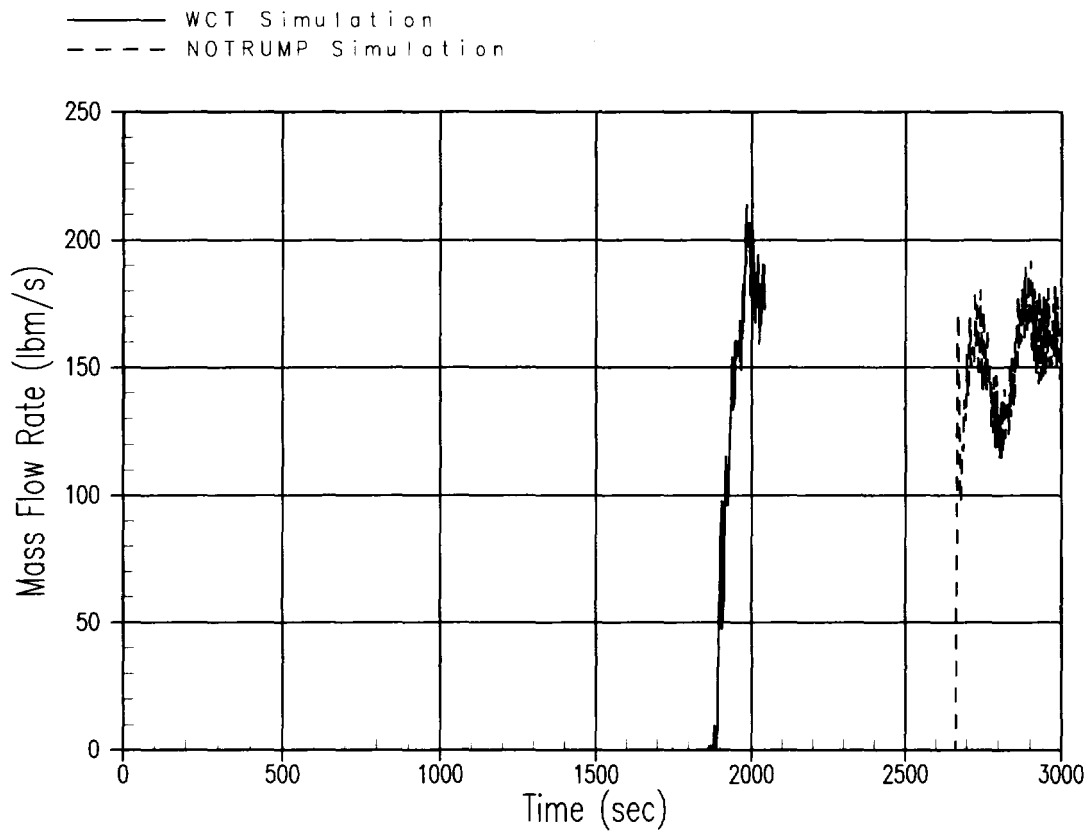


Figure 3-19 AP1000 Inadvertent ADS Actuation Scenario – Total IRWST Injection Flow Rate

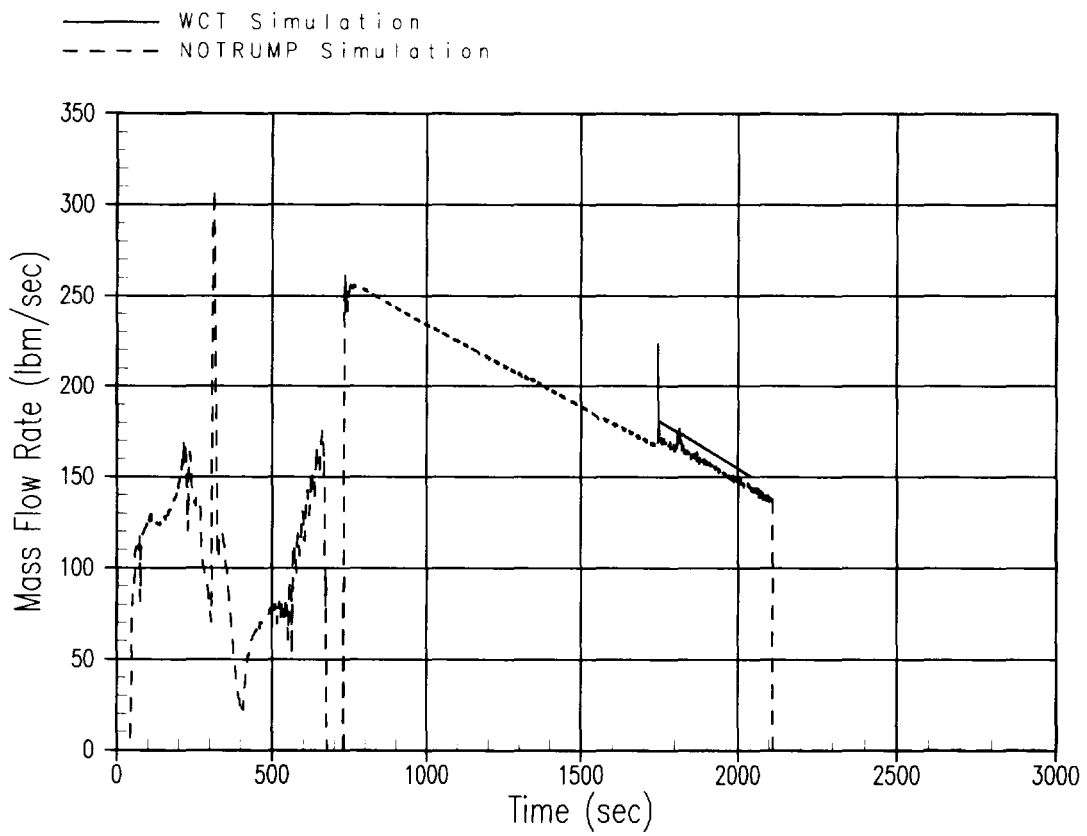


Figure 3-20 AP1000 Inadvertent ADS Actuation Scenario – Total CMT Injection Flow Rate

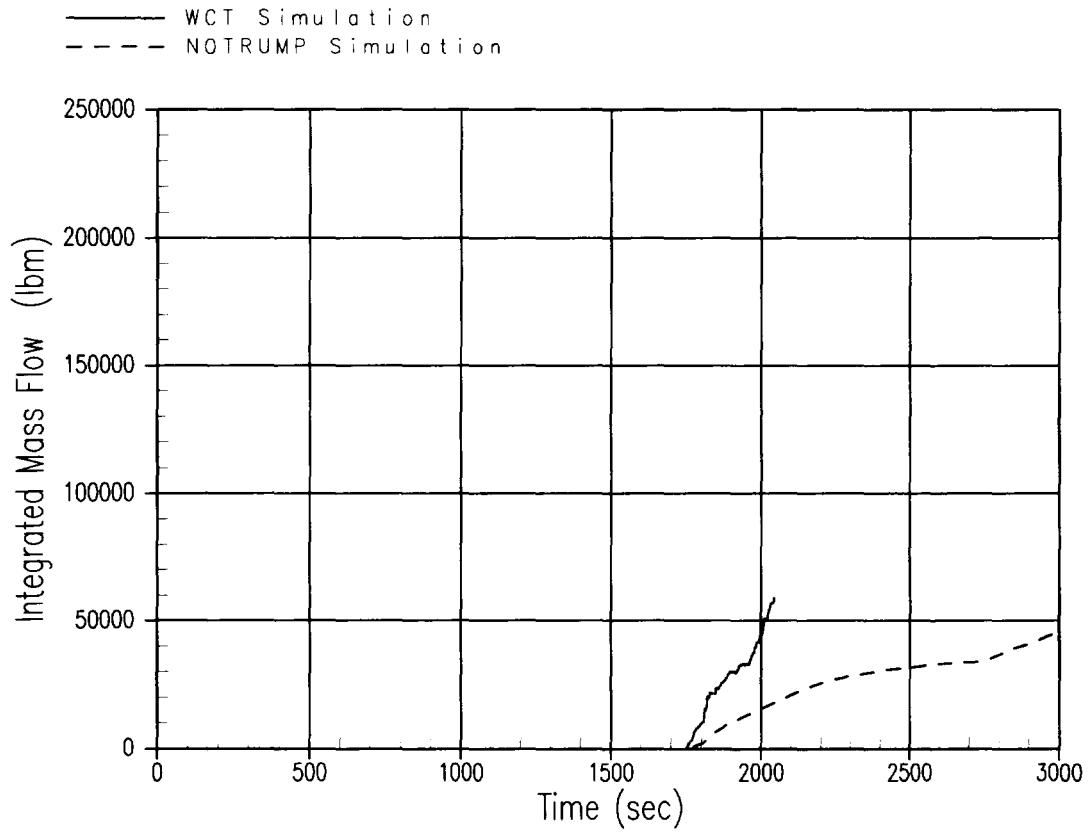


Figure 3-21 AP1000 Inadvertent ADS Actuation Scenario Intact Loop ADS-4 – Integrated Liquid Flow

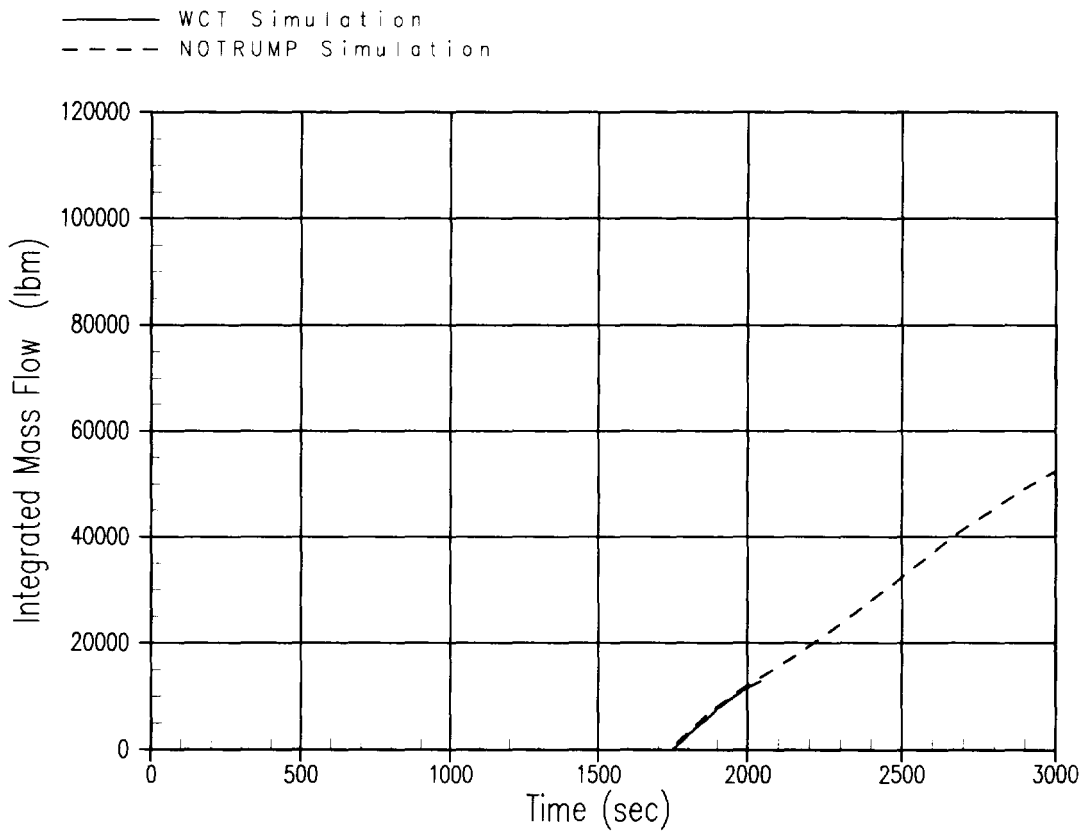


Figure 3-22 AP1000 Inadvertent ADS Actuation Scenario Intact Loop ADS-4 – Integrated Vapor Flow

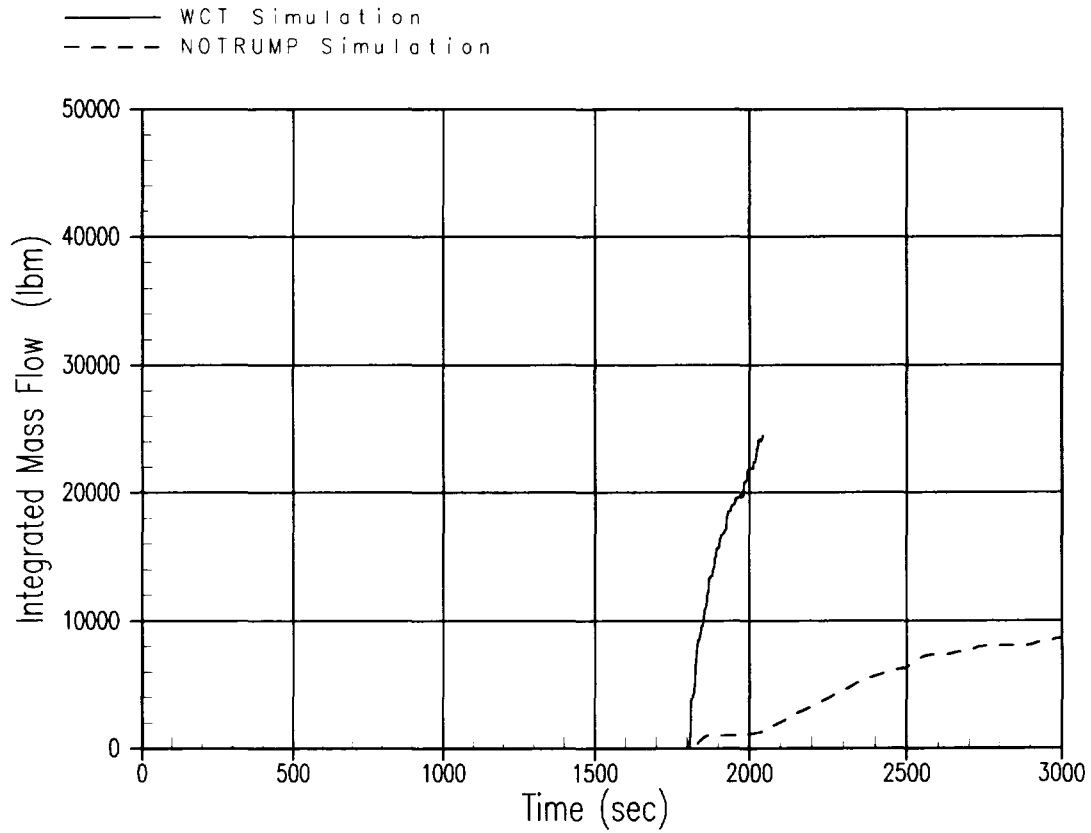


Figure 3-23 AP1000 Inadvertent ADS Actuation Scenario Single Failure Loop ADS-4 – Integrated Liquid Flow

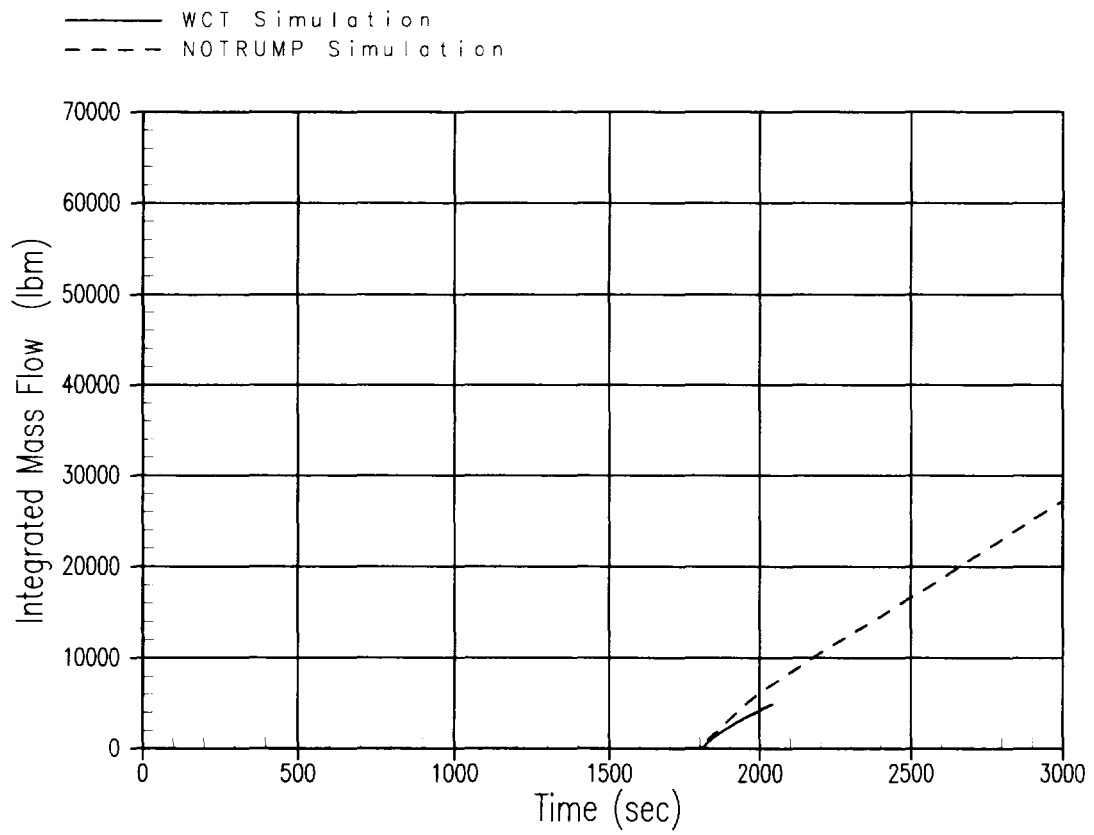


Figure 3-24 AP1000 Inadvertent ADS Actuation Scenario Single Failure Loop ADS-4 – Integrated Vapor Flow

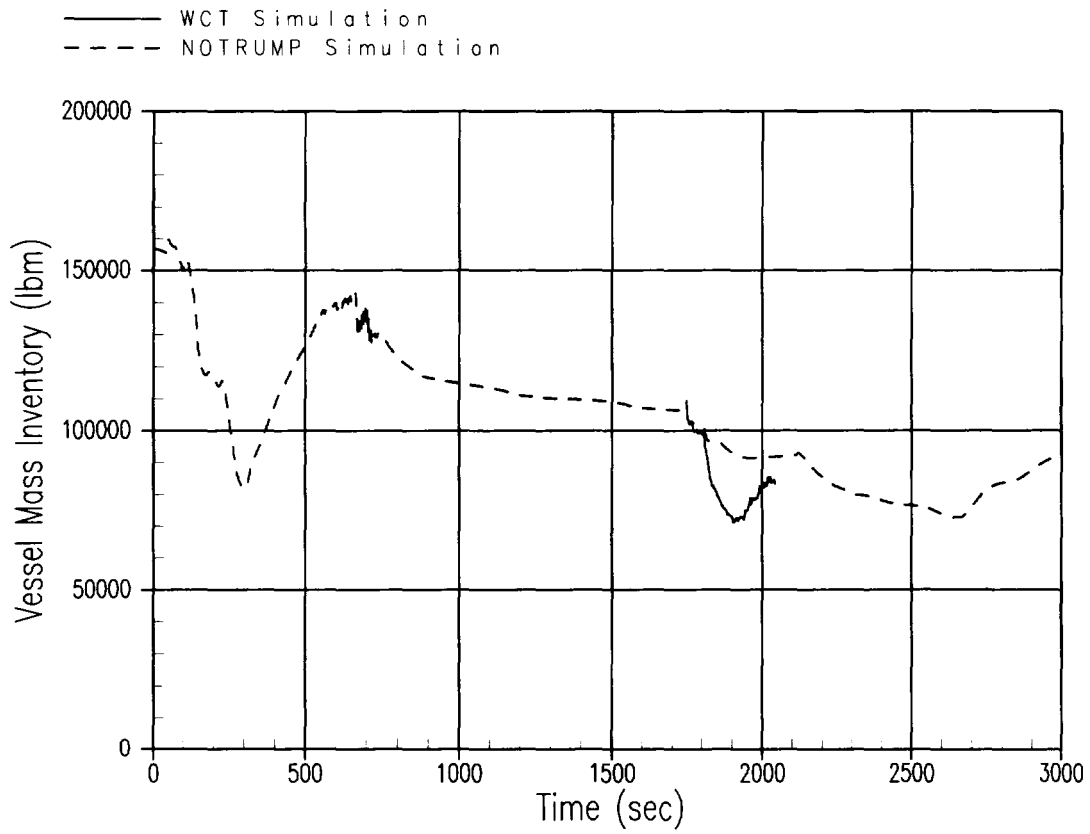


Figure 3-25 AP1000 Inadvertent ADS Actuation Scenario Break Vessel Mass Inventory

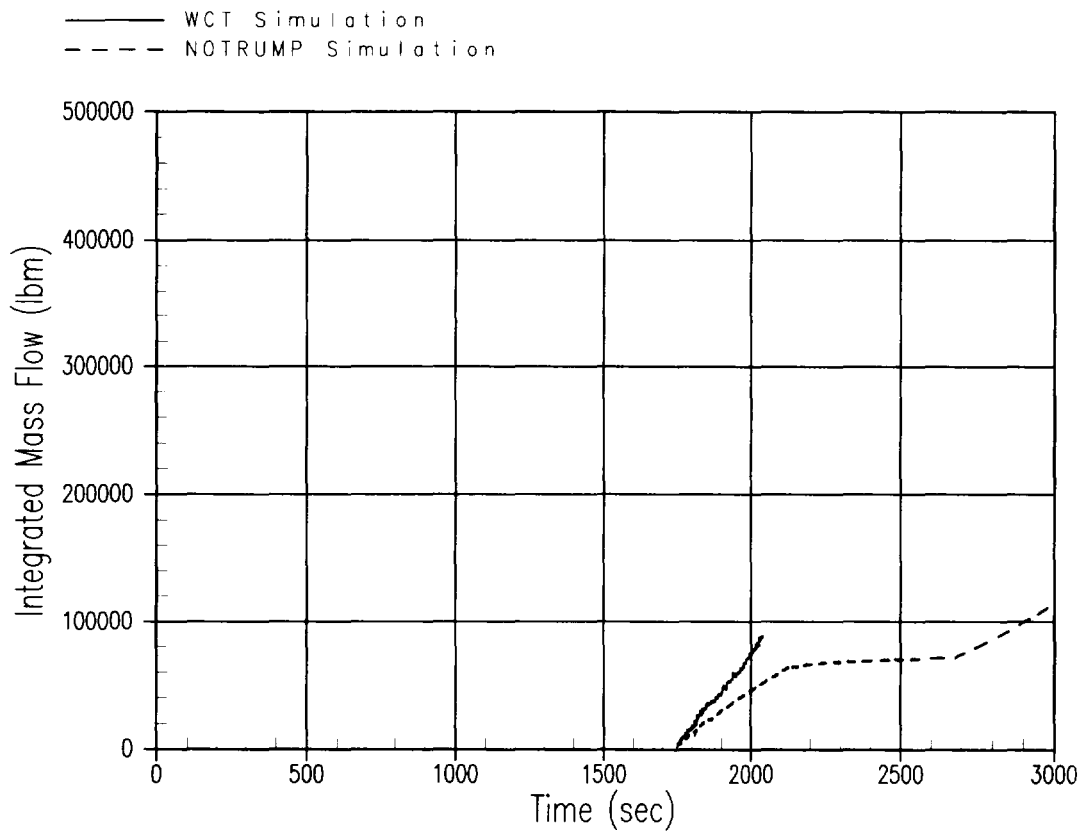


Figure 3-26 AP1000 Inadvertent ADS Actuation Scenario Break Integrated Core Inlet Flow

4 CONCLUSIONS

A version of the WCOBRA/TRAC computer code which contains physically based models for hot leg flow and entrainment phenomena has been created to analyze the AP1000 ADS-4 IRWST initiation phase. The code version has been validated against separate effects test data and against OSU APEX Facility Test SB18. The WCOBRA/TRAC-AP code version is then used to analyze the ADS-4 IRWST initiation phase transients for the DEDVI break and inadvertent ADS actuation AP1000 plant scenarios, using the same methodology as in the test simulations.

Core cooling heat transfer is a function of mass flow rate through the core. During the ADS to IRWST transition the flow through the core is controlled by the ability to remove mass and energy via flow out the ADS vents. WCOBRA/TRAC predicts more flow through the core as expected due to its small-break LOCA break flow modeling. NOTRUMP stabilizes at somewhat higher pressure as the energy being discharged comes into near equilibrium with the decay heat and metal heat.

This comparison of NOTRUMP and WCOBRA/TRAC for the ADS to IRWST transition phase shows that:

- NOTRUMP modeling of ADS venting results in a slower depressurization of the primary system following a SBLOCA in comparison to the prediction with WCOBRA/TRAC.
- The higher pressure in NOTRUMP delays the onset of IRWST injection relative to WCOBRA/TRAC.
- Minimum vessel inventory during the ADS to IRWST transition phase is predicted to occur later for NOTRUMP relative to WCOBRA/TRAC, mainly due to the delayed depressurization in NOTRUMP.
- NOTRUMP and WCOBRA/TRAC both predict core heat transfer rates that maintain clad temperatures near the fluid saturation temperature.

The comparison of NOTRUMP with WCOBRA/TRAC for the limiting SBLOCA events confirms that NOTRUMP can adequately simulate the overall core cooling behavior during the ADS to IRWST transition phase of an AP1000 SBLOCA event. The methodology developed for NOTRUMP for AP600 provides a conservative simulation of ADS-4 venting and the onset of IRWST injection for AP1000.

The NOTRUMP DCD analysis is performed under Appendix K restrictions, including the use of ANS 1971 + 20% core decay heat. Additional conservatism account for plant design uncertainties: the passive safety systems resistances are set at design upper bound values, and the minimum effective critical flow area and maximum flow resistance are used in the ADS flow paths. Overall, the NOTRUMP thermal-hydraulic model predictions of critical flow and ADS-4 flow path pressure drop with the flow resistance penalty included adequately compensate for the lack of detailed momentum flux and liquid entrainment models in the code. The NOTRUMP DCD analysis provides a conservative prediction of the ECCS performance of the AP1000 for postulated small break LOCA events.

Appendix A provides the assessments performed to address the importance of upper plenum and hot leg entrainment on the AP1000 passive safety system performance following a small-break LOCA. Conclusions from these assessments are provided in Appendix A.

APPENDIX A

**ASSESSMENT OF THE EFFECTS OF
ENTRAINMENT IN AP1000 SBLOCA ANALYSIS**

A.1 INTRODUCTION

Westinghouse and the NRC performed a pre-certification review of the AP1000 to determine whether the testing performed in support of AP600 Design Certification are applicable to the AP1000 Design Certification. In addition, the analysis codes that were validated against the AP600 passive safety system tests were reviewed for their applicability to AP1000. The results of this review were documented in NRC letter "Applicability of AP600 Standard Plant Design Analysis Codes, Test Program and Exemptions to the AP1000 Standard Plant Design," dated March 25, 2002.

In this letter, the NRC staff concludes that the tests and analysis codes used to support AP600 Design Certification can be used to support AP1000. In this letter, the staff also identified exceptions to this conclusion that need to be resolved during Design Certification. The most notable of these exceptions is that Westinghouse had not demonstrated that the existing AP600 tests provide data over the range of conditions necessary to validate entrainment models in the NOTRUMP and WCOBRA/TRAC codes that are used for small-break LOCA analyses. This issue is addressed in Appendix A of this report.

A.1.1 Hot Leg Entrainment

In the detailed assessment of the AP1000 scaling assessments provided in WCAP-15613, the staff made the following conclusions:

"Although Westinghouse's bottom-up scaling analysis of entrainment onset showed that the APEX facility is well-scaled for the AP1000 standard plant design, the staff finds that this analysis contains several shortcomings.

- *Westinghouse's scaling analysis is based on an entrainment onset correlation in which the applicability to the AP1000 geometry has not been confirmed. This correlation is founded on experimental data with a small branch line to main pipe diameter ratio (d/D), which may not be appropriate for the AP1000 design because it has a large d/D ratio.*
- *Existing correlations are based on tests performed with small offtake diameter more than 10 times smaller than the main pipe diameter, as summarized by Ardron and Bryce (Reference 17). In the AP1000 design, the ADS-4 branch pipe diameter is 14 inches relative the hot leg diameter of 31 inches, yielding a (d/D) ratio much larger than the AP600 test data.*
- *The general entrainment onset correlation does not account for the effect of viscosity and liquid surface tension, which may affect the liquid entrainment. Correlations that account for these parameters suggest that significant entrainment will occur for the AP1000 design, but will not occur in the tests Westinghouse has used for code validation."*

To address this issue, Westinghouse performed scaling evaluations and sensitivity studies with WCOBRA-TRAC to gain a better understanding of the importance of hot leg entrainment on the performance of the AP1000 passive safety systems following a small-break LOCA.

A.1.2 Upper Plenum Entrainment

In the detailed assessment of the AP1000 scaling assessments provided in WCAP-15613, the staff made the following conclusions:

“The staff also finds upper plenum pool entrainment to be an issue for the AP1000 design.

Experiments in the APEX facility as well as in simulations of the AP600 design showed that the double-ended guillotine break (DEGB) of one of the DVI lines and a 10-inch cold leg break could lead to the minimum vessel inventory or core uncover. Entrainment of liquid from the upper plenum will be significant, and will be more important in the AP1000 design than in the AP600 design. RES considered bottom-up scaling of upper plenum entrainment. Pool entrainment is a complex process that is highly dependent on the gas velocity bubbling through the pool, and the height to which droplets and other entrained liquid must be elevated to exit the vessel.

The AP1000 core power is 75 percent higher than in the AP600 design, but the upper plenum design is nearly identical. The entrainment is often defined as the ratio of the droplet upward mass flux to the gas mass flux:

$$E_{fg} = \rho_f J_{fe} / (\rho_g J_g)$$

Where ρ_f and ρ_g are liquid and gas phase densities, J_g is the gas superficial velocity, and J_{fe} is the entrained phase superficial velocity.

Expressions for E_{fg} show the functional dependence:

$$E_{fg} \propto (J_g)^n$$

The exponent n is generally 3 or higher. Assuming pressure similitude and preserving the dimensionless height ratio, the AP1000 upper plenum pool entrainment can be expected to be at least 1.75³ or 5.36 times as large as that in the AP600 design. Consideration of experimental tests scaled to the AP600 design power levels leads to the conclusion that the AP1000 upper plenum entrainment is significantly higher than entrainment in the integral-effects tests.

To address this issue, Westinghouse performed sensitivity studies and comparisons of the WCOBRA-TRAC predictions of entrainment to the known entrainment correlations. These studies were performed to gain a better understanding of the importance of upper plenum entrainment on the performance of the AP1000 passive safety systems following a small-break LOCA.

A.2 SCALING ASSESSMENT OF ENTRAINMENT

Liquid entrainment in the AP1000 vessel following ADS-4 actuation consists of two mechanisms:

- Entrainment of liquid in the bottom of the hot leg from steam flowing from the upper plenum to the ADS-4. This condition applies when the liquid level in the vessel is at or above the bottom of the hot leg.
- Entrainment of liquid in the upper plenum resulting from steam flow through a pool with a defined free surface. This entrainment mechanism is dominant when the liquid level in the vessel is below the bottom of the hot leg.

A.2.1 Hot Leg Entrainment Scaling

In WCAP-15613 (Reference 1), Westinghouse showed that liquid entrainment in the hot leg was properly scaled from the standpoint of both the flow regime and the onset of entrainment.

Flow Regime

Froude number scaling between AP1000 and OSU tests was acceptable

$$(\pi_{Fr})_R = j_g / \sqrt{gd} * [\rho_g / \Delta\rho] \quad (A.2-1)$$

where:

- j_g is the steam velocity
- g is the gravitational constant
- d is the pipe diameter
- ρ_g is the vapor density
- $\Delta\rho$ is the difference between the liquid and vapor density

Assuming that there is pressure similitude between the test and the plant, and relating the core power to the steam velocity,

$$(\pi_{Fr})_R = [q_{core} / d_{HL}^{5/2}]_R \quad (A.2-2)$$

where:

- q_{core} is the core power
- d_{HL} is the hot leg pipe diameter

The scaling ratio for the Froude Number is:

$$(\pi_{Fr})_R = [\quad]^{a,b,c}$$

between AP1000 and OSU, which is considered acceptable.

Entrainment Inception

Scaling of parameters important to the inception of entrainment from the hot leg into ADS-4 results in the following relationship

$$(\pi_{Ent})_R = [q_{core} / (d_{ADS4-inlet}^{1/2} * d_{HL}^2)]_R \tag{A.2-3}$$

where:

$d_{ADS4-inlet}$ is the diameter of the ADS-4 inlet piping

The scaling of this entrainment inception number is

$$[\quad]^{a,b,c}$$

between AP1000 and OSU, which is considered acceptable.

Based on these results, it was concluded that the tests were adequately scaled for both flow regime and entrainment onset.

Subsequent review by the staff indicated that the entrainment correlation used in WCOBRA/TRAC is based on experiments with geometry outside the range of AP1000. These tests consisted of a small standpipe atop a larger horizontal pipe containing a separated liquid level. The ratio of the diameter of the small pipe to the larger pipe was on the order of 0.1. The ratio of the diameters for AP1000 is nearer to 0.5.

The correlation used in WCOBRA/TRAC for hot leg entrainment is based on the best available test data (Ardron and Bryce, Reference 3), even though the geometry tested is not the same as AP1000. In WCOBRA/TRAC, the entrainment onset in the hot leg is determined according to the work first performed by Craya (Reference 4) for discharge to a point sink. Soliman and Sims (Reference 5) extended the work of Craya to consider the onset of liquid entrainment for discharge of a stratified mixture through a side orifice of finite diameter. Their model indicated that the ratio of the critical height for the onset of entrainment (z), to offtake diameter (d) is uniquely dependent on the Froude number, irrespective of the value of d. If the (z/d) value is not dependent on the value of d, then the geometry of the test facilities is not of primary importance.

For high values of Froude number (≥ 30), the Soliman/Sims values of (z/d) agree within 1% of Craya's predictions. Soliman and Sims present a comparison of both theirs and Craya's predictions for the experimental data of Armstrong et al. (Reference 6). At the Froude number values for flow into the two ADS-4 flow paths of the AP1000, which are typically in the range of 2 to 4, the difference between the

two predictions is shown to be less than 10%, with the data in between the two predictions. At a Froude number of 3.5 the difference between the data and the Craya prediction is only approximately 1%. Therefore, the approach is judged to be reasonable for AP1000 plant analysis.

Hot leg entrainment can only occur when there is a water level in the hot legs. This condition is indicative of a large margin to core uncover.

A.2.2 Upper Plenum Entrainment Scaling

To demonstrate scaling of the entrainment in the upper plenum, the pool entrainment correlation by Kataoka-Ishii (Reference 2) is used. This correlation is discussed in detail in Section A.3, and determines the liquid droplets that are carried upward, as a result of steam bubbling through a pool at a given velocity. The correlation shows that the entrainment is highly dependent on the distance, h , that the liquid droplets are carried above the pool surface. For the case of the upper plenum, h is defined as the distance from the pool surface to the bottom of the hot leg.

The correlation is used to calculate the entrainment ratio, E_{fg} , which is defined as:

$$E_{fg} = \rho_f j_{fe} / (\rho_g j_g) \quad (\text{A.2-4})$$

where:

- ρ_f is the liquid phase density
- ρ_g is the vapor phase density
- j_g is the vapor velocity
- j_{fe} is the entrained liquid velocity

The correlation is divided into three regions, depending on h :

- **Near Surface Region**

Entrainment ratio, E_{fg} , depends only on the ratio of the densities. Since, at the time of ADS-4 actuation, both OSU and SPES-2 were sufficiently scaled with respect to pressure, pool entrainment is adequately scaled for the condition where the pool surface is at or just below the level of the hot leg. Throughout this region, the entrainment rate is constant as the distance above the pool is increased. For AP1000, this distance was determined to be approximately 0.15 m (see Section A.3).

- **Momentum Controlled Region**

Since the velocities in the upper plenum are below the critical counter current flow limit, momentum-controlled entrainment can be applied to the upper plenum region. Entrainment ratio, E_{fg} , depends on the thermodynamic properties of the liquid and vapor phases, as well as the

distance from the pool surface, h , and the vapor velocity, j_g , which is proportional to the core power. The functional relationship of E_{fg} is given by:

$$E_{fg} \propto (j_g / h)^n \quad (\text{A.2-5})$$

For the high gas flux regime typical of AP1000, n ranges from 2 to 7. Reference 2 shows that the entrainment rate in this region is bounded by the value calculated for the near surface region, and drops orders of magnitude as h increases. For AP1000, this region is applied when the pool surface is between 0.15 m (the limit of the near surface region) and 0.5 m below the bottom of the hot leg. Although higher core power levels for AP1000 effects the magnitude of the entrainment calculated in this region, the decrease in the magnitude of the entrainment as h is increased offsets the importance of this phenomenon for these conditions.

- **Deposition Controlled Region**

Entrainment ratio, E_{fg} , depends on the distance from the pool surface, h , to a much greater degree. For this region, the entrainment rate is bounded by the lower bound of the momentum controlled region and falls several orders of magnitude as h is increased. For AP1000, this region is applied when the pool surface is between 0.5 m below the bottom of the hot leg and the top of the core, which is 1.43 m below the bottom of the hot leg. As with the momentum controlled region, the very small magnitude of the entrainment in this region further reduces the importance of this phenomena for these conditions.

A.2.3 Conclusions

The following conclusions can be reached:

- Entrainment in the hot leg is well scaled from the standpoint of the flow regime (Froude number) and the onset of entrainment.
- While the entrainment correlation in WCOBRA/TRAC is based on tests where the geometry is different from AP1000, the correlation acceptably calculates the entrainment rate in the hot leg.
- Hot leg entrainment can only occur when there is a water level in the hot legs. This condition is indicative of a large margin to core uncover.
- When the level in the upper plenum is at or just below the bottom of the hot leg, the Kataoka-Ishii pool entrainment model predicts an entrainment ratio (E_{fg}) that depends on the local thermodynamic conditions. For these conditions, the tests are well scaled at the time of ADS-4 actuation.
- When the level in the upper plenum is below the “near surface region” as described by Kataoka-Ishii, the entrainment rate depends strongly on the distance between the pool surface and the bottom of the hot legs. Thus, the magnitude of the entrainment falls rapidly as this distance is increased.

A.2.4 References

1. WCAP-15613, "AP1000 PIRT and Scaling Assessment," July 2001.
2. Kataoka, I. and Ishii, M., "Mechanistic Modeling and Correlations for Pool Entrainment Phenomenon," NUREG/CR-3304, 1983.
3. Ardron, K. H. and Bryce, W. M., "Assessment of Horizontal Stratification Entrainment Model in RELAP5/MOD2 by Comparison with Separate Effects Experiments," Nuclear Engineering and Design, Vol. 122, pp. 263-271, 1990.
4. Craya, A., "Theoretical Research on the Flow of Non-homogeneous Fluids," La Houille Blanche, pp. 44-55, 1949.
5. Soliman, H. M. and Sims, G. E., "Theoretical Analysis of the Onset of Liquid Entrainment for Orifices of Finite Diameter," Int. J. Multiphase Flow, Vol. 18, No. 2, pp. 229-235, 1992.
6. Armstrong, K. F. et al., "Theoretical and Experimental Study of the Onset of Liquid Entrainment During Dual Discharge from Large Reservoirs," Int. J. Multiphase Flow, Vol. 18, pp. 217-227.

A.3 EFFECT OF ENTRAINMENT IN THE AP1000 UPPER PLENUM FOLLOWING LOCA EVENTS

The purpose of this calculation is to quantify the effect of liquid entrainment in the AP1000 upper plenum following a LOCA. The WCOBRA/TRAC computer code was used to simulate a direct vessel injection (DVI) line break and an inadvertent ADS actuation. Both of these events eventually result in the RCS being depressurized, first by the break, then by the first three stages of the ADS, and, finally, by the ADS Stage 4 valves. During the period following ADS-4 actuation, WCOBRA/TRAC predicts significant liquid discharged through the ADS-4. This liquid results from the level in the vessel swelling after the sudden pressure decrease, or liquid being entrained from the upper plenum due to steam production in the core.

The WCOBRA/TRAC entrainment model calculates entrainment/de-entrainment rate in a computational cell, dependent on conditions in the cell. Three flow fields are tracked: continuous liquid, liquid droplets, and continuous vapor. The drag between the vapor and continuous liquid results in either liquid entrainment, when the liquid moves from the continuous liquid field to the entrained liquid field due to the interfacial shear forces of the vapor acting on the liquid, or liquid de-entrainment, which is caused by the entrained liquid interacting with the continuous liquid in the form of liquid film on structures.

Entrainment of liquid drops from the continuous liquid can occur under a variety of conditions. The physical models used to determine the average net mass rate of entrainment and the entrained drop size will be different for each condition. Entrainment mechanisms that may have a significant influence on reactor thermal-hydraulics include entrainment from liquid films, reflood entrainment, entrainment resulting from vapor bubbling through liquid pools, and entrainment resulting from vapor flow across rod structures, such as the upper plenum internals of a pressurized water reactor (PWR).

The net mass entrainment rate is defined as:

$$S = S'' \cdot V$$

where:

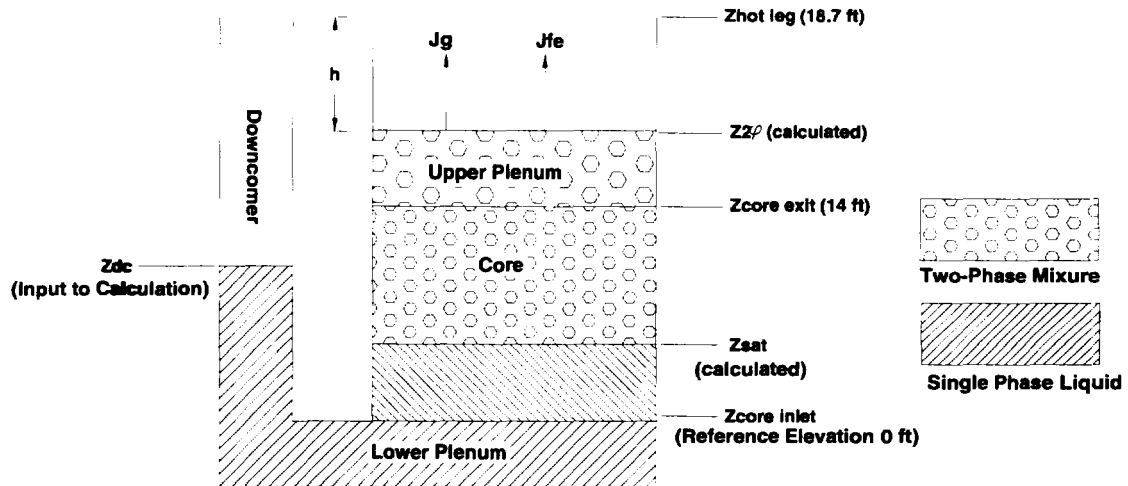
- V is the cell volume
- S'' is the volumetric drop generation rate

The net mass entrainment rate has units of mass per unit time and is the net result of the opposing mechanisms of entrainment and de-entrainment.

WCOBRA/TRAC calculates different film entrainment rates using a stable film as a basis and comparing the entrainment rate based on the stable film to empirical correlations for entrainment from films. The code then chooses the maximum entrainment from either the stable film model or the empirical correlation.

The void fraction at which a stable liquid film will exist depends on the flow channel size and the vapor velocity.

The Kataoka-Ishii entrainment model assumes that liquid is entrained from vapor flowing through a two-phase pool with a defined level (Reference 1). The entrained liquid flow is a function of the vapor velocity and the height above the pool surface (see figure below).



Analytical Model of Reactor Vessel

A.3.1 Kataoka-Ishii Pool Entrainment Model

To determine the amount of liquid entrainment, the Kataoka-Ishii model (Reference 1) is compared with information from the WCOBRA/TRAC run. The Kataoka-Ishii (KI) model depends on the distance from the liquid level in the upper plenum to the bottom of the hot leg. The maximum distance that can be attained for AP1000 is assumed to be the top of the active fuel, which is 1.43 m from the bottom of the hot leg. The KI model identifies three distinct regions:

- Near surface region
- Momentum controlled region
- Deposition controlled region

A.3.1.1 Near Surface Region

The liquid entrainment in this region is independent of the height above the pool surface, h . The region is defined by:

$$0 \leq h^* \leq 1.038E3 j_g^* N_{\mu g}^{0.5} D_h^{*0.42} (\rho_g / \Delta\rho)^{0.23} \tag{A.3-1}$$

where:

$$h^* = h / (\sigma / g \Delta\rho)^{0.5} \tag{A.3-2}$$

$$N_{\mu g} = \mu_g / [\rho_g \sigma (\sigma / g \Delta\rho)^{0.5}]^{0.5} \tag{A.3-3}$$

$$D_h^* = D_h / ((\sigma/g \Delta\rho)^{0.5}) \quad (\text{A.3-4})$$

$$j_g^* = j_g / (\sigma g \Delta\rho / \rho_g^2)^{0.25} \quad (\text{A.3-5})$$

and:

- j_g is the vapor phase velocity leaving the pool surface
- ρ_g is the vapor phase density
- $\Delta\rho$ is the density difference between the liquid and vapor phases
- σ is the liquid surface tension
- μ_g is the vapor phase dynamic viscosity
- d_h is the hydraulic diameter of the upper plenum
- h is the distance from the free surface to the bottom of the hot leg

The entrainment factor in this region is only a function of the thermodynamic properties of the two-phase pool, and is given by:

$$E_{fg} = 4.84E-3 (\rho_g / \Delta\rho)^{-1.0} \quad (\text{A.3-6})$$

where:

$$E_{fg} = \rho_f j_{fe} / (\rho_g j_g) \quad (\text{A.3-7})$$

and:

- ρ_f is the liquid phase density
- j_{fe} is the entrained liquid velocity

A.3.1.2 Momentum Controlled Region

The entrainment in this region is dependent on the vapor velocity, the height above the free surface, and the thermodynamic properties of the two-phase pool. From Reference 1, this region is limited to the intermediate height range given by:

$$1.038E3 j_g^* N_{\mu g}^{0.5} D_h^{*0.42} (\rho_g / \Delta\rho)^{0.23} \leq h^* \leq 1.97E3 N_{\mu g}^{0.33} D_h^{*0.42} (\rho_g / \Delta\rho)^{0.23} \quad (\text{A.3-8})$$

This region is divided into three regimes depending on the vapor velocity:

A.3.1.2.a Low Gas Flux Regime

This regime is limited to:

$$j_g^* / h^* < 6.39E-4 \quad (\text{A.3-9})$$

and the entrainment is given by:

$$E_{fg} = 2.213 N_{\mu g}^{1.5} D_h^{*1.25} (\rho_g / \Delta\rho)^{-0.31} j_g^* h^{*-1} \quad (\text{A.3-10})$$

A.3.1.2.b Intermediate Gas Flux Regime

For the intermediate gas flux regime bounded by:

$$6.39\text{E-}4 < j_g^* / h^* < 5.7\text{E-}4 N_{\mu g}^{-0.5} D_h^{*-0.42} (\rho_g / \Delta\rho)^{0.1} \quad (\text{A.3-11})$$

the entrainment is:

$$E_{fg} = 5.417\text{E}6 j_g^{*3} h^{*-3} N_{\mu g}^{1.5} D_h^{*-1.25} (\rho_g / \Delta\rho)^{-0.31} \quad (\text{A.3-12})$$

A.3.1.2.c High Gas Flux Regime

For the high gas flux regime limited to:

$$j_g^* / h^* > 5.7\text{E-}4 N_{\mu g}^{-0.5} D_h^{*-0.42} (\rho_g / \Delta\rho)^{0.1} \quad (\text{A.3-13})$$

the entrainment increases very rapidly as:

$$E_{fg} \propto (j_g^* / h^*)^{7-20} \quad (\text{A.3-14})$$

But, in no case is the entrainment greater than the Near Surface Region.

A.3.1.3 Deposition Controlled Region

Above the height given by:

$$h^* \geq 1.97\text{E}3 N_{\mu g}^{0.33} D_h^{*0.42} (\rho_g / \Delta\rho)^{0.23} \quad (\text{A.3-15})$$

the entrainment decreases gradually with h, due to deposition, and is given by:

$$E_{fg} = 7.13\text{E-}4 j_g^{*3} N_{\mu g}^{0.5} (\rho_g / \Delta\rho)^{-1.0} \exp [-0.205 (h / D_h)] \quad (\text{A.3-16})$$

A.3.2 Application of Entrainment Model to AP1000

To apply the pool entrainment model described above to AP1000, geometric and thermal-hydraulic information must be specified. In Section 3 of this report, the upper plenum nodes are defined by the volume just above the core support plate (15), and the volume above that at the level of the hot legs (20). The areas and hydraulic diameters for these nodes are:

[

$j^{a,b,c}$

Since the code calculates entrainment for both nodes, the total entrainment rate will be used for comparison to the Kataoka-Ishii correlation. Since the liquid level in the upper plenum is expected to be in the vicinity of the hot legs, the geometric parameters for node 20 will be used. The maximum height above the pool surface is measured from the top of the core to the bottom of the hot leg, as follows:

$$[\quad]^{a,b,c}$$

A.3.2.1 DVI Line Break

Figure A.3-1 shows the RCS pressure as a function of time for the DVI break, after the second ADS-4 valve is opened. A representative pressure is 33 psia (2.28 bar). From Reference 3, at 2.28 bar:

$$\begin{aligned} \rho_f &= 938.35 \text{ kg/m}^3 \\ \rho_g &= 1.273 \text{ kg/m}^3 \\ \mu_g &= 12.98\text{E-}6 \text{ N-s/m}^2 \\ \sigma &= 0.05403 \text{ N/m} \end{aligned}$$

From the WCOBRA/TRAC run in Section 3 of this report, the steam velocity entering node 20 is shown in Figure A.3-2. At the time of interest, the steam velocity is:

$$[\quad]^{a,b,c}$$

For these parameters, the dimensionless groups become:

$$[\quad]^{a,b,c}$$

and, as h is varied from [\quad]^{a,b,c}, the results are shown in Figure A.3-3.

The entrained liquid flow rate from WCOBRA/TRAC is shown in Figure A.3-4. Also shown are the entrainment limits defined by the Kataoka-Ishii correlation for these conditions. Figure A.3-5 shows the same curve with the upper limit on a linear scale. This figure shows that, for this event, the entrainment rate calculated by WCOBRA/TRAC compares very well with the Kataoka-Ishii correlation for entrainment near the surface of a liquid pool.

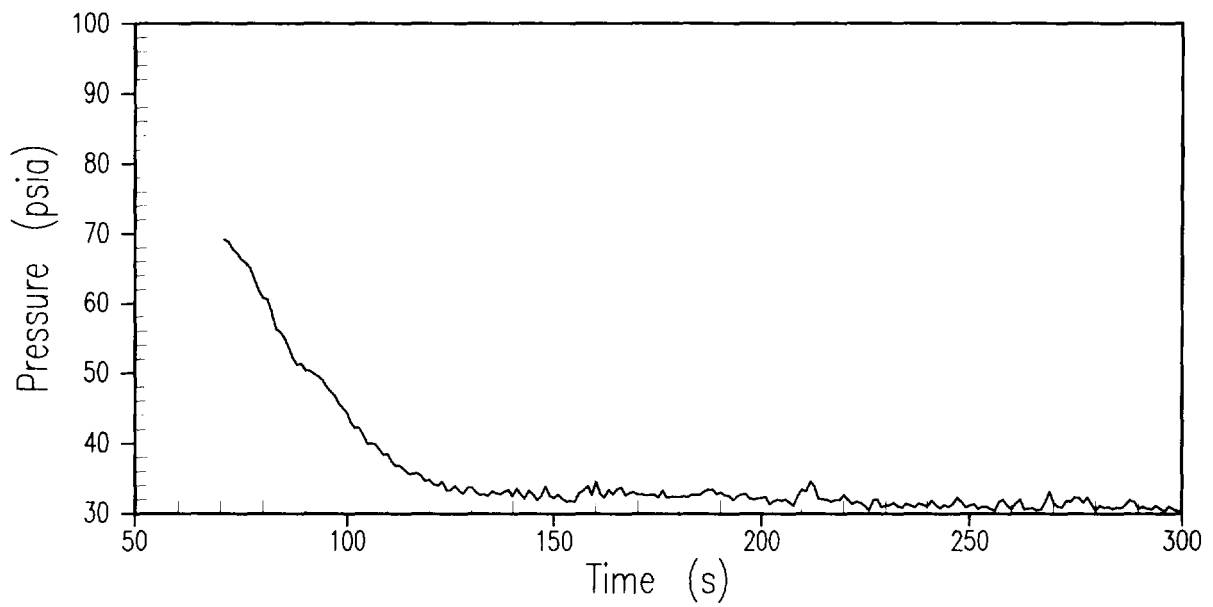


Figure A.3-1 DVI Break Pressure vs. Time – All ADS-4 Open

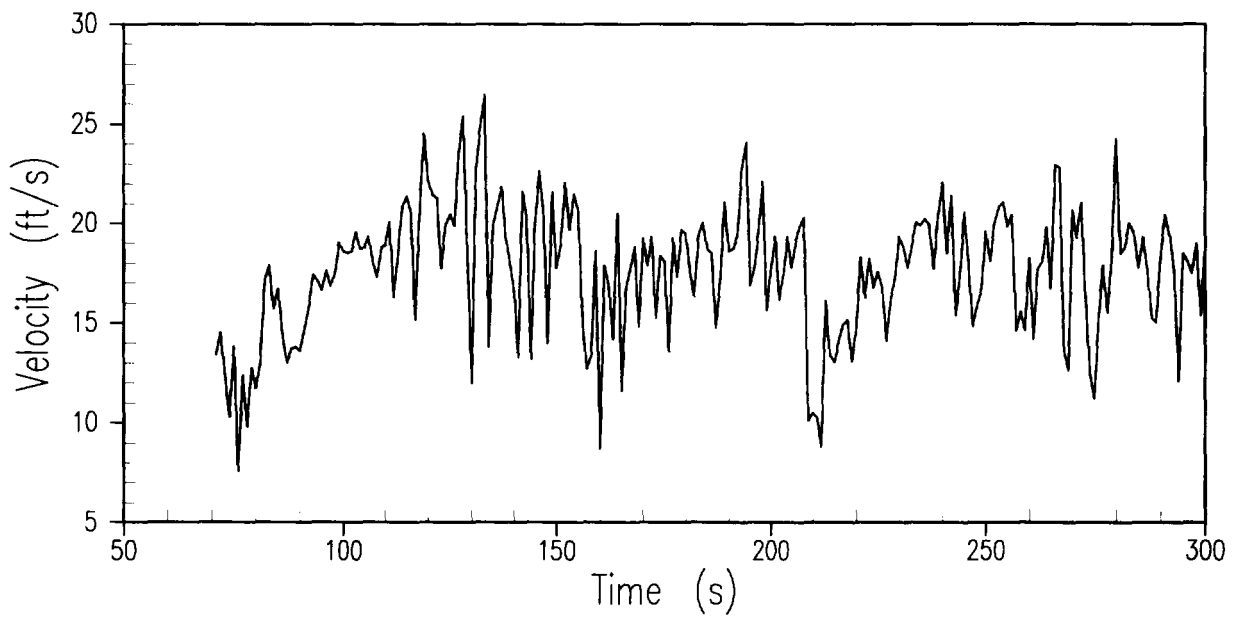


Figure A.3-2 DVI Break Vapor Velocity vs. Time – All ADS-4 Open

a,b,c

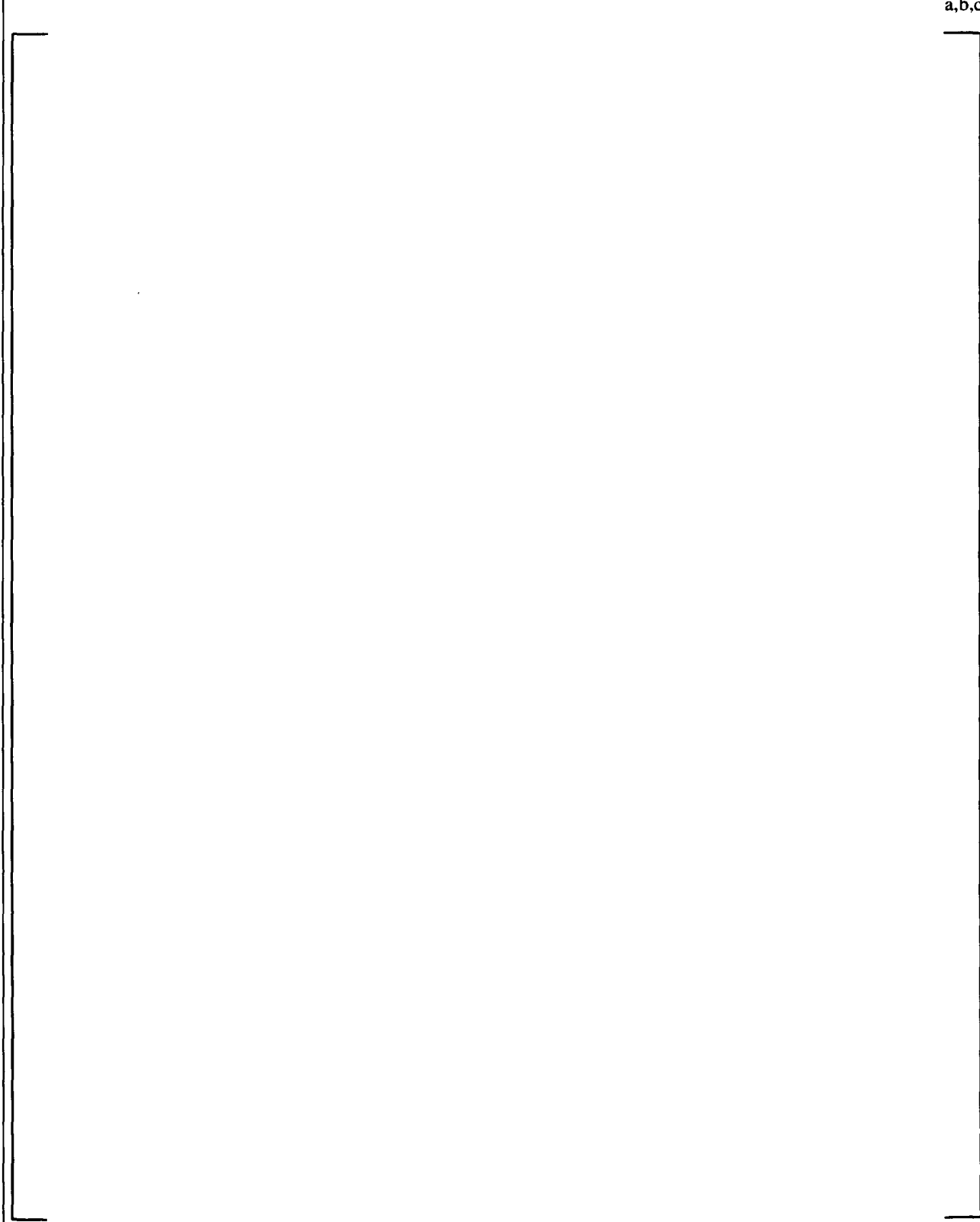


Figure A.3-3 DVI Break – Kataoka-Ishii Entrainment Limits

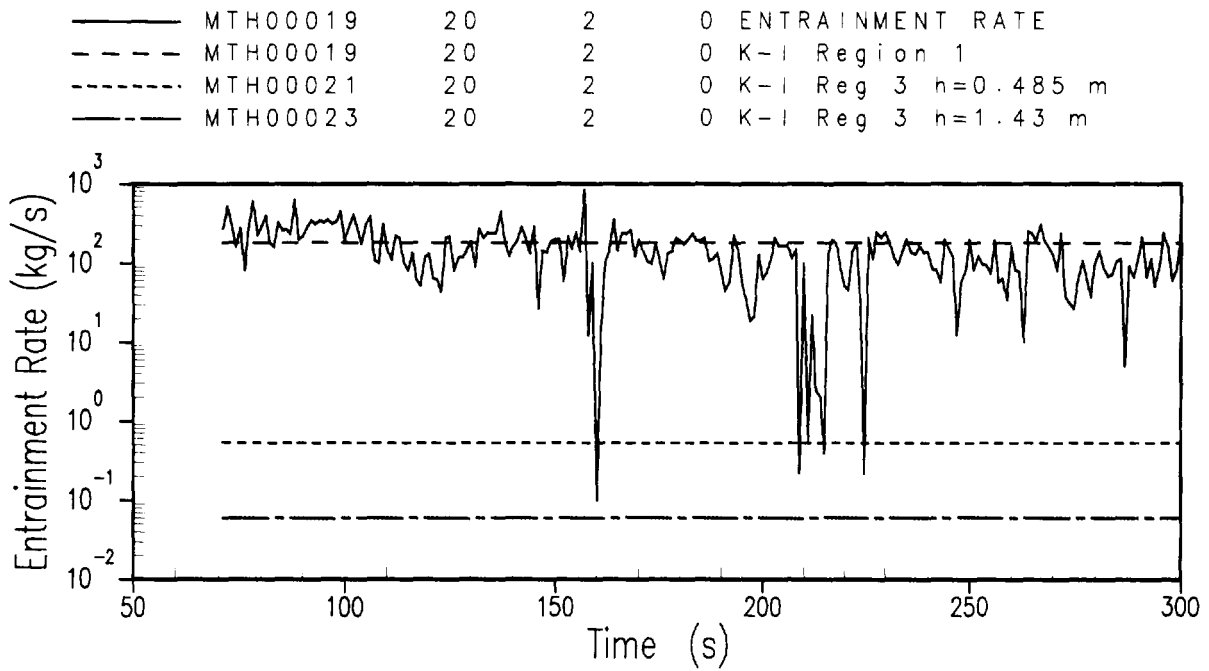


Figure A.3-4 DVI Break WCOBRA/TRAC Entrainment vs. Time – All ADS-4 Open

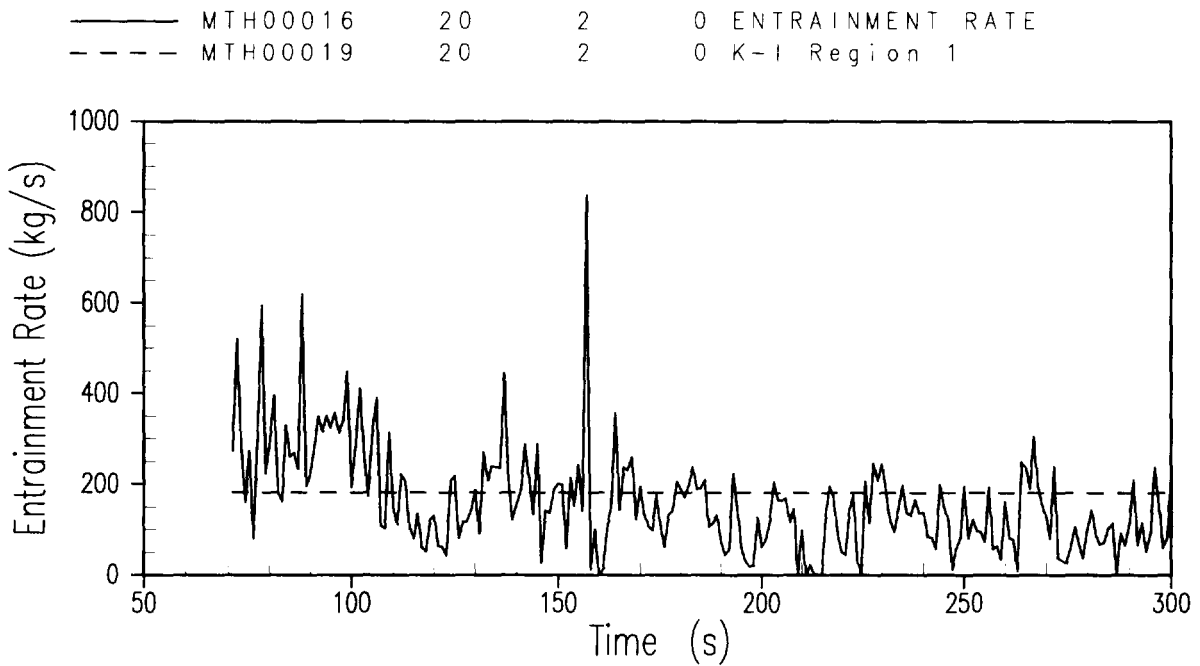


Figure A.3-5 DVI Break Entrainment vs. Time – K-I Entrainment Limit Region 1

A.3.2.2 Inadvertent ADS

Figure A.3-6 shows the RCS pressure as a function of time for the Inadvertent ADS break, after the second ADS-4 valve is opened. A representative pressure is 27 psia (1.86 bar). From Reference 3, at 1.86 bar:

$$\begin{aligned} \rho_f &= 943 \text{ kg/m}^3 \\ \rho_g &= 1.055 \text{ kg/m}^3 \\ \mu_g &= 12.75\text{E-}6 \text{ N-s/m}^2 \\ \sigma &= 0.0553 \text{ N/m} \end{aligned}$$

From the WCOBRA/TRAC run in Section 3 of this report, the steam velocity entering node 20 is shown in Figure A.3-7. At the time where all ADS-4 valves are open, the steam velocity is:

$$[\quad]^{a,b,c}$$

For these parameters, the dimensionless groups become:

$$[\quad]^{a,b,c}$$

and, as h is varied from [\quad]^{a,b,c}, the results are shown in Figure A.3-8.

The entrained liquid flow rate from WCOBRA/TRAC is shown in Figure A.3-9. Also shown are the entrainment limits defined by the Kataoka-Ishii correlation for these conditions. Figure A.3-10 shows the same curve with the upper limit on a linear scale. This figure shows that, for this event, the entrainment rate calculated by WCOBRA/TRAC compares very well with the Kataoka-Ishii correlation for entrainment near the surface of a liquid pool. Therefore, WCOBRA/TRAC predicts conservatively high levels of entrainment for liquid levels in the upper plenum, below the level of the hot legs.

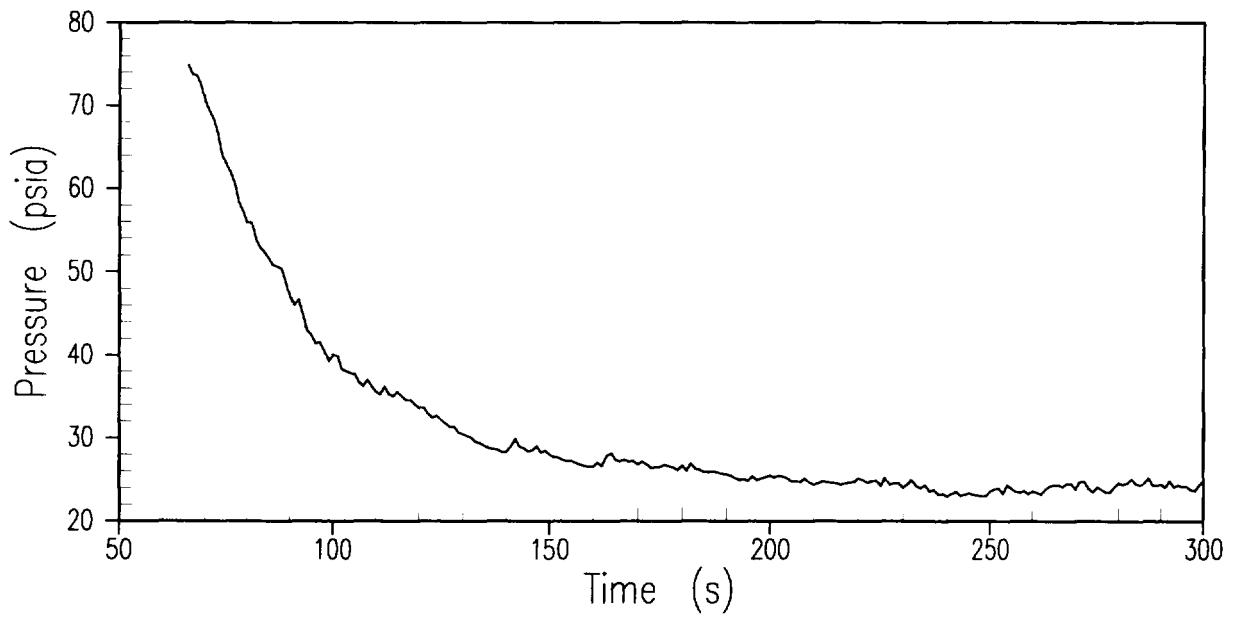


Figure A.3-6 Inadvertent ADS Pressure vs. Time – All ADS-4 Open

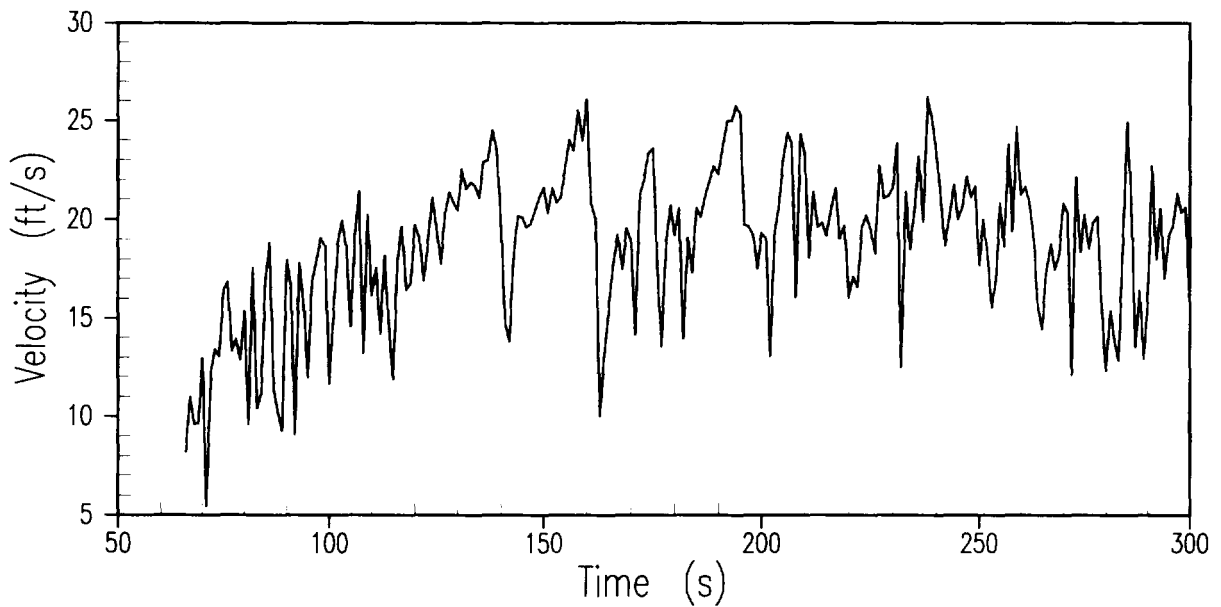


Figure A.3-7 Inadvertent ADS Vapor Velocity vs. Time – All ADS-4 Open

a,b,c

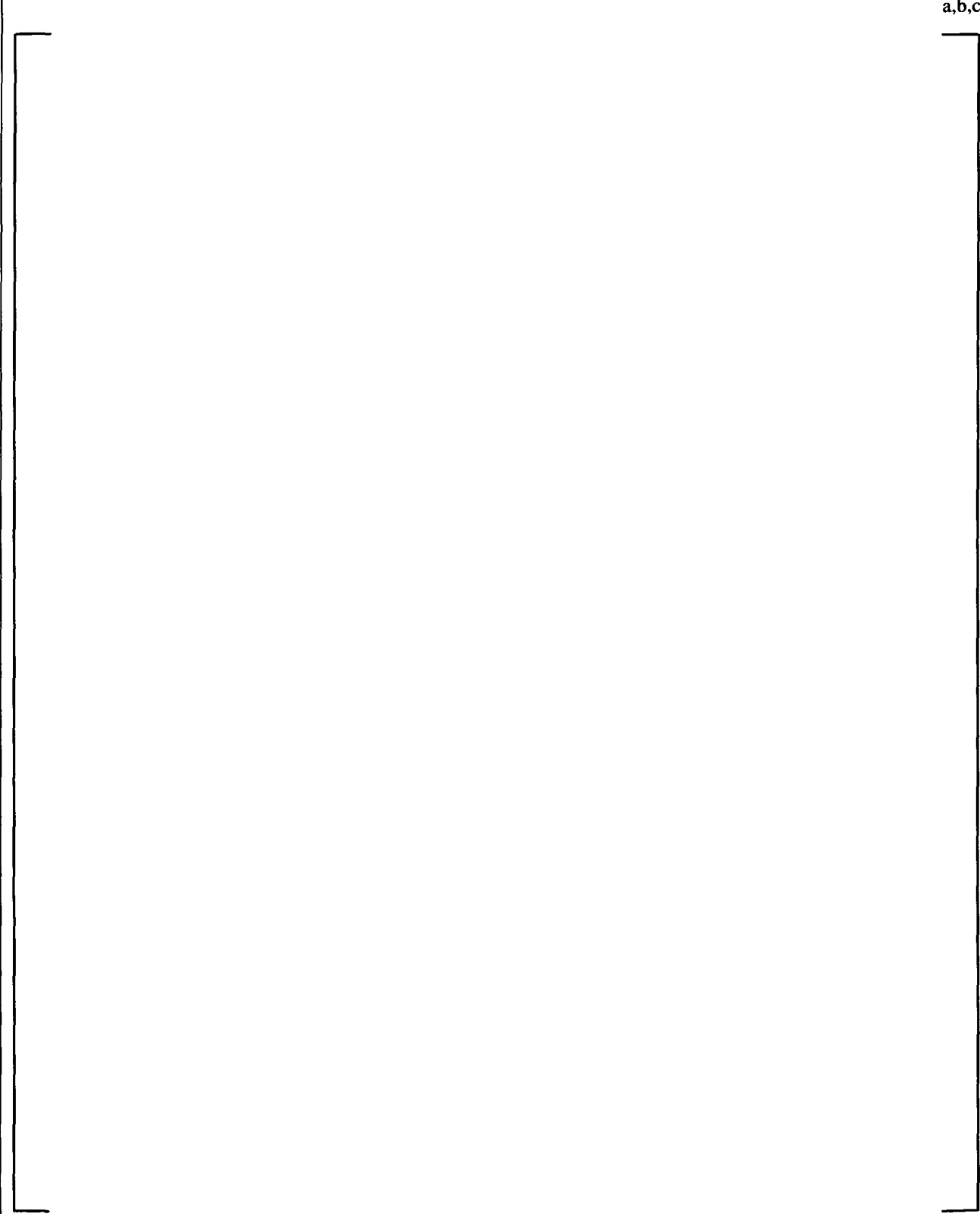


Figure A.3-8 Inadvertent ADS – Kataoka-Ishii Entrainment Limits

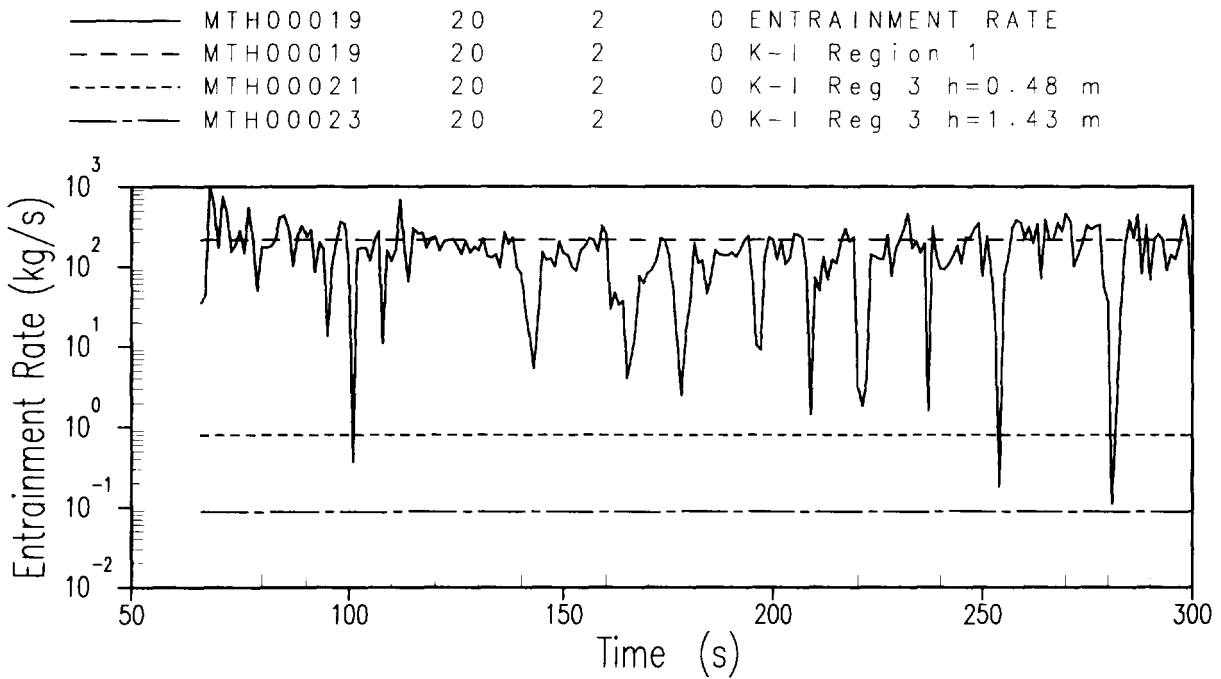


Figure A.3-9 Inadvertent ADS WCOBRA/TRAC Entrainment vs. Time – All ADS-4 Open

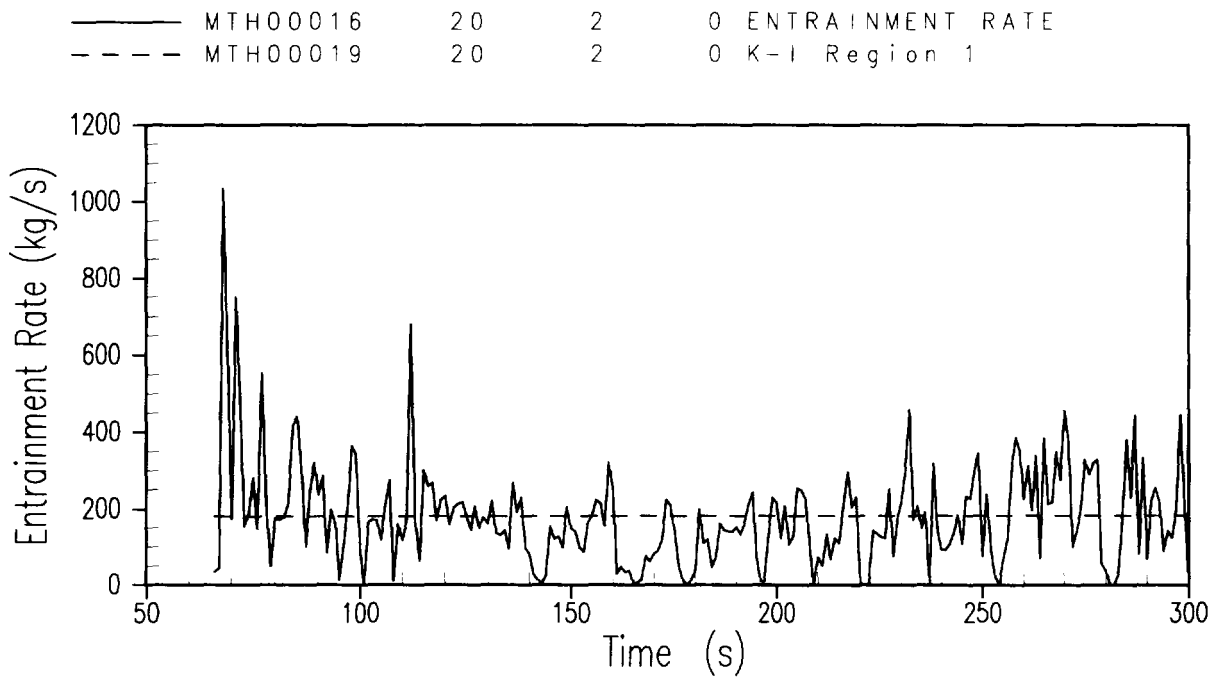


Figure A.3-10 Inadvertent ADS Entrainment vs. Time – K-I Entrainment Limit Region 1

A.3.3 Conclusions

The results of this calculation show that, even though the model used in WCOBRA-TRAC considers entrainment from a liquid film instead of a pool surface, the calculated entrainment rate compares well to the Kataoka-Ishii pool correlation, when assuming that the liquid level is at, or very near to, the level of the hot leg. This entrainment rate is the highest of the rates predicted by the KI pool correlation and bounds rates that may occur at lower levels of the pool surface. This conclusion is consistent for both the DVI break and the inadvertent ADS during the time period when all ADS-4 valves are open.

Based on the Kataoka-Ishii pool entrainment correlation, the pool entrainment phenomena for the AP1000/AP600 upper plenum geometry and the gas flux during this time of the transient has self limiting characteristics. The entrained liquid flux at the hot leg level decreases very rapidly as the pool level moves down from the hot leg, decreasing more than two orders of magnitude within the first 0.5 meter below the hot leg. The gas flux for AP1000 is about 1.75 times that for AP600 (power ratio), but a decrease of a few inches in the upper plenum pool level would compensate for this difference and result in entrained liquid flux at the hot leg level becoming the same as for AP600.

A.3.4 References

1. Kataoka, I. and Ishii, M., "Mechanistic Modeling and Correlations for Pool Entrainment Phenomenon," NUREG/CR-3304, 1983.
2. WCAP-15833, "WCOBRA/TRAC AP1000 ADS-4/IRWST Phase Modeling," Revision 0, May 2002.
3. Todreas, N. E. and Kazimi, M. S., "Nuclear Systems I – Thermal Hydraulic Fundamentals," Hemisphere Publishing, 1989.

A.4 ENTRAINMENT SENSITIVITY STUDIES WITH WCOBRA/TRAC

Section A.3 of this report compared the entrainment rate predicted by WCOBRA/TRAC in the reactor vessel upper plenum in the AP1000 simulations, presented in Section 3 of this report, with the Kataoka-Ishii correlation prediction (Reference 1). The comparisons show the WCOBRA/TRAC entrainment rate is similar to the Kataoka-Ishii correlation region 1 predicted pool entrainment rate, during the ADS-4/IRWST initiation phase for these small break LOCA events. Because the magnitudes of the predicted rates are similar, meaningful sensitivity studies may be performed with WCOBRA/TRAC to investigate the impact of varying parameters that affect liquid entrainment or discharge through the ADS-4 paths for AP1000. WCOBRA/TRAC calculates the entrainment of liquid drops from the continuous liquid phase using a model based on a stable liquid film as described in Section 4.6.2 of Reference 2.

The Inadvertent ADS actuation scenario is the case chosen for the sensitivity study. The choice is based on several factors. First of all, this case exhibits a significantly lower minimum mass inventory than the DEDVI break at the time that IRWST injection is predicted to occur. Therefore, any variation that leads to a reduction in vessel mass inventory would be more likely to approach core uncover in the Inadvertent ADS case. Also, the accumulator injects for approximately 100 seconds of the DEDVI break case ADS-4/IRWST initiation phase, providing a large safety injection flow rate to accommodate any change in the predicted rate of mass removal from the vessel which extends almost to the time of IRWST initiation; safety injection comes only from the core makeup tanks in the Inadvertent ADS case during the time interval of interest. Further, the absolute pressure to which the reactor coolant system (RCS) must be depressurized, in the Inadvertent ADS case, to achieve IRWST injection is 10 psi lower than for the DEDVI case, so any steam binding phenomena that occur and hinder depressurization are expected to have a greater effect on the Inadvertent ADS case.

Sensitivity cases have been performed for the AP1000 that vary the vessel upper plenum entrainment rate directly and that vary other parameters that might affect the ability to depressurize the RCS to achieve IRWST injection. The important figures of merit in assessing the ADS-4/IRWST initiation phase predictions of ECCS performance are the establishment of IRWST injection and the minimum reactor vessel mass inventory that occurs. The studies performed are described in the subsections that follow.

A.4.1 Addition of Fluid Cells to the Upper Plenum Modeling

The WCOBRA/TRAC cases in Section 3 are performed using one vertical cell in the upper plenum channels located in VESSEL component Section 3. To facilitate performing the sensitivity studies, the nodalization in the upper plenum is increased by placing three equal size vertical cells in Section 3 of the WCOBRA/TRAC model shown in Figure 3-1. The WCOBRA/TRAC – predicted results for the Inadvertent ADS actuation scenario are insensitive to the nodalization change. In particular, the depressurization rate and the minimum reactor vessel inventory are essentially the same for the two cases.

Figure A.4.1-1 shows the reactor vessel mass inventory comparison for the single and multi-level nodalizations of the upper plenum. In all figures in this section the 3-cell upper plenum channel representation is the solid line, and the Section 3 case is the dashed line. The minimum inventories differ by less than 500 lbm between the two cases. Moreover, the downcomer pressure values agree as shown in Figure A.4.1-2, leading to the initiation of IRWST injection in both cases between 140–150 seconds, as

shown for one of the injection line flow paths in Figure A.4.1-3. Once the IRWST injection begins, the 3-node upper plenum case exhibits both a slightly higher IRWST injection flow rate and a slightly higher liquid release through the ADS-4 flow paths. The increase in the fluid mass inventory in the reactor vessel therefore occurs slightly more slowly, as shown in Figure A.4.1-1. Figures A.4.1-4 through A.4.1-7 compare the liquid and vapor flow rates through the open ADS-4 flow paths; very close agreement is again predicted through the 140–150 second time frame. Overall, the two upper plenum channel nodalizations produce an equivalent prediction of the important figures of merit for the ADS-4/IRWST initiation phase performance of the AP1000 from WCOBRA/TRAC. Therefore, the three channel upper plenum nodalization can serve as the base case for studies that investigate the sensitivity to several pertinent parameters.

A.4.2 Variation of the Predicted Entrainment Rate in the Upper Plenum

The sensitivity of the ADS-4/IRWST initiation phase transient to the calculated entrainment rate in WCOBRA/TRAC is investigated by applying a multiplier to the entrainment rate calculated by the code. The multiplier as specified in input is non-mechanistic and is not based on any physical consideration; nevertheless, its use permits an assessment of the impact on the WCOBRA/TRAC prediction of varying the entrainment levels within the range of variation between the code and the Kataoka-Ishii region 1 predictions of entrainment observed in the previous section.

Consider first the impact of decreasing the entrainment rate prediction in the upper plenum channels by applying a multiplier of 0.50 to the WCOBRA/TRAC calculated value. Figure A.4.2-1 shows the reactor vessel mass inventory comparison for the base three-cell upper plenum channel representation and the reduced upper plenum entrainment case. In all figures in this section, the base three-cell upper plenum channel case from subsection 5.1 is the solid line, and the reduced entrainment case is the dashed line. The minimum vessel mass inventory of the reduced entrainment case is 4000 lbm higher than the base case, and its downcomer pressure value closely tracks that of the base case, as shown in Figure A.4.2-2. The flow rate from the IRWST at its initiation also agrees well between the cases, as shown in Figure A.4.2-3. The reduction in entrainment produces a steadily widening difference in vessel mass inventory between the two cases after the second set of ADS-4 valves open at 66 seconds until the minimum inventory condition occurs in the base case.

While the reduction in upper plenum entrainment does result in additional mass remaining in the reactor vessel, the impact is rather modest. To understand this, a comparison of the liquid field mass flow rates from the two cases at the upper plenum/hot leg point of contact is instructive. WCOBRA/TRAC calculates the flow rate of both an entrained droplet field and a continuous liquid field through the gap connecting the upper plenum channel to either hot leg channel. Figures A.4.2-4 and A.4.2-5 compare the integrated flows of entrained liquid into the hot leg in which both of the ADS-4 valves are assumed to open and into the hot leg that is equipped with the ADS-4 valve that is assumed to fail, respectively. For both loops, the entrained flow is lower when the entrainment multiplier of 0.50 is applied, because the entrained liquid fraction in the upper plenum channel connected to the hot legs is lower.

Figures A.4.2-6 and A.4.2-7 compare the integrated flow of the continuous liquid field into the hot leg with no failure of an ADS-4 valve and into the hot leg that contains the ADS-4 valve that is assumed to fail to open, respectively. Figure A.4.2-7 exhibits a negative flow before the ADS-4 valve in that loop is opened, as liquid that has been entrained into the loop flows back into the vessel because no ADS-4 flow

path is open. For both loops, the continuous liquid flow is higher when the multiplier of 0.5 is applied, because the continuous liquid fraction in the upper plenum channel connected to the hot leg is higher. The increase in the continuous liquid flow rate comes close to fully compensating for the lower flow of entrained liquid; the difference between the sums of the two liquid field flows entering both of the hot legs equals the additional 4000 lbm that is predicted to remain in the vessel for the reduced entrainment case.

Next, consider the impact of increasing the entrainment prediction in the upper plenum channels by applying a multiplier of 2.0 to the WCOBRA/TRAC-calculated entrainment rate. Figure A.4.2-8 shows the vessel mass inventory comparison for the base three-cell upper plenum channel representation and the increased upper plenum entrainment case. In all figures in this comparison the base three-cell upper plenum channel case is the solid line, and the increased entrainment case is the dashed line. The impact of increasing the entrainment rate by a factor of two on the reactor vessel mass inventory is smaller and less dramatic than is that of decreasing the entrainment rate by a factor of two. The minimum vessel mass inventory of the increased entrainment case is 1500 lbm lower than the base case, and the comparison in Figure A.4.2-8 shows no divergence between the cases until 160 seconds have elapsed. Figure A.4.2-9 indicates that the calculated depressurization is less favorable in the case with the 2.0 multiplier on the entrainment rate calculation. As a result, IRWST injection is initiated later and as a result lags in flow delivery relative to the base case, as shown in Figure A.4.2-10.

Figures A.4.2-11 and A.4.2-12 compare the integrated flows of entrained liquid into the hot leg with no failure of an ADS-4 valve and into the hot leg containing the ADS-4 valve that is assumed to fail to open, respectively. For both loops, the entrained flow is higher when the entrainment multiplier of 2.00 is applied because the entrained fraction in the upper plenum channel connected to the hot leg is higher. The magnitude of the change in entrained droplet flow caused by doubling the entrainment rate as calculated by the code is considerably less than that observed when the entrainment rate is halved through 150 seconds. The decrease in entrained flow into the hot legs in the 0.5 entrainment multiplier case approximates the factor of two reduction, while the net increase in entrained flow into the two hot legs when a multiplier of 2.0 is applied is only 25%. It appears that an effective upper bound on the entrainment prediction is in effect, because the higher the entrainment rate, the less continuous liquid there is to be entrained in an upper plenum channel.

To carry this further, a case that increases the entrainment prediction in the upper plenum channels by applying a multiplier of 4.0 to the WCOBRA/TRAC calculation of entrainment is performed. Figure A.4.2-13 shows the vessel mass inventory comparison for the base three-cell upper plenum channel representation and the increased upper plenum entrainment case. In all figures showing this comparison the base three-cell upper plenum channel case is the solid line, and the increased entrainment case is the dashed line. The minimum vessel mass inventory of the increased entrainment case is 2200 lbm lower than the base case, and only 750 lbm lower than the 2.0 multiplier case. The reactor vessel pressure transient comparison to the base case shown in Figure A.4.2-14 is very similar to that of the 2.0 multiplier case comparison, as is the IRWST flow behavior shown in Figure A.4.2-15.

Figures A.4.2-16 and A.4.2-17 compare the integrated flows of entrained liquid into the hot leg with no failure of an ADS-4 valve and into the hot leg containing the ADS-4 valve that is assumed to fail to open, respectively. Combining both loops, the entrained flow total is higher than the base case when the entrainment multiplier of 4.0 is applied because the entrained fraction in the upper plenum channel

connected to the hot leg is higher. However, the net increase in entrained flow into the two hot legs when a multiplier of 4.0 is applied is only about 5% above the 2.0 entrainment multiplier case total shown in Figures A.4.2-11 and -12.

The reduction in continuous liquid phase mass present in the upper plenum when the entrainment rate is increased depletes the continuous liquid present to such an extent that there is little left to entrain. In other words, the entrainment from the upper plenum into the hot legs as predicted by WCOBRA/TRAC for AP1000 is self-limiting; as the entrainment rate is increased, the continuous liquid phase mass decreases, and the propensity to entrain liquid also diminishes. The 4.00 multiplier approximates the largest difference between the WCOBRA/TRAC and Kataoka-Ishii predictions of entrainment, so no larger value is considered.

A.4.3 Variation of the Interfacial Drag in the Upper Plenum

During the ADS-4/IRWST initiation phase depressurization, vapor can be generated by the flashing of liquid in the core and reactor vessel upper plenum. This vapor combined with the vapor generated from decay heat power will exert an interfacial shear on the liquid present in the upper plenum, increasing the two-phase mixture level above the level that the liquid in a collapsed state would otherwise occupy. This mixture level swell is a function of several processes but largely depends upon the interfacial drag prediction between the vapor and liquid phases. WCOBRA/TRAC computes the interfacial drag as a function of the vertical flow regime map model in the code; simulations of blowdown test void fraction distributions have in some instances implied that the code overestimates interfacial drag.

The sensitivity of the ADS-4/IRWST initiation phase transient to interfacial drag in vertical flow in the upper plenum channels of the AP1000 WCOBRA/TRAC model is investigated by applying a multiplier to the interfacial drag calculated by the code in those channels. The multiplier range is used to investigate potential uncertainty in the code prediction of the level swell physical phenomenon; the use of a multiplier facilitates the assessment of the impact of level swell modeling on the WCOBRA/TRAC prediction of entrainment from the upper plenum into the hot legs.

Consider first the impact of decreasing the interfacial drag prediction in the upper plenum channels a relatively large amount by applying a multiplier of 0.65 to the WCOBRA/TRAC calculation. Figure A.4.3-1 shows the reactor vessel mass inventory comparison between the base three-cell upper plenum channel representation and the reduced interfacial drag case. In all figures in this subsection the base three-cell upper plenum channel case is the solid line, and the altered interfacial drag case is the dashed line. The vessel mass inventory of the reduced interfacial drag case tracks very closely the base case value, but it does not reach quite as low a minimum value. Its minimum value is less than 800 lbm greater than the base case value. As shown in Figures A.4.3-2 and A.4.3-3, the reactor vessel pressure values also closely track one another through IRWST actuation, and IRWST injection is achieved at approximately the same time with approximately the same injection flow rate through 200 seconds.

Consider next the impact of increasing the interfacial drag prediction in the upper plenum channels by a similar amount by applying a multiplier of 1.30 to the WCOBRA/TRAC calculation. Figure A.4.3-4 shows the reactor vessel mass inventory comparison between the base three-cell upper plenum channel representation and case with increased interfacial drag. The vessel mass inventory of the increased interfacial drag case tracks very closely the base case value until just before 150 seconds, when the

1.30 multiplier case shows a vessel inventory increase due the flow of some liquid from hot leg into the upper plenum. The depressurization rate also becomes a bit slower in the 1.30 multiplier case just before 140 seconds as shown in Figure A.4.3-5, so IRWST injection begins later, as shown in Figure A.4.3-6. The net result of these minor effects is negligible; the two cases exhibit almost identical minimum reactor vessel mass inventories.

The two cases performed varying the upper plenum interfacial drag prediction in WCOBRA/TRAC show that AP1000 ADS-4/IRWST initiation phase transient performance is insensitive to variations in the interfacial drag prediction in the reactor vessel upper plenum.

A.4.4 Variation of the Coefficients for the Inception of Entrainment into ADS-4

The second location within the RCS where entrainment phenomena are of interest during the AP1000 ADS-4/IRWST initiation phase transient is in the hot legs. The entrainment of liquid from the two hot legs into the respective open ADS-4 flow paths influences the venting capability and the effectiveness of the ADS-4 in depressurizing the RCS to achieve IRWST injection.

A number of correlations have been proposed for determining the liquid level at which entrainment into an offtake pipe will occur for various piping geometries. The general form of most entrainment onset correlations found in the literature is:

$$Fr_g \left(\frac{\rho_g}{\rho_l - \rho_g} \right)^{0.5} = C_1 \left[\frac{z}{d} \right]^{C_2}$$

The key elements of this correlation form consist of the Froude number (Fr), density ratio ($\rho/\Delta\rho$), and a geometric ratio (z/d) of entrainment onset height (z) to offtake diameter (d). The coefficient C_1 and exponent C_2 are functions of the orientation and geometry of the offtake.

Side Offtake Orientation

Craya (Reference 3) developed a theoretical onset of liquid entrainment for discharge from a side offtake neglecting viscosity and surface tension effects. Craya's theoretical result was obtained by treating the offtake as a potential flow point sink. From this, he arrived at onset correlations for orifice-type offtakes and slot-type offtakes, as follows:

$$Fr_g \left(\frac{\rho_g}{\rho_l - \rho_g} \right)^{0.5} = C_1 \left[\frac{z}{d} \right]^{2.5} \quad \text{for orifice}$$

$$Fr_g \left(\frac{\rho_g}{\rho_l - \rho_g} \right)^{0.5} = C_1 \left[\frac{z}{d} \right]^{1.5} \quad \text{for slot}$$

Note that the form is similar for orifice and slot, however, the exponents for the geometric ratio (z/d) are 2.5 and 1.5 respectively.

Top Offtake Orientation

Rouse, 1956 (Reference 5) developed a correlation for onset of liquid entrainment for top offtake configurations, as follows:

$$Fr_g \left(\frac{\rho_g}{\rho_l - \rho_g} \right)^{0.5} = C_1 \left[\frac{z}{d} \right]^2$$

It is important to note here that the exponent for the geometric ratio is 2.0, which is different from those obtained by Craya for side offtake orientations. Ardron and Bryce (Reference 4) provide a summary of exponents and coefficients recommended for use in Froude number type correlations in the open literature. It appears from several data sets that the general correlation form for entrainment onset provides reasonable agreement and representation.

In the AP1000 application, the geometry of interest involves entrainment at the top of the main pipe (hot leg) through a vertical connection into an offtake pipe. The coefficient and exponent recommended by Ardron and Bryce for top offtake configurations in the correlation based on the Froude number are the base values in the WCOBRA/TRAC calculations. The impact of varying the coefficient and the exponent in the correlation is assessed by independently varying the multiplier C_1 and the exponent C_2 from the base values of 0.35 and 2.50, respectively.

Consider the impact of decreasing the exponent C_2 in the WCOBRA/TRAC entrainment onset correlation to the value of 2.00 recommended by Rouse. Figure A.4.4-1 shows the reactor vessel mass inventory comparison between the base three-cell upper plenum channel representation and the reduced entrainment onset exponent case. In all figures in this subsection the base three-cell upper plenum channel case is the solid line, and the altered correlation case is the dashed line. The vessel mass inventory of the reduced exponent case tracks slightly above the base case value, but its minimum value is less than 800 lbm different from the base case value. As shown in Figures A.4.4-2 and A.4.4-3, the reactor vessel pressure becomes slightly greater in the reduced exponent case as the time of IRWST actuation approaches, so IRWST injection is achieved at a slightly later time with approximately the same injection flow rate.

Consider next the impact of increasing the coefficient C_1 in the entrainment onset correlation by 50% to a value of 0.525 in a WCOBRA/TRAC calculation. Figure A.4.4-4 shows the reactor vessel mass inventory comparison between the base three-cell upper plenum channel representation and the increased entrainment onset coefficient case. In all figures the base three-cell upper plenum channel case is the solid line, and the altered coefficient case is the dashed line. The vessel mass inventory of the increased coefficient case tracks very closely the base case value until shortly before IRWST injection, when it increases relative to the base case; its minimum value is 1000 lbm different from the base case value. As shown in Figures A.4.4-5 and A.4.4-6, the reactor vessel pressure values also closely track one another until just before IRWST actuation, when a pressure increase in the increased coefficient case causes IRWST injection to be delayed.

Consider also the impact of decreasing the coefficient C_1 in the entrainment onset correlation by 50% to a value of 0.175 in an AP1000 WCOBRA/TRAC case. Figure A.4.4-7 shows the reactor vessel mass inventory comparison between the base three-cell upper plenum channel representation and the reduced

entrainment onset coefficient case. The vessel mass inventory of the reduced coefficient case diverges very slightly from the base case value, and its minimum value is less than 600 lbm greater than the base case value. As shown in Figures A.4.4-8 and A.4.4-9, the reactor vessel pressure values also closely track one another through IRWST actuation, and IRWST injection is achieved at approximately the same time with approximately the same injection flow rate.

A.4.5 Comparison of WCOBRA/TRAC Entrainment Predictions to Kataoka-Ishii

The WCOBRA/TRAC predictions of upper plenum entrainment during the AP1000 ADS-4/IRWST initiation phase are shown to be similar in magnitude with the Kataoka-Ishii correlation, region 1 prediction in the preceding section. The Kataoka-Ishii model identifies two other distinct regions that apply when the pool level drops below the hot leg elevation, and the entrainment predicted for these two regions is orders of magnitude less than for region 1. It is instructive to identify a "level" in the upper plenum associated with the WCOBRA/TRAC-predicted void fractions in Channels 47 and 20 to draw further conclusions about the code simulation of AP1000. The nodalization of these channels with the three-cell representation is shown in detail in Figure A.4.5-1. Positions are identified in Figure A.4.5-1 for the discussion in the following paragraph. In WCOBRA/TRAC terminology, [

]^{a,c} Positions identified by half-number values in the figure are at the boundaries between cells.

The void profile in the upper plenum for the base three-cell upper plenum case is presented in Figure A.4.5-2. Each cell in channel 47 is 0.48 meters high. Position 1 in the axis of this figure is position 1 of Figure A.4.5-1. It shows the void fraction value of cell 2 in channel 47; position 2 shows the void fraction value of cell 3 in channel 47; position 3 shows the void fraction value of cell 4 in channel 47; and position 4 shows the void fraction value of cell 2 in channel 20. The curves on Figure A.4.5-2 show the upper plenum void profiles at various times during the subject WCOBRA/TRAC case, and the WCOBRA/TRAC void fraction value corresponds specifically to the center of the cell. At 66 seconds, the time immediately after the second set of two ADS-4 valves open, the void profile shows that cell (20,2) is in the liquid-continuous void fraction range at a value less than 0.8. By 104 seconds cell (20,2) exceeds 0.8 in void fraction, indicating a vapor-continuous condition in WCOBRA/TRAC, while cell (47,4), position 3 of the figure, remains below the 0.8 value. By 120 seconds the void fractions of both cells (20,2) and (47,4) exceed 0.8, the value above which the vapor phase-continuous annular flow regime is presumed in WCOBRA/TRAC. By 130 seconds, cell (20,2) within the hot leg perimeter is just about totally void, while the void fraction in cell (47,3) is still in the liquid-continuous void fraction regime at a value well below 0.8. This strongly suggests that a two-phase mixture level exists somewhere below the hot leg bottom elevation in the upper plenum, where a high velocity flow is entering the two hot legs.

When the void fraction of cell (47,4) is greater than 0.8, a two-phase mixture elevation may in fact exist significantly below the hot leg bottom elevation. To estimate the elevation at which a two-phase mixture level may be present in the WCOBRA/TRAC upper plenum, compare the void fractions at the boundaries of cell (47,4), which are indicated in Figure A.4.5-2 (for instance, the void fraction at position 2.5, which is the cell boundary between cell (47,4) and cell (47,3), is 0.78 at 120 seconds), with the cell center values. If the difference in void fraction between position 3 and position 2.5 exceeds 0.05, a two-phase level can be presumed to exist somewhere in the bottom half of cell (47,4). Likewise, if the difference in

void fraction between position 3 and position 3.5 exceeds 0.05, a two-phase level can be presumed to exist somewhere in the top half of cell (47,4). At a time when both of these criteria are met, the two-phase level is considered to be indeterminate and therefore not to exist. The prediction obtained using this approach is presented in Figure A.4.5-3. The index value of 1 in this figure indicates that a two-phase mixture level estimated to exist in the bottom half of the upper plenum cell (47,4) in WCOBRA/TRAC; a value of 0 indicates that no two-phase mixture level is predicted at this elevation. Beginning at 117 seconds, when the level is at such an elevation, which is approximately one foot below the bottom of the hot leg, region 2 of the Kataoka-Ishii pool entrainment correlation is in effect. It specifies an entrainment rate orders of magnitude less than the correlation region 1 value, a rate that is significantly less than the WCOBRA/TRAC-calculated value. Because the WCOBRA/TRAC calculation continues to predict liquid entrainment at rates consistent with the Kataoka-Ishii correlation region 1 result even when a mixture level is indicated well below the hot leg elevation, the WCOBRA/TRAC calculation of minimum reactor vessel mass inventory during the ADS-4/IRWST initiation is judged to be conservative for AP1000.

A.4.6 Conclusions about Upper Plenum Entrainment

Overall, the AP1000 ADS-4/IRWST initiation phase performance exhibits a modest sensitivity to varying the entrainment rate calculated in WCOBRA/TRAC. Cutting the entrainment rate in half through the use of a multiplier results in a somewhat increased minimum mass inventory. Increasing the entrainment rate calculated in the code through the use of the multiplier reduces the minimum mass inventory by a somewhat lesser amount, and the effect obtained from increasing the entrainment rate calculated in WCOBRA/TRAC diminishes by the time the increase multiplier equals a factor of four. The AP1000 has adequate ADS-4 venting capacity to depressurize the RCS to achieve IRWST injection in a timely manner for any of the entrainment rates analyzed. In each case analyzed, the heat transfer regime on the fuel rods enables cladding temperatures to remain near the coolant saturation temperature.

The AP1000 ADS-4/IRWST initiation phase performance exhibits a lack of sensitivity to the level swell calculated in the upper plenum channels in WCOBRA/TRAC. Increasing and decreasing the interfacial drag calculated by the code by one-third results in very minor changes in the ADS-4/IRWST initiation phase transient prediction.

A.4.7 Conclusions about Hot Leg Entrainment

Correlations published to determine the liquid level at which entrainment will occur from a horizontal pipe into an offtake pipe are based on the Froude number for flow in the horizontal pipe. The base values of the multiplier coefficient and the exponent in this form of correlation have been varied in WCOBRA/TRAC in the two hot legs, to vary the prediction of entrained liquid flow into the respective open ADS-4 flow paths. The purpose of varying the parameters is to assess the impact that the prediction of the entrainment of liquid from the hot legs exerts on the AP1000 ADS-4/IRWST injection phase performance. Little sensitivity is observed to varying the parameters in the correlation used in WCOBRA/TRAC from their recommended values.

A.4.8 Overall Conclusions about Entrainment in the AP1000

The sensitivity of the AP1000 ADS-4/IRWST initiation phase performance, as predicted by WCOBRA/TRAC, to varying the entrainment rate in the upper plenum is modest. The sensitivity of the AP1000 ADS-4/IRWST initiation phase performance, in WCOBRA/TRAC, to varying the interfacial drag in the upper plenum is minimal. The sensitivity of the AP1000 ADS-4/IRWST initiation phase performance, as predicted by WCOBRA/TRAC, to varying the entrainment onset correlation for flow from the hot legs into the ADS-4 flow paths is minimal. In all cases analyzed, the predicted depressurization rate led to the initiation of IRWST injection at a reactor vessel mass inventory that is close to that of the base inadvertent ADS actuation case from Section 3 of this report.

The upper plenum entrainment rate predicted in WCOBRA/TRAC is of the same order of magnitude as that predicted by the Kataoka-Ishii pool entrainment correlation for the near surface region, which applies when the liquid phase level is at or near the hot leg elevation and represents a conservative bound on the entrainment for other regions. After all the ADS-4 valves have opened and before the minimum reactor vessel mass inventory occurs, the estimated two-phase mixture level in the upper plenum in WCOBRA/TRAC is located well below the bottom of the hot leg. A pool level at this elevation corresponds to region 2, the momentum controlled region of the Kataoka-Ishii pool entrainment correlation, and to an entrainment rate much less than is predicted by the code. Therefore, WCOBRA/TRAC provides a conservative entrainment rate prediction in the reactor vessel upper plenum for the ADS-4/IRWST initiation phase of small break LOCA events.

Overall, the AP1000 is equipped with ADS-4 flow paths that are adequate to depressurize the RCS to achieve IRWST injection, even when a postulated single failure and when a conservatively high entrainment rate prediction in the reactor vessel upper plenum are assumed. Credible variations in the entrainment in either the upper plenum or the hot legs do not adversely impact the safety of the AP1000 for the ADS-4/IRWST initiation phase of small break LOCA events. In each sensitivity study case, the heat transfer regime on the fuel rods enables the cladding temperatures to remain near the coolant saturation temperature.

A.4.9 References

1. NUREG/CR-3304, "Mechanistic Modeling and Correlations for Pool Entrainment Phenomenon," I. Kataoka and M. Ishii, 1983.
2. Bajorek, S. M., et al., "Code Qualification Document for Best-Estimate LOCA Analysis," WCAP-12945-P-A, Volume 1, 1998.
3. Craya, A., "Theoretical Research on the Flow of Non-homogeneous Fluids," La Houille Blanche, pp. 44-55, 1949.
4. Rouse, H., "Seven Exploratory Studies in Hydraulics," Proc. ASCE, Vol. 82, 1956.
5. Ardron, K. H. and Bryce, W. M., "Assessment of Horizontal Stratification Entrainment Model in RELAP5/MOD2 by Comparison with Separate Effects Experiments," Nuclear Engineering and Design, Vol. 122, pp. 263-271, 1990.

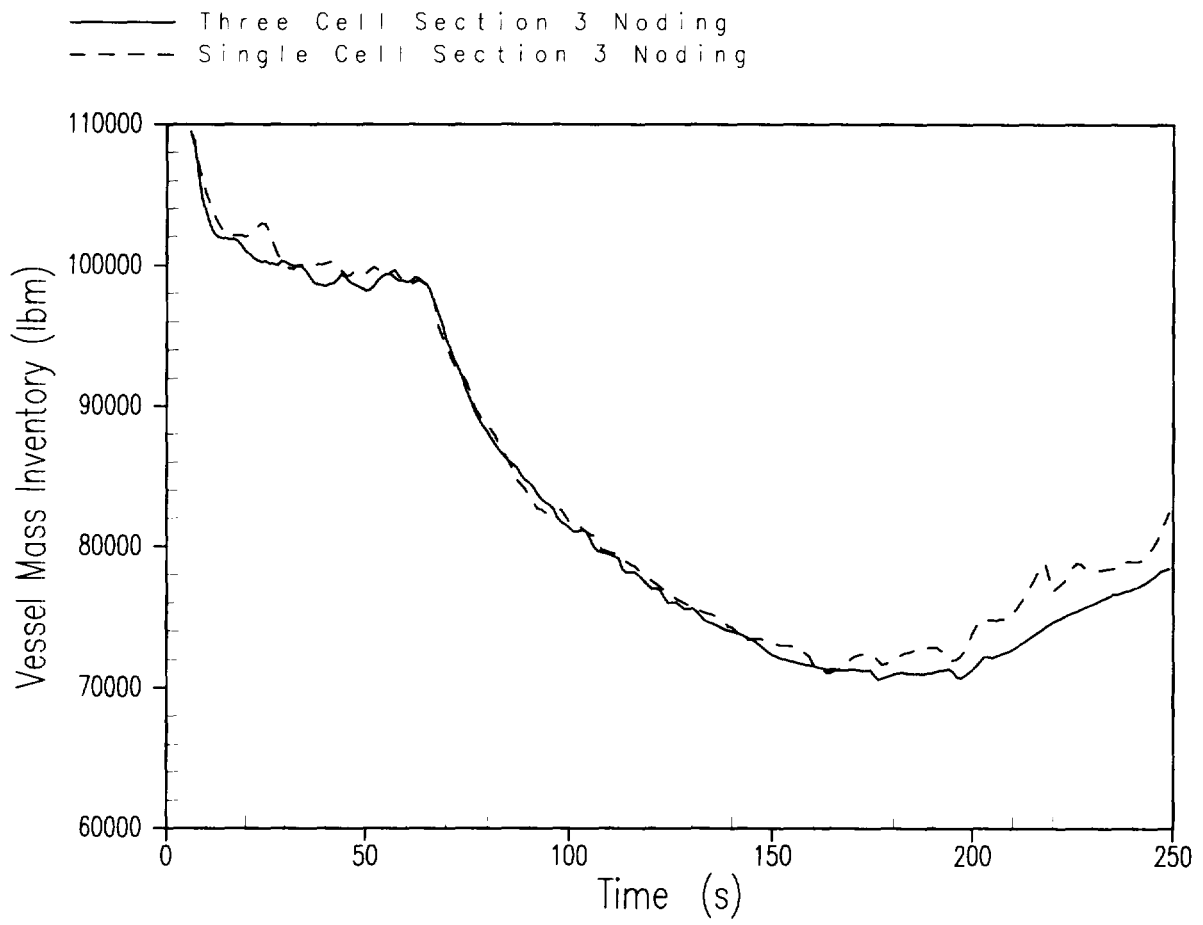


Figure A.4.1-1 Nodalization Study Vessel Mass Inventory

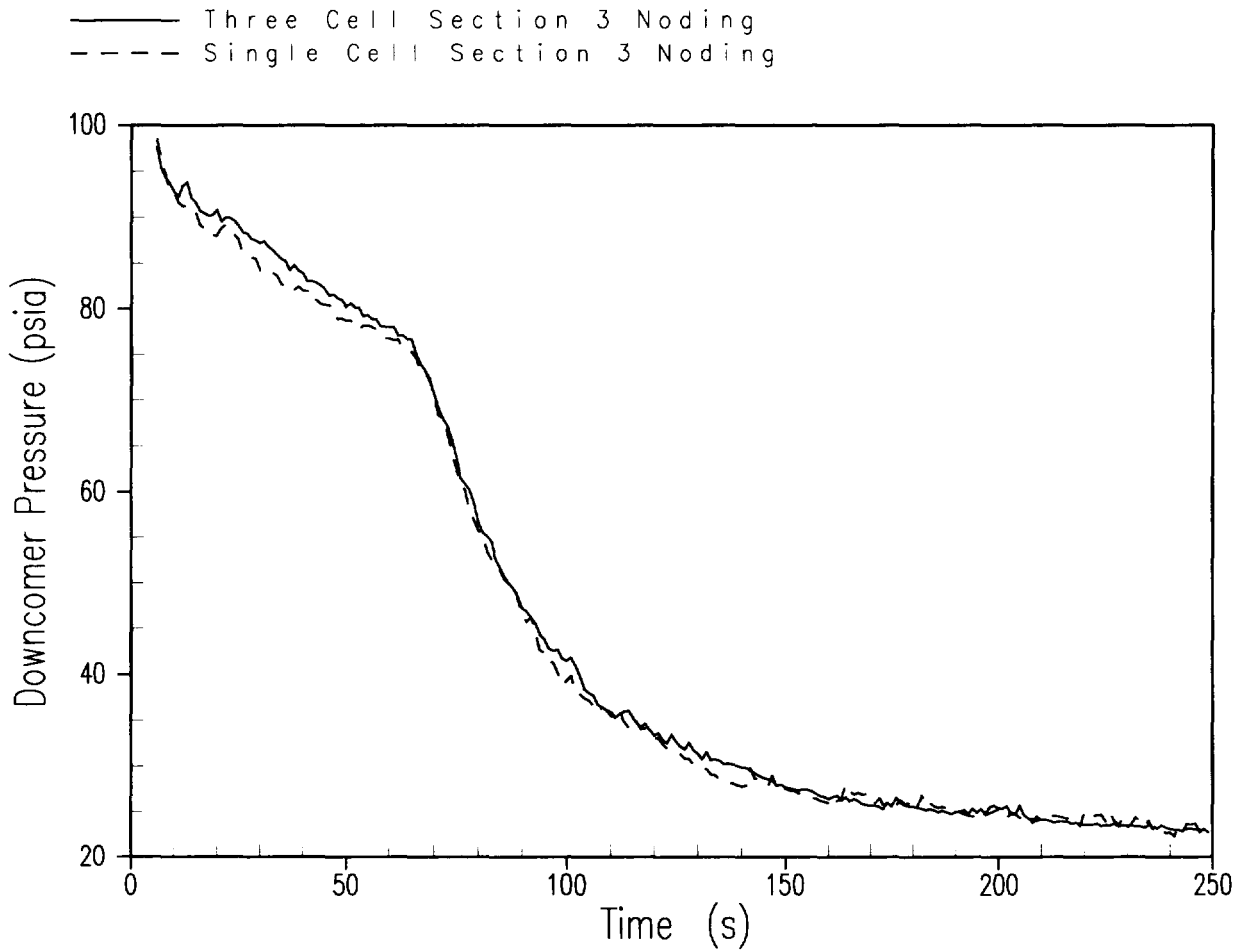


Figure A.4.1-2 Nodalization Study Downcomer Pressure

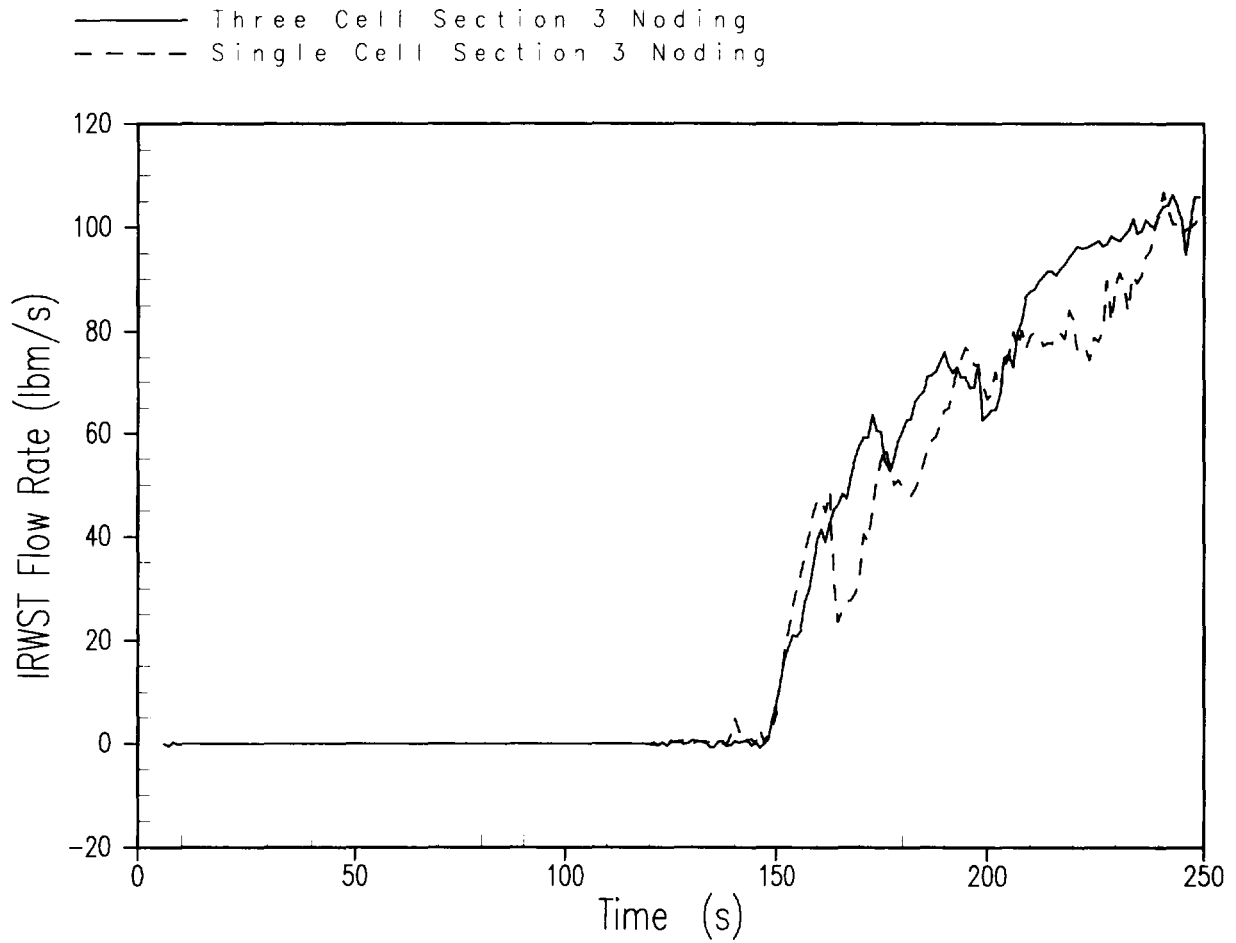


Figure A.4.1-3 Nodalization Study IRWST Injection Flow Rate

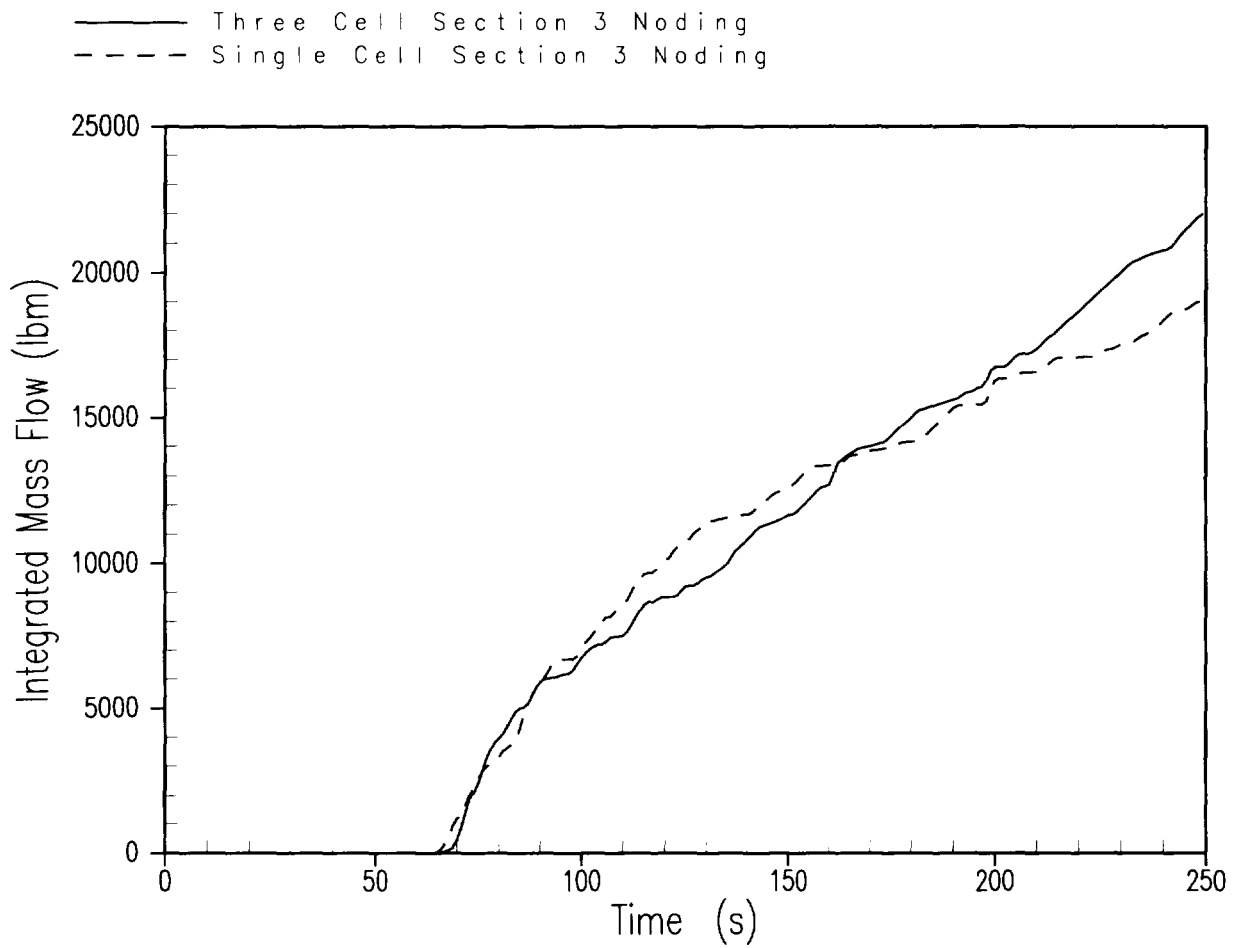


Figure A.4.1-4 Nodalization Study ADS-4 Integrated Liquid Flow, Single Failure Loop

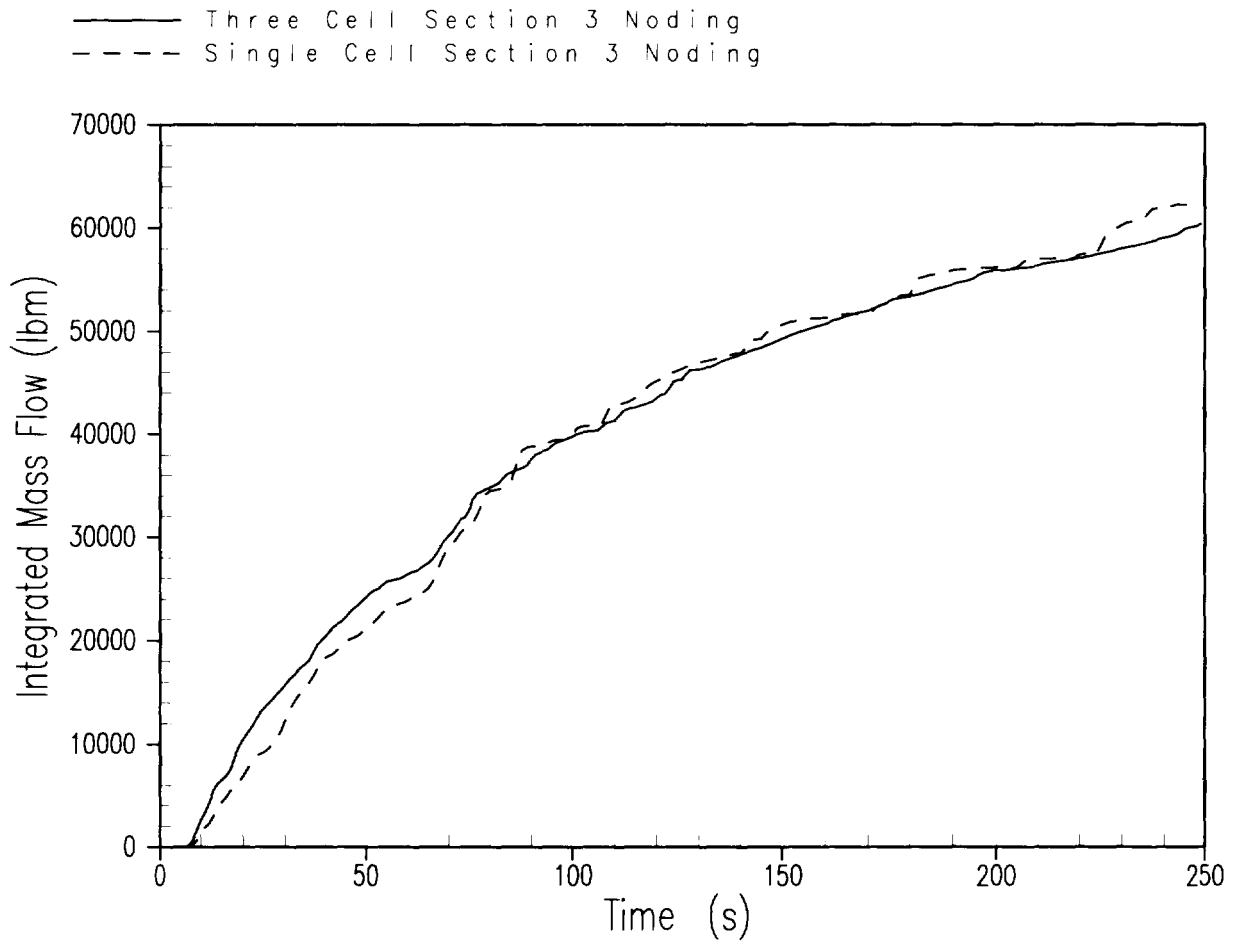


Figure A.4.1-5 Nodalization Study ADS-4 Integrated Liquid Flow, Intact Loop

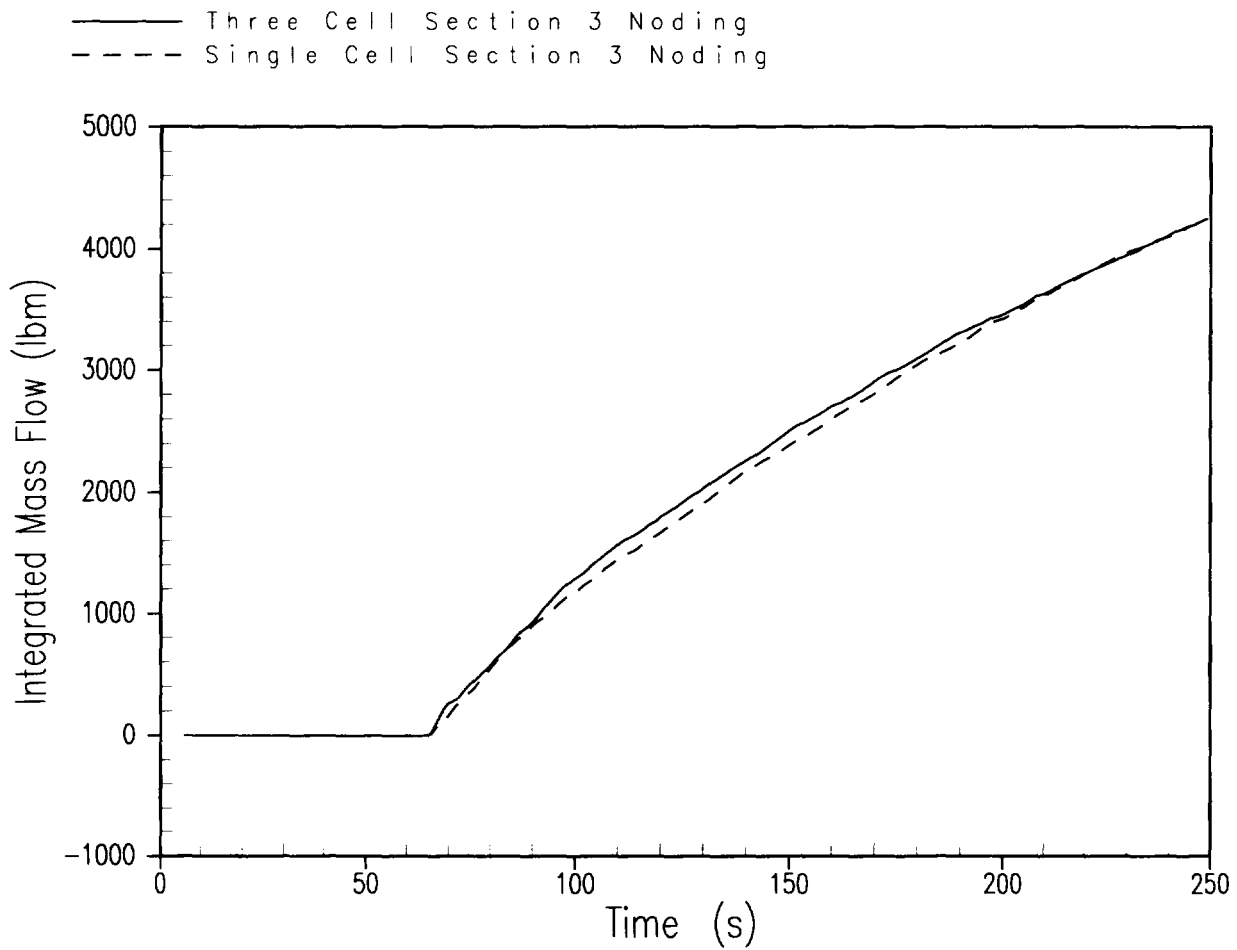


Figure A.4.1-6 Nodalization Study ADS-4 Integrated Vapor Flow, Single Failure Loop

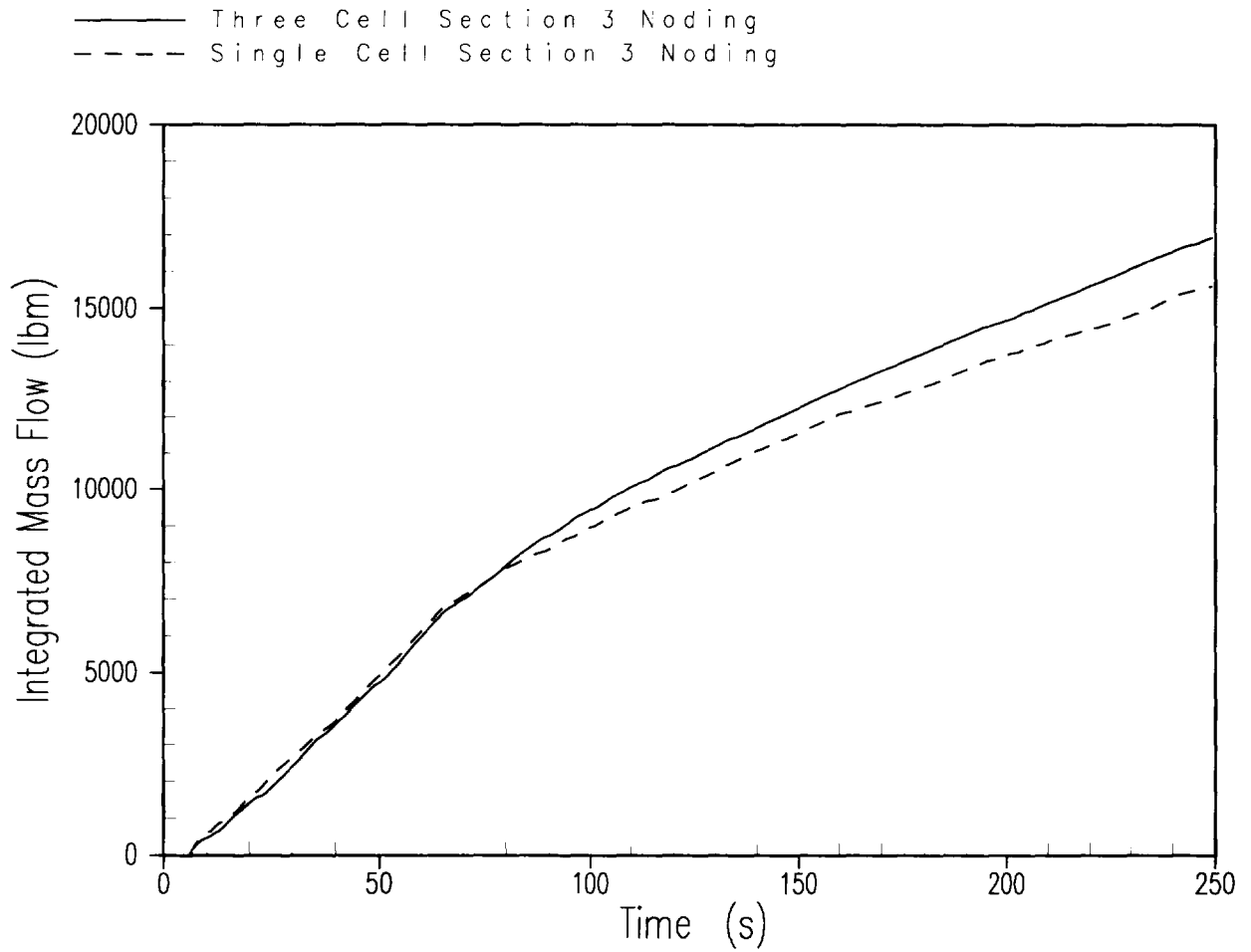


Figure A.4.1-7 Nodalization Study ADS-4 Integrated Vapor Flow, Intact Loop

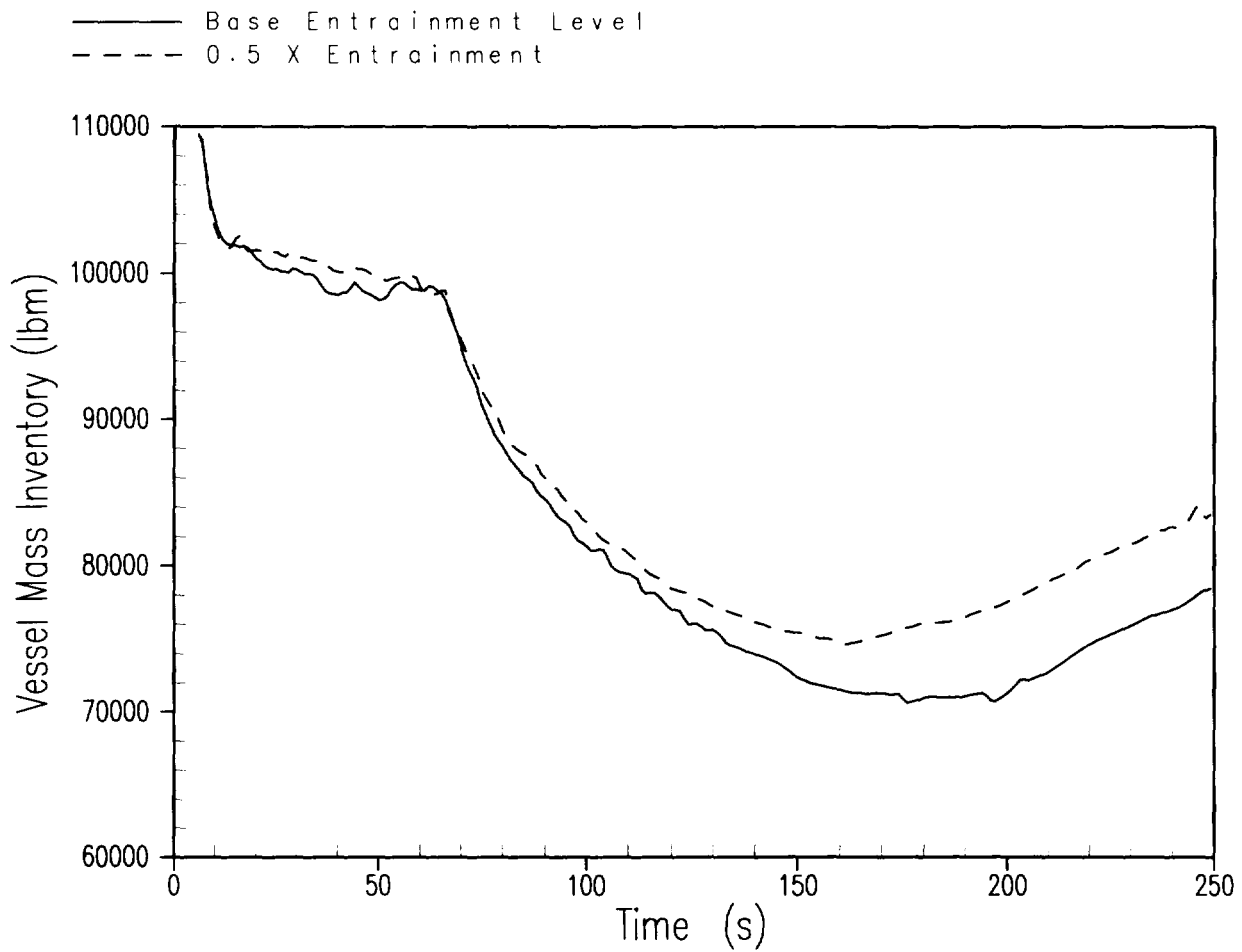


Figure A.4.2-1 0.5 Entrainment Rate Case Vessel Mass Inventory

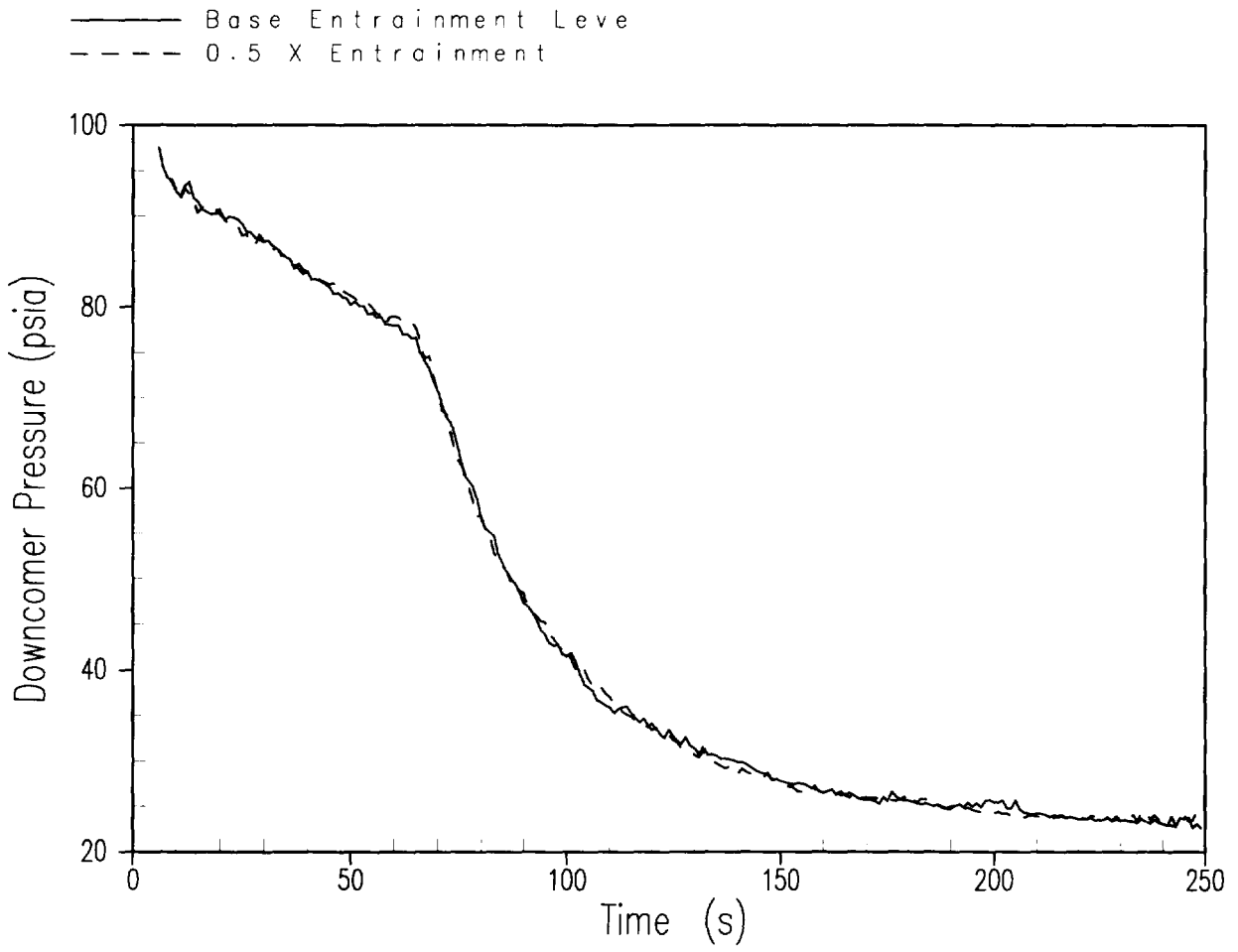


Figure A.4.2-2 0.5 Entrainment Rate Case Downcomer Pressure

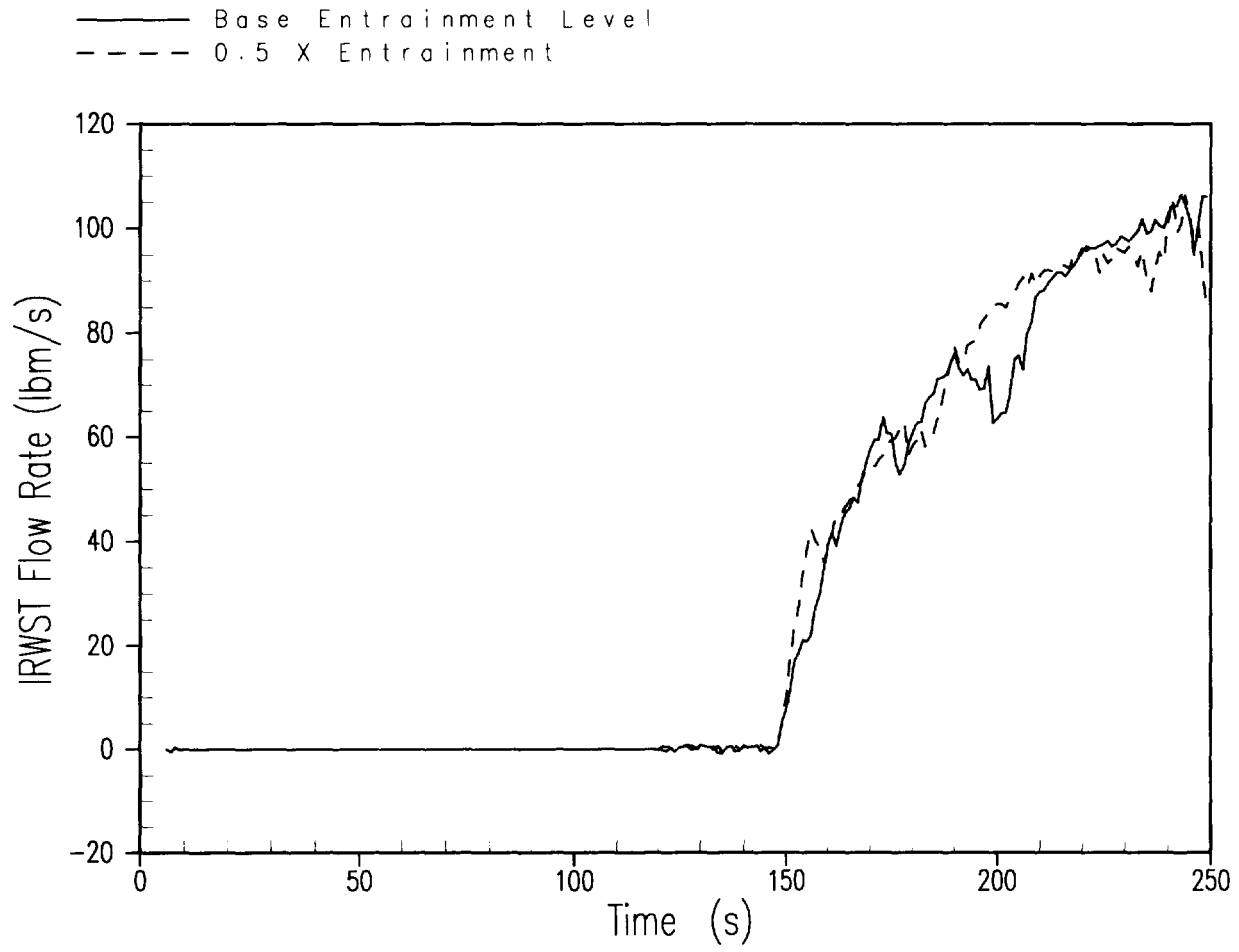


Figure A.4.2-3 0.5 Entrainment Rate Case IRWST Injection Flow Rate

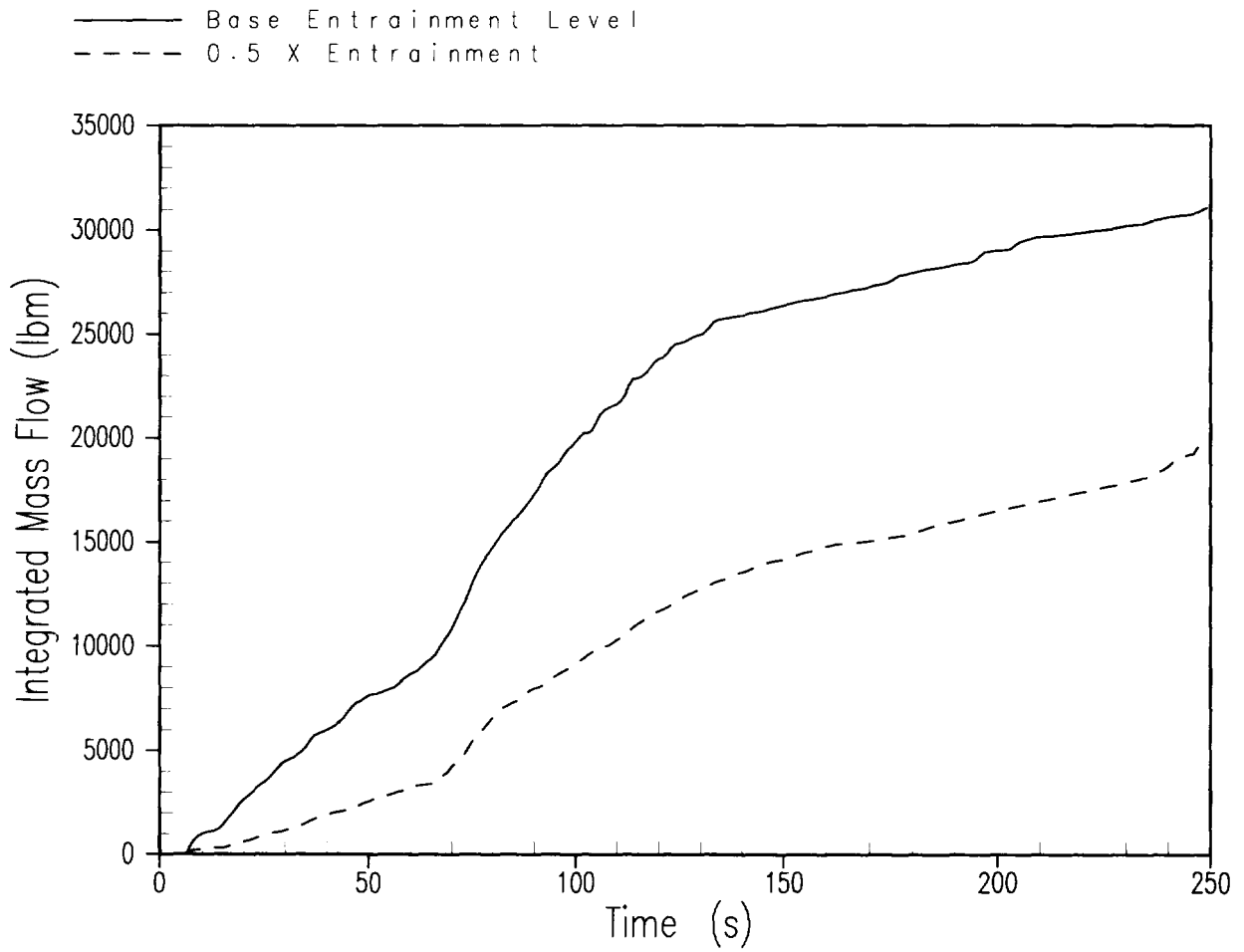


Figure A.4.2-4 0.5 Entrainment Rate Case Entrained Flow into the Intact Loop Hot Leg

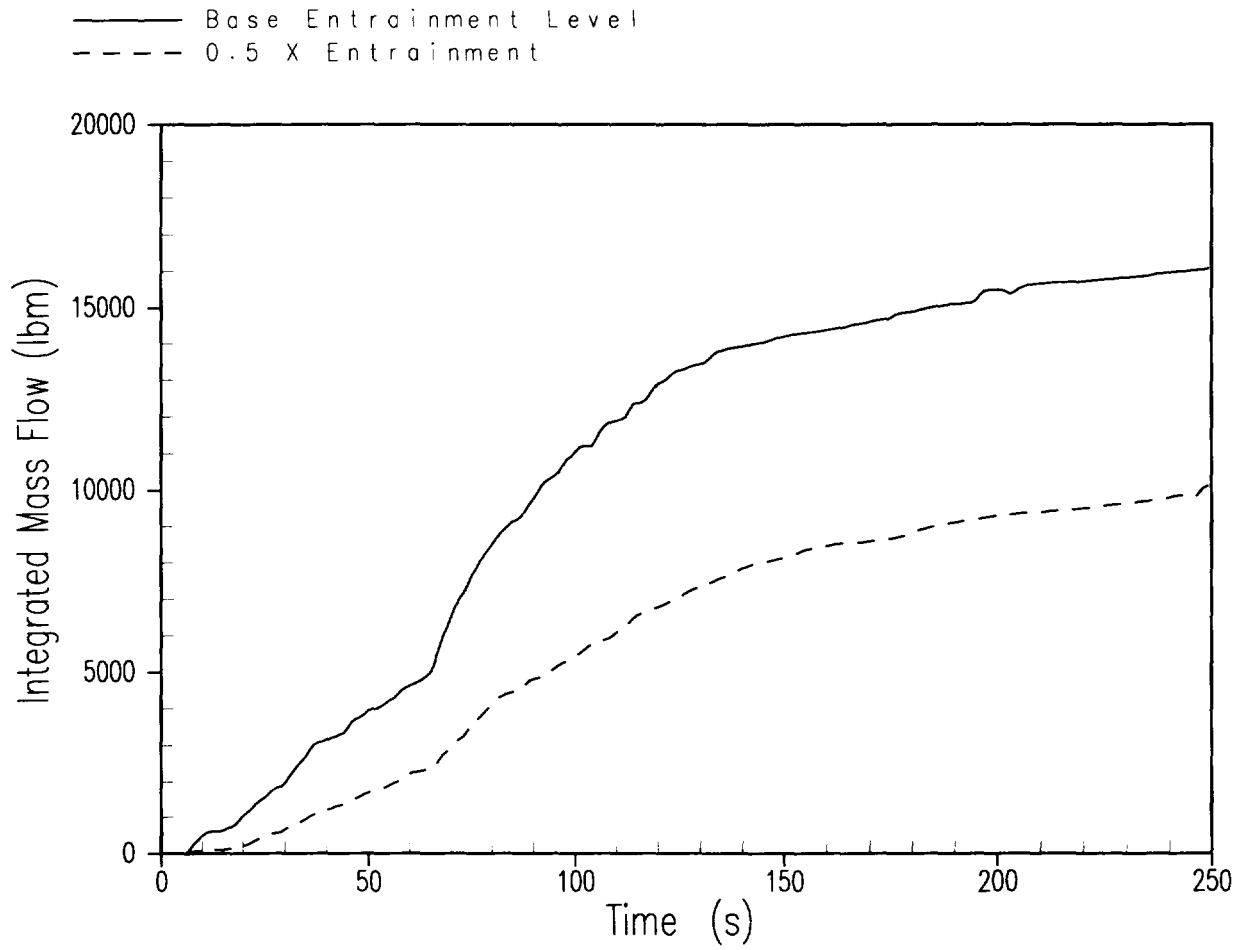


Figure A.4.2-5 0.5 Entrainment Rate Case Entrained Flow into the Single Failure Loop Hot Leg

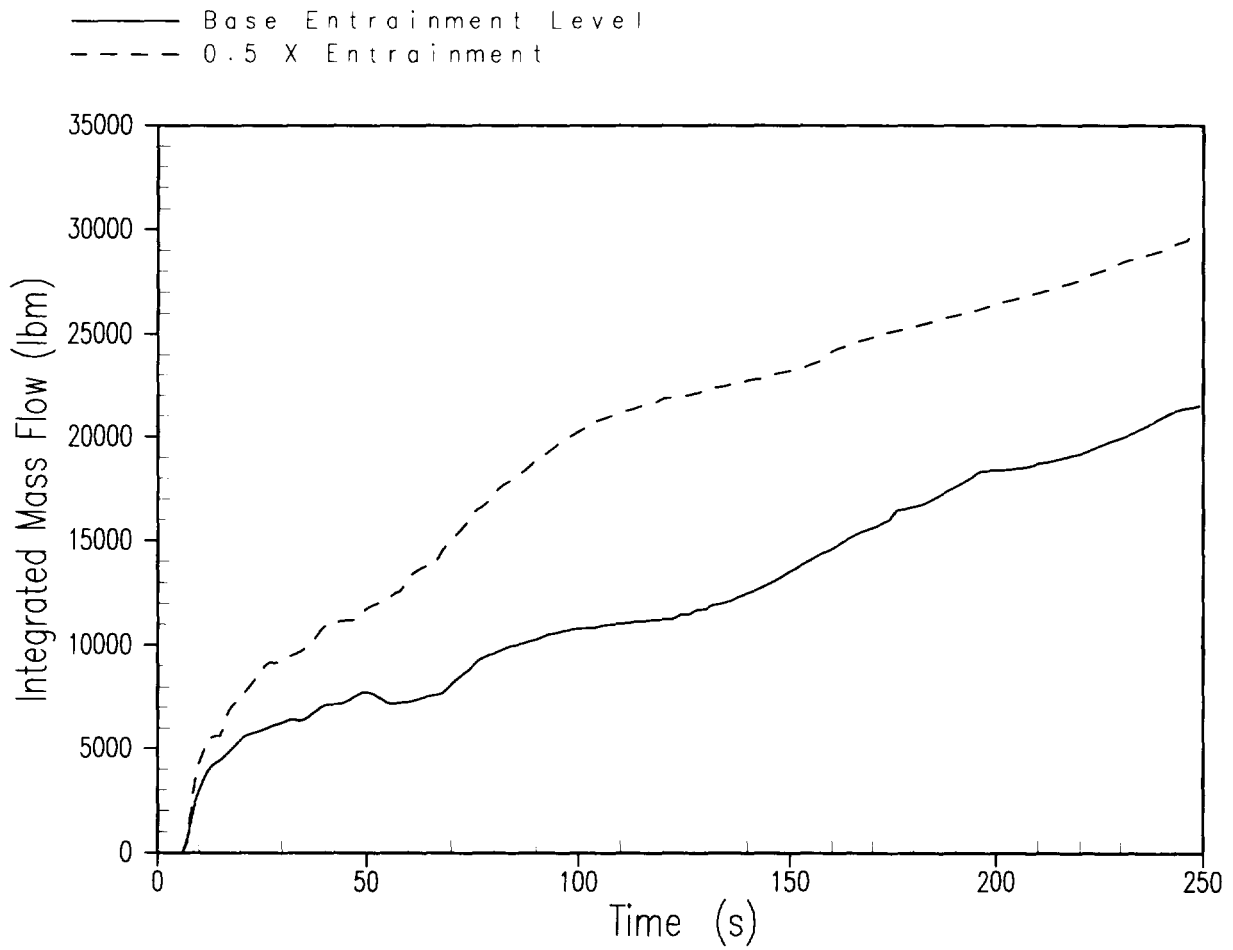


Figure A.4.2-6 0.5 Entrainment Rate Case Liquid Field Flow into the Intact Loop Hot Leg

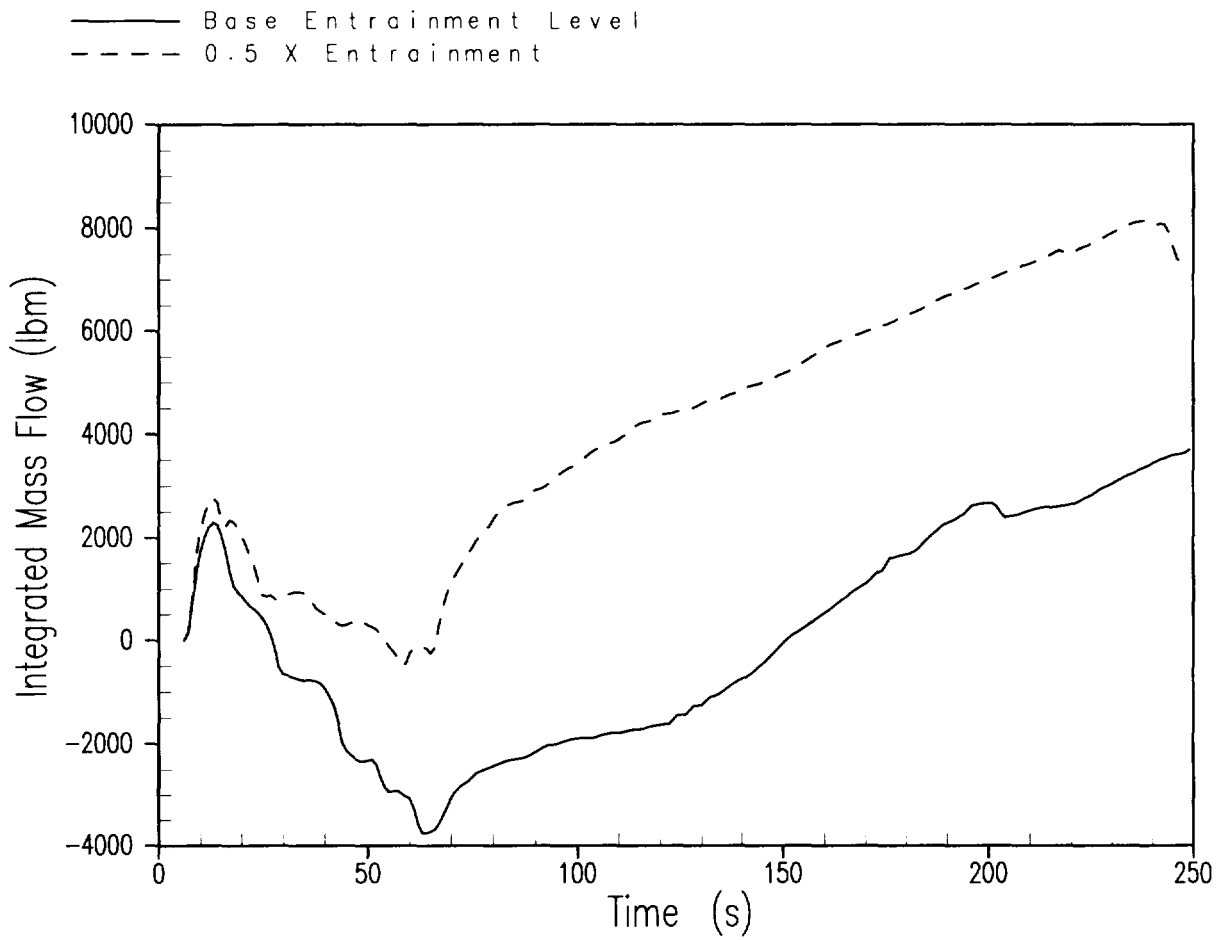


Figure A.4.2-7 0.5 Entrainment Rate Case Liquid Field Flow into the Single Failure Loop Hot Leg

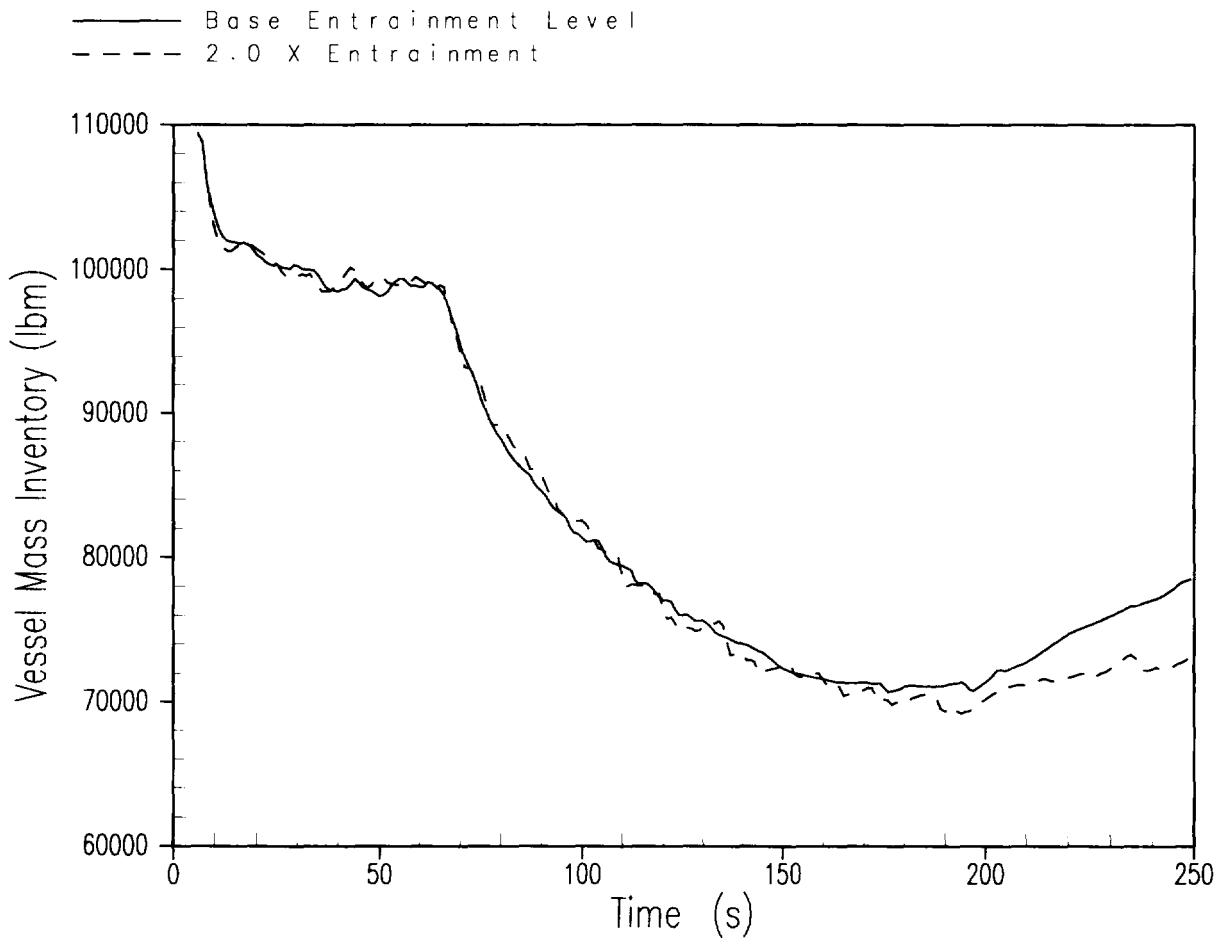


Figure A.4.2-8 2.0 Entrainment Rate Case Vessel Mass Inventory

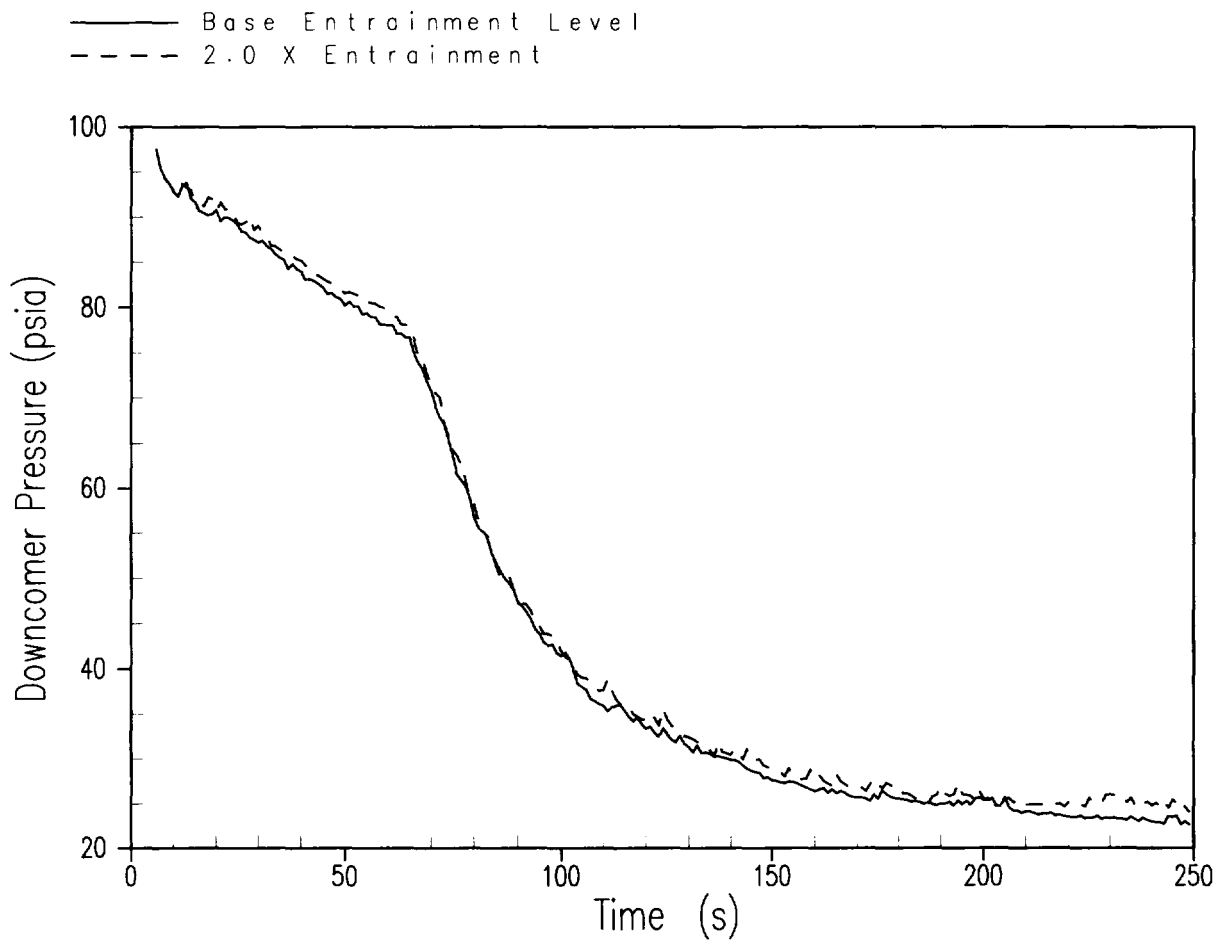


Figure A.4.2-9 2.0 Entrainment Rate Case Downcomer Pressure

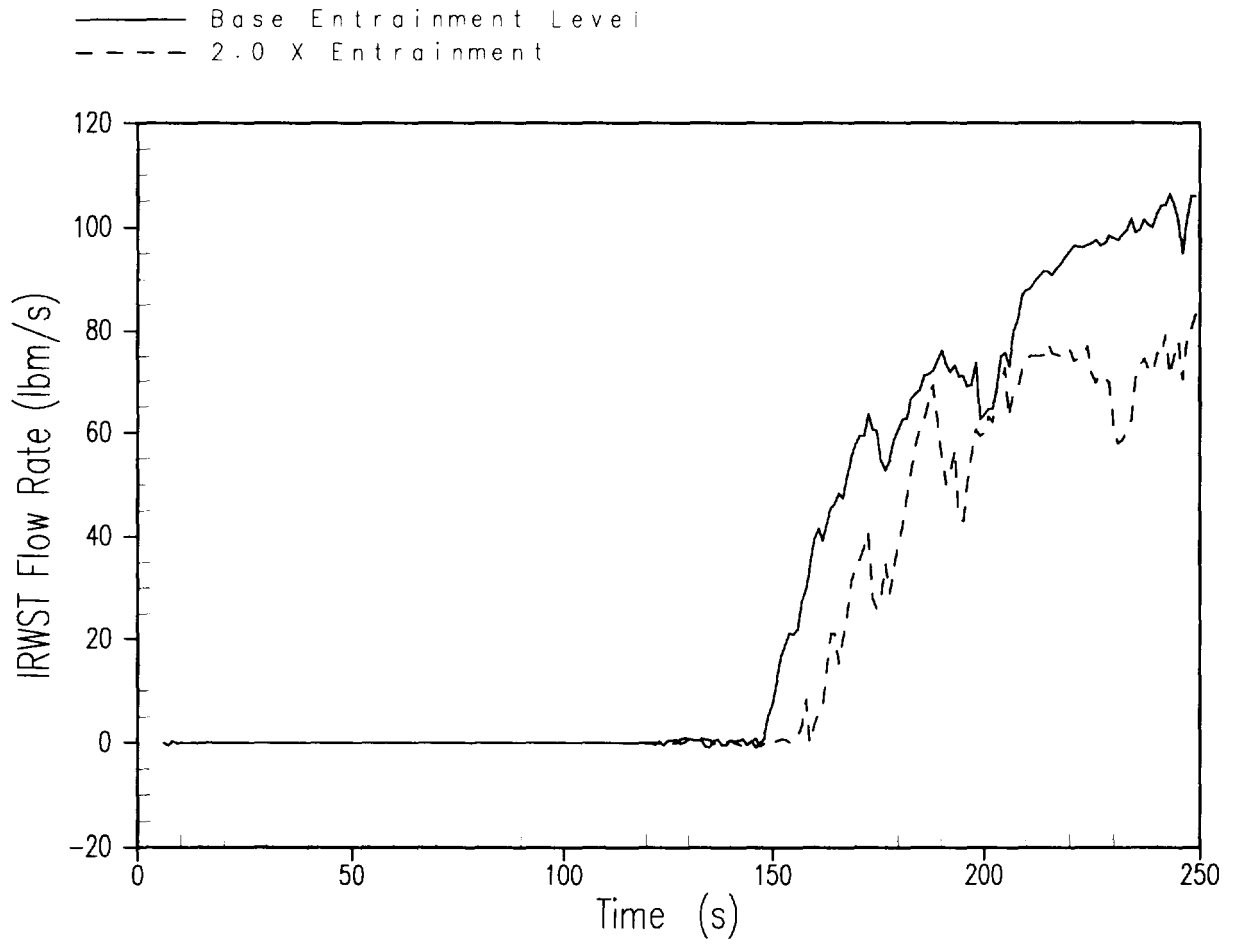


Figure A.4.2-10 2.0 Entrainment Rate Case IRWST Injection Flow Rate

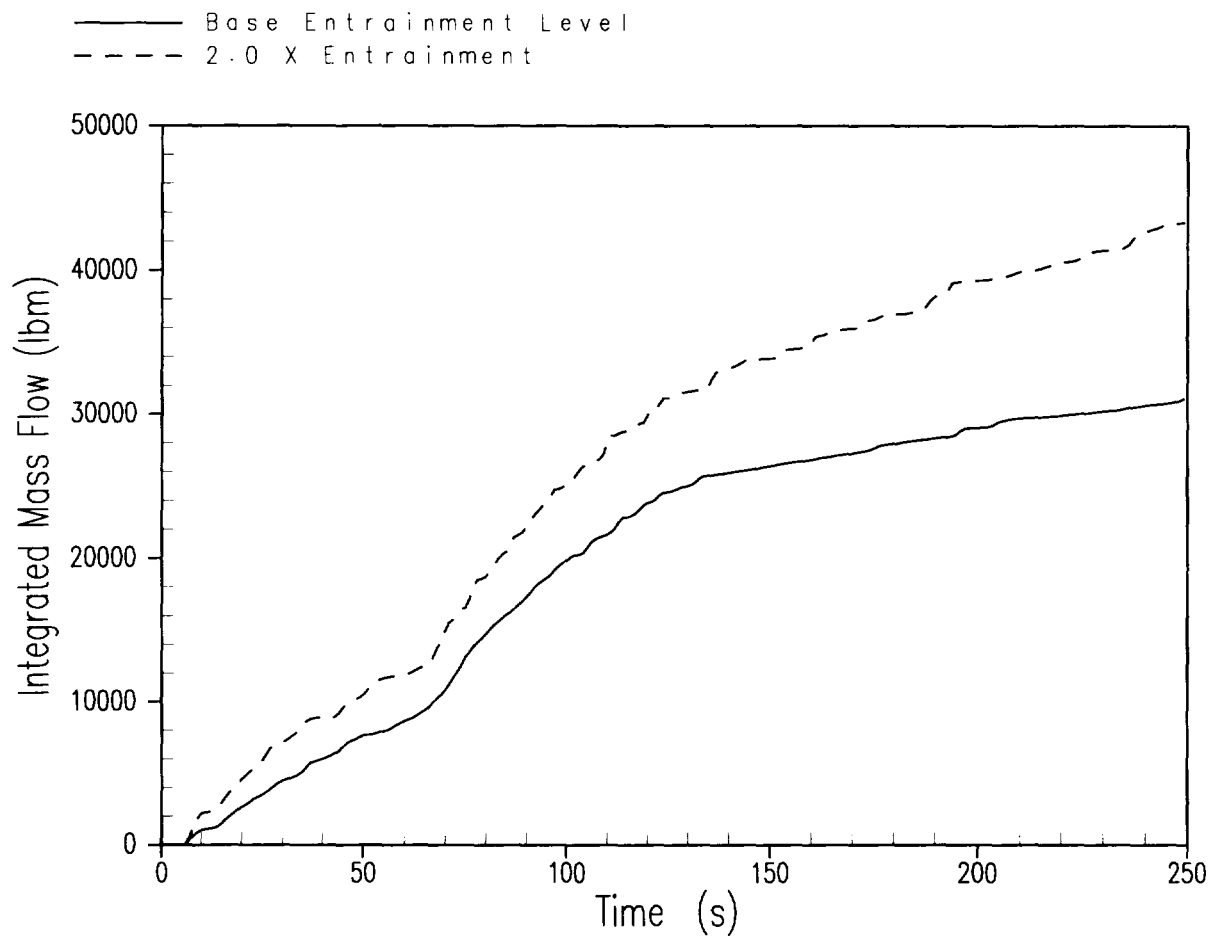


Figure A.4.2-11 2.0 Entrainment Rate Case Entrained Flow into the Intact Loop Hot Leg

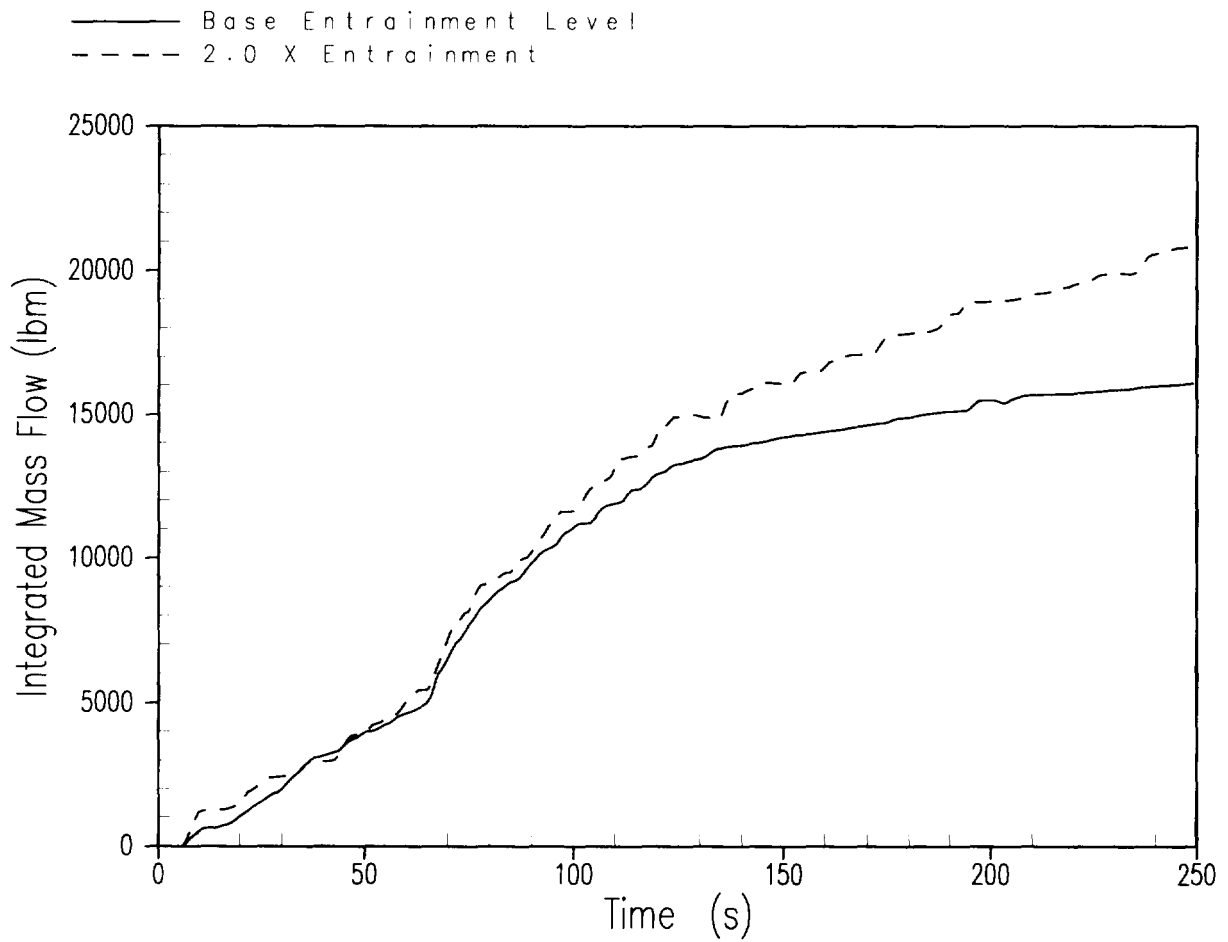


Figure A.4.2-12 2.0 Entrainment Rate Case Entrained Flow into the Single Failure Loop Hot Leg

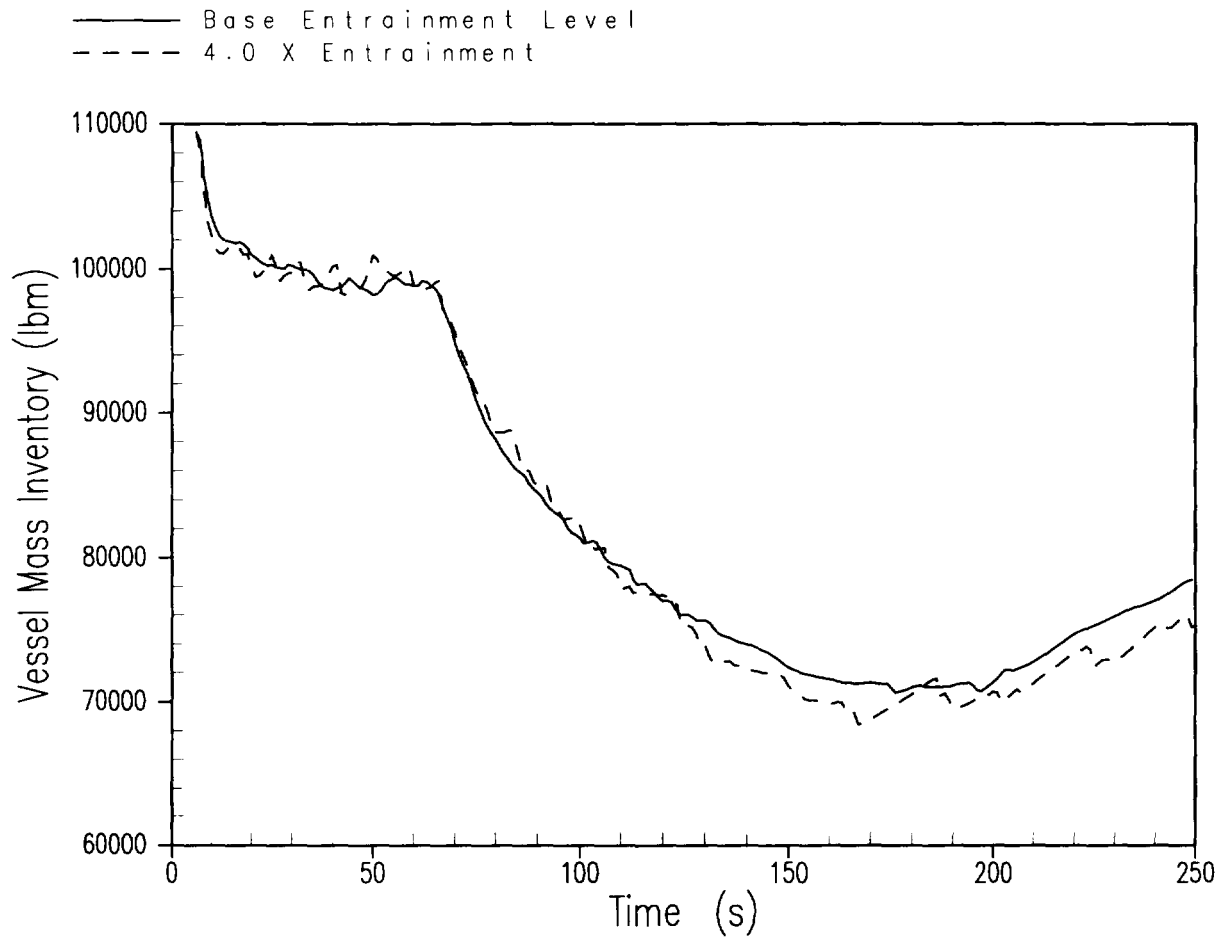


Figure A.4.2-13 4.0 Entrainment Rate Case Vessel Mass Inventory

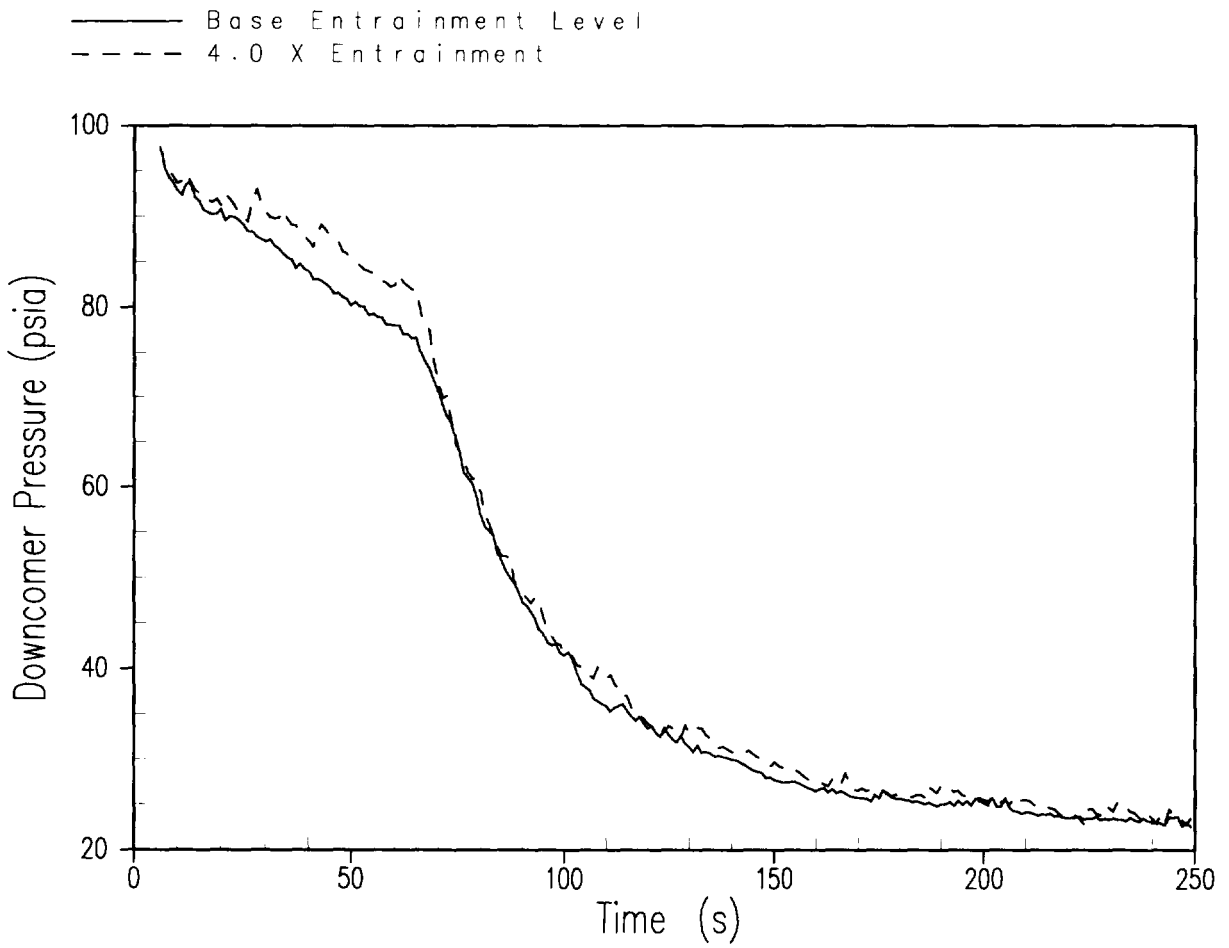


Figure A.4.2-14 4.0 Entrainment Rate Case Downcomer Pressure

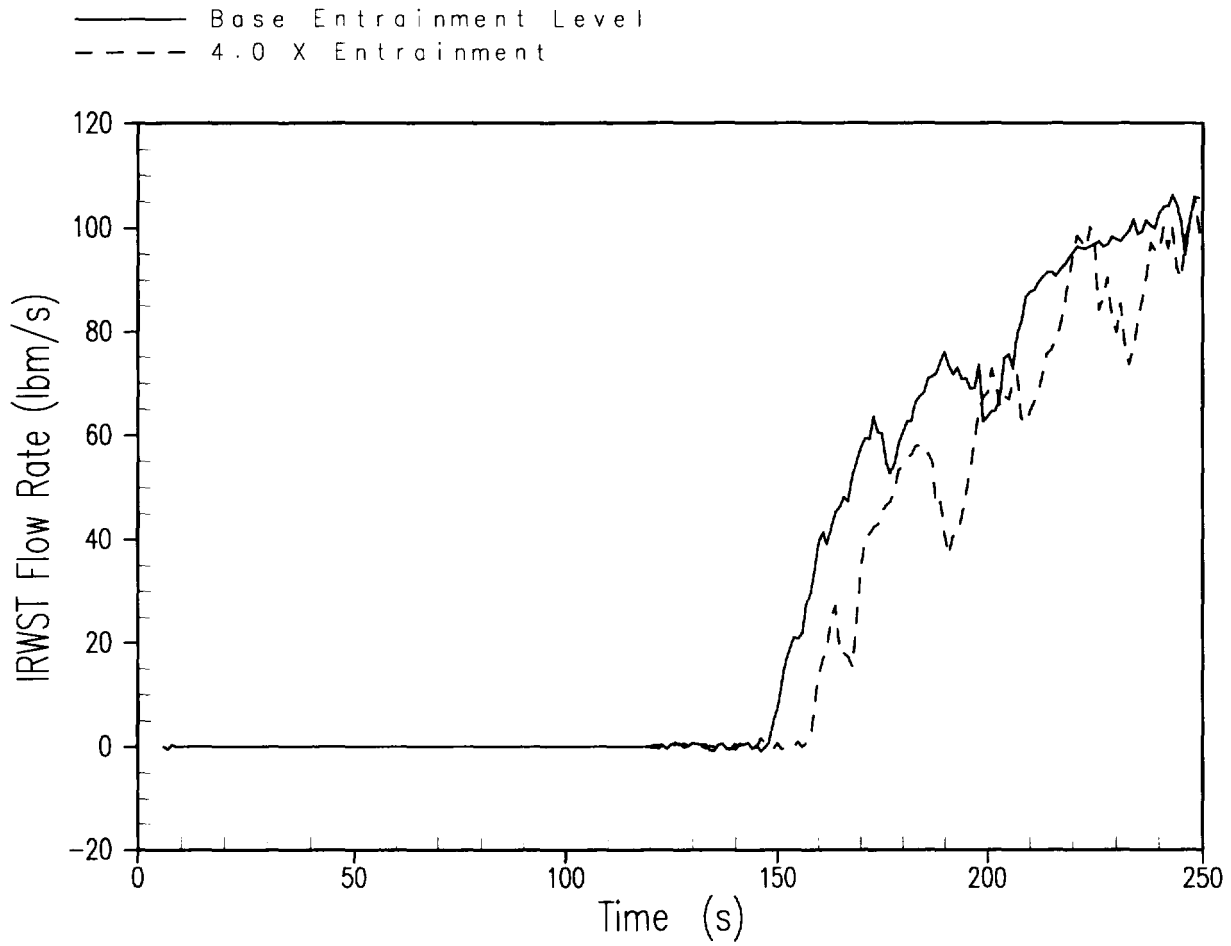


Figure A.4.2-15 4.0 Entrainment Rate Case IRWST Injection Flow Rate

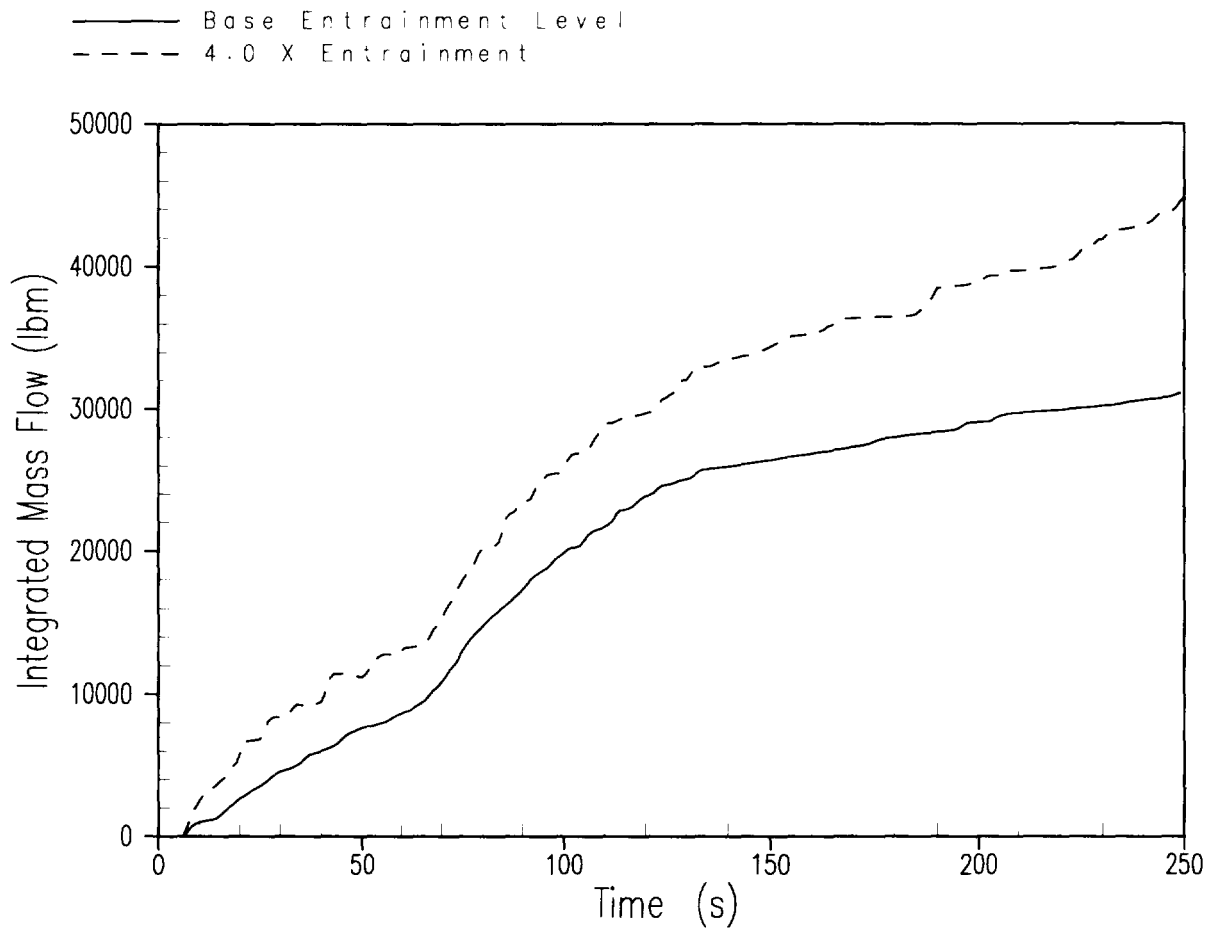


Figure A.4.2-16 4.0 Entrainment Rate Case Entrained Flow into the Intact Loop Hot Leg

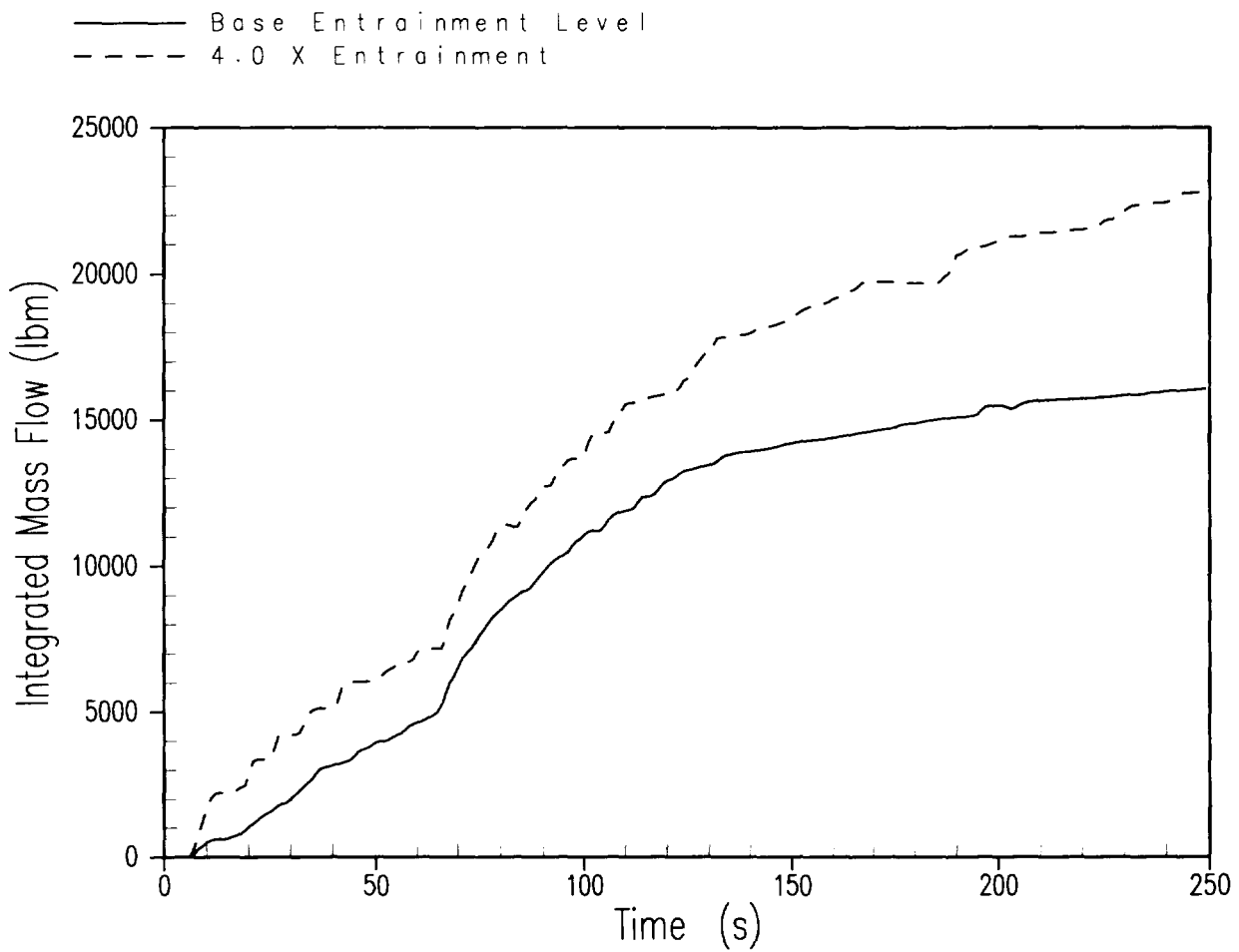


Figure A.4.2-17 4.0 Entrainment Rate Case Entrained Flow into the Single Failure Loop Hot Leg

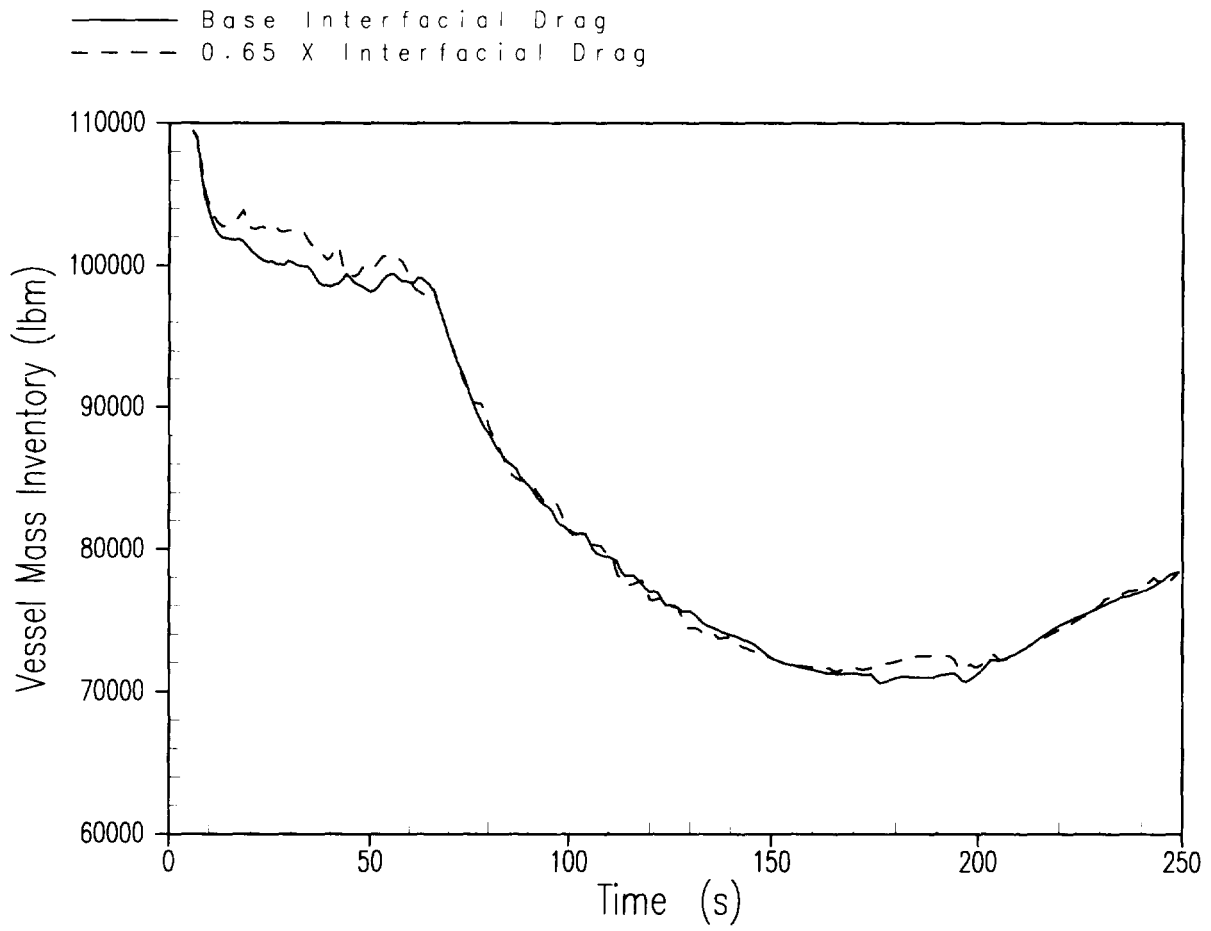


Figure A.4.3-1 Reduced Upper Plenum Interfacial Drag Vessel Mass Inventory

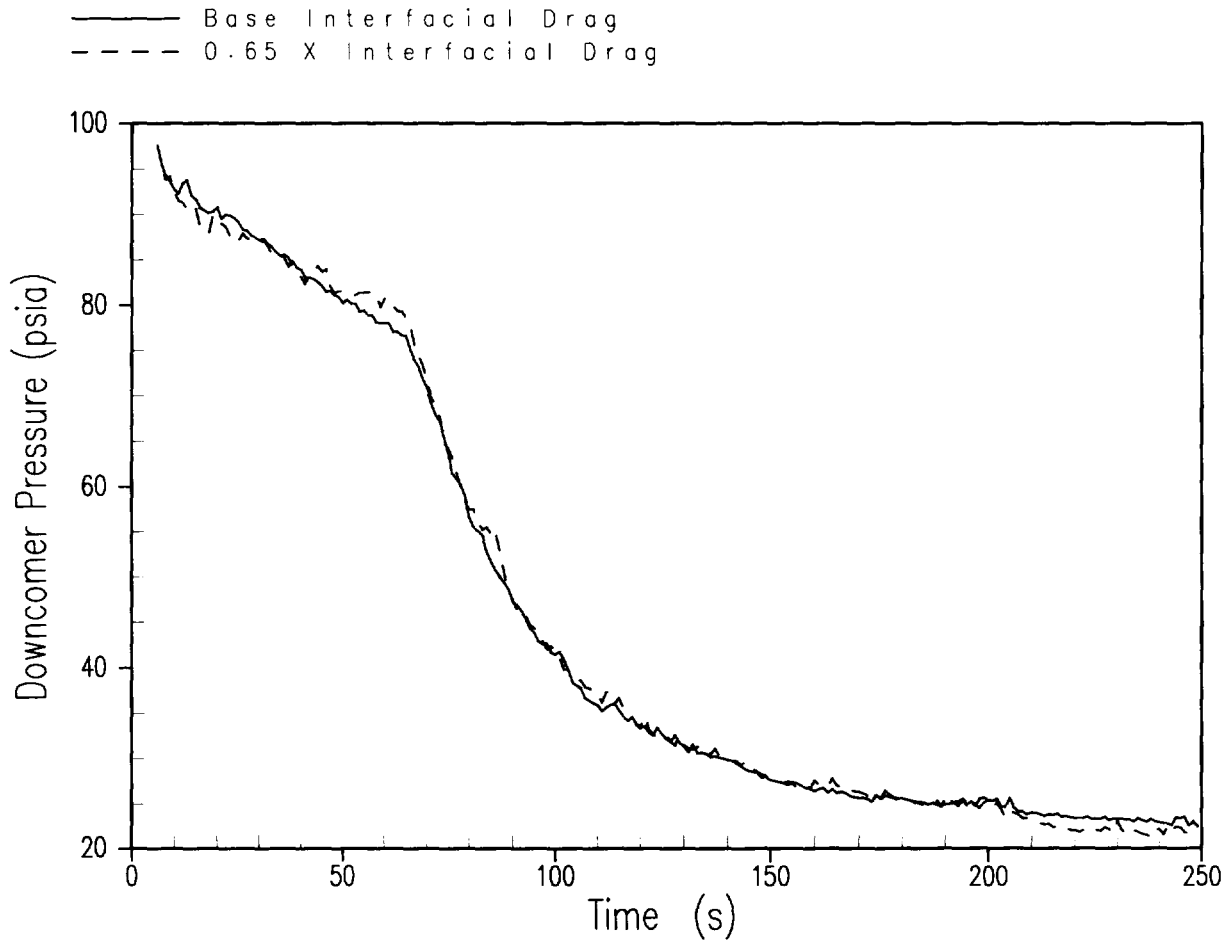


Figure A.4.3-2 Reduced Upper Plenum Interfacial Drag Downcomer Pressure

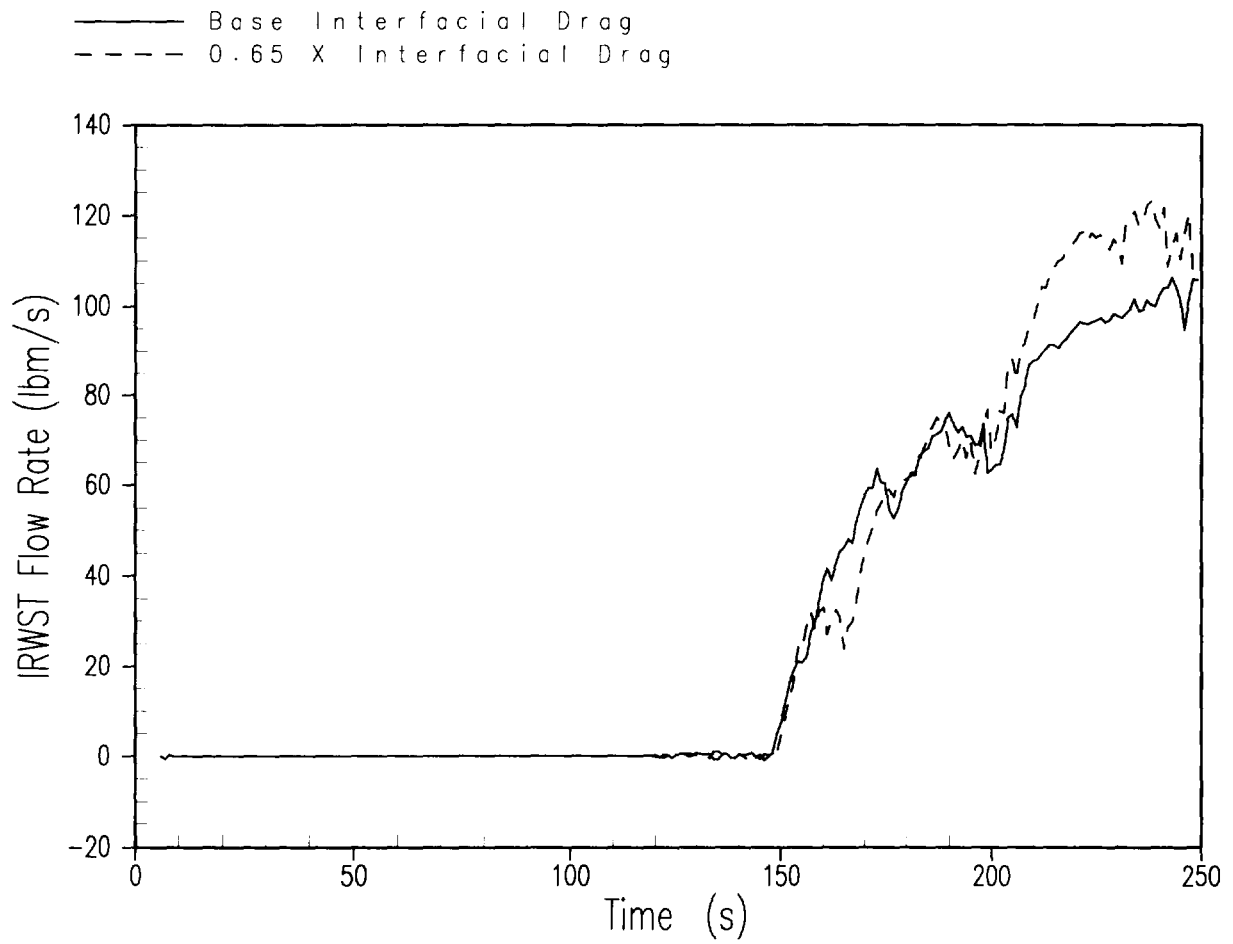


Figure A.4.3-3 Reduced Upper Plenum Interfacial Drag IRWST Injection Flow Rate

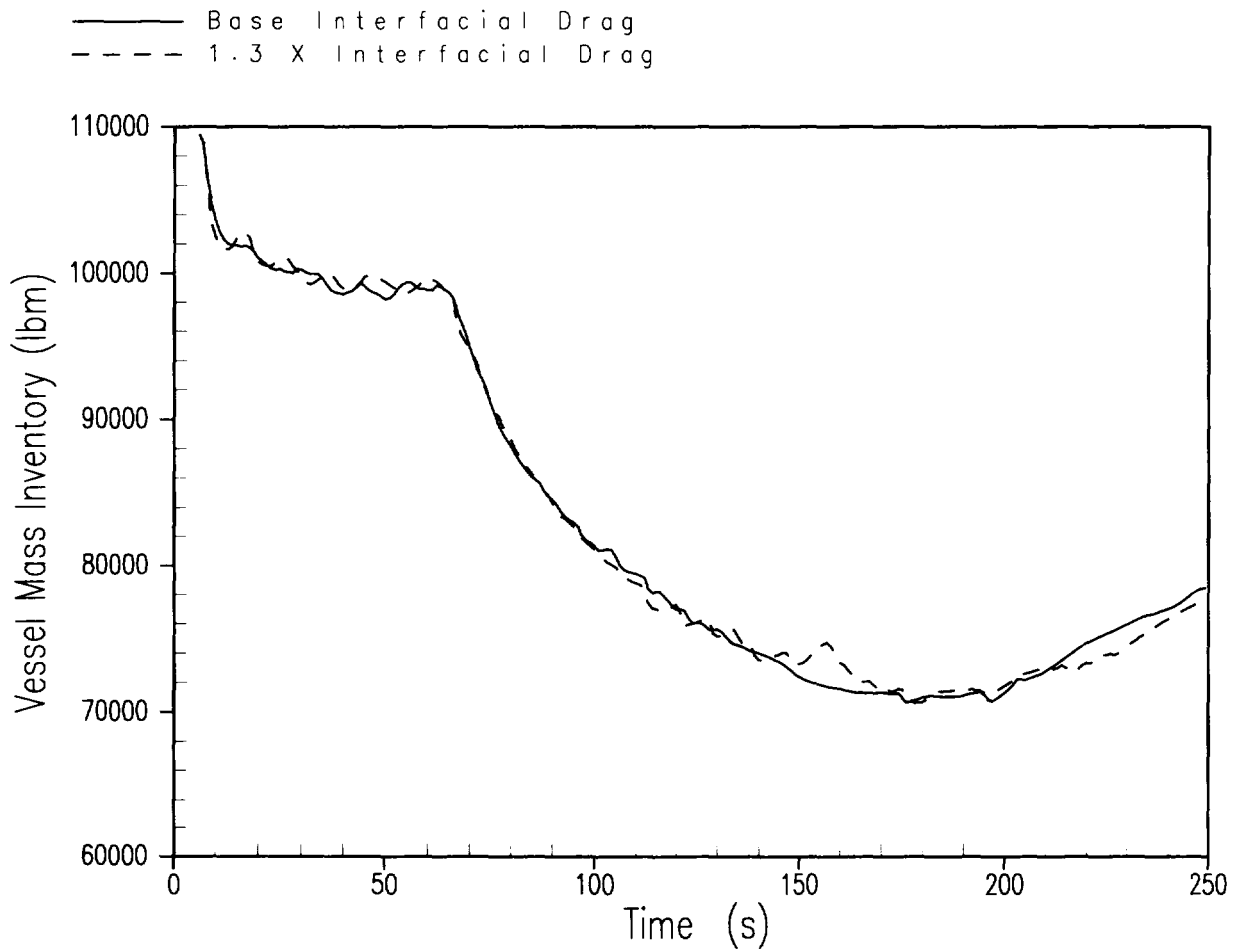


Figure A.4.3-4 Increased Upper Plenum Interfacial Drag Vessel Mass Inventory

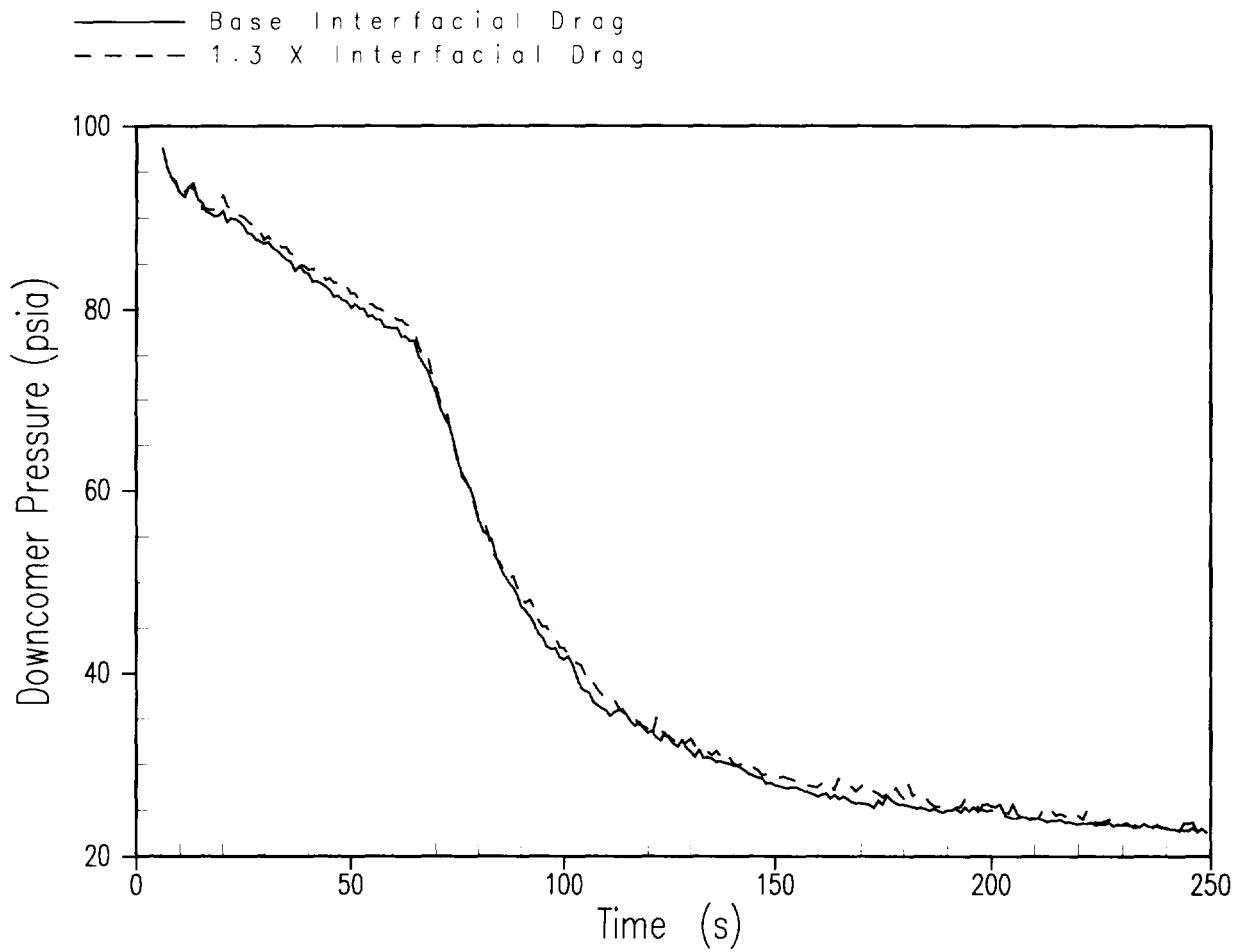


Figure A.4.3-5 Increased Upper Plenum Interfacial Drag Downcomer Pressure

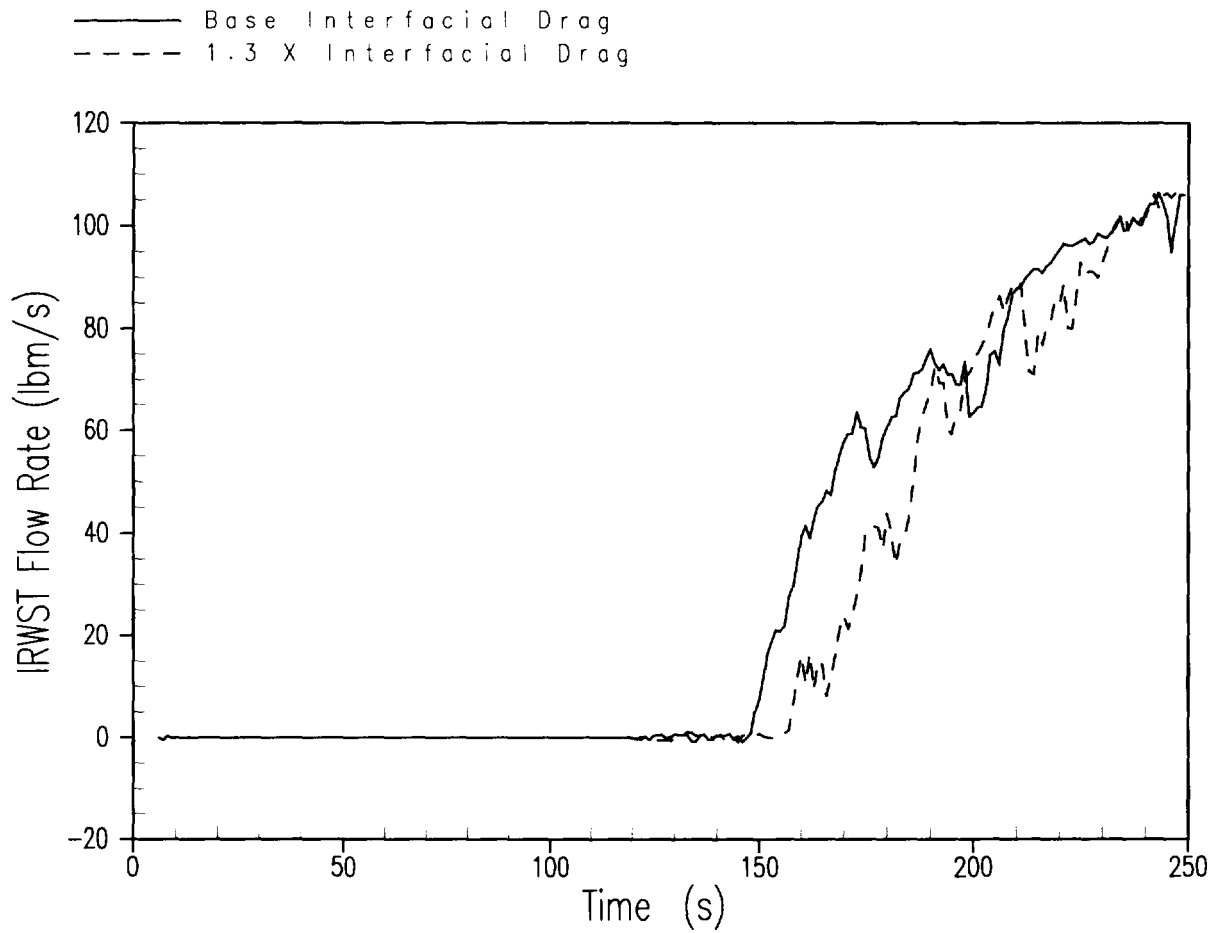


Figure A.4.3-6 Increased Upper Plenum Interfacial Drag IRWST Injection Flow Rate

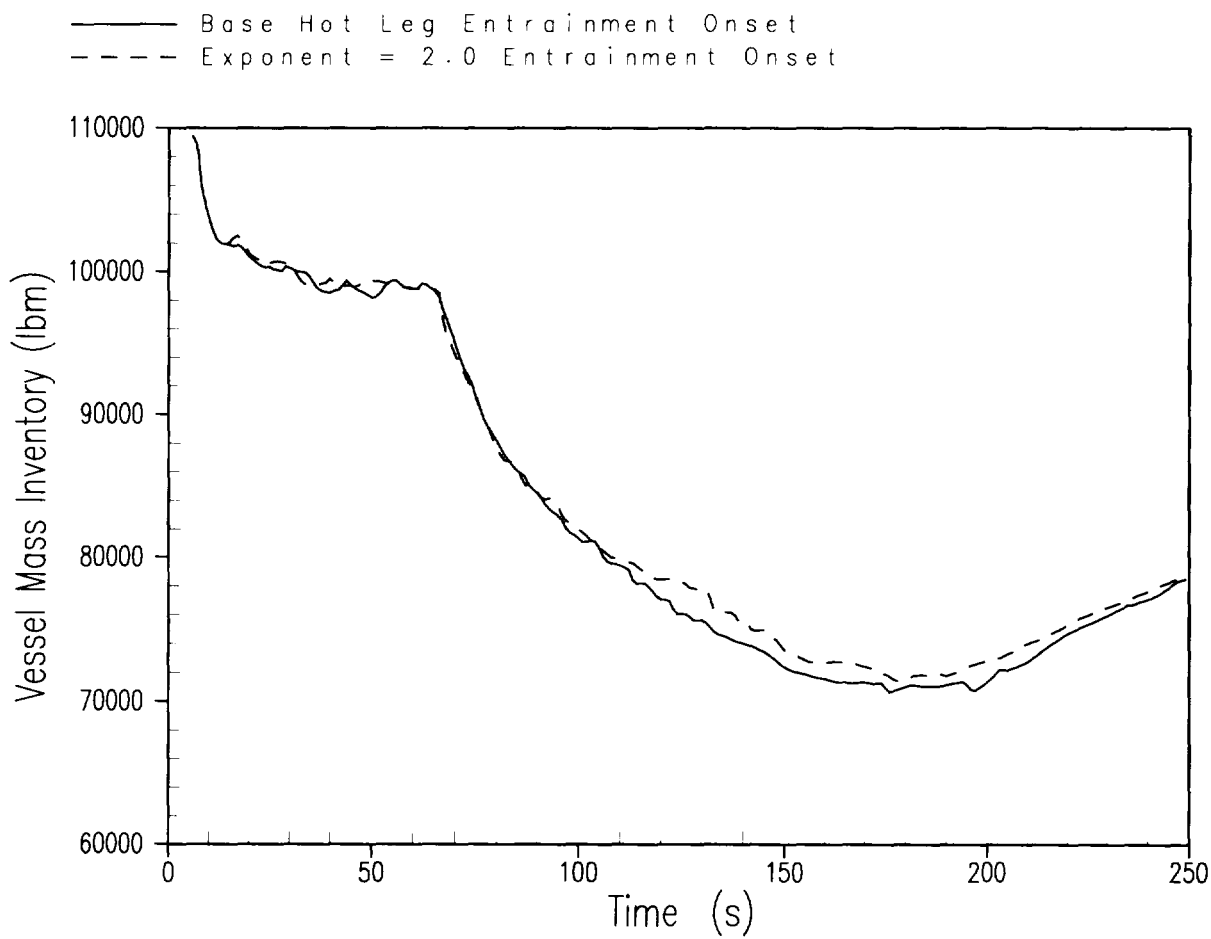


Figure A.4.4-1 Reduced Entrainment Onset Correlation Exponent Vessel Mass Inventory

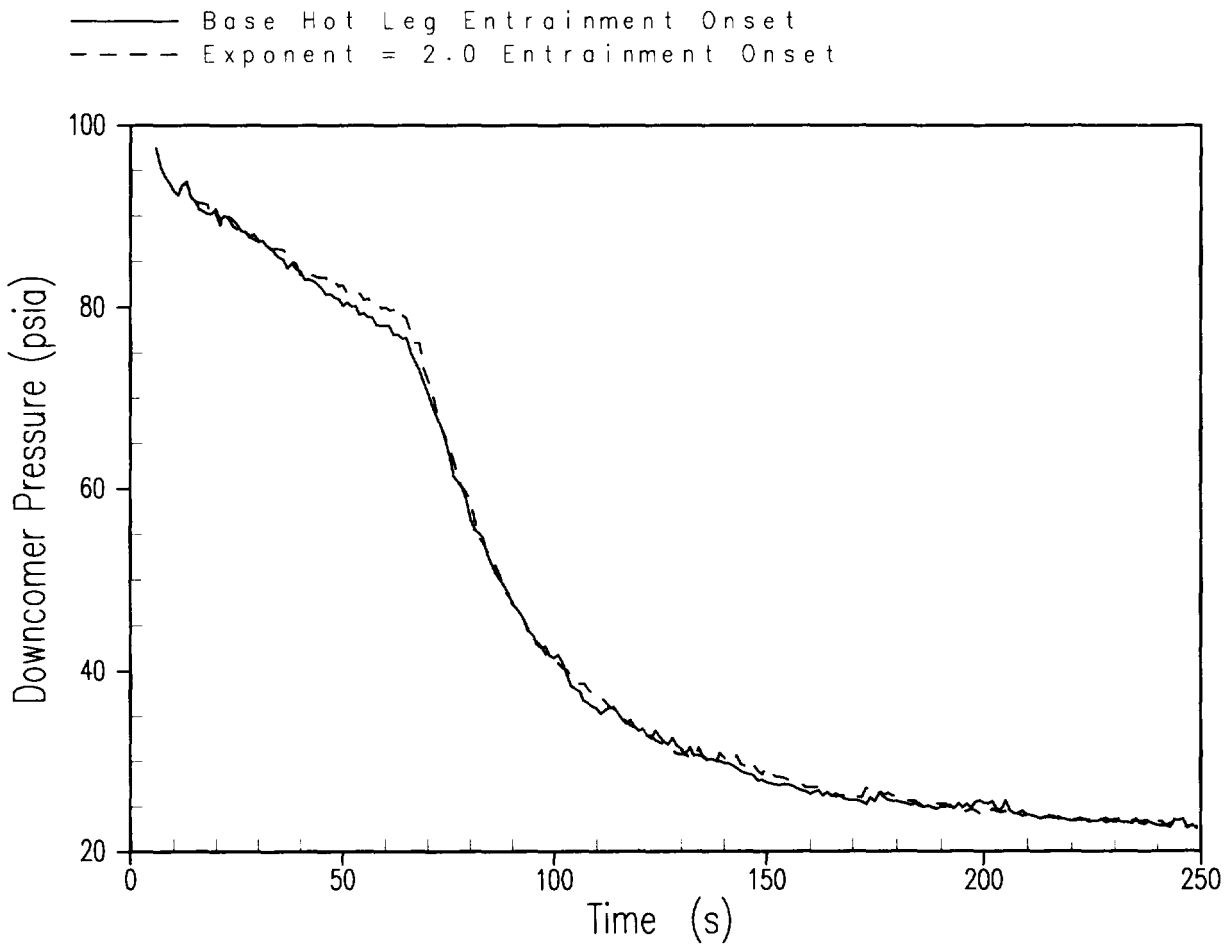


Figure A.4.4-2 Reduced Entrainment Onset Correlation Exponent Downcomer Pressure

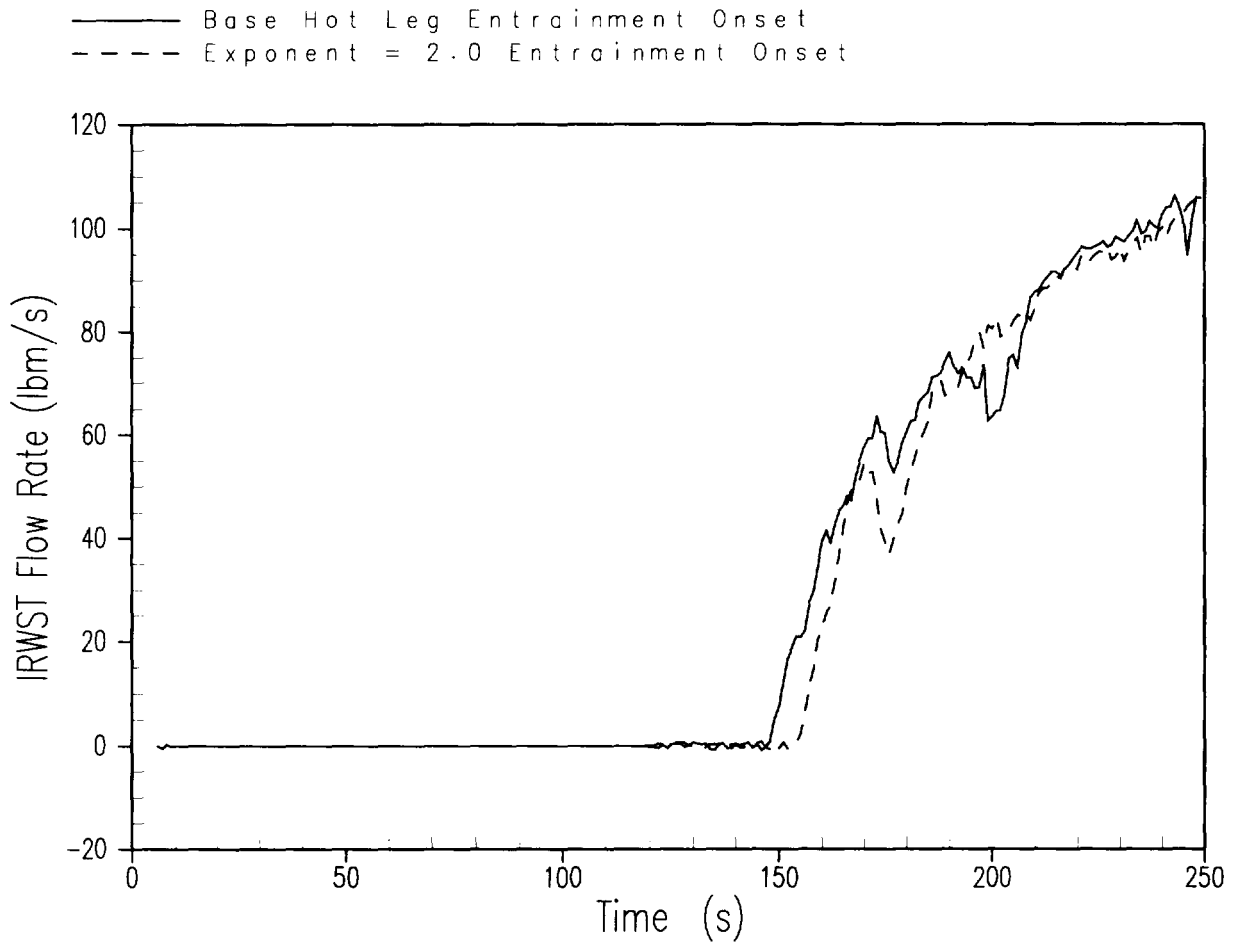


Figure A.4.4-3 Reduced Entrainment Onset Correlation Exponent IRWST Injection Flow Rate

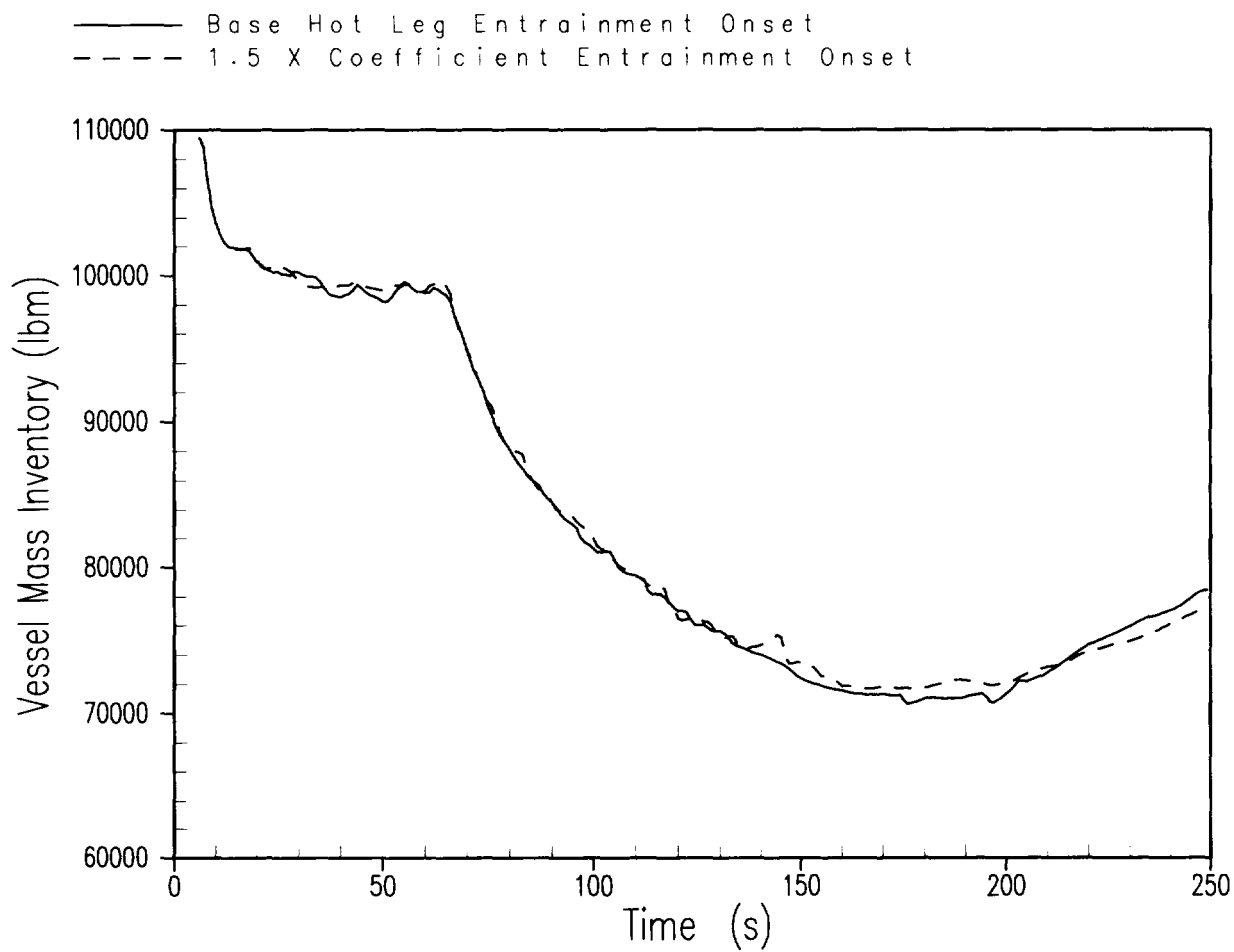


Figure A.4.4-4 Increased Entrainment Onset Correlation Coefficient Vessel Mass Inventory

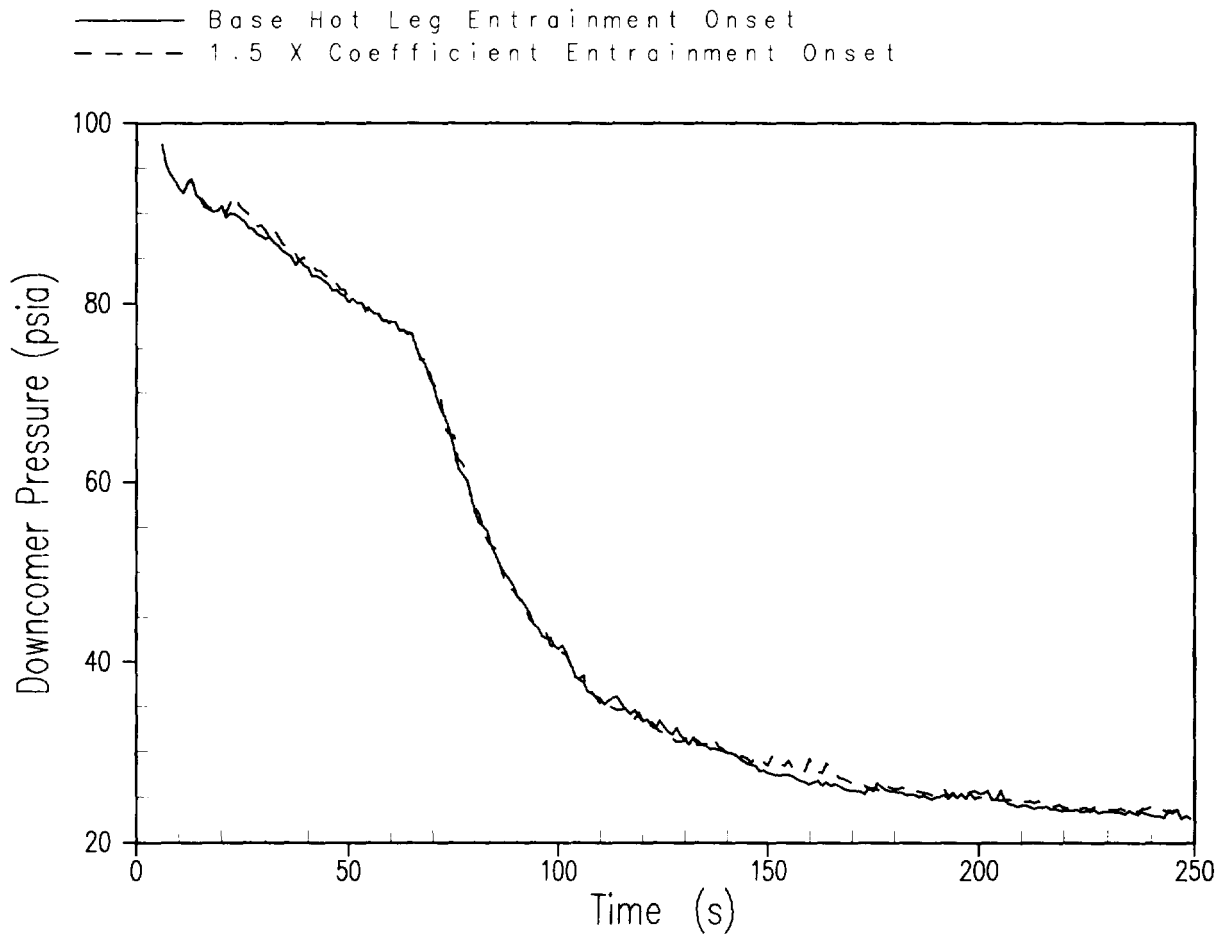


Figure A.4.4-5 Increased Entrainment Onset Correlation Coefficient Downcomer Pressure

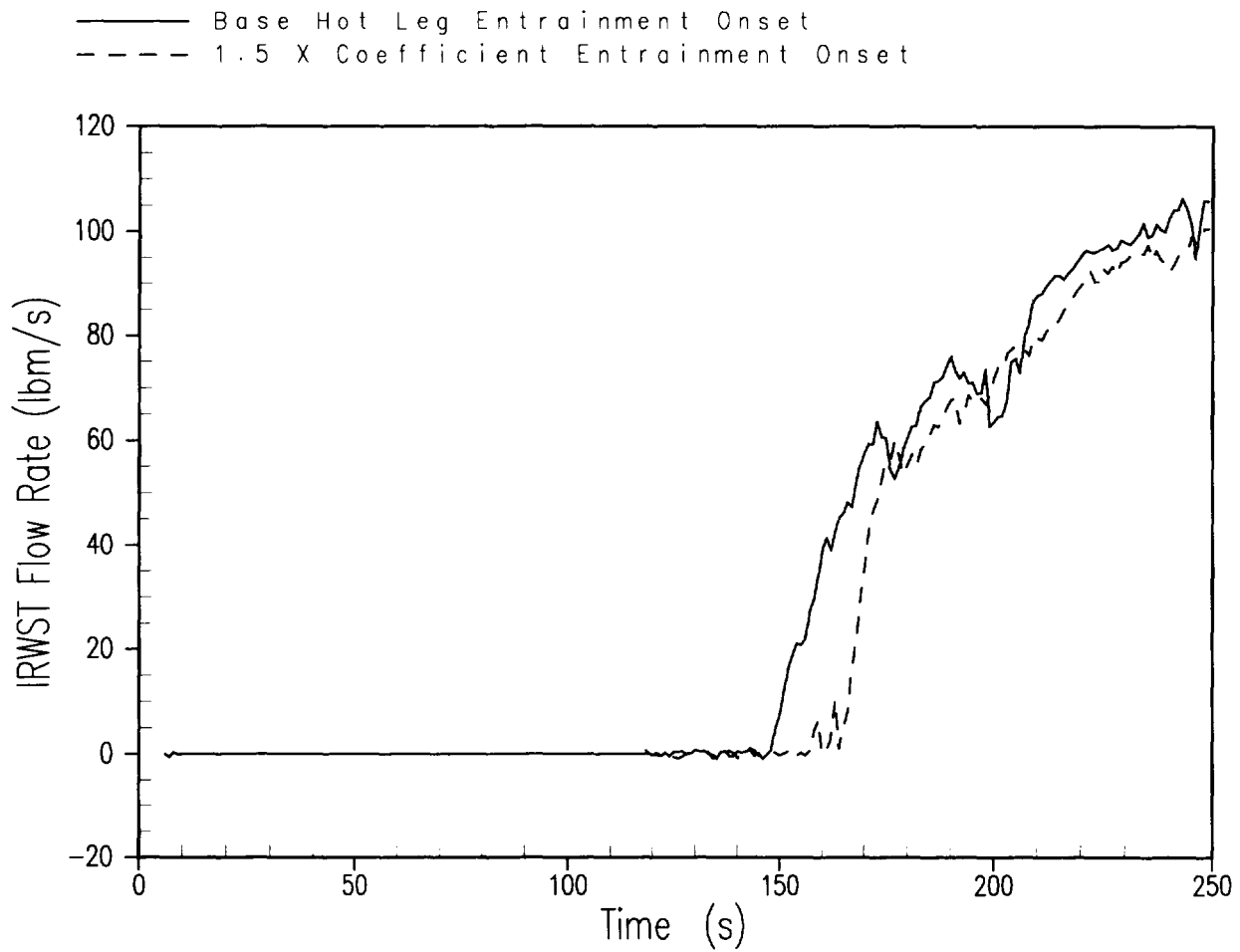


Figure A.4.4-6 Increased Entrainment Onset Correlation Coefficient IRWST Injection Flow Rate

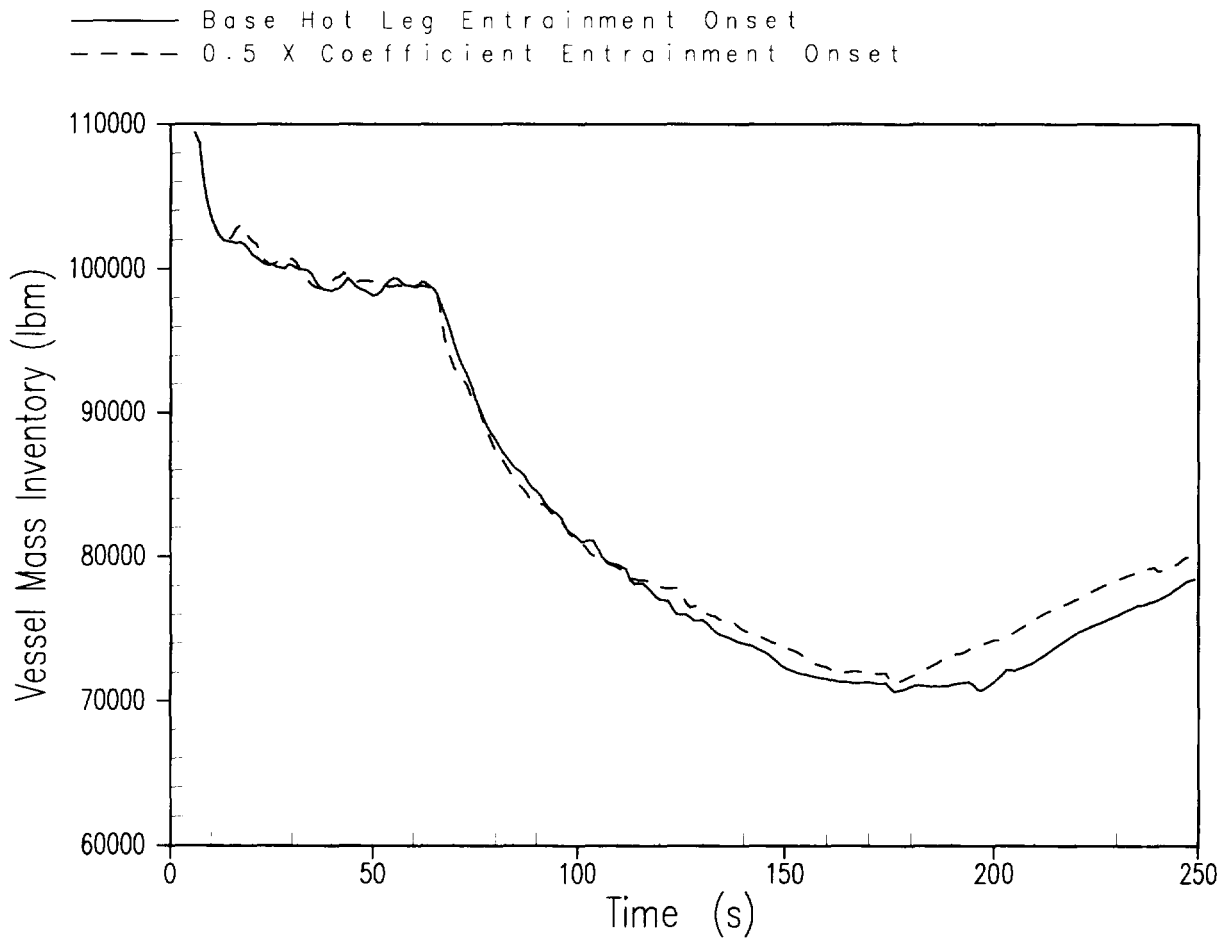


Figure A.4.4-7 Reduced Entrainment Onset Correlation Coefficient Vessel Mass Inventory

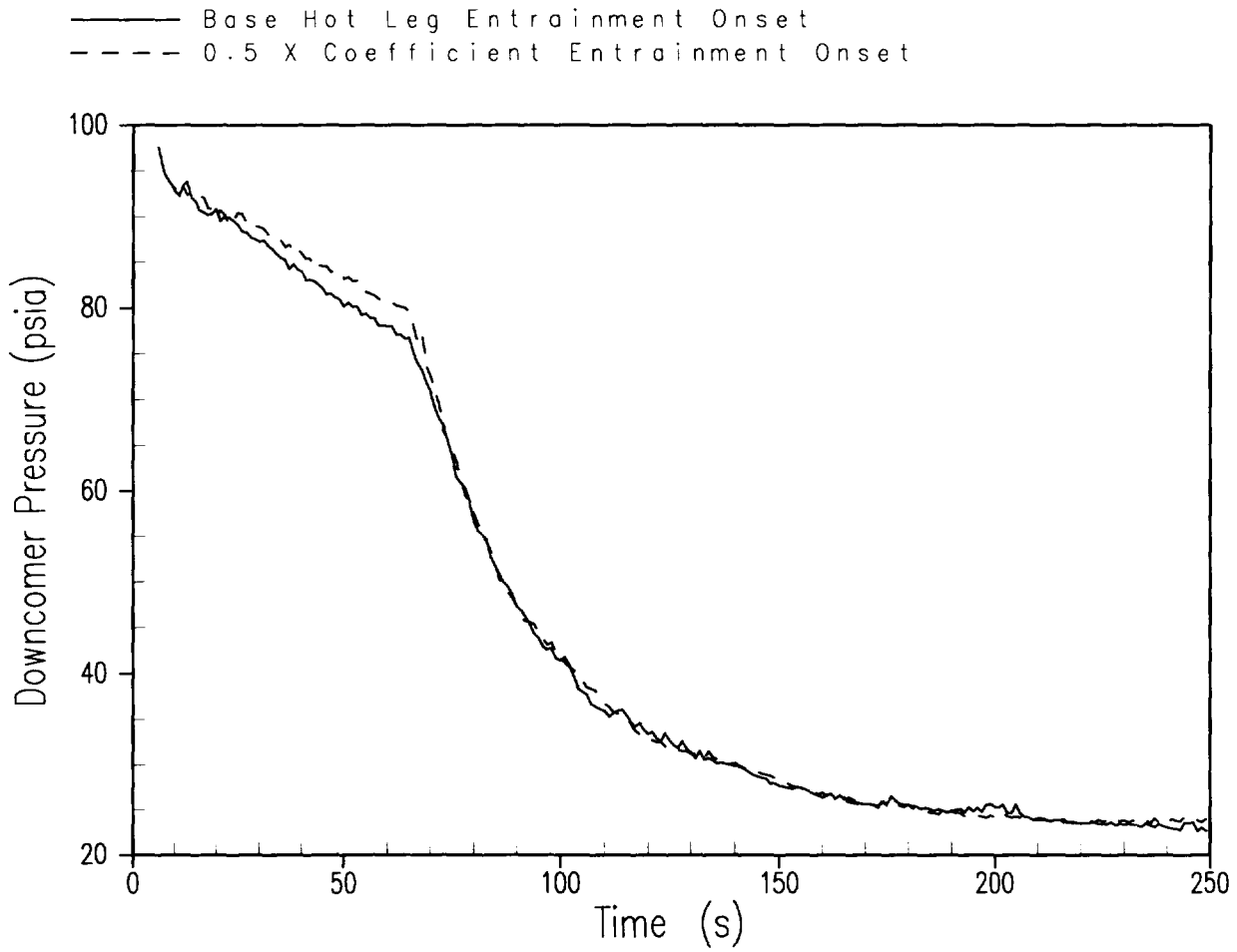


Figure A.4.4-8 Reduced Entrainment Onset Correlation Coefficient Downcomer Pressure

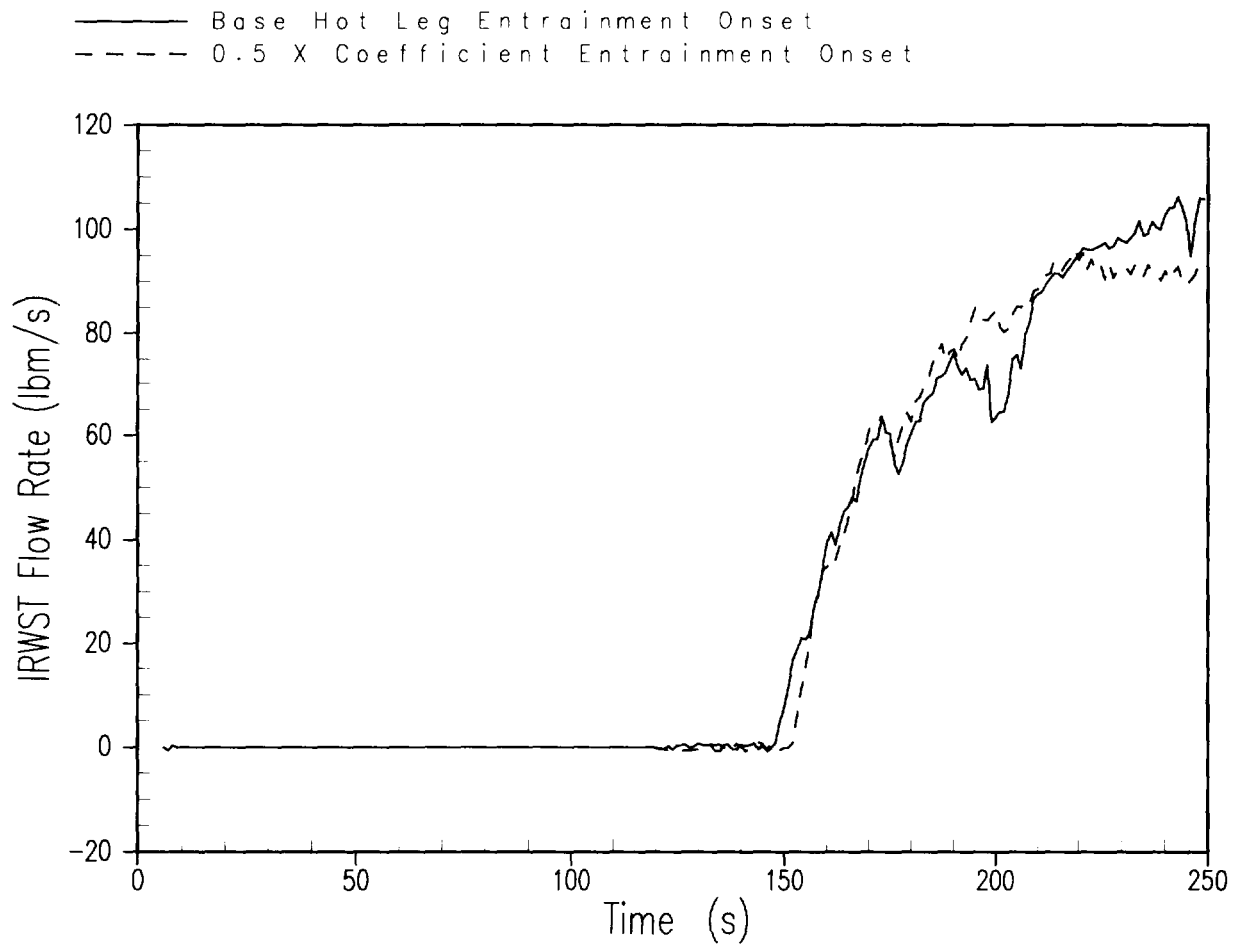


Figure A.4.4-9 Reduced Entrainment Onset Correlation Coefficient IRWST Injection Flow Rate

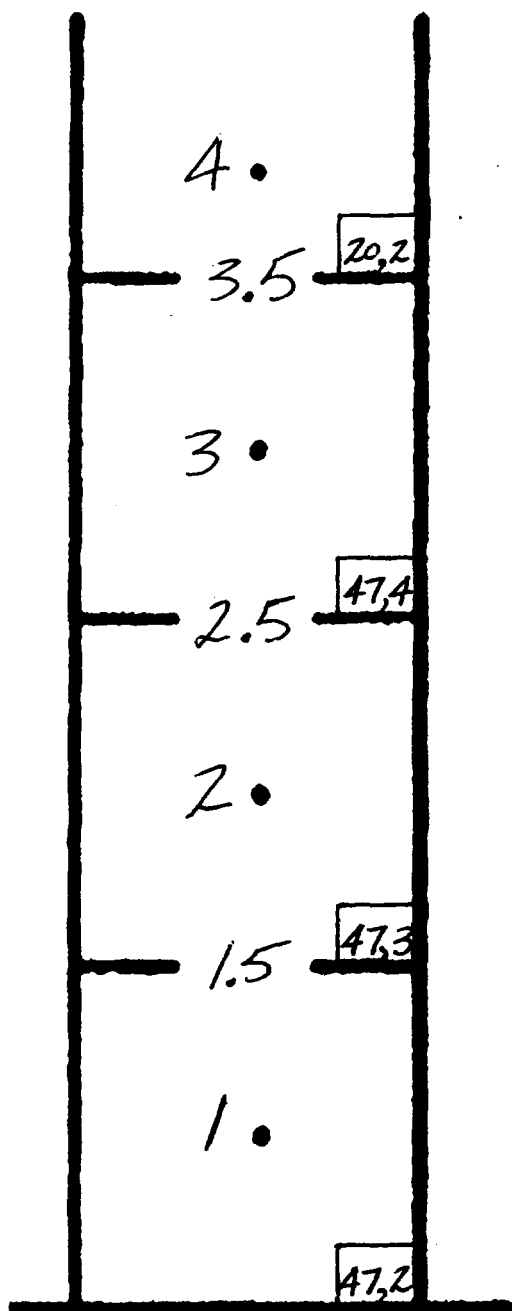


Figure A.4.5-1 AP1000 WCOBRA/TRAC Upper Plenum Channel Detail Indicating Positions

| | | | | |
|-----------|----|-----|---|--------------------|
| — | AL | 1 | 0 | 0 TIME = 66.0 SEC |
| - - - | AL | 39 | 0 | 0 TIME = 104.0 SEC |
| - - - - - | AL | 55 | 0 | 0 TIME = 120.0 SEC |
| - · - · - | AL | 65 | 0 | 0 TIME = 130.0 SEC |
| - - - - - | AL | 81 | 0 | 0 TIME = 146.0 SEC |
| - · - · - | AL | 97 | 0 | 0 TIME = 162.0 SEC |
| - - - - - | AL | 120 | 0 | 0 TIME = 185.0 SEC |

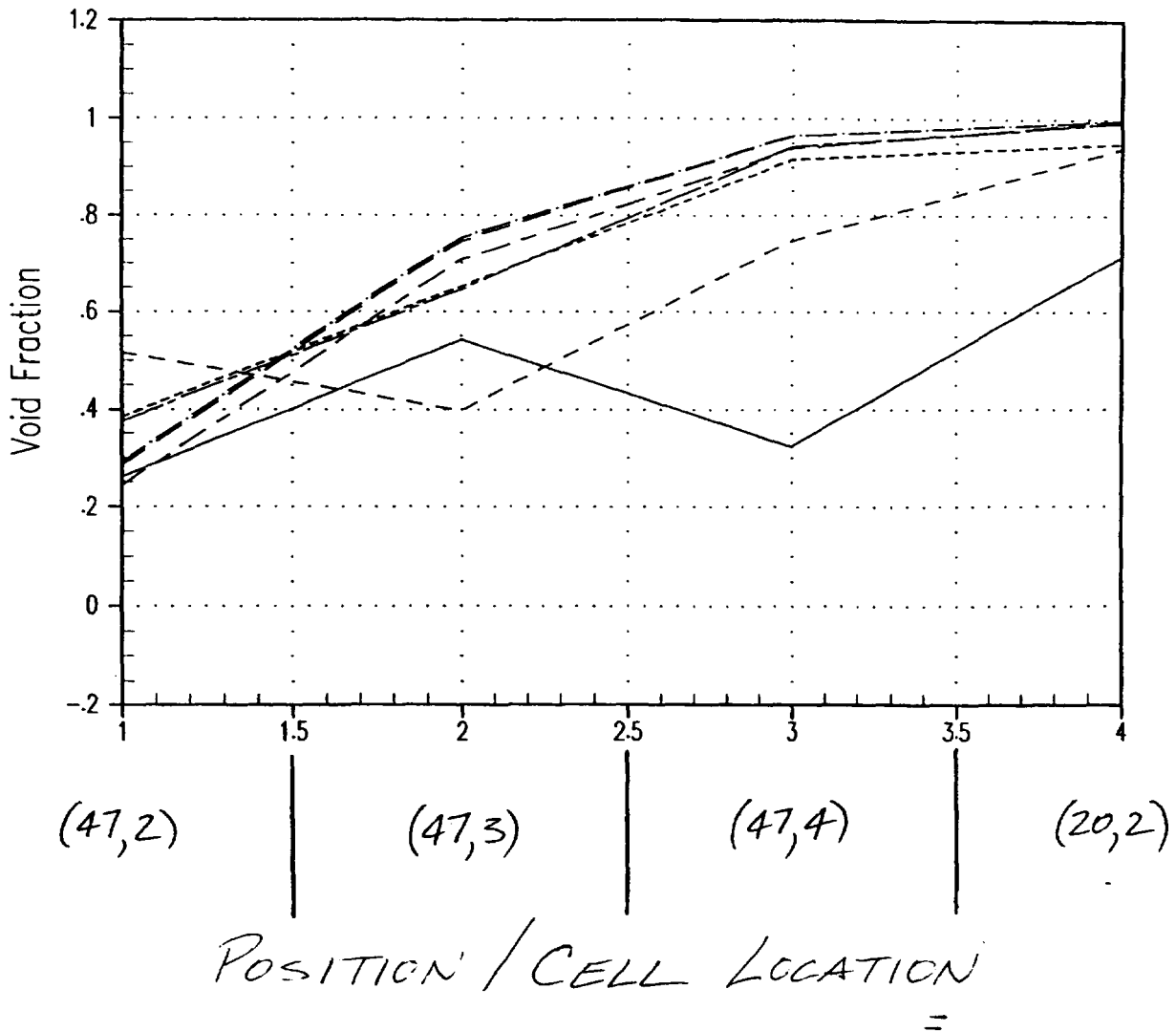


Figure A.4.5-2 WCOBRA/TRAC Upper Plenum Void Fraction Profile

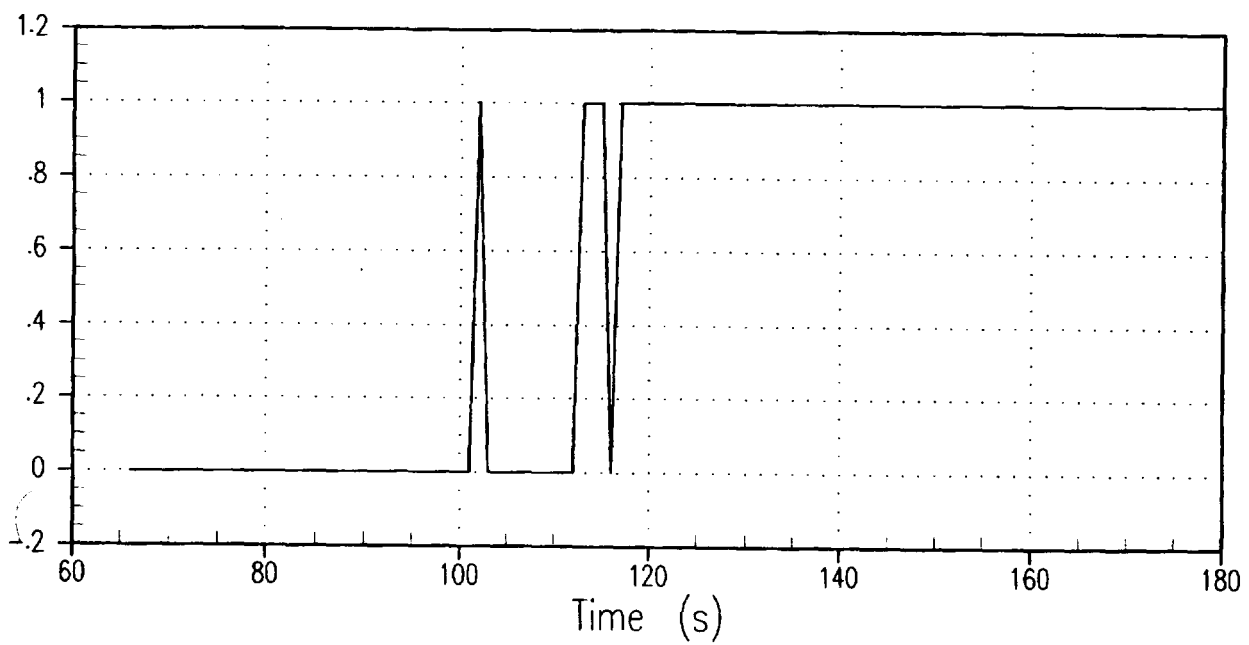


Figure A.4.5-3 Index of the WCOBRA/TRAC Upper Plenum Two-Phase Mixture Level

A.5 CONCLUSIONS

This appendix addresses the issues raised by the NRC staff during the pre-certification review regarding hot leg entrainment and upper plenum entrainment and their effect on the performance of the passive core cooling system following a small break LOCA. In the AP1000 pre-certification review, the staff concludes that the tests and analysis codes used to support AP600 Design Certification are sufficiently scaled for AP1000 such that they are applicable to support AP1000 Design Certification. An open issue with this conclusion is the treatment of hot leg and upper plenum entrainment in the analysis of a small break LOCA. The staff's findings regarding hot leg and upper plenum entrainment are presented in Section A.1 of this appendix.

In Section A.2 of this appendix, scaling evaluations of upper plenum and hot leg entrainment are presented. Based on these evaluations, the following conclusions are made:

- Entrainment in the hot leg is acceptably scaled for AP1000 in the OSU test facility from the standpoint of the flow regime (Froude number) and the geometry.
- Published investigations indicate that the onset to hot leg entrainment is uniquely dependent on Froude number, irrespective of the ratios of the diameter of the off-take piping to the hot leg piping (i.e., d/D). While the entrainment correlation in WCOBRA/TRAC is based on tests where the geometry is different from AP1000, the correlation acceptably calculates the entrainment rate in the hot leg.
- Hot leg entrainment can only occur when there is a water level in the hot legs. This condition is indicative of a large margin to core uncover.
- When the level in the upper plenum is at or just below the bottom of the hot leg, the Kataoka-Ishii pool entrainment model predicts entrainment ratio (E_{fg}) that depends on the local thermodynamic conditions. For these conditions, the tests are well scaled at the time of ADS-4 actuation.
- When the level in the upper plenum is below the "near surface region" as described by Kataoka-Ishii, the entrainment rate depends strongly on the distance between the pool surface and the bottom of the hot legs. Thus, the magnitude of the entrainment falls rapidly as this distance is increased.

In Section A.3, the models used in WCOBRA/TRAC to calculate upper plenum entrainment are compared with predictions using the Kataoka-Ishii correlation that has been used to predict pool entrainment. The following conclusions regarding these comparisons are made:

- The results of the comparison of the WCOBRA-TRAC models to Kataoka-Ishii show that, even though the model used in WCOBRA-TRAC considers entrainment from a liquid film instead of a pool surface, the calculated entrainment rate compares well to the Kataoka-Ishii correlation, when assuming that the liquid level is at, or very near to, the level of the hot leg. This conclusion is consistent for both the DVI break and the inadvertent ADS during the time period when all ADS-4 valves are open. Therefore, the WCOBRA-TRAC correlation tends to overpredict the upper plenum entrainment when the water level in the vessel is below the bottom of the hot leg.

- Based on the Kataoka-Ishii pool entrainment correlation, the pool entrainment phenomena for the AP1000/AP600 upper plenum geometry and the gas flux during this time of the transient has self limiting characteristics. The entrained liquid flux at the hot leg level decreases very rapidly as the pool level moves down from the hot leg, decreasing more than two orders of magnitude within the first 0.5 meter below the hot leg. The gas flux for AP1000 is about 1.75 times that for AP600 (power ratio), but a decrease of a few inches in the upper plenum pool level would compensate for this difference and result in entrained liquid flux at the hot leg level becoming the same as for AP600.

In Section A.4, sensitivity studies are made using WCOBRA/TRAC to assess the effect of entrainment on the WCOBRA/TRAC predictions. The following conclusions from these studies are made:

- Overall, the AP1000 ADS-4/IRWST initiation phase performance exhibits a modest sensitivity to varying the entrainment rate calculated in WCOBRA/TRAC. Cutting the entrainment rate in half through the use of a multiplier results in a somewhat increased minimum mass inventory. Increasing the entrainment calculated in the code through the use of the multiplier reduces the minimum mass inventory by a somewhat lesser amount, and the effect obtained from increasing the entrainment rate calculated in WCOBRA/TRAC diminishes by the time the increase multiplier equals a factor of four. The AP1000 has adequate ADS-4 venting capacity to depressurize the RCS to achieve IRWST injection in a timely manner for any of the entrainment rates analyzed.
- The AP1000 ADS-4/IRWST initiation phase performance exhibits a lack of sensitivity to the level swell calculated in the upper plenum channels in WCOBRA/TRAC. Increasing and decreasing the interfacial drag calculated by the code by one-third results in very minor changes in the ADS-4/IRWST initiation phase transient prediction.
- Correlations published to determine the liquid level at which entrainment will occur from a horizontal pipe into an offtake pipe are based on the Froude number for flow in the horizontal pipe. The base values of the multiplier coefficient and the exponent in this form of correlation have been varied in WCOBRA/TRAC in the two hot legs, to vary the prediction of entrained liquid flow into the respective open ADS-4 flow paths. The purpose of varying the parameters is to assess the impact that the prediction of the entrainment of liquid from the hot legs exerts on the AP1000 ADS-4/IRWST injection phase performance. The results of these studies show little impact on the calculated minimum inventory.
- The sensitivity of the AP1000 ADS-4/IRWST initiation phase performance, as predicted by WCOBRA/TRAC, to varying the entrainment rate in the upper plenum is modest. The sensitivity of the AP1000 ADS-4/IRWST initiation phase performance, in WCOBRA/TRAC, to varying the interfacial drag in the upper plenum is minimal. The sensitivity of the AP1000 ADS-4/IRWST initiation phase performance, as predicted by WCOBRA/TRAC, to varying the entrainment onset correlation for flow from the hot legs into the ADS-4 flow paths is minimal. In all cases analyzed, the predicted depressurization rate led to the initiation of IRWST injection at a reactor vessel mass inventory that is close to that of the base inadvertent ADS actuation case from Section 3 of this report.

- The upper plenum entrainment rate predicted in WCOBRA/TRAC is of the same order of magnitude as that predicted by the Kataoka-Ishii pool entrainment correlation for the near surface region, which applies when the liquid phase level is at or near the hot leg elevation, and represents a conservative bound on the entrainment for other regions. After all the ADS-4 valves have opened and before the minimum reactor vessel mass inventory occurs, the estimated two-phase mixture level in the upper plenum in WCOBRA/TRAC is located well below the bottom of the hot leg. A pool level at this elevation corresponds to region 2, the momentum controlled region of the Kataoka-Ishii pool entrainment correlation, and to an entrainment rate much less than is predicted by the code. Therefore, WCOBRA/TRAC provides a conservative entrainment rate prediction in the reactor vessel upper plenum for the ADS-4/IRWST initiation phase of small break LOCA events. In each sensitivity study case, the heat transfer regime on the fuel rods enables the cladding temperatures to remain near the coolant saturation temperature.

In summary, the AP1000 is equipped with ADS-4 flow paths that are adequately sized to depressurize the RCS to achieve sufficient IRWST injection, even when a postulated single failure and when a conservatively high entrainment rate prediction in the reactor vessel upper plenum are assumed. Credible variations in the entrainment in either the upper plenum or the hot legs do not adversely impact the safety of the AP1000 for the ADS-4/IRWST initiation phase of small break LOCA events. Based on these assessments, Westinghouse concludes that additional testing to develop AP1000 plant-specific upper plenum and/or hot leg entrainment correlations for the purposes of updating the NOTRUMP or WCOBRA-TRAC analysis codes is not necessary.

As demonstrated in this report, the NOTRUMP plant predictions provided in the AP1000 DCD provide a conservative prediction of the plant performance following a small break LOCA, and the results of these conservative analyses demonstrate large margin to regulatory limits. Furthermore, when compared to the WCOBRA/TRAC plant calculations, it is shown that the NOTRUMP predictions conservatively under-predict the depressurization rate of the ADS, and therefore conservatively delay the time of IRWST injection. The analyses demonstrate that the AP1000 is equipped with ADS-4 flow paths that are adequate to depressurize the RCS to achieve sufficient IRWST injection, even when a postulated single failure and when a conservatively high entrainment rate prediction in the reactor vessel upper plenum are assumed. Credible variations in the entrainment in either the upper plenum or the hot legs do not adversely impact the safety of the AP1000 for the ADS-4/IRWST initiation phase of small break LOCA events. Based on these assessments, Westinghouse concludes that additional testing to develop AP1000 plant-specific upper plenum and/or hot leg entrainment correlations for the purposes of incorporating these models into either NOTRUMP or WCOBRA-TRAC is not necessary.